Gene identification in Hereditary Spastic Paraplegias and characterization of spastic paraplegia type 58 (SPG58)

Dissertation

zur Erlangung des Grades eines

Doktors der Naturwissenschaften

der Mathematisch-Naturwissenschaftlichen Fakultät

und

der Medizinischen Fakultät

der Eberhard-Karls-Universität Tübingen

vorgelegt

von

Andrés Caballero García de Oteyza
aus Madrid, Spanien

Oktober - 2016

Tag der mündlichen Prüfung:	14 Oktober 2016
Dekan der Math.-Nat. Fakultät:	Prof. Dr. W. Rosenstiel
Dekan der Medizinischen Fakultät:	Prof. Dr. I. B. Autenrieth
1. Berichterstatter:	Prof. Dr. Ludger Schöls
2. Berichterstatter:	Prof. Dr. Doron Rapaport
Prüfungskommission:	Prof. Dr. Peter Heutink
	Prof. Dr. Thomas Gasser
	Prof. Dr. Ludger Schöls
	Dr. Michela Deleidi

I hereby declare that I have produced the work entitled: “Gene Identification in Hereditary Spastic Paraplegias and Characterization of spastic paraplegia type 58 (SPG58)”, submitted for the award of a doctorate, on my own (without external help), have used only the sources and aids indicated and have marked passages included from other works, whether verbatim or in content, as such. I swear upon oath that these statements are true and that I have not concealed anything. I am aware that making a false declaration under oath is punishable by a term of imprisonment of up to three years or by a fine.

Tübingen, October 21st 2016 Andrés Caballero García de Oteyza

Date Signature

Acknowledgements

I would like to start thanking Dr. Rebecca Schüle for having given me the opportunity to start such an exciting project together. I also thank her because she believed in me even though I had little experience when I started. She has guided and taught me patiently as much as I have asked for. During these 4 years she has been my mentor and a role model; her example has made me grow not only professionally but personally. Without her, this exciting journey would have never been possible and for that I will always thank her.

Of course I also want to thank Prof. Dr. Ludger Schöls for having sheltered me in his group with his arms wide open. I thank him also for his support, knowledge and advice whenever needed, but most importantly I am thankful because of his always constant kind words and efforts to make everyone feel like family in the group.

I would like to thank all the people in the group for their constant attempts to make me feel like one more and always welcome. Especially I would like to mention Yvonne Theurer for her endless patience and help, and Jennifer Reichbauer because of her constant willingness to help not only with lab duties but with personal matters. More than a lab mate, she has been a good friend; and the best colleague anyone could ask for. I am also grateful for the rest of my lab mates and people in the department, because they were always there to give me a hand whenever I needed it.

Finally I would like to thank all my friends, especially David, Manuel, Akshay, Mohammad Mario, Ángel, Juan, Nacho and Akbar for having made this journey more pleasant and unforgettable. Of course I thank my family, specially my mum for her endless love and support that helped me move forward and I thank the most important person in my life – Marta – because I simply could not have completed this quest without you by my side.

Table of contents

Summary

Hereditary spastic paraplegias (HSPs) are a large group of inherited neurodegenerative disorders characterised by a progressive spasticity and weakness of the lower limbs. Additional symptoms variably occur and define so-called complicated forms of the disease. HSPs exhibit a very high genetic and clinical variability, with at least 84 loci identified and 67 known causative genes. They can be inherited in autosomal dominant, autosomal recessive, and X-linked manner. However, they all share a common trait: a progressive length-dependent distal axonopathy of the motor neurons that form the corticospinal tracts.

The use of whole exome sequencing (WES) has dramatically increased the speed of gene discovery in HSP. This technique granted the conjunct identification of the five genes described here, which are responsible for causing different forms of spastic paraplegia: SPG28, SPG46, SPG26, SPG54 and SPG58. These genes are respectively involved in mitochondrial function, different aspects of lipid metabolism and RNA metabolism.

The in-depth study of SPG58 shows how mutations in *KIF1C* alter the cellular localization of KIF1C protein and affect endogenous protein levels if mutations locate to the ATP-binding domain. This work also elucidates that KIF1C interacts with known RNA-binding proteins (RBPs) and that it also binds RNA directly and is thus itself an RBP. Transcripts bound to KIF1C correspond to genes involved in key mechanisms of cell cycle and gene regulation and in various aspects of RNA metabolism. In addition to the enrichment of ribosomal RNAs, KIF1C also interacts with ribosomal proteins and influences cellular ribosome distribution. This suggests that KIF1C might have a role in the regulation and or transport of ribosomes.

Synopsis

I. Hereditary Spastic Paraplegias

HSPs are a diverse group of inherited neurodegenerative disorders characterized by progressive spasticity and weakness of the lower limbs. Although they are overall rare with a prevalence of about 4 - 6 per 100.000 individuals (1), they are among the most heterogeneous Mendelian diseases. Up to date, at least 84 different loci have been associated with HSPs and 67 corresponding spastic paraplegia genes (SPG) have been identified (2) (Figure 1).

All Mendelian modes of inheritance: autosomal dominant, autosomal recessive and X-linked have been described in HSP. SPG4 is by far the most common subtype and mutations in the associated *SPAST* gene explain about 50% of autosomal dominant HSP cases. The majority of the remaining subtypes are rare and individually account for less than 5% of cases. Clinically, HSPs are classified into pure and complex forms depending on the absence or presence of additional signs and symptoms. Common complicating features comprise peripheral neuropathy, muscle atrophy, cerebellar ataxia, mental retardation and/or dementia, epilepsy, optic neuropathy, deafness, and many others (3). Complicated forms therefore phenotypically overlap with other neurodegenerative disorders such as amyotrophic lateral sclerosis (ALS), hereditary cerebellar ataxias, Charcot-Marie Tooth (CMT) disease, epileptic encephalopathies, and others (4–6). These phenotypic overlap-syndromes further increase the genetic heterogeneity of HSP and related disorders.

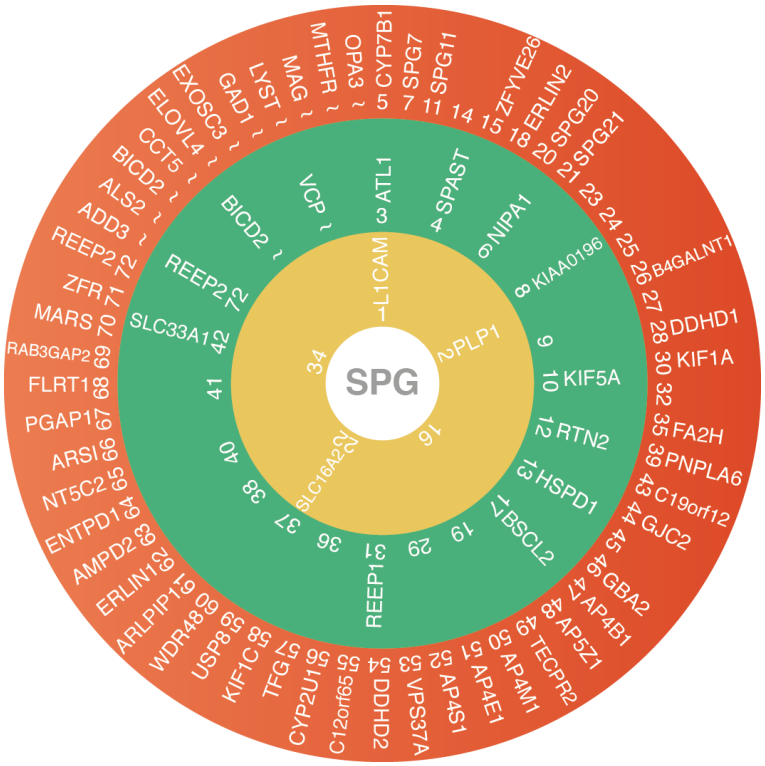

Figure 1. Overview over known HSP loci and genes. HSP loci are named by the acronym SPG (Spastic Paraplegia Gene), followed by a number. All modes of inheritance occur: X-linked (yellow), autosomal dominant (green) and autosomal recessive (orange). Reference: Schule, R. and L. Schols, *Genetics of Hereditary Spastic Paraplegias (HSP)*, in *Movement disorder genetics*, S.A. Schneider and J.M.T. Brás, Editors. 2015, Springer Berlin Heidelberg: New York, NY. p. 353-385.

Due to poor phenotype-genotype correlation and the extraordinary genetic heterogeneity, molecular diagnostic testing in HSP based on single-gene analysis has posed a huge challenge in clinical practice. Identification of novel disease genes required large pedigrees to allow meaningful linkage analysis, followed by often time consuming screening of candidate genes by Sanger sequencing or related techniques. The advent of Next Generation Sequencing (NGS) technology has revolutionized both diagnostic testing as well as research-based gene identification studies. This has led to an exponential increase in the number of newly identified HSP genes (Figure 2). Moreover, unbiased screenings of HSP genes in large cohorts of patients have led to a broadening of the phenotypic spectrum of many HSP subtypes, thus even increasing the phenotypic overlap with other hereditary neurodegenerative disorders.

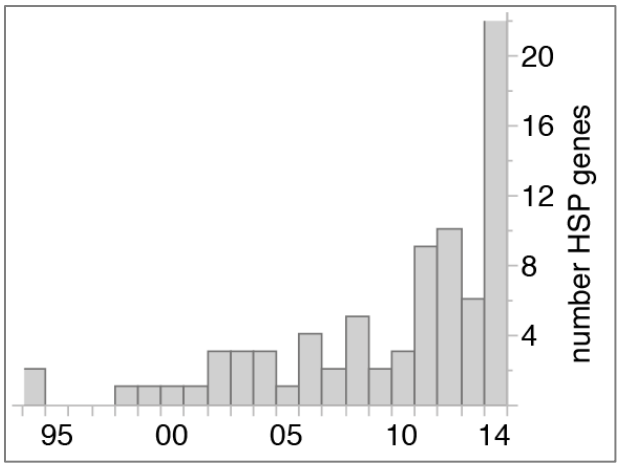

Figure 2. **Number of HSP genes published by year**. Bars represent the number of HSP genes published per year (not cumulative). First WES publications came out in 2011.

In spite of their high clinical and genetic variability, all HSPs share a common pathological hallmark in form of a progressive length-dependent distal axonopathy of the motor neurons that comprise the corticospinal tracts. Identification of disease genes in HSP has thus not only clinical applications but offers a chance to identify pathways that are important for axon formation and maintenance. Several cellular processes and pathways with its responsible proteins have been identified in HSP pathogenesis (Figure 3). For instance *SPAST* (SPG4) and *KIF5A* (SPG10) are involved in axonal transport (7, 8); *ATL1* (SPG3) and *REEP1* (SPG31) in endoplasmic reticulum membrane modelling and shaping (9); *PARAPLEGIN* (SPG7) is essential for mitochondrial function (10); *AP5Z1* (SPG48), *MARS* (SPG70) and *NT5C2* (SPG65) are involved in DNA repair and nucleotide metabolism (11, 12); *SPATACSIN* (SPG11) and *SPASTIZIN* (SPG15) in autophagy (13); *CYP7B1* (SPG5), *B4GALNT1* (SPG26), *DDHD1* (SPG28) *FA2H* (SPG35), *GBA2* (SPG46), *DDHD2* (SPG54) are all involved in diverse aspects of lipid metabolism (14–19); *NIPA1* (SPG6) and *SPARTIN* (SPG20) in cellular signalling for protein morphogenesis (20); and the family of adaptors *AP4* (SPG47,50-52) or *Strumpellin* (SPG8) (part of the WASH complex) are involved in endosome membrane trafficking and vesicle formation (21).

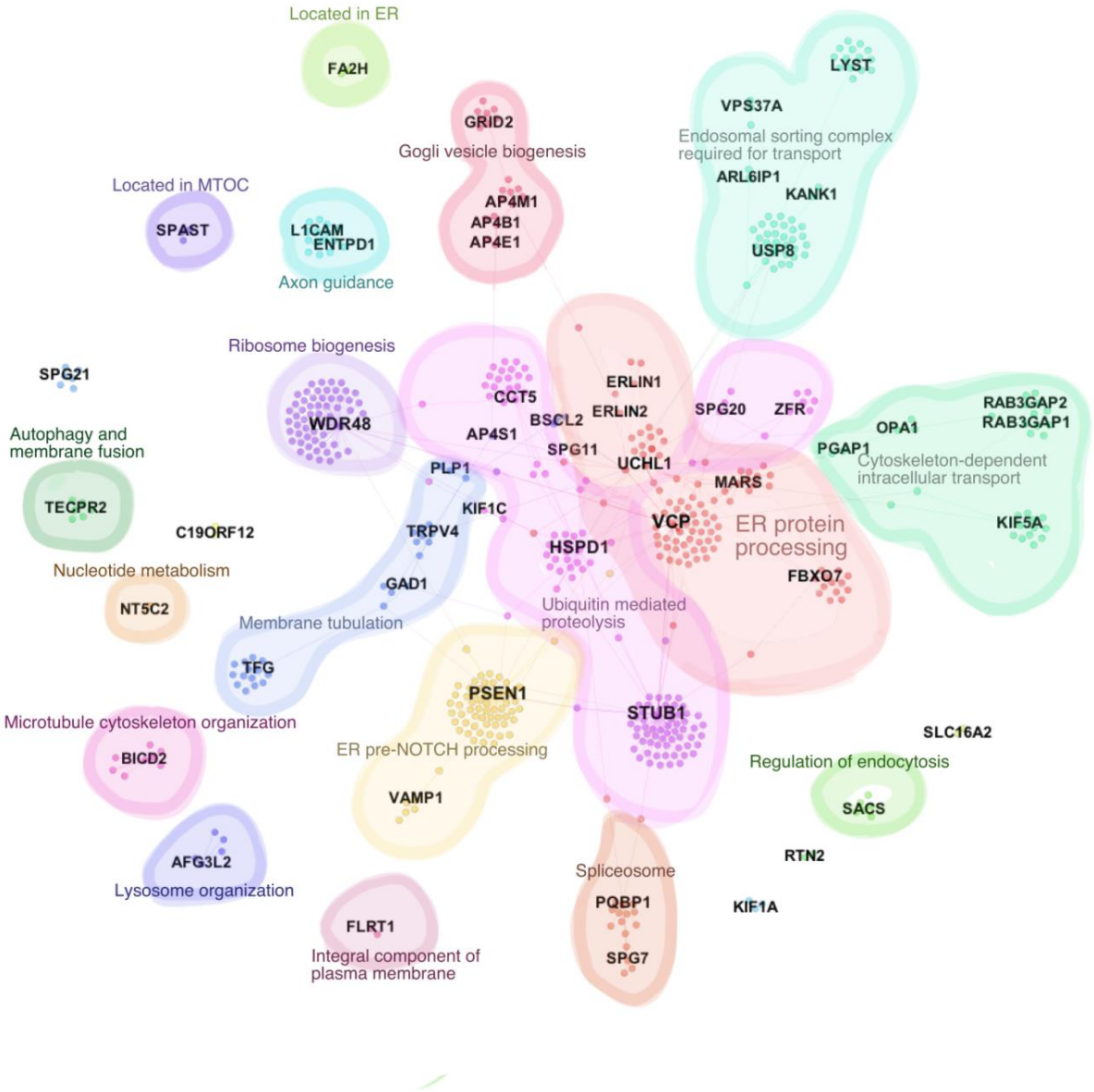

Figure 3. **Network of HSP-associated proteins based on protein-protein interactions and functional annotations.** The iRefScape plugin in Cytoscape was used to generate a protein-protein interaction map based on iRefIndex (includes BIND, BioGRID, CORUM, DIP, HPRD, InnateDB, IntAct, MatrixDB, MINT, MPact, MPIDB and MPPI). The resulting network was then uploaded to Gephi and clustered by modularity. Clusters were functionally annotated using ConsensusPathDB; over-representation analysis for pathways and GO terms was performed and the resulting significant pathways/terms for each cluster were then overlaid manually onto the network. Reprinted with permission from Dana Bis, University of Miami.

The huge variety of functional mechanisms involved makes the heterogeneity of the disease very tangible. However there are still cases to be solved and therefore it is plausible that other important pathways, such as RNA metabolism, could also be altered in HSP pathogenesis. The continuous discovery of new HSP genes has shed light into the overall picture of this network and it is helping to link existing affected pathways, which improves the way we can address and understand the disease.

II. Gene identification in HSPs

In spite of the large number of genes already identified in HSP, mutations in these genes still only explain about 70% of autosomal dominant and less than half of autosomal recessive and sporadic cases (22). We therefore employed a WES-based approach to identify novel genes causing autosomal recessive HSP.

Our centre runs one of the largest HSP specialty clinics in the world and has collected detailed clinical data and biomaterials of > 1000 HSP cases, including 544 simplex cases with HSP, 115 families with multiplex recessive HSP and 557 autosomal dominant pedigrees. From this cohort we selected multiplex recessive families, where several affected and unaffected family members were available, in which Sanger sequencing based approaches had so far failed to provide a genetic diagnosis. WES was carried out at the Hussman Institute for Human Genomics at the University of Miami Miller School of Medicine (collaboration: Stephan Zuchner). Data were then analysed using the web-based GEM.app/Genesis platform developed by the Zuchner lab (23). Resulting exome variants were filtered for allele frequency in public databases and GEM.app/Genesis, segregation pattern, variant ontology, and genotyping quality; resulting variants were then prioritized

based on conservation across species and predicted effect on protein function. In ~27% of families we identified pathogenic mutations in known autosomal recessive genes associated with HSP and related disorders. In the remaining families we created shortlists of candidate genes, typically between 1 and 20 genes per family. Sanger sequencing in additional family members was then performed to evaluate the segregation pattern within the family and thus reject variants based on failed co-segregation with the disease. The resulting final candidate gene lists were then intersected across families both within our own cohort as well as with candidate genes obtained by international collaborators. In genes mutated in two or more families with a similar phenotype additional genetic as well as functional evidence was then obtained as detailed below.

SPG28

WES in two brothers of Turkish origin and consanguineous family background revealed a homozygous truncating mutation (c.1874delT) in the *DDHD1* gene. Both affected siblings in Family THI26002 showed progressive spastic gait developing since adolescence, complicated by a mild cerebellar oculomotor phenotype in one of them. Sanger segregation confirmed co-segregation of the mutation with the disease. Identification of two additional HSP families with truncating *DDHD1* mutations led to our joint identification of *DDHD1* as a novel HSP gene (SPG28) (17) (paper attached). DDHD1 is a phospholipase that hydrolyses phosphatidic acid (PA) and is transiently associated with cytosolic membranes. We demonstrated that DDHD1 causes mitochondrial dysfunction, including reduced respiration and ATP production. As PA is a natural substrate for DDHD1 it can be speculated that the mitochondrial bioenergetic dysfunction observed in DDHD1 deficiency, might be a result of an accumulation of PA in the mitochondria (24). Mitochondrial dysfunction could also result

from an altered mitochondrial morphogenesis, as in *Paraplegin* mutations (25) or from a mitochondrial respiratory impairment, due to increased reactive oxygen species (ROS) as observed in SPG28 cells. Such overproduction of ROS could play a role in neuronal degeneration, as previously suggested for HSP pathophysiology (26).

SPG46

In a Turkish family (F18310) with consanguineous family background and two siblings affected by spastic ataxia we were able to narrow down the candidate gene list carrying rare homozygous coding variants to 22 genes. *GBA2* was the only gene harbouring a truncating mutation. Sanger sequencing confirmed that both affected siblings in this family carried the nonsense homozygous mutation c.700C>T (p.Arg234*) in the *GBA2* gene. A targeted query of *GBA2* across the GEM.app/Genesis database pointed us to a Belgian family (de Jonghe group, Antwerp) with a similar phenotype also carrying two truncating *GBA2* alleles, thus adding genetic evidence towards the pathogenicity of *GBA2* variants. Finally, collaboration with additional partners allowed us to increase the total number of GBA2 families to four and publish our findings in the American Journal of Human genetics (19) (paper attached). Affected SPG46 family members presented a complex HSP phenotype characterized by cerebral and cerebellar atrophy, thinning of the corpus callosum, cataract and hypogonadism in males.

GBA2 is a non-lysosomal glucosylceramidase that hydrolyses glucosylceramide into glucose and ceramide. It also catalyses the reverse reaction by adding glucose to diverse lipid substrates (27). GBA2 is thus involved in key aspects of sphingolipid metabolism. It synthetises various signalling molecules and plasma membrane components which are essential for composition and dynamics of membranes (28). GBA2 localises to the

endoplasmic reticulum (ER) and the cell surface, where ceramide molecules produced by this enzyme are used to synthetize sphingomyelin (29).

Pathogenic *GBA2* mutations resulted in a complete loss of enzymatic function in both untransformed leukocytes and lymphoblasts from affected SPG46 patients (19). Loss of β-glucosylceramidase activity thus suggests a link between glucosylceramide metabolism and HSP pathogenesis.

SPG26

Three out of 10 siblings of Family THI26004 were affected by childhood onset cognitive disability, followed about a decade later by a predominantly lower limb spastic tetraparesis with pseudobulbar dysarthria, and organic psychosis. The family originated from a small village in former Yugoslavia, making a founder mutation likely. Exome sequencing in one affected sibling yielded possible biallelic variants in a total of 3 candidate genes (2 with potentially compound heterozygous and 1 with homozygous changes), including a homozygous missense mutation in *B4GALNT1* (c.1298A>C, p.N433A). We matched these disease gene candidates with results from our collaborators and were able to identify a total of seven families with mutations in the *B4GALNT1* gene (14) (paper attached).

B4GALNT1 encodes the enzyme β-1,4-N-acetyl-galactosaminyl transferase 1 which is involved in the biosynthesis of complex gangliosides. Gangliosides belong to the large family of glycosphingolipids, components of the synaptic plasma membrane involved in synaptic plasticity, signal transduction and endocytosis, which are essential for CNS development (30). B4GALNT1 catalyses the transfer of N-acetyl-galactosamine into ganglioside mono- and di- sialic acid 3 (GM3, GD3) and globotriaosylceramide, therefore mutations in *B4GALNT1* will lead to a deficit of gangliosides G[M/D/T]3 and globotriaosylceramide. Concomitantly,

the B4galnt1 -/- mouse resembles to a certain extent the gait phenotype seen in SPG26. Lack of complex gangliosides in SPG26 might reduce myelination in the spinal cord, thus resulting in degeneration due to increased unmyelinated fibres (31).

SPG54

Following the same strategy of WES and Sanger confirmation in family THI26003 we were able to identify *DDHD2* as the gene causing spastic paraplegia 54 (SPG54) (32) (paper attached). The SPG54 phenotype is characterized by early onset of spasticity, mental retardation, short stature and dysgenesis of the corpus callosum. Sequencing results revealed that both affected siblings in THI26003, a consanguineous family from Azerbaijan, presented a homozygous nonsense variant in *DDHD2* (c.859C4T, p.Arg287*). The transcript containing this early stop codon produces – if it escapes nonsense mediated decay - a protein lacking the DDHD catalytic domain. This domain ensures membrane localization, phosphoinositide binding and homo-oligomerization; loss of this domain therefore likely leads to a loss of crucial DDHD2 functions. DDHD2 is phospholipase, and like DDHD1, also possesses phospholipase A1 activity to catalyse phosphatidic acid (PA) and other phospholipids (33). PA is an essential structural component of biological membranes, it is involved in lipid signalling and it is also a substrate for the biosynthesis of triacylglycerols and phosphoglycerols (34). A cytosolic and membrane-associated pool of DDHD2 localises to the ER-Golgi intermediate compartment (ERGIC). This pool may be involved in membrane trafficking because DDHD2 overexpression leads to Golgi dispersion and ERGIC enlargement (35). DDHD2 involvement in lipid metabolism and Golgi-ER membrane trafficking highlight the importance of these mechanisms for motor neuron maintenance and sheds light into the complex network of HSP pathogenesis.

SPG58

Lastly, WES of the index patient of family THI26001 permitted the identification of two compound heterozygous missense mutations in *KIF1C* c.[305G>C];[527C>T], p.[Gly102Ala];[Pro176Leu]. Sanger sequencing of this German family confirmed co-segregation of these variants with the disease. The other two affected siblings also carried both heterozygous missense mutations, while each of the parents presented one of the heterozygous mutations. Targeted analysis of KIF1C in the Genesis/GEMapp database allowed identification of Family IHG25215, of Turkish origin and consanguineous family background, also carrying mutations in *KIF1C.* The less severely affected brother of this family ported the heterozygous missense variant c.901A>G, p.Arg301Gly whereas the severely affected brother carried the variant in homozygous state. The identification of these three different missense mutations in these two families and their later characterization allowed us to conclude that mutations in *KIF1C* cause spastic paraplegia type 58 (SPG58) (36) (paper attached). Therefore we defined SPG58 as a new form of spastic paraplegia which can be complicated by cervical dystonia and cerebellar ataxia.

III. KIF1C, what is known?

Prior to KIF1C involvement in human neurodegeneration, diverse functions for the motor had been described. These included retrograde vesicle transport from Golgi apparatus to the endoplasmic reticulum in mouse fibroblast cells (37), regulation of podosome dynamics in primary human macrophages (38), control of pericentrosomal localization and anterograde transport of Rab6 secretory vesicles in hippocampal neurons, when interacting with BICDR-1

(39), and transport of α5β1-integrins to stabilize trailing focal adhesions in migrating human RPE1 cells (40).

Recent investigations also describe how the role of KIF1C in podosome formation and maintenance in human macrophages is influenced by microtubule acetylation (41), and induced by protein kinase C (PKC) which prompts KIF1C to translocate to the cell periphery in a CLASP dependent manner (42). Furthermore, KIF1C has been reported to transport Rab6A-vesicles and influence Golgi's membrane organization through its direct binding with Rab6A via both its motor and C-terminus domain, which causes a reduction in KIF1C motility (43).

In spite of this broad and diverse functional spectrum, KIF1C had never been reported as an axonal transporter nor had it been linked to neurodegeneration. Therefore, a different approach was needed to tackle KIF1C role in motor neurons and its involvement in SPG58 pathogenesis.

IV. Characterization of SPG58 mutations

Analysis of mRNA expression levels of *KIF1C* in all members of family THI26001 revealed that expression did not differ significantly between the compound heterozygous affected siblings and the heterozygous parents. In contrast, analysis of protein levels showed a reduction of about 50% in all carriers of the c.305G>C mutation when compared to controls or the heterozygous mother (carrier of c.527C>T change) (36) (paper attached). The c.305G>C allele therefore likely translates into a protein that is recognized as non-functional and is therefore targeted for degradation.

KIF1C belongs to the super family of kinesins, and has been defined as a retrograde (37) and anterograde (40) microtubule-based transporter. All mutations found in our HSP families reside in the protein's motor domain; more precisely they are located at the ATP-binding domain (p.G102A), the Loop 8 microtubule-binding domain (p.P176L) and the Loop 12 microtubule-binding domain (p.R301G). Therefore, mutations within these locations will likely affect processivity of KIF1C. KIF1C is expressed ubiquitously and is sparsely distributed in the cytoplasm, accumulating around the nucleus and the centrosome. When overexpressed in COS-7 cells, we found that $KIF1C_{WT}$ tended to redistribute to the cell periphery and accumulate at the verges of cellular protrusions. However, overexpressed mutant $KIF1C_{G102A}$ or $KIF1C_{R301G}$ failed to reach the tips of cellular processes, showing instead a non-specific cytoplasmic localisation. Overexpressed $KIF1C_{P176L}$ surprisingly showed a distribution comparable to that of $KIF1C_{WT}$ (36). Patients simultaneously express two pathogenic *KIF1C* alleles; in the case of family THI26001 the affected siblings carry both the P176L and the G102A mutation, while the unaffected parents carry only one mutation in combination with a wildtype allele. To mimic this situation in cell culture we therefore performed double-overexpression of different *KIF1C* alleles. The mis-localisation of the mutant $KIF1C_{G102A}$ can be almost completely rescued by simultaneous overexpression of $KIF1C_{WT}$. In contrast, $KIF1C_{P176L}$ fails to rescue the mis-localisation caused by expression of mutant $KIF1C_{G102A}$ allele (36). We hypothesize that this might be explained by a reduced microtubule binding affinity of the $KIF1C_{P176L}$ allele. Therefore the $KIF1C_{P176L}$ allele, despite its putatively normal mobility, fails to make up for $KIF1C_{G102A}$'s motility defect in dimeric state. The transport deficit caused by *KIF1C* mutations likely translates into a lack of cargo delivery at the verge of cellular processes (i.e. at the synapse in neurons) essential for synapse maintenance and cell survival in motor neurons.

V. Determination of KIF1C function

With whom does KIF1C interact?

To better understand KIF1C function we decided to look for interaction partners, because identification of new protein interactors may shed light on previously unknown functional pathways. To this end we immunoprecipitated KIF1C complexes in HEK293T cells overexpressing $KIF1C_{WT}$ or $KIF1C_{MUT}$ (G102A, P176L) (manuscript attached). Mass spectrometry analysis of a protein band of about 70 KDa revealed the presence of several RNA-binding proteins: PABPC1 (PABP), IGF2BP1 (IMP-1), IGF2BP3 (IMP-3) and HSPA8, all of them known to be involved in a certain aspect of RNA metabolism (44–46). Mutual interactions between KIF1C and candidates PABP, IMP-1 or HSPA8 could be confirmed by western-blotting of co-immunoprecipitated complexes in HEK293T cells. Moreover, immunofluorescent (IF) imaging of fibroblast-like COS-7 cells and neuron-like SH-SY5Y cells confirmed the co-localisation of KIF1C with all three putative novel interaction partners. In addition, quantitative analysis of KIF1C complexes demonstrated that mutations in the KIF1C motor domain ($KIF1C_{G102A}$, $KIF1C_{P176L}$, $KIF1C_{R301G}$) have no effect on binding properties, at least in an overexpression setting.

KIF1C binds RNA

The fact that PABP, IMP-1 and HSPA8 are known RNA-binding proteins raised the question of whether KIF1C might as well share that role. The way we addressed this possibility, with an RNAse-mediated IP, permitted to elucidate that KIF1C-PABP interaction is RNA dependent. Co-Immunoprecipitation (CO-IP) of HA-tagged fusion protein KIF1C-HA with PABP in HEK293T lysates demonstrated that the mutual interaction diminishes with increasing concentrations of RNAse I, an enzyme that hydrolyses single-stranded RNA to nucleoside 3'-

monophosphates. This outcome was not compromised by an under-representation of PABP, because mutual CO-IP of fusion proteins KIF1C-HA and PABP-GFP was likewise RNAse-sensitive. Moreover, CO-IP of endogenous KIF1C and PABP in HeLa lysates was equally abolished after RNAse I addition (manuscript attached). Consistency of these results proved that PABP-KIF1C interaction is RNA-mediated and suggested that KIF1C could bind RNA directly and thus be an RBP itself.

To test this hypothesis and identify potential transcripts bound to KIF1C we performed an individual-nucleotide resolution crosslinked immunoprecipitation (iCLIP) (47) in HEK293T cells transiently expressing the fusion protein KIF1C-mCherry. The iCLIP protocol notably includes an UV-light irradiation step, which leads to formation of covalent bonds at sites of protein-RNA interaction, thus specifically preserving direct protein-RNA interactions during the following rigorous washing and purification steps (48). iCLIP interactions are therefore highly specific. This procedure permitted detection of positive RNA signal and isolation of RNA fragments ranging between 250-450bp (retro-transcribed to cDNA) which were bound to KIF1C.

Analysis of RNA transcripts bound to KIF1C

Recovered RNA fragments were used to create a cDNA library that was submitted to high-throughput sequencing and resulted in an average of 157 million read-pairs. Later alignment with Galaxy, a web-based genome analysis tool (49), mapped an average of 48 million read-pairs to the genome. Subsequent analysis with PIPE-CLIP, a tool that provides data processing and statistical analysis to determine candidate protein-RNA cross-linking regions (50), showed that the transcripts mapped to a total of 515 unique genes (manuscript attached). The top four genes represented by transcripts with the highest peak scores were

KIF1C, *HYDIN* (hydrocephalus inducing protein homologue) and two ribosomal DNA genes: *RNA45S5* from which the ribosomal 28S, 5.8S, and 18S subunits are transcribed, and *RNA5-8S5* that encodes the ribosomal 5S subunit.

Validation of transcripts found after iCLIP data analysis was performed using recovered RNA from an RNA-IP of HEK293T lysates (from both endogenous and KIF1C overexpressed conditions) and quantitative PCR. For this purpose we chose five genes *KIF1C, HYDIN, HFM1, PDE3 & RAPGEF*, all of which were among the 10 highest scoring genes in the analysis. The assay proved not only the presence of the five genes in the KIF1C-IP sample but also their over-representation in comparison to the input sample, thus confirming the results from iCLIP data analysis.

To uncover functional connections of bound transcripts and analyse functionally over-represented pathways we used DAVID (51), a web resource that allows annotation of genes with terms derived from multiple databases including GO terms, KEGG and Panther pathways, BioGrid and many more, and constructed a network of overrepresented pathways in Cytoscape. Strongly enriched functions include RNA/DNA binding, RNA processing and splicing, gene expression and cell cycle. These results reflect the importance of KIF1C as an RBP in RNA metabolism and its involvement in further key cellular functions; none of which had been previously described for KIF1C.

KIF1C interacts with Ribosomes

The strong over-representation of RNA-related functional pathways among of transcripts bound to KIF1C, plus the enrichment of rRNA transcripts, suggested that KIF1C might cooperate with ribosomes. Therefore we studied the interaction between KIF1C and the ribosomal protein S6 (RPS6), a ribosomal marker that has been previously used to measure

dendritic mRNA transport in form of RNA granules in hippocampal neurons (52). Immunofluorescent imaging revealed that $KIF1C_{WT}$ overexpression induces a ribosomal recruitment to the cell periphery and accumulation at the tips of cellular processes; whereas $KIF1C_{G102A}$ overexpression causes a redistribution of ribosomes to the cytoplasm. Ribosomal localization thereby strictly follows the localization pattern of overexpressed KIF1C. Moreover KIF1C-ribosome interaction is supported by the mutual co-immunoprecipitation of KIF1C and RPS6, as shown by western blotting (manuscript attached). These findings strongly suggest that KIF1C interacts with ribosomes and strengthen our hypothesis that KIF1C is an axonal transporter for ribosomes in neurons that might be involved in maintenance and regulation of synaptic translation through transport and regulation of local protein translation.

VI. Conclusion

Gene discovery in HSPs has progressed enormously over the last few years thanks to the use of whole-exome sequencing in clinical practice. This technique facilitated the discovery of five distinct spastic paraplegia genes during the course of this study: SPG28, SPG46, SPG26, SPG54 and SPG58, respectively involved in mitochondrial function, different aspects of lipid metabolism and RNA metabolism.

SPG58 mutations located in the motor domain provoke a change in KIF1C distribution and impact protein stability if the mutation localises to the ATP-binding domain. KIF1C directly binds RNA as well as RNA-binding proteins. Transcripts bound to KIF1C map preferentially to RNA-related cellular processes and ribosomal components are strongly enriched among

KIF1C-bound transcripts. Overexpression of KIF1C recruits ribosomes to the tips of cellular processes, a distribution that is lost when overexpressing mutant KIF1C.

In conclusion we hypothesize that KIF1C transports ribosomes along the axons and is involved in regulation of local protein translation at the synapse. Alteration of RNA transport and regulation of translation, caused by mutations in RNA-binding proteins, is increasingly recognized as an important pathogenic mechanism in other neurological and neurodegenerative diseases such as ALS and Fronto-Temporal Dementia (FTD) (53), however it would be the first case in HSP pathogenesis.

References

1. Schule R, Schols L. Genetics of hereditary spastic paraplegias.. *Semin. Neurol.* 2011;31(5):484–493.

2. Tesson C, Koht J, Stevanin G. Delving into the complexity of hereditary spastic paraplegias: how unexpected phenotypes and inheritance modes are revolutionizing their nosology.. *Hum. Genet.* 2015;134(6):511–538.

3. Depienne C, Stevanin G, Brice A, Durr A. Hereditary spastic paraplegias: an update.. *Curr. Opin. Neurol.* 2007;20:674–680.

4. Oates EC et al. Mutations in BICD2 cause dominant congenital spinal muscular atrophy and hereditary spastic paraplegia.. *Am. J. Hum. Genet.* 2013;92(6):965–973.

5. Vantaggiato C, Clementi E, Bassi MT. ZFYVE26/SPASTIZIN: a close link between complicated hereditary spastic paraparesis and autophagy.. *Autophagy* 2014;10(2):374–375.

6. Daoud H et al. Exome sequencing reveals SPG11 mutations causing juvenile ALS. *Neurobiol. Aging* 2012;33(4). doi:10.1016/j.neurobiolaging.2011.11.012

7. Denton KR et al. Loss of spastin function results in disease-specific axonal defects in human pluripotent stem cell-based models of hereditary spastic paraplegia.. *Stem Cells* 2014;32(2):414–423.

8. Campbell PD et al. Unique function of Kinesin Kif5A in localization of mitochondria in axons.. *J. Neurosci.* 2014;34(44):14717–14732.

9. Park SH, Zhu PP, Parker RL, Blackstone C. Hereditary spastic paraplegia proteins REEP1, spastin, and atlastin-1 coordinate microtubule interactions with the tubular ER network. *J. Clin. Invest.* 2010;120(4):1097–1110.

10. McDermott CJ et al. Investigation of mitochondrial function in hereditary spastic paraparesis. [Internet]. *Neuroreport* 2003;14(3):485–488.

11. S??abicki M et al. A genome-scale DNA repair RNAi screen identifies SPG48 as a novel gene associated with hereditary spastic paraplegia. *PLoS Biol.* 2010;8(6). doi:10.1371/journal.pbio.1000408

12. Novarino G et al. Exome sequencing links corticospinal motor neuron disease to common neurodegenerative disorders. [Internet]. *Science* 2014;343(6170):506–11.

13. Chang J, Lee S, Blackstone C. Spastic paraplegia proteins spastizin and spatacsin mediate autophagic lysosome reformation. *J. Clin. Invest.* 2014;124(12):5249–5262.

14. Boukhris A et al. Alteration of ganglioside biosynthesis responsible for complex hereditary spastic paraplegia. *Am. J. Hum. Genet.* 2013;93(1):118–123.

15. Tsaousidou MK et al. Sequence Alterations within CYP7B1 Implicate Defective Cholesterol Homeostasis in Motor-Neuron Degeneration. *Am. J. Hum. Genet.* 2008;82(2):510–515.

16. Dick KJ et al. Mutation of FA2H underlies a complicated form of hereditary spastic paraplegia (SPG35). *Hum. Mutat.* 2010;31(4). doi:10.1002/humu.21205

17. Tesson C et al. Alteration of fatty-acid-metabolizing enzymes affects mitochondrial form and function in hereditary spastic paraplegia. *Am. J. Hum. Genet.* 2012;91(6):1051–1064.

18. Gonzalez M et al. Mutations in phospholipase DDHD2 cause autosomal recessive hereditary spastic paraplegia (SPG54). [Internet]. *Eur. J. Hum. Genet.* 2013;21(11):1214–8.

19. Martin E et al. Loss of function of glucocerebrosidase GBA2 is responsible for motor neuron defects in hereditary spastic paraplegia. *Am. J. Hum. Genet.* 2013;92(2):238–244.

20. Tsang HTH et al. The hereditary spastic paraplegia proteins NIPA1, spastin and spartin are inhibitors of mammalian BMP signalling.. *Hum. Mol. Genet.* 2009;18(20):3805–3821.

21. Freeman C, Seaman MNJ, Reid E. The hereditary spastic paraplegia protein strumpellin: Characterisation in neurons and of the effect of disease mutations on WASH complex assembly and function. *Biochim. Biophys. Acta - Mol. Basis Dis.* 2013;1832(1):160–173.

22. Schule R et al. Hereditary Spastic Paraplegia -clinico-genetic lessons from 608 patients.. *Ann. Neurol.* [published online ahead of print: February 2016]; doi:10.1002/ana.24611

23. Gonzalez M et al. Innovative genomic collaboration using the GENESIS (GEM.app) platform.. *Hum. Mutat.* 2015;36(10):950–956.

24. Higgs HN, Han MH, Johnson GE, Glomset JA. Cloning of a phosphatidic acid-preferring phospholipase A1 from bovine testis. *J. Biol. Chem.* 1998;273(10):5468–5477.

25. Casari G et al. Spastic paraplegia and OXPHOS impairment caused by mutations in paraplegin, a nuclear-encoded mitochondrial metalloprotease. *Cell* 1998;93(6):973–983.

26. Gucuyener K et al. Is oxidative damage in operation in patients with hereditary spastic paraparesis? [Internet]. *Brain Dev.* 2010;32(2):130–136.

27. Boot RG et al. Identification of the non-lysosomal glucosylceramidase as β-glucosidase 2. *J. Biol. Chem.* 2007;282(2):1305–1312.

28. Mencarelli C, Martinez-Martinez P. Ceramide function in the brain: When a slight tilt is enough. *Cell. Mol. Life Sci.* 2013;70(2):181–203.

29. van Weely S, Brandsma M, Strijland A, Tager JM, Aerts JM. Demonstration of the existence of a second, non-lysosomal glucocerebrosidase that is not deficient in Gaucher disease.. *Biochim. Biophys. Acta* 1993;1181(1):55–62.

30. Xu Y-H, Barnes S, Sun Y, Grabowski GA. Multi-system disorders of glycosphingolipid and ganglioside metabolism. [Internet]. *J. Lipid Res.* 2010;51(7):1643–1675.

31. Sheikh K a et al. Mice lacking complex gangliosides develop Wallerian degeneration and myelination defects.. *Proc. Natl. Acad. Sci. U. S. A.* 1999;96(June):7532–7537.

32. Gonzalez M et al. Mutations in phospholipase DDHD2 cause autosomal recessive hereditary spastic paraplegia (SPG54). [Internet]. *Eur. J. Hum. Genet.* 2013;21(11):1214–8.

33. Nakajima KI et al. A novel phospholipase A1 with sequence homology to a mammalian Sec23p-interacting protein, p125. *J. Biol. Chem.* 2002;277(13):11329–11335.

34. Wang X, Devaiah SP, Zhang W, Welti R. Signaling functions of phosphatidic acid. *Prog. Lipid Res.* 2006;45(3):250–278.

35. Morikawa RK et al. Intracellular phospholipase A1gamma (iPLA1gamma) is a novel factor involved in coat protein complex I- and Rab6-independent retrograde transport between the endoplasmic reticulum and the Golgi complex.. *J. Biol. Chem.* 2009;284(39):26620–26630.

36. Caballero Oteyza A et al. Motor protein mutations cause a new form of hereditary spastic paraplegia. [Internet]. *Neurology* [published online ahead of print: 2014]; doi:10.1212/WNL.0000000000000479

37. Dorner C et al. Characterization of KIF1C, a new kinesin-like protein involved in vesicle transport from the Golgi apparatus to the endoplasmic reticulum.. *J. Biol. Chem.* 1998;273(32):20267–20275.

38. Kopp P et al. The kinesin KIF1C and microtubule plus ends regulate podosome dynamics in macrophages.. *Mol. Biol. Cell* 2006;17(6):2811–2823.

39. Schlager MA et al. Pericentrosomal targeting of Rab6 secretory vesicles by Bicaudal-D-related protein 1 (BICDR-1) regulates neuritogenesis.. *EMBO J.* 2010;29(10):1637–1651.

40. Theisen U, Straube E, Straube A. Directional Persistence of Migrating Cells Requires Kif1C-Mediated Stabilization of Trailing Adhesions. *Dev. Cell* 2012;23(6):1153–1166.

41. Bhuwania R, Castro-Castro A, Linder S. Microtubule acetylation regulates dynamics of KIF1C-powered vesicles and contact of microtubule plus ends with podosomes. *Eur. J. Cell Biol.* 2014;93(10-12):424–437.

42. Efimova N et al. Podosome-regulating kinesin KIF1C translocates to the cell periphery in a CLASP-dependent manner. [Internet]. *J. Cell Sci.* 2014;127(24):5179–88.

43. Lee PL, Ohlson MB, Pfeffer SR. Rab6 regulation of the kinesin family KIF1C motor domain contributes to Golgi tethering. [Internet]. *Elife* 2015;4. doi:10.7554/eLife.06029

44. Zhang H et al. PABPC1 interacts with AGO2 and is responsible for the microRNA mediated gene silencing in high grade hepatocellular carcinoma.. *Cancer Lett.* 2015;367(1):49–57.

45. Bley N et al. Stress granules are dispensable for mRNA stabilization during cellular stress.. *Nucleic Acids Res.* 2015;43(4):e26.

46. Kakumani PK et al. Dengue NS3, an RNAi suppressor, modulates the human miRNA pathways through its interacting partner.. *Biochem. J.* 2015;471(1):89–99.

47. Huppertz I et al. iCLIP: Protein-RNA interactions at nucleotide resolution. *Methods* 2014;65(3):274–287.

48. Smirnov YA, Rodrigues-Molto MP, Famadas MT. Protein-RNA interaction in encephalomyocarditis virus as revealed by UV light-induced covalent linkages.. *J. Virol.*

1983;45(3):1048–1055.

49. Goecks J, Nekrutenko A, Taylor J. Galaxy: a comprehensive approach for supporting accessible, reproducible, and transparent computational research in the life sciences [Internet]. *Genome Biol.* 2010;11(8):1–13.

50. Chen B, Yun J, Kim MS, Mendell JT, Xie Y. PIPE-CLIP: a comprehensive online tool for CLIP-seq data analysis. [Internet]. *Genome Biol.* 2014;15(1):R18.

51. Huang DW, Sherman BT, Lempicki RA. Systematic and integrative analysis of large gene lists using DAVID bioinformatics resources.. *Nat. Protoc.* 2009;4(1):44–57.

52. Kim HK, Kim Y-B, Kim E-G, Schuman E. Measurement of dendritic mRNA transport using ribosomal markers.. *Biochem. Biophys. Res. Commun.* 2005;328(4):895–900.

53. Lagier-Tourenne C, Polymenidou M, Cleveland DW. TDP-43 and FUS/TLS: emerging roles in RNA processing and neurodegeneration.. *Hum. Mol. Genet.* 2010;19(R1):R46–64.

Statement of contributions

1. Tesson C et al. Alteration of fatty-acid-metabolizing enzymes affects mitochondrial form and function in hereditary spastic paraplegia. *Am. J. Hum. Genet.* 2012;91(6):1051–1064.

Contributed analysing data retrieved from Genesis/GEM.app after whole exome sequencing of index patient of family THI26002. Sanger sequencing of all available family members of THI26002 and subsequent co-segregation analysis of candidate variants. Critical revision of the drafted manuscript.

2. Martin E et al. Loss of function of glucocerebrosidase GBA2 is responsible for motor neuron defects in hereditary spastic paraplegia. *Am. J. Hum. Genet.* 2013;92(2):238–244.

Contributed analysing data retrieved from Genesis/GEM.app after whole exome sequencing of index patient of family F18310. Sanger sequencing of all available family members of F18310 and subsequent co-segregation analysis of candidate variants. Critical revision of the drafted manuscript.

3. Boukhris A et al. Alteration of ganglioside biosynthesis responsible for complex hereditary spastic paraplegia. *Am. J. Hum. Genet.* 2013;93(1):118–123.

Contributed analysing data retrieved from Genesis/GEM.app after whole exome sequencing of index patient of family THI26004. Sanger sequencing of all available family members of THI26004 and subsequent co-segregation analysis of candidate variants. Critical revision of the drafted manuscript.

4. Gonzalez M et al. Mutations in phospholipase DDHD2 cause autosomal recessive hereditary spastic paraplegia (SPG54). [Internet]. *Eur. J. Hum. Genet.* 2013;21(11):1214–8.

Contributed to analyse data retrieved from Genesis/GEM.app after whole exome sequencing of index patient of family THI26003. Sanger sequencing of all available family members of THI26003 and subsequent co-segregation analysis of candidate variants. Critical revision of the drafted manuscript.

4. Caballero Oteyza A et al. Motor protein mutations cause a new form of hereditary spastic paraplegia. [Internet]. *Neurology* [published online ahead of print: 2014]; doi:10.1212/WNL.0000000000000479

Andrés Caballero-Oteza was involved in the conception of the study and in the analysis of exome sequencing data retrieved from Genesis/GEM.app of family THI26001. Performed sanger sequencing of all available family members of THI26001 and subsequent co-segregation analysis of candidate variants. Experiments and analysis for the study of the protein localization of genetic mutations and their impact on KIF1C expression levels. Experiments and analysis of cellular distribution of endogenous, overexpressed wild-type and mutant KIF1C proteins. Also involved in the drafting of the manuscript.

Esra Battaloglu was involved in the conception of the study and analysis of genetic data on family IHG25215, and critically revised the manuscript.

Levent Ocek recruited and examined family IHG25215 and participated in drafting of the article.

Tobias Lindig acquired and interpreted the MRI of family THI26001 and participated in drafting of the article.

Jennifer Reichbauer helped with Sanger sequencing of family THI26001 and critically revised the manuscript.

Michael A. Gonzalez performed exome sequencing in both families and critically revised the manuscript.

Yasar Zorlu recruited and examined family IHG25215 and critically revised the article.

Burcak Ozes performed sequencing and segregation analysis of variants in family IHG25215 and critically revised the manuscript.

Dagmar Timmann recruited and examined family IHG25215 and critically revised the manuscript.

Benjamin Bender acquired and analysed the MRIs of family THI26001 and critically revised the article.

Günther Woehlke was involved in the analysis of the position of KIF1C mutations and participated in the drafting of the article.

Stephan Züchner was involved in the design of the study and critically revised the manuscript.

Ludger Schöls was involved in the design of the study and critically revised the article.

Rebecca Schüle was responsible for conception and design of the study, analysed and interpreted the exome sequencing data, supervised and coordinated the study, and drafted the article.

5. (Manuscript in preparation, planning to submit to Journal of Clinical Investigations) Caballero-Oteyza et al. RNA metabolism meets axonopathy: the HSP protein KIF1C binds RNA and ribosomal components (April 2016)

Andrés Caballero-Oteyza was responsible for conceptualization and design of the study. Experiments and analysis for: the identification and validation of KIF1C interacting partners, the study of KIF1C cellular distribution and KIF1C interactions, and the effect of KIF1C pathogenic mutation in interactions and distribution. Experiments and analysis for the study of KIF1C interaction with RNA and the identification and confirmation of transcripts bound to KIF1C. Experiments and analysis for the study of KIF1C interaction with ribosomes. Drafting of the manuscript.

Stephan Kotschote contributed to the experiments for the study of KIF1C interaction with RNA (iCLIP) and critically reviewed the manuscript.

Beibei Chen contributed to the analysis and interpretation of iCLIP data using PIPE-CLIP analysis tool; and critically revised the manuscript.

Jennifer Reichbauer contributed to the experiments for the study of KIF1C interaction with Ribosomes and critically reviewed the manuscript.

Angelos Skodras contributed to the data analysis for the study of KIF1C interaction with Ribosomes and critically reviewed the manuscript.

Alleene Strickland contributed to the analysis and processing of iCLIP data and critically revised the manuscript.

Adriana Rebelo contributed to the experiments for the study of KIF1C candidate interactors and critically revised the manuscript.

Günther Woehlke contributed critically reviewing the manuscript.

Ludger Schöls contributed to the project supervision and critically revised the article.

Stephan Züchner contributed critically reviewing the manuscript.

Michael Bonin contributed with iCLIP experiment supervision and critically revised the manuscript.

Rebecca Schüle contributed to the conceptualization, design and supervision of the study and to the analysis and interpretation of all experimental data. Performed pathway enrichment analysis of KIF1C transcripts. Critically revised the manuscript.

Papers & Manuscript

Alteration of Fatty-Acid-Metabolizing Enzymes Affects Mitochondrial Form and Function in Hereditary Spastic Paraplegia

Christelle Tesson,[1,2,3,4,26] Magdalena Nawara,[1,2,3,26] Mustafa A.M. Salih,[5,26] Rodrigue Rossignol,[6,26] Maha S. Zaki,[7] Mohammed Al Balwi,[8,9] Rebecca Schule,[10] Cyril Mignot,[11] Emilie Obre,[6] Ahmed Bouhouche,[12] Filippo M. Santorelli,[13] Christelle M. Durand,[6] Andrés Caballero Oteyza,[10] Khalid H. El-Hachimi,[1,2,3,4] Abdulmajeed Al Drees,[14] Naima Bouslam,[12] Foudil Lamari,[15] Salah A. Elmalik,[14] Mohammad M. Kabiraj,[16] Mohammed Z. Seidahmed,[17] Typhaine Esteves,[1,2,3] Marion Gaussen,[1,2,3] Marie-Lorraine Monin,[1,2,3] Gabor Gyapay,[18] Doris Lechner,[19] Michael Gonzalez,[20] Christel Depienne,[1,2,3,11] Fanny Mochel,[1,2,3,11] Julie Lavie,[6] Ludger Schols,[10,21] Didier Lacombe,[6,22] Mohamed Yahyaoui,[12] Ibrahim Al Abdulkareem,[9] Stephan Zuchner,[20] Atsushi Yamashita,[23] Ali Benomar,[12,24] Cyril Goizet,[6,22] Alexandra Durr,[1,2,3,11] Joseph G. Gleeson,[25] Frederic Darios,[1,2,3] Alexis Brice,[1,2,3,11,*] and Giovanni Stevanin[1,2,3,4,11,*]

Hereditary spastic paraplegia (HSP) is considered one of the most heterogeneous groups of neurological disorders, both clinically and genetically. The disease comprises pure and complex forms that clinically include slowly progressive lower-limb spasticity resulting from degeneration of the corticospinal tract. At least 48 loci accounting for these diseases have been mapped to date, and mutations have been identified in 22 genes, most of which play a role in intracellular trafficking. Here, we identified mutations in two functionally related genes (*DDHD1* and *CYP2U1*) in individuals with autosomal-recessive forms of HSP by using either the classical positional cloning or a combination of whole-genome linkage mapping and next-generation sequencing. Interestingly, three subjects with *CYP2U1* mutations presented with a thin corpus callosum, white-matter abnormalities, and/or calcification of the basal ganglia. These genes code for two enzymes involved in fatty-acid metabolism, and we have demonstrated in human cells that the HSP pathophysiology includes alteration of mitochondrial architecture and bioenergetics with increased oxidative stress. Our combined results focus attention on lipid metabolism as a critical HSP pathway with a deleterious impact on mitochondrial bioenergetic function.

Introduction

Hereditary spastic paraplegia (HSP), also known as Strümpell-Lorrain disease, is recognized as one of the most clinically and genetically heterogeneous groups of inherited neurodegenerative disorders. These disorders are mainly characterized by slowly progressive lower-limb spasticity that worsens over time. The symptoms are the consequence of corticospinal-tract degeneration.[1–3] Affected subjects are clinically classified according to the absence (uncomplicated or pure HSP) or presence (complicated or complex HSP) of additional neurological or extraneurological signs. This clinical heterogeneity partially underlies the large genetic heterogeneity of this group of disorders; at least 48 loci have been mapped to date and account for all classical modes of inheritance.[4,5] So far, mutations have been identified in 22 genes,[5] most of which play a role in intracellular trafficking.[6–8]

Autosomal-recessive HSP (AR-HSP) is less common than the autosomal-dominant form, except in countries with a high rate of consanguinity.[9,10] It is more often associated with clinically complex phenotypes, but pure forms of the

[1]Unité 975, Institut National de la Santé et de la Recherche Médicale, 75013 Paris, France; [2]Unité Mixte de Recherche S975, Centre de Recherche de l'Institut du Cerveau et de la Moelle Épinière, Pitié-Salpêtrière Hospital, Université Pierre et Marie Curie (Paris 6), 75013 Paris, France; [3]Unité Mixte de Recherche 7225, Centre National de la Recherche Scientifique, 75013 Paris, France; [4]Laboratoire de Neurogénétique de l'Ecole Pratique des Hautes Etudes, 75013 Paris, France; [5]Division of Pediatric Neurology, College of Medicine, King Saud University, 11461 Riyadh, Saudi Arabia; [6]Equipe d'Accueil 4576, Laboratoire Maladies Rares: Génétique et Métabolisme, University Bordeaux Segalen, 33076 Bordeaux, France; [7]National Research Centre, 12311 Cairo, Egypt; [8]King Abdulaziz Medical City, 11426 Riyadh, Saudi Arabia; [9]King Abdullah International Medical Research Center, 11426 Riyadh, Saudi Arabia; [10]Department of Neurodegenerative Disease, Hertie Institute for Clinical Brain Research and Center for Neurology, 72076 Tuebingen, Germany; [11]Fédération de Génétique, Pitié-Salpêtrière Hospital, Assistance Publique-Hôpitaux de Paris, 75013 Paris, France; [12]Equipe de Recherche des Maladies Neurodégénératives, Faculté de Médecine et de Pharmacie de Rabat, Université Mohammed V Souissi, 6402 Rabat, Morocco; [13]Istituto di Ricovero e Cura a Carattere Scientifico Fondazione Stella Maris, Calambrone, 56018 Pisa, Italy; [14]Department of Physiology, College of Medicine, King Saud University, 11461 Riyadh, Saudi Arabia; [15]Service de Biochimie, Pitié-Salpêtrière Hospital, Assistance Publique-Hôpitaux de Paris, 75013 Paris, France; [16]Department of Neurosciences, Armed Forces Hospital, 11159 Riyadh, Saudi Arabia; [17]Department of Pediatrics, Security Forces Hospital, 11481 Riyadh, Saudi Arabia; [18]Genoscope, 91057 Evry, France; [19]Centre National de Génotypage, 91057 Evry, France; [20]Department of Human Genetics and Hussman Institute for Human Genomics, Miller School of Medicine, University of Miami, FL 33136, USA; [21]German Center of Neurodegenerative Diseases, 72076 Tuebingen, Germany; [22]Service de Génétique Médicale, Centre Hospitalier Universitaire de Bordeaux, 33076 Bordeaux, France; [23]Department of Life and Health Sciences, Faculty of Pharmaceutical Sciences, Teikyo University, Kaga 2-11-1, Itabashi-Ku, Tokyo 173-8605, Japan; [24]Faculté de Médecine et de Pharmacie de Rabat, Centre de Recherche en Épidemiologie Clinique et Essai Thérapeutique, Université Mohammed V Souissi, 6402 Rabat, Morocco; [25]Department of Neurosciences, Howard Hughes Medical Institute, University of California, San Diego, La Jolla, CA 92093-0665, USA
[26]These authors contributed equally to this work
*Correspondence: giovanni.stevanin@upmc.fr (G.S.), alexis.brice@upmc.fr (A.B.)
http://dx.doi.org/10.1016/j.ajhg.2012.11.001.

disease can be due to mutations in *SPG5/CYP7B1* (MIM 603711), *SPG7/PGN* (MIM 602783), and *SPG30/KIF1A* (MIM 601255) or can be linked to *SPG28* (MIM 609340).[11–15] Mutations in *SPG11/KIAA1840* (MIM 610844) account for ~20% of the autosomal-recessive (AR) forms,[16] but many genes remain to be discovered given that 60% of AR-HSP is still genetically unexplained.[5]

Here, we report the identification of causative mutations in two genes after the use of next-generation sequencing focused on all exons of the *SPG28* interval, as well as linkage mapping combined with systematic candidate-gene analysis in *SPG49*, identified in this study. These combined approaches enabled us to identify in individuals from three families four truncating mutations in *DDHD1* (MIM 614603), encoding for a phosphatidic-acid (PA)-preferring phospholipase A1. In subjects from five different families, we also found five mutations in *CYP2U1* (MIM 610670), encoding a P450 hydroxylase. We demonstrate in human cells that the pathophysiology of SPG28 and SPG49 includes alteration of mitochondrial architecture and bioenergetics with increased oxidative stress.

Subjects and Methods

Subjects

Ninety-nine index individuals from families affected by AR-HSP and without identified mutations in *SPG11*, *SPG5*, and *SPG7*, were included in this study and originated mainly from France, Italy, the Middle East, and North Africa. This study was approved by the local Bioethics Committee (approval number 03-12-07 from the Comité Consultatif pour la Protection des Personnes et la Recherche Biomédicale Paris-Necker to A. Durr and A. Brice). Written informed consent was signed by all index persons and by 39 additional participating members of the families before blood samples were collected for DNA extraction. All clinical evaluations included a full medical history and examination, estimation of the age of onset, observation of additional neurological signs, electroneuromyographic studies, and, when possible, brain MRI and/or computed-tomography (CT) scans.

Next-Generation Sequencing in Family FSP445

After exclusion of large genomic rearrangements in the *SPG28* linkage interval by comparative genomic hybridization (CGH) in subjects FSP445-V.3 and FSP445-V.1 by chromosome-14-specific 385K NimbleGen arrays (data not shown), targeted enrichment and next-generation sequencing were performed on the DNA of individual FSP445-V.3 from the original SPG28-affected family.[11] Enrichment of all 723 exons in chr14: 49,100,775–55,305,189 was performed by hybridization of shotgun fragment libraries to a custom Roche NimbleGen microarray according to the manufacturer's recommendations. Three micrograms of amplified enriched DNA was used as input for massively parallel sequencing on a Roche 454-GS-FLX sequencer with Titanium reagents. Sequence data were then aligned with hg18 human genome as a reference. In total, 285,704 reads were obtained with an average length of 399 bp; 283,483 (99%) of those reads could be mapped, and 68% of them were on target. From the total of 723 enriched regions, 689 (95%) were covered entirely, and 99% of targeted bases were covered at least 10× (95% of all captured exons were covered entirely). The real coverage of enriched regions was 80×. Variants with fewer than three reads or accounting for less than 25% of all reads were excluded from the analysis. A total of 1,062 variations were identified. We excluded known validated SNPs present in dbSNP and the HapMap database. As expected, 88 of the remaining 239 variants were homozygous in this disease: 17 were intergenic, 63 were intronic, and 8, including 2 exonic variants, were in the mRNA.

Genome-wide Scan in Family FSP719

Exclusion of linkage to some of the most common AR-HSP-associated loci (*SPG5*, *SPG15* [MIM 270700], *SPG24* [MIM 607584], *SPG28*, *SPG30*, and *SPG32* [MIM 611252]) and of mutations in *SPG7* and *SPG11* was performed prior to this study (data not shown).

A genome scan with 6,090 SNP markers (LINKAGE_V panel, Illumina) covering all chromosomes was performed on family FSP719. Genotypes were generated with BeadStudio software (Illumina) and analyzed with MERLIN 1.0,[17] and all family members were considered. An AR inheritance, a penetrance of 95% without phenocopy, a disease allele frequency of 0.00001, equal allele frequencies for each marker, and equal male-female recombination rates were considered.

Linked and uninformative regions were explored by genotyping of 47 additional microsatellite markers in all family members. PCR amplicons were resolved on an ABI 3730 sequencer with the use of fluorescent primers, and the results were analyzed with GeneMapper 4 (Applied Biosystems). We manually constructed haplotypes by minimizing the number of recombination events. Genetic distances were taken from the MAP-O-MAT consortium.

Candidate-Gene Analysis

After exclusion of large genomic rearrangements by CGH in one person of SPG49-linked family FSP1015 (data not shown), all coding exons of genes in the *SPG49* candidate interval, including flanking splicing sites and at least 50 bp of intronic sequence on each side, were analyzed by direct sequencing (primers are available from the authors upon request) with BigDye Chemistry (Applied Biosystems). The sequence products were run on an ABI 3730 sequencer, and electrophoretic profiles were compared with the reference hg18 sequence with the use of SeqScape 2.5 (Applied Biosystems).

Mutation screening of *DDHD1* (RefSeq accession number NM_030637.2; hg19) and *CYP2U1* (RefSeq NM_183075.2; hg19) was performed in 96 index cases by classical Sanger sequencing (primers and PCR conditions are available upon request).

The effects of mutations and amino acid conservation in other species were analyzed with ALAMUT 2.2 (Interactive Biosoftware), PolyPhen-2, and MutationTaster.[18,19]

Rearrangement Analysis

Exon deletions or duplications in *CYP2U1* and *DDHD1* were explored by quantitative multiplex PCR of short fragments (QMPSF; primers and PCR conditions are available from the authors upon request) and analyzed with GeneMapper 4.

Investigation of Mitochondrial Energetics and Oxidative Stress

The mitochondrial respiratory rate was measured in lymphocytes and fibroblasts grown in RPMI 1640 medium and

DMEM, respectively, both of which contained 5 mM glucose and 2 mM glutamine (Glutamax) supplemented with 10% fetal bovine serum (PAA), 100 U/ml penicillin, and 100 U/ml of streptomycin. All experiments were performed with the same number of flask divisions in culture between cases and controls. For the lymphoblast cells (nonadherent), respiration was measured in real time on 1×10^6 cells per ml by polarography, with the use of the Hansatech Oxygraph system (Oxy 1, Hansatech), at 37°C in growth medium containing glucose and glutamine as energy substrates. We assessed respiratory coupling by adding oligomycin, a specific inhibitor of mitochondrial F_1F_0-ATPsynthase, in the cuvette of the oxygraph. The coupling of mitochondrial respiration with ADP phosphorylation was evaluated by the ratio of the routine respiratory rate to the rate measured in the presence of oligomycin (at steady state). Respiration was expressed as ngatom O per min per one million cells. Each cell culture was assayed at least three times (minimum of three different cultures according to the sample). For the fibroblasts, respiration was assayed on 96-well plates with the extracellular flux analyzer XF96 (Seahorse Bioscience).

The amount of mitochondria was compared on protein extracts from lymphoblastoid cell lines by immunoblot analysis according to standard procedures[20] and by labeling of actin C4 (Abcam, 1/1,000) and TOM20 (BD Biosciences, 1/1,000). The total cellular ATP content and the mitochondrial contribution to cellular ATP production were measured by bioluminescence with the ATP Roche assay Kit II on 1×10^6 cells as described elsewhere.[21] The concentration of reactive oxygen species was measured with the CMH2DCFDA fluorescent probe on a fluorometer (SAFAS) as previously reported.[21]

The measurement of respiratory-chain-enzyme activities was performed spectrophotometrically with standardized techniques as described previously.[22] In brief, fibroblasts and lymphoblasts of affected and control subjects were grown in DMEM or RPMI and harvested at 70% confluency. We performed cell- and mitochondrial-membrane disruption by freezing the cells in liquid nitrogen, thawing them at room temperature, and subsequent sonication. Total protein content was measured with the bicinchoninic acid assay, and maximal activities of respiratory-chain complex I (NADH: ubiquinone oxidoreductase), complex II (succinate dehydrogenase), complex III (ubiquinol cytochrome c reductase), and complex IV (cytochrome c oxydase) were assayed at 30°C and expressed as nmol/min/mg of protein. Mitochondrial transmembrane electric potential ($\Delta\psi$) was measured on a fluorometer (SAFAS Xenius) with the potentiometric dye tetramethylrhodamine methyl esther (TMRM) obtained from Invitrogen as previously detailed.[23]

mRNA-Expression Analysis

Total RNA was extracted from various tissues and different development stages of four wild-type c57bl6 mice with the RNeasy Mini kit (QIAGEN) and was used for generating cDNA with the Superscript III First-Strand Synthesis SuperMix for quantitative RT-PCR (Invitrogen). Real-time quantitative expression analysis of *DDHD1*, *CYP2U1*, and *RAD51* (control [MIM 179617]) was performed on a Roche LC480-1536 with QIAGEN Quantitect primer assays in triplicate. Expression levels relative to *PGK1* (MIM 311800) or *PP1A*, used as reference genes, were determined with qbase Plus software (Biogazelle) and were then compared with the Pearson test.

In lymphoblasts from individuals FSP445-4 and FSP445-6, we analyzed the effect on mRNA splicing of a variant affecting the last codon of exon 7 of *DDHD1* and predicted to alter splicing by the Splice Site Prediction by Neural Network. This was done on polyA+ RNA that was reversely transcribed with the 1st Strand cDNA Synthesis Kit (Roche) according to the manufacturer's random primer protocol and was followed by subcloning and direct sequencing of the PCR products with specific primers (available upon request).

Overexpression Analysis

HeLa cells used for transient transfection of the *CYP2U1* cDNA fused to green fluorescent protein (GFP) (Origen) were maintained in DMEM (Invitrogen) supplemented with fetal calf serum and antibiotics (100 UI/ml penicillin and 100 μg/ml streptomycin). Cells (10,000 cells per well) were transfected with the use of Fugene Xtreme Gene according to the manufacturer's instructions (Promega). After 48 hr, cells were fixed with 4% paraformaldehyde, washed, permeabilized with 0.25% Triton/PBS, blocked for 1 hr with 10% normal goat serum (NGS) before being incubated for 1 hr with primary antibodies at room temperature in 3% NGS/PBS, and then washed in PBS and incubated for 45 min with secondary antibodies in 3% NGS/PBS. Cultures were mounted with Vectashield HardSet Mounting Medium (Eurobio) or counterstained with DAPI (1 μg/ml, Sigma) and mounted with Fluoromount-G (Southern Biotech). Immunocytochemistry was performed with the following primary antibodies: rabbit anti-SDHA (Abcam), anti-Calregulin (Santa Cruz Biotechnology), and mouse anti-FLAG (Sigma). Secondary antibodies were alexa-fluor 568 and 647 (Invitrogen) anti-mouse and anti-rabbit. Images of CYP2U1 overexpression were acquired with a Zeiss VivaTome microscope with a 60× objective. AxioVision software (Zeiss) was used for analyzing one stack for visualizing the colocalization. For quantitative colocalization analysis of CYP2U1 with mitochondria or endoplasmic reticulum (ER), all images were processed identically with MBF Image J software and were quantified with Intensity Correlation Analysis plug-in (ICA) as defined elsewhere.[24] For each stack, similar background signal was subtracted, and images were analyzed as a z-series projection taken in intervals 0.2 mm deep. Two coefficients were calculated for each cell: (1) Rr is the Pearson's correlation coefficient and ranges from −1 to +1 (a value of 1 represents perfect correlation, −1 represents perfect exclusion, and 0 represents random localization) and (2) ICQ is the intensity correlation quotient in which colocalization is defined as the synchronous increase or decrease in fluorescence intensities.[24,25] The ICQ is based on the nonparametric sign-test analysis of the PDM (product of the differences from the mean) values and is equal to the ratio of the number of positive PDM values to the total number of pixel values. The ICQ values are distributed between −0.5 and +0.5 (−0.5 represents a random staining, and +0.5 represents perfect overlap). Each experiment was performed on three independent cells preparations, and 25–30 cells were quantified for each condition.

Fibroblasts were transfected with a pCMV/mito/GFP vector (Invitrogen) in which the Myc epitope was deleted[26] with the use of the Neon system (Invitrogen) according to the manufacturer's instructions. Twenty four hours after transfection, live cells were observed on a Zeiss Axiovert 200 inverted video-microscope with a 63× oil objective. Metamorph 7.7.7.0 software was used for acquiring the image.

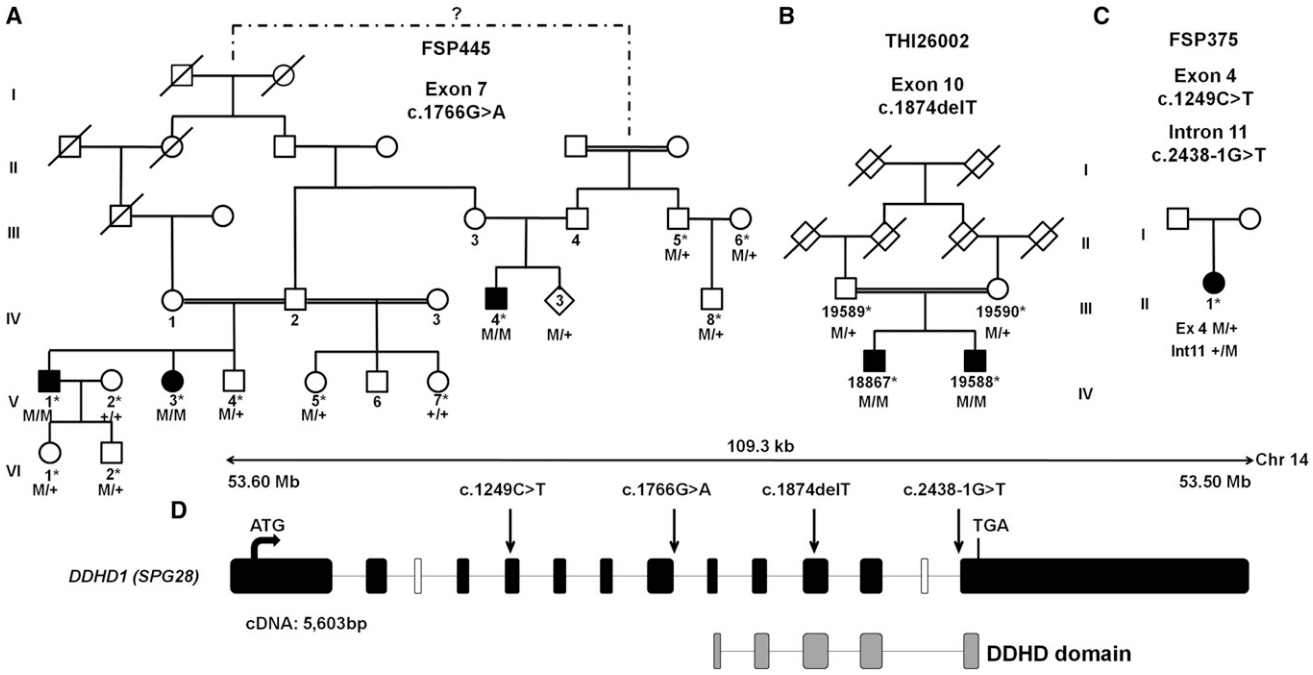

Figure 1. Mutations in *DDHD1*

(A–C) Family trees and segregation analysis of the mutations identified in families FSP445 (A), THI26002 (B) and FSP375 (C). Squares represent males, circles represent females, diamonds indicate anonymized subjects, filled symbols represent affected individuals, and a double line indicates consanguinity. The following abbreviations are used: M, mutation; +, wild-type; and *, sampled individuals. The electrophoregrams are shown in Figure S2.

(D) A graphical representation of *DDHD1* (RefSeq NM_030637.2) on chromosome 14 indicates the DDHD domain (gray boxes) and the location of the mutations (c.1249C>T [p.Gln417*], c.1766G>A [p.Arg589Gln; r.spl?], c.1874delT [p.Leu625*], and c.2438-1G>T [r.spl?]) (arrows). Black and white boxes represent coding and noncoding exons, respectively. The *DDHD1* transcript is 5,603 bp long and is composed of 12 exons that encode an 872 amino acid protein. There are three known isoforms of DDHD1; isoforms b and c are longer than isoform a because they include an alternate in-frame coding exon (white box). The sequence contains a lipase consensus domain and also includes a putative coiled-coil-forming region and a DDHD domain between residues 611 and 858 of isoform a; the four conserved residues that can form a metal binding site are seen in phosphoesterase domains. This domain is found in retinal degeneration B proteins, as well as in a family of probable phospholipases.

Results

Identification of Mutations in *SPG28/DDHD1*

We previously described a consanguineous Moroccan family (with AR inheritance) in which we mapped the disease locus, *SPG28*, to chromosome 14q.[11] We sequenced all exons of the *SPG28* interval in one affected subject (FSP445-V.3) from the original SPG28-affected kindred by using a custom Roche-NimbleGen Capture assay and massively parallel sequencing on a Roche 454-GS-FLX sequencer. From 239 variants identified, we focused our analysis on the two homozygous exonic variants not reported as polymorphisms: (1) the c.427G>T (p.Ala143Ser) transversion in *SAMD4A* (MIM 610747; RefSeq NM_015589.4), encoding SMAUG1, an RNA-binding protein involved in mRNA silencing and deadenylation in postsynaptic densities, and (2) the c.1766G>A (p.Arg589Gln) variant located in the last nucleotide of exon 7 of *DDHD1* (encoding an enzyme of lipid metabolism) and affecting correct *DDHD1* mRNA splicing (Figure 1A, Figures S1 and S2, and Table S1, available online). These two variants cosegregated with the disease and were absent in controls. The deleterious nature of the *DDHD1* mutation let us focus on this gene. Further screening of all *DDHD1* coding exons by Sanger sequencing and QMPSF in 96 index cases affected by HSP with an unknown genetic cause identified mutations absent in controls in two individuals (Figures 1B and 1C, Figure S2, and Table S1). One simplex French case (FSP375-II.1) harbored heterozygous mutations c.1249C>T (p.Gln417*) and c.2438-1G>T in exon 4 and intron 11, respectively. DNA of relatives or mRNA was not available, so we could not exclude that the mutations were in *cis*, although this is unlikely given their rarity (Table S1). One Turkish boy and his affected brother harbored the homozygous c.1874del (p.Leu625*) mutation, which was also present at the heterozygous state in their healthy parents.

Clinical data from the three additional SPG28-affected subjects identified in this study extended the clinical spectrum of this disease compared to the pure phenotype originally described.[11] When examined at 30 years of age, the two Turkish brothers showed progressive spastic gait (which had been developing since adolescence), and one had a cerebellar oculomotor disturbance with saccadic eye pursuit. No other signs were noticed, and brain and spine MRI, sensory-evoked potentials (tibial nerve and median nerve),

and nerve-conduction studies were normal. The French SPG28-affected woman, aged 62 years at her latest examination, had suffered since infancy from HSP with axonal neuropathy but had unremarkable spinal and brain MRI.

Mapping of an AR-HSP-Associated Locus, *SPG49*

A genome scan with the Illumina LINKAGE Mapping V SNP Set was performed in family FSP719, composed of two nuclear consanguineous kindreds from Saudi Arabia. Multipoint linkage analysis (Figure S3A) identified on chromosomes 4, 19, and X three genomic regions with uninformative multipoint LOD scores between 0 and +1; these regions were later excluded with the use of 23 additional markers (data not shown). A fourth region of 34 consecutive SNPs on chromosome 4 presented a significant multipoint LOD score of +3.97 between markers rs1528381 and rs1525760. Further genotyping of 24 additional microsatellite markers and haplotype reconstructions restricted the region and confirmed a 5.9 Mb (6.29 cM) region of homozygosity by descent between markers D4S3256 and D4S2309 in all four affected individuals of the family (Figure S4). A maximum and significant multipoint LOD score of +4.76 was then reached (Figure S3B). This locus was named *SPG49* according to the Human Genome Organization. A second Saudi Arabian AR-HSP-affected family was found to be linked to this locus with a multipoint LOD score of +2.4. Both families shared a portion of the same homozygous haplotype, suggesting a common ancestry and narrowing down the *SPG49* candidate interval to the 3.8 Mb (4.42 cM) between markers D4S3256 and D4S2940 (Figure S4).

Identification of Mutations in *SPG49/CYP2U1*

In all coding exons of the 23 genes assigned to the *SPG49* region, we identified a single *CYP2U1* variant, c.947A>T (p.Asp316Val), which segregated with the disease at the homozygous state in the two SPG49-affected families (Figure 2A and Figure S2) and was not detected in healthy controls (Table S1). This variant affected an amino acid highly conserved during evolution among orthologs of CYP2U1 (Figure 2B) but also among other cytochrome P450 proteins (data not shown), including CYP7B1 (SPG5).[15] The mutation was localized in the cytochrome P450 functional domain and was predicted to be damaging.[18,19] Sanger sequencing and QMPSF analysis of all exons of *CYP2U1* in 94 index cases affected by HSP with an undetermined genetic basis identified four mutations predicted to be damaging and absent in controls (Figures 2C–2E, Figure S2, and Table S1). A homozygous missense mutation affecting a conserved amino acid (c.1139A>G [p.Glu380Gly]) was detected in an Italian simplex case (ITAP9-II.1) with suspected consanguinity. A homozygous 13 bp deletion (in exon 1) leading to a frameshift (c.61_73del [p.Leu21Trpfs*19]) segregated with the disease in two Egyptian brothers (from family HSP1363). Finally, two heterozygous mutations (c.784T>C [p.Cys262Arg] and c.1462C>T [p.Arg488Trp]) segregated in *trans* in two siblings with Spanish and Vietnamese ancestry.

Phenotype Associated with the SPG49 Clinicogenetic Entity

The overall SPG49 phenotype (Table 1) was an early-onset (2.5 ± 2.5 SD years; range = birth to 8 years) spastic paraplegia frequently involving the upper limbs (7/11 cases) and rarely associated with dystonic postures (n = 2) and cognitive alterations (n = 3). Among eight tested subjects, all had normal conduction velocities of the median and peroneal nerves, but the facts that five of them had a slight reduction in the amplitude of compound muscle action potentials and that three of them had a reduction in the amplitude of sensory-nerve action potential indicate the presence of infraclinical axonal neuropathy, predominantly in the lower limbs (data not shown). On brain MRI, thinning of the corpus callosum (n = 1) and white-matter lesions (3/8) were observed but were not inaugural MRI features in two affected subjects (Figure S5). Interestingly, globus pallidus hypointensities were detected during follow-up analysis of two siblings and were confirmed as calcifications by CT scans; they were reminiscent of the familial idiopathic basal-ganglia calcification (Fahr syndrome) (see GeneReviews in Web Resources). Therefore, SPG49 can be added to the growing number of mixed forms (pure and complex) of HSP, such as SPG5 or SPG7.[12,13] The severity of symptoms varied widely among affected subjects, even in the same family, and independently of the nature of the mutation; two individuals (FSP719-V.5 and HSP1363-IV.4) never walked, and a third (FSP719-IV.3) was limited in his running capacities, although he had otherwise fully conserved autonomy at 30 years of age.

Expression Profiles of *CYP2U1* and *DDHD1* mRNA

DDHD1 and *CYP2U1* transcripts have been shown to be expressed in the brain.[27–29] To identify a possible relationship between these two genes, we explored their expression profiles in multiple CNS and non-CNS mouse tissues by quantitative RT-PCR. We observed that *DDHD1* and *CYP2U1* mRNA levels increased during development in all tested tissues, including the cerebral cortex, but not in peripheral tissues in the case of *DDHD1* (Figure S6). Moreover, we showed that their expression levels were significantly coregulated at the embryonic and adult stages in the CNS (Figure S6), but not in non-neuronal tissues, a result compatible with a concomitant need for the two proteins in the CNS.

Subcellular Localization of CYP2U1 and DDHD1 and Exploration of Mitochondrial Functions and Network Organization

We then investigated how these mutations affect cell physiology in HSP. At a subcellular level, DDHD1 fused with a FLAG tag displayed a diffuse distribution pattern almost exclusively in the cytosol (data not shown), but it has also been observed partially in microsomes and mitochondria.[30] Because of its PLA1 activity, DDHD1 must transiently

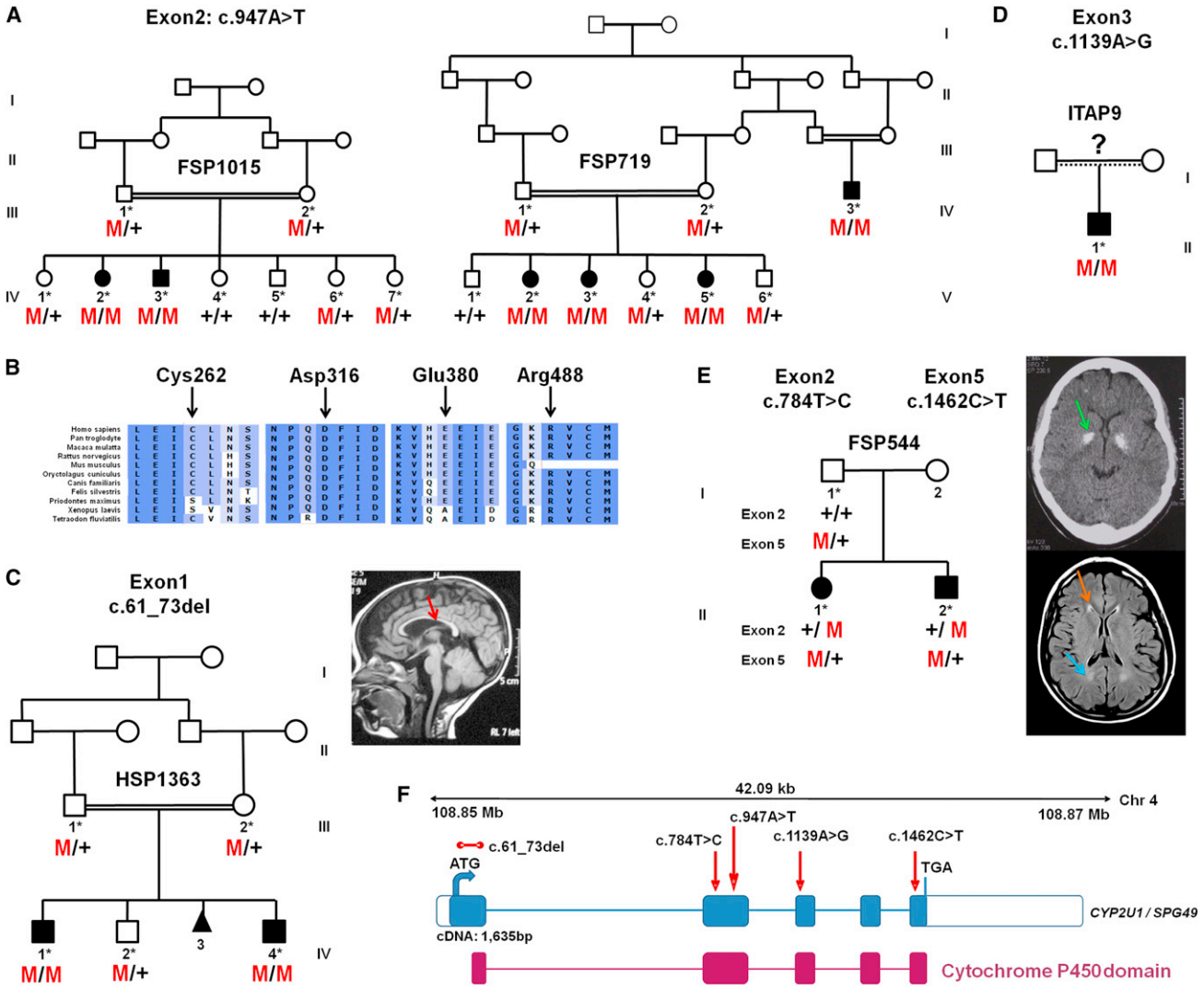

Figure 2. ***CYP2U1*** **Mutations in SPG49-Affected Subjects**

(A) Segregation analysis of the c.947A>T mutation in two Saudi Arabian families. Their corresponding electrophoregrams are in Figure S2.

(B) Conservation of the amino acids affected by missense variations with the use of ALAMUT software.

(C–E) Pedigrees and segregation of mutations in AR-HSP-affected families HSP1363 (C), ITAP9 (D), and FSP544 (E). A T1-weighted sagittal cerebral MRI from individual HSP1363-IV.4 shows a thin corpus callosum (C, red arrow). A CT scan of individual FSP544-III.1 (E, top view) shows bilateral globus pallidus calcifications (E, green arrow), and a brain MRI (E, bottom view) shows white-matter abnormalities (E, blue arrow), including the "ear of the lynx" aspect of frontal horns of the lateral ventricles (E, orange arrow).

(F) Schematic representation of *CYP2U1* (coding exons are represented by blue boxes). The locations of the identified mutations (c.61_73del [p.Leu21Trpfs*19], c.784T>C [p.Cys262Arg], c.947A>T [p.Asp316Val], c.1139A>G [p.Glu380Gly], and c.1462C>T [p.Arg488Trp]) are shown with red arrows, and the cytochrome P450 domain is indicated by red boxes. The five exons of *CYP2U1* (RefSeq NM_183075.2) cover 1,635 bp and encode a 544 amino acid protein with potential transmembrane domains and a heme binding site in the cytochrome P450 domain.

interact with membranes from the cytosolic pool to process its substrates. We also showed that CYP2U1 fused with enhanced GFP partially colocalized with ER and mitochondria (Figure S7), as previously reported.[31]

Given the partial mitochondrial localization of both proteins and the implication of this organelle in other HSPs,[12,32] we investigated mitochondrial functions in lymphoblasts. At steady state in growth medium, the mean routine respiration was significantly lower in SPG49 and SPG28 cells than in controls (Figure 3A; controls versus SPG49: $p = 0.053$, which is very close to the limit of significance; controls versus SPG28: $p = 0.011$). No cell death was observed (trypan-blue staining and count), suggesting that mitochondrial alterations were not a consequence of a reduction in cell viability. As expected from the respiratory data, total and mitochondrial ATP contents were significantly reduced in SPG49 and SPG28 lymphoblasts (Figure 3B). Furthermore, a concomitant increase of the concentration of cytosolic hydrogen peroxide as measured by CM-H_2DCFDA fluorescence (Figure 3C) was also observed in SPG49 and SPG28 cells when compared to controls. No major difference in mitochondrial content,

Table 1. Clinical Phenotypes in 11 SPG49-Affected Individuals

	SPG49-Affected Subject										
	FSP719-IV.3	**FSP719-V.2**	**FSP719-V.3**	**FSP719-V.5**	**FSP1015-IV.2**	**FSP1015-IV.3**	**HSP1363-IV.1**	**HSP1363-IV.4**	**ITAP9-II.1**	**FSP544-II-1**	**FSP544-II-2**
Gender	male	female	female	female	female	male	male	male	male	female	male
Age (years)	33	21	18	11	25	21	12	5	31	29	27
Duration of follow up (years)	3	12	13	10	12	13	2	2	4	9	9
Age at onset	3 years	5 years	1.5 years	8 months	birth	5 years	1.5 years	birth	8 years	13 months	16 months
Symptoms at onset	delayed walking, spastic gait	unsteadiness, spastic gait	delayed walking, unsteadiness	delayed walking, spasticity	delayed walking, toe walking	toe walking	unsteady gait, tip-toe walking	spasticity since birth	cannot run, frequent falls	delayed walking, spastic gait	spastic gait
Age at walking	3 years	1.5 years	1.5 years	never walked	6 years (after surgery)	1 year	2 years	never walked	2 years	delayed	normal
Cognitive delay or mental retardation	no	no	no	yes	no	no	no	no speech	no	yes	yes
Lower-limb hyperreflexia and positive extensor response (Babinski)	yes	yes	yes	yes	yes	yes	yes	yes	yes	yes	yes
Upper-limb hyperreflexia	no	no	no	yes	yes	yes	no	yes	yes	yes	yes
Dysarthria	no	no	no	no	no	no	no	no speech	no	yes, mild	yes, mild
Extrapyramidal signs	no	no	no	dystonia in upper limbs	no	no	no	dystonia in upper limbs	no	no	no
Other signs	no	no	no	no	no	no	no	no	no	maculopathy	no
Disability stage[a] (at age)	2 (30 years)	2 (21 years)	2 (18 years)	6 (11 years)	5 (25 years)	2 (21 years)	4	4	2 (28 years)	6 (16 years)	5
MRI cerebral (at age)	ND	normal (20 years)	normal (17 years)	normal (10 years)	ND	ND; CT normal	normal (5 years)	TCC, WMLs, mild cortical changes (2.5 years)	normal (28 years)	normal (14 years), then WMLs and globus pallidus hypointensities (26 years)	WMLs and globus pallidus hypointensities (26 years)
MRI of spine (at age)	ND	normal (20 years)	normal (17 years)	normal (10 years)	ND	normal	normal (4 years)	ND	normal (28 years)	normal	normal (19 years)
Nerve-conduction studies (at age)	ND	subclinical axonal neuropathy (21 years)	subclinical axonal neuropathy (18 years)	subclinical axonal neuropathy (10 years)	subclinical axonal neuropathy (25 years)	subclinical axonal neuropathy (21 years)	normal	normal	normal (28 years)	ND	ND

None of the affected persons presented with muscle wasting, dysphagia, cerebellar signs, superficial sensory loss, or auditory loss. Muscle biopsy in one subject was unremarkable. The following abbreviations are used: CT, computed tomography; ND, not done; TCC, thin corpus callosum; and WML, white-matter lesion.

[a]Disability scale: 1, minimal disability (slight stiffness of the legs); 2, mild disability (unable to run but full autonomy); 3, moderate disability in walking (reduced perimeter and frequent falls); 4, severe disability (unilateral assistance required for walking); 5, bilateral assistance required for walking; 6, wheelchair bound; and 7, bedridden.

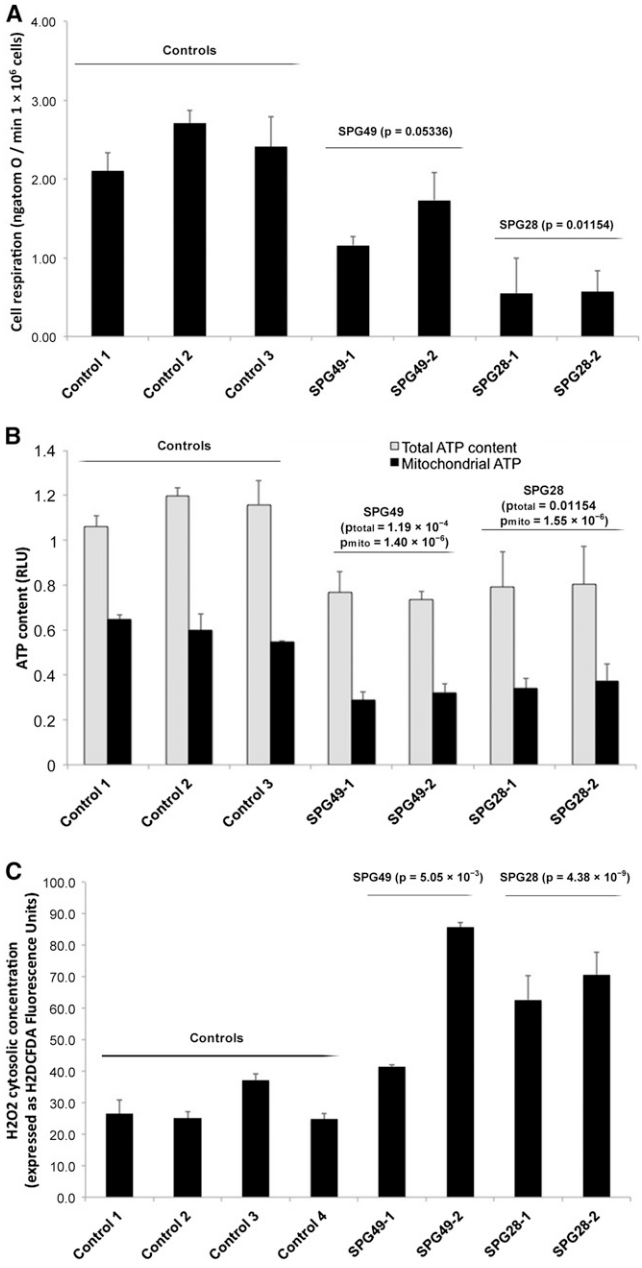

Figure 3. Mitochondrial Dysfunctions in Lymphoblasts from SPG28- and SPG49-Affected Individuals

(A) Mitochondrial respiration rate in SPG28-affected subjects (FSP445-V.3 [SPG28-1] and FSP445-V.1 [SPG28-2] aged 44 and 42 years, respectively, at sampling), SPG49-affected subjects (FSP719-V.3 [SPG49-1] and FSP1015-IV.3 [SPG49-2] aged 18 and 21 years, respectively, at sampling), and three control lymphoblastoid cell lines (aged 34, 37, and 40 years at sampling). The routine respiration data are shown. These measurements were taken after trypan-blue staining and a count for the exclusion of the presence of massive cell death.

(B) Total cellular (light gray bar) and mitochondrial (black bars) ATP content expressed as relative light unit (RLU) measured in SPG28, SPG49, and control lymphoblasts.

(C) H2DCFDA fluorescence gives a measure of the concentration of cytosolic hydrogen peroxide in control cells (white bar) and in *CYP2U1* (light gray bar) and *DDHD1* (black bars) mutant cells. The p values comparing mutant cells to control cells are indicated above each histogram (Student's t test). Error bars represent the SD.

measured by the comparison of the level of mitochondrial TOM20, was detected in lymphoblasts of affected cases (data not shown), suggesting that the observed reduction in mitochondrial energy fluxes results from a functional oxidative-phosphorylation-system alteration caused by mutations in *SPG28/DDHD1* and *SPG49/CYP2U1*.

Reduced oxygen consumption could be confirmed in skin fibroblasts of an SPG49-affected individual compared to controls (Figure S8A). Given that respiration originates from the activity of the respiratory chain and the consecutive buildup of an electrochemical gradient of protons, we measured those two parameters. As seen in Figure S8B, the transmembrane electric potential ($\Delta\psi$) measured with TMRM was 30% lower in the SPG49 fibroblasts than in the three controls (respective p values of 0.0011, 0.0010, and 0.0033). To take into account the nonspecific fluorescence due to TMRM (data not shown), we obtained the same results with the $\Delta\psi$ dissipating agent FCCP (uncoupler, p-trifluoromethoxy carbonyl cyanide phenyl hydrazone). However, the catalytic activities of each of the respiratory-chain complexes assayed in vitro were not altered in the SPG49 fibroblasts or in the lymphoblasts obtained from subjects with *SPG28* and *SPG49* mutations (Figure S9). This spectrophotometric assay of complexes I–IV was performed in experimental conditions of a so-called "isolated enzyme" with mechanical disruption of mitochondrial membranes and the addition of excess exogenous substrates. In contrast, mitochondrial respiration, ATP synthesis, and $\Delta\psi$ were measured in cells with intact mitochondrial membranes, so alteration in membrane properties could be responsible for the observed bioenergetic failure in cells of affected individuals. Interestingly, we observed structural abnormalities of the mitochondrial membrane, given that the mitochondrial network presented with unusual signs of tubule self-fusions in the SPG49 fibroblasts. These abnormalities included the presence of numerous (1) "donut-like" vesicles 800 nm in diameter within the mitochondrial tubules and (2) circular subnetworks 5 μm in diameter (Figure 4). These features were observed with either outer-membrane TOM20 labeling (Figure 4) or mitochondrial-matrix dyes such as mitotracker (data not shown) or mito-GFP (Figure S10). All together, our findings indicate mitochondrial-membrane-organization alteration associated with a reduction of energy production. Previous studies revealed that such remodeling of mitochondrial tubules could influence the internal diffusion of energy metabolites, the sequestration and conduction of the electric membrane potential ($\Delta\Psi$), the stability of the respirasome, the efficiency of oxidative phosphorylation, the diffusion of proteins, or the delivery of newly synthesized ATP to various cellular areas.[33]

Discussion

We have described a clinicogenetic entity, SPG49, associated with a wide range of phenotypes from pure to

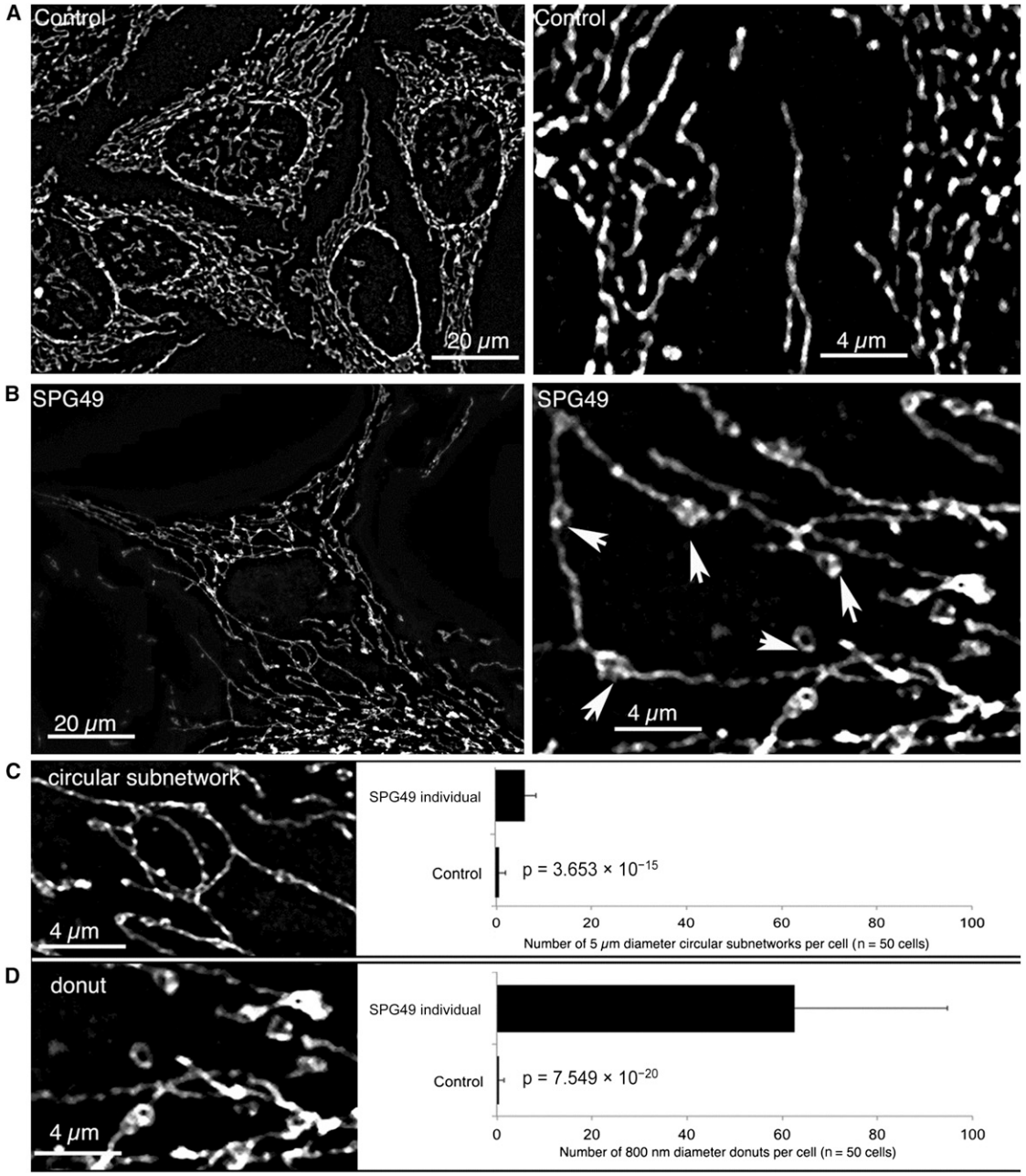

Figure 4. Abnormal Structures in the Mitochondrial Network of SPG49-Affected Skin Fibroblasts
Mitochondrial-network morphology was analyzed by confocal microscopy of skin fibroblasts obtained from control individuals (A) and from individual HSP1363-IV.1 (B). The images on the right are high magnifications (5× zoomed in) of the images on the left. The mitochondrial network was labeled by immunocytochemistry with specific antibodies directed against TOM20, an outer-membrane mitochondrial protein, and fluorescence confocal imaging on a Zeiss Vivatome microscope followed. Three-dimensional stacks were obtained, and the projection images are shown here. We observed two types of abnormal structures on the mitochondrial network of SPG49 cells: small "donut-like" vesicles (800 nm in diameter) suggestive of self-fused mitochondrial filaments (D) and larger circular subnetworks (5 μM in diameter) (C). Counting of these two types of abnormal structures was performed on 50 control cells and 50 cells from the tested subject (right panels). Mean values and p values (Student's t test) are shown, and error bars represent the SD.

complex forms causing a thin corpus callosum and mental impairment, as in SPG11 and SPG15,[34,35] or basal-ganglia calcification (see GeneReviews in Web Resources). Second, the identification of the causative mutations in SPG28- and SPG49-affected families highlights lipid metabolism as a critical pathway in HSP given that *CYP2U1* and *DDHD1* encode fatty-acid- and/or phospholipid-metabolizing enzymes.

DDHD1 was previously identified as a PA-preferring phospholipase A1 (PA-PLA1) but is also known to serve as a substrate for phosphatidylinositol to form 2-arachidonoyl lysophosphatidylinositol.[27,36] DDHD1 is

ubiquitously expressed in human tissues such as the brain and testis, but the physiological role of this enzyme has not been fully established. DDHD1 orthologs, p125 and DDHD2 (KIAA0725p), are involved in the maintenance of the ER and/or Golgi structures.[37,38] Therefore, DDHD1 might also be involved in similar functions in the maintenance of organelle membranes and intracellular trafficking.

CYP2U1 is one of the oldest identifiable vertebrate cytochrome P450 proteins implicated in ω- and ω-1 fatty-acid (C16–C22) hydroxylation.[28] In vitro, CYP2U1 is able to catalyze the hydroxylation of arachidonic acid and related long-chain fatty acids such as eicosapentaenoic (EPA) and docosahexaenoic (DHA) acids. Two known metabolites, 19- and 20-hydroxyeicosatetraenoic (HETE) acids, are local mediators of signal transduction.[28,39–41]

These two enzymes most likely act in the same pathway related to phospholipid degradation and fatty-acid metabolism, which is in agreement with (1) the coregulation of the expression of *DDHD1* and *CYP2U1*, specifically in the CNS, (2) the identification of mutations in both genes in affected subjects with relatively similar clinical presentations, and (3) similar consequences of these mutations for mitochondrial physiology. In addition, other enzymes involving the metabolism of fatty acids and phospholipids have been implicated in neurodegeneration.[8,42–44] PA and phosphatidylinositol, as well as the bioactive lipids resulting from their metabolism, modulate membrane properties and play a role in signal-transduction pathways.[45,46] Alterations of this pathway (Figure 5) in individuals with HSP could thus have various consequences leading to the observed phenotypes.

First, phospholipids and fatty acids can serve as precursors of a wide variety of bioactive lipid messengers[45,46] that exhibit hormone- or neurotransmitter-like activity through membrane receptors. Previously, one of the authors found that the major molecular species of phosphatidylinositol (PI), 1-stearoyl-2-arachidonoyl PI, was able to serve as substrate of DDHD1 to generate 2-arachidonoyl lysophosphatidylinositol, a potent agonist of GPR55,[47,48] considered a cannabinoid receptor,[49] like CB1 or CB2.[30,50] Arachinonic acid is metabolized to various eicosanoids through cyclooxygenase and lipoxygenase pathways. CYP2U1 is known to convert arachidonic acid into 19- and 20-HETE acids, which are known to regulate ion channels and neurotransmitter release.[28,51,52] In particular, 20-HETE acid has recently been reported as a potent activator of the transient receptor potential vanilloid 1 (TRPV1) channel. TRPV1 colocalizes with cannabinoid receptors CB1 and CB2 in brain and sensory neurons and seems to be gated by endocannabinoids, such as anandamide and N-arachidonoyl dopamine.[51,52] Although the bioactive lipids synthesized by DDHD1 and CYP2U1 have not been shown to act directly on mitochondria, their action on receptors might mediate their effect, as has been demonstrated for the CB1 cannabinoid receptors, which can regulate mitochondrial respiration and energy production.[53]

Second, mitochondrial-membrane lipid composition is critical for maintaining proper bioenergetic functions,[23,54] and the alteration of phospholipid metabolism has already been shown to impact mitochondrial functions and trigger secondary cellular dysfunction.[54–56] Indeed, maintenance of membrane composition, particularly of the mitochondrial membrane, should be critical for the functions of the long axons of the corticospinal tracts. The shape of the mitochondrion is also known to be linked to mitochondrial functions, including respiration, and the dysregulation of the mitochondria dynamics causes mitochondrial dysfunction.[57] PA, a fusogenic phospholipid at the mitochondrion surface, is postulated to regulate the fusion of mitochondria.[56] Overexpression of mitochondria phospholipase D (MitoPLD) causes continuous giant perinuclear mitochondria, but the reduced function of MitoPLD causes noncontiguous mitochondrial fragments. In the present study, the mutation of *DDHD1* (SPG28) was shown to cause mitochondrial dysfunction, including reduced respiration and ATP production. It is tempting to postulate that the associated mitochondrial bioenergetic dysfunction might result from the accumulation of PA in mitochondria given that DDHD1 exhibits PA-degrading activity (PA-PLA1). SPG28 fibroblasts were not available for exploring this finding, but the abnormal mitochondrial organization in SPG49 fibroblasts suggests that the pathway implicated in SPG28 and SPG49 has a role in this process. Mitochondrial abnormalities could also result from other, unknown, mechanisms because the link between altered mitochondrial morphogenesis and neuronal impairment has already been shown in other diseases, including other forms of HSP.[12,32,58–63] Furthermore, because these results on mitochondrial-network disorganization were derived from results from one single fibroblast culture, additional individuals with *CYP2U1* and *DDHD1* mutations are required for making firm conclusions.

Lastly, other mechanisms could also contribute to the disease. Indeed, in numerous conditions of mitochondrial respiratory impairment, increased reactive oxygen species (ROS) were observed, as in SPG28 and SPG49 cells. Such ROS overproduction could play a role in neuronal degeneration, as previously suggested for HSP pathophysiology.[64]

In conclusion, our identification of causative mutations in two genes demonstrates the importance of combining systematic gene mapping with large-scale sequencing for elucidating the molecular basis of HSP. Unraveling the role of different proteins involved in the same biological pathway might pave the way for common therapeutic possibilities for individuals with different gene mutations. Our results suggest that the membrane itself or membrane-derived mediators are very important for the neuronal functions in the corticospinal tracts.

The wide expression of *DDHD1* and *CYP2U1* suggests that it should be possible to explore metabolic

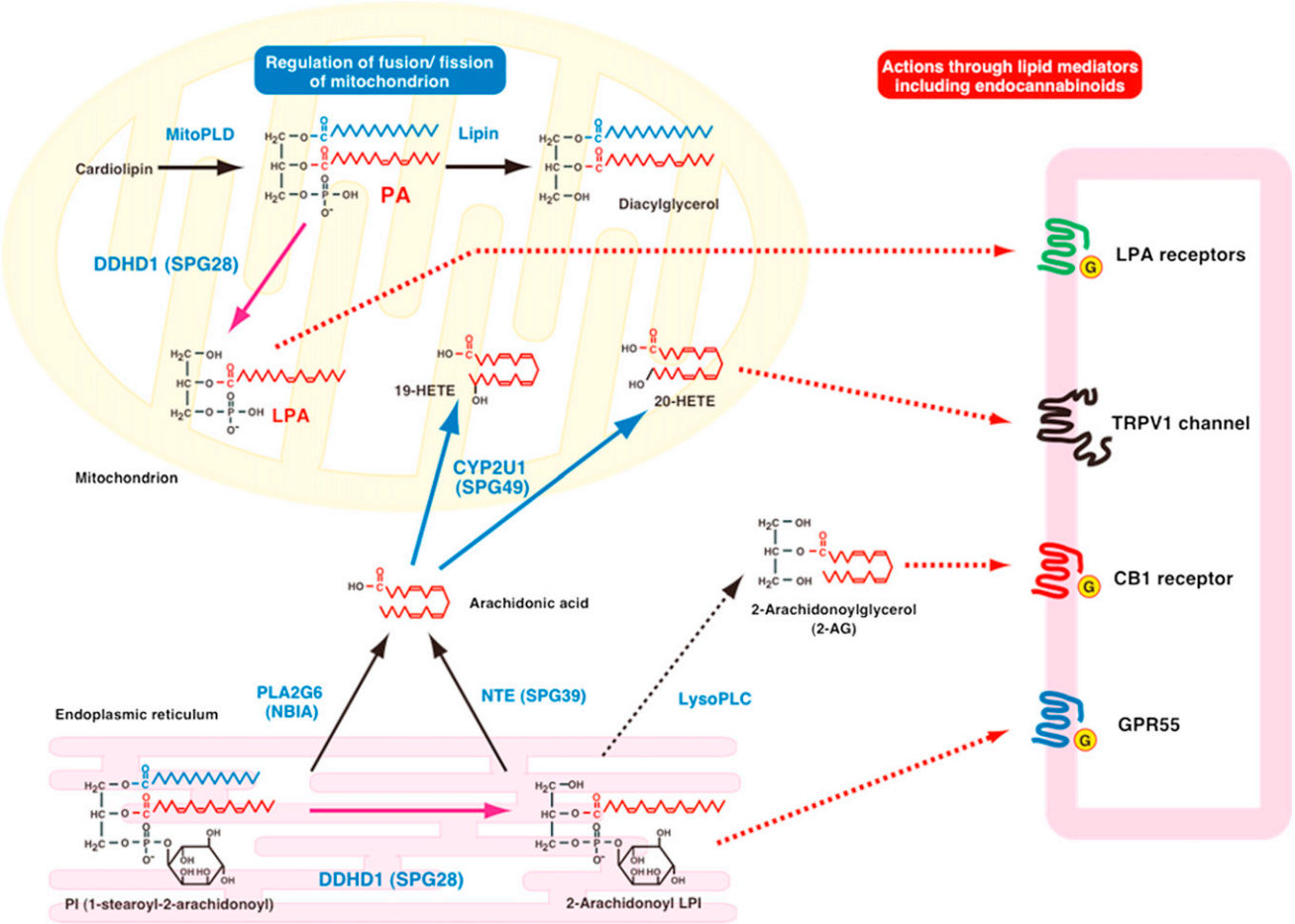

Figure 5. Schematic Representation of the Metabolic Connections between DDHD1 and CYP2U1 Enzymatic Activities
The content of PA on the surface of mitochondria is known to regulate mitochondrial fusion; PA is generated by mitochondrial phospholipase D (MitoPLD) and is further degraded by lipin PA phosphatase. DDHD1 was previously identified as PA-phospholipase A1 (PLA1). The action of DDHD1 might regulate the content of PA on the surface of mitochondria and then be involved in mitochondrial fusion. The *DDHD1* mutation causes reduced PA-PLA1 activity, and the resultant increased PA content on the surface of mitochondria might cause the impairment of mitochondrial fusion and lead to the dysfunction of mitochondria. In contrast, phosphatidylinositol (PI) serves as a substrate of DDHD1 to form 2-arachidonoyl lysophosphatidylinositol (LPI). 2-arachidonoyl LPI is known to act on GPR55, which is assumed to be a cannabinoid receptor. 2-arachidonoyl LPI might be hydrolyzed by lysophospholipase C into 2-arachidonoylglycerol, which is an endogenous agonist for cannabinoid receptors CB1 and CB2. Arachidonic acid can be released from PI through phospholipase A2, which includes PLA2G6 (iPLA2 and PNPLA9), and can also be generated from 2-arachidonoyl LPI by neuropathy target esterase (NTE, PNPLA6) given that this enzyme exhibits high lysophospholipase activity. Arachidonic acid is converted to various eicosanoids through the cyclooxygenase and lipoxygenase pathways. In addition, arachidonic acid is known to be the preferred substrate of CYP2U1 to form 19- or 20-HETE acids. Among these, 20-HETE acid is reported as a potent activator of the TRPV1 cation channel, which is a receptor of endocannabinoids, including anandamide and N-arachidonoyl dopamine. CYP2U1 can also metabolize esterified forms of arachidonic acid (EPA and DHA). These common arachidonic-acid metabolites can have effects on the endocannabinoid system through the CB1, GPR55, and TRPV1 receptors.

dysregulation in peripheral tissues, as in SPG5,[65] and develop biomarkers for potential treatment outcome. In particular, the probable implication of mitochondria in the pathophysiology of SPG28 and SPG49 could allow the development of innovative therapeutic strategies focused on organelle dynamics and bioenergetics, as well as ROS scavenging.

Supplemental Data

Supplemental Data include ten figures and one table and can be found with this article online at http://www.cell.com/AJHG/.

Acknowledgments

We are grateful to the affected family members and their relatives who participated in this study. We thank S. Rivaud-Pechoux and C. Gautier for their advice and D. Zelenika, E. Mundwiller, L. Orlando, D. Bouteiller, A. Rastetter, A. Méneret, the DNA and Cell Bank of the Centre de Recherche de l'Institut du Cerveau et de la Moelle Épinière, and the Plateforme d'Imagerie de la Pitié-Salpêtrière for their contribution. We also thank J.-P. Azulay, A. Lossos, and A. Cherif, who referred some of the affected individuals. This work was supported by the Association Strumpell-Lorrain (to the Spastic Paraplegia and Ataxia Network and C.G.), the Association contre les Maladies Mitochondriales (to C.G. and

R.R.), the Agence Nationale de la Recherche (to A.D., G.S., and C.G.), the Association Française contre les Myopathies (to C.G. and G.S.), the European Union E-Rare program (to A.Br.), the University of Tübingen (to R.S.), the Conseil Régional d'Aquitaine (to C.G.), and the Verum Foundation (to A.Br.). M.A.M.S. was supported by the College of Medicine Research Center (project 07-581) at King Saud University, Saudi Arabia. M.Al.B. and I.Al.A. were supported by the King Abdullah International Medical Research Center, Riyadh, Saudi Arabia. M.N. and C.T. were recipients of fellowships from the Neuroscience Research Pole in Ile de France and the French Ministry of Research, respectively. F.M.S. was supported by Fondazione Telethon project GGP10121A. This study also received funding from the program "Investissements d'avenir" ANR-10-IAIHU-06 (to the Institut du Cerveau et de la Moelle Épinière).

Received: June 28, 2012
Revised: September 4, 2012
Accepted: November 5, 2012
Published online: November 21, 2012

Web Resources

The URLs for data presented herein are as follows:

GeneReviews, Sobrido, M.J., Hopfer, S., and Geschwind, D.H. (2004). Familial Idiopathic Basal Ganglia Calcification, http://www.ncbi.nlm.nih.gov/books/NBK1421
MAP-O-MAT, http://compgen.rutgers.edu/mapomat/
Mutation Taster, http://www.mutationtaster.org/
Online Mendelian Ihneritance in Man (OMIM), http://www.omim.org
PolyPhen-2, http://genetics.bwh.harvard.edu/pph2/
Splice Site Prediction by Neural Network, http://www.fruitfly.org/seq_tools/splice.html

References

1. Harding, A.E. (1983). Classification of the hereditary ataxias and paraplegias. Lancet *1*, 1151–1155.
2. Tallaksen, C.M., Dürr, A., and Brice, A. (2001). Recent advances in hereditary spastic paraplegia. Curr. Opin. Neurol. *14*, 457–463.
3. Fink, J.K. (2003). Advances in the hereditary spastic paraplegias. Exp. Neurol. *184*(*Suppl 1*), S106–S110.
4. Schüle, R., and Schöls, L. (2011). Genetics of hereditary spastic paraplegias. Semin. Neurol. *31*, 484–493.
5. Finsterer, J., Löscher, W., Quasthoff, S., Wanschitz, J., Auer-Grumbach, M., and Stevanin, G. (2012). Hereditary spastic paraplegias with autosomal dominant, recessive, X-linked, or maternal trait of inheritance. J. Neurol. Sci. *318*, 1–18.
6. Salinas, S., Proukakis, C., Crosby, A., and Warner, T.T. (2008). Hereditary spastic paraplegia: Clinical features and pathogenetic mechanisms. Lancet Neurol. *7*, 1127–1138.
7. Stevanin, G., Ruberg, M., and Brice, A. (2008). Recent advances in the genetics of spastic paraplegias. Curr. Neurol. Neurosci. Rep. *8*, 198–210.
8. Blackstone, C., O'Kane, C.J., and Reid, E. (2011). Hereditary spastic paraplegias: Membrane traffic and the motor pathway. Nat. Rev. Neurosci. *12*, 31–42.
9. Coutinho, P., Barros, J., Zemmouri, R., Guimarães, J., Alves, C., Chorão, R., Lourenço, E., Ribeiro, P., Loureiro, J.L., Santos, J.V., et al. (1999). Clinical heterogeneity of autosomal recessive spastic paraplegias: Analysis of 106 patients in 46 families. Arch. Neurol. *56*, 943–949.
10. Boukhris, A., Stevanin, G., Feki, I., Denora, P., Elleuch, N., Miladi, M.I., Goizet, C., Truchetto, J., Belal, S., Brice, A., and Mhiri, C. (2009). Tunisian hereditary spastic paraplegias: Clinical variability supported by genetic heterogeneity. Clin. Genet. *75*, 527–536.
11. Bouslam, N., Benomar, A., Azzedine, H., Bouhouche, A., Namekawa, M., Klebe, S., Charon, C., Durr, A., Ruberg, M., Brice, A., et al. (2005). Mapping of a new form of pure autosomal recessive spastic paraplegia (SPG28). Ann. Neurol. *57*, 567–571.
12. Casari, G., De Fusco, M., Ciarmatori, S., Zeviani, M., Mora, M., Fernandez, P., De Michele, G., Filla, A., Cocozza, S., Marconi, R., et al. (1998). Spastic paraplegia and OXPHOS impairment caused by mutations in paraplegin, a nuclear-encoded mitochondrial metalloprotease. Cell *93*, 973–983.
13. Goizet, C., Boukhris, A., Durr, A., Beetz, C., Truchetto, J., Tesson, C., Tsaousidou, M., Forlani, S., Guyant-Maréchal, L., Fontaine, B., et al. (2009). CYP7B1 mutations in pure and complex forms of hereditary spastic paraplegia type 5. Brain *132*, 1589–1600.
14. Klebe, S., Lossos, A., Azzedine, H., Mundwiller, E., Sheffer, R., Gaussen, M., Marelli, C., Nawara, M., Carpentier, W., Meyer, V., et al. (2012). KIF1A missense mutations in SPG30, an autosomal recessive spastic paraplegia: Distinct phenotypes according to the nature of the mutations. Eur. J. Hum. Genet. *20*, 645–649.
15. Tsaousidou, M.K., Ouahchi, K., Warner, T.T., Yang, Y., Simpson, M.A., Laing, N.G., Wilkinson, P.A., Madrid, R.E., Patel, H., Hentati, F., et al. (2008). Sequence alterations within CYP7B1 implicate defective cholesterol homeostasis in motor-neuron degeneration. Am. J. Hum. Genet. *82*, 510–515.
16. Stevanin, G., Azzedine, H., Denora, P., Boukhris, A., Tazir, M., Lossos, A., Rosa, A.L., Lerer, I., Hamri, A., Alegria, P., et al.; SPATAX consortium. (2008). Mutations in SPG11 are frequent in autosomal recessive spastic paraplegia with thin corpus callosum, cognitive decline and lower motor neuron degeneration. Brain *131*, 772–784.
17. Abecasis, G.R., Cherny, S.S., Cookson, W.O., and Cardon, L.R. (2002). Merlin—Rapid analysis of dense genetic maps using sparse gene flow trees. Nat. Genet. *30*, 97–101.
18. Adzhubei, I.A., Schmidt, S., Peshkin, L., Ramensky, V.E., Gerasimova, A., Bork, P., Kondrashov, A.S., and Sunyaev, S.R. (2010). A method and server for predicting damaging missense mutations. Nat. Methods *7*, 248–249.
19. Schwarz, J.M., Rödelsperger, C., Schuelke, M., and Seelow, D. (2010). MutationTaster evaluates disease-causing potential of sequence alterations. Nat. Methods *7*, 575–576.
20. Murmu, R.P., Martin, E., Rastetter, A., Esteves, T., Muriel, M.-P., El Hachimi, K.H., Denora, P.S., Dauphin, A., Fernandez, J.C., Duyckaerts, C., et al. (2011). Cellular distribution and subcellular localization of spatacsin and spastizin, two proteins involved in hereditary spastic paraplegia. Mol. Cell. Neurosci. *47*, 191–202.
21. Jose, C., Hébert-Chatelain, E., Bellance, N., Larendra, A., Su, M., Nouette-Gaulain, K., and Rossignol, R. (2011). AICAR inhibits cancer cell growth and triggers cell-type distinct effects on OXPHOS biogenesis, oxidative stress and Akt activation. Biochim. Biophys. Acta *1807*, 707–718.

22. Benard, G., Faustin, B., Passerieux, E., Galinier, A., Rocher, C., Bellance, N., Delage, J.-P., Casteilla, L., Letellier, T., and Rossignol, R. (2006). Physiological diversity of mitochondrial oxidative phosphorylation. Am. J. Physiol. Cell Physiol. *291*, C1172–C1182.
23. Benard, G., Bellance, N., James, D., Parrone, P., Fernandez, H., Letellier, T., and Rossignol, R. (2007). Mitochondrial bioenergetics and structural network organization. J. Cell Sci. *120*, 838–848.
24. Li, Q., Lau, A., Morris, T.J., Guo, L., Fordyce, C.B., and Stanley, E.F. (2004). A syntaxin 1, Galpha(o), and N-type calcium channel complex at a presynaptic nerve terminal: analysis by quantitative immunocolocalization. J. Neurosci. *24*, 4070–4081.
25. Brown, M., Adyshev, D., Bindokas, V., Moitra, J., Garcia, J.G.N., and Dudek, S.M. (2010). Quantitative distribution and colocalization of non-muscle myosin light chain kinase isoforms and cortactin in human lung endothelium. Microvasc. Res. *80*, 75–88.
26. Darios, F., Lambeng, N., Troadec, J.-D., Michel, P.P., and Ruberg, M. (2003). Ceramide increases mitochondrial free calcium levels via caspase 8 and Bid: role in initiation of cell death. J. Neurochem. *84*, 643–654.
27. Higgs, H.N., Han, M.H., Johnson, G.E., and Glomset, J.A. (1998). Cloning of a phosphatidic acid-preferring phospholipase A1 from bovine testis. J. Biol. Chem. *273*, 5468–5477.
28. Chuang, S.S., Helvig, C., Taimi, M., Ramshaw, H.A., Collop, A.H., Amad, M., White, J.A., Petkovich, M., Jones, G., and Korczak, B. (2004). CYP2U1, a novel human thymus- and brain-specific cytochrome P450, catalyzes omega- and (omega-1)-hydroxylation of fatty acids. J. Biol. Chem. *279*, 6305–6314.
29. Karlgren, M., Backlund, M., Johansson, I., Oscarson, M., and Ingelman-Sundberg, M. (2004). Characterization and tissue distribution of a novel human cytochrome P450-CYP2U1. Biochem. Biophys. Res. Commun. *315*, 679–685.
30. Yamashita, A., Kumazawa, T., Koga, H., Suzuki, N., Oka, S., and Sugiura, T. (2010). Generation of lysophosphatidylinositol by DDHD domain containing 1 (DDHD1): Possible involvement of phospholipase D/phosphatidic acid in the activation of DDHD1. Biochim. Biophys. Acta *1801*, 711–720.
31. Dutheil, F., Dauchy, S., Diry, M., Sazdovitch, V., Cloarec, O., Mellottée, L., Bièche, I., Ingelman-Sundberg, M., Flinois, J.-P., de Waziers, I., et al. (2009). Xenobiotic-metabolizing enzymes and transporters in the normal human brain: Regional and cellular mapping as a basis for putative roles in cerebral function. Drug Metab. Dispos. *37*, 1528–1538.
32. Rugarli, E.I., and Langer, T. (2012). Mitochondrial quality control: A matter of life and death for neurons. EMBO J. *31*, 1336–1349.
33. Benard, G., and Rossignol, R. (2008). Mitochondrial fluidity matters. Focus on "Inherited complex I deficiency is associated with faster protein diffusion in the matrix of moving mitochondria". Am. J. Physiol. Cell Physiol. *294*, C1123.
34. Hanein, S., Martin, E., Boukhris, A., Byrne, P., Goizet, C., Hamri, A., Benomar, A., Lossos, A., Denora, P., Fernandez, J., et al. (2008). Identification of the SPG15 gene, encoding spastizin, as a frequent cause of complicated autosomal-recessive spastic paraplegia, including Kjellin syndrome. Am. J. Hum. Genet. *82*, 992–1002.
35. Stevanin, G., Santorelli, F.M., Azzedine, H., Coutinho, P., Chomilier, J., Denora, P.S., Martin, E., Ouvrard-Hernandez, A.-M., Tessa, A., Bouslam, N., et al. (2007). Mutations in SPG11, encoding spatacsin, are a major cause of spastic paraplegia with thin corpus callosum. Nat. Genet. *39*, 366–372.
36. Higgs, H.N., and Glomset, J.A. (1994). Identification of a phosphatidic acid-preferring phospholipase A1 from bovine brain and testis. Proc. Natl. Acad. Sci. USA *91*, 9574–9578.
37. Tani, K., Mizoguchi, T., Iwamatsu, A., Hatsuzawa, K., and Tagaya, M. (1999). p125 is a novel mammalian Sec23p-interacting protein with structural similarity to phospholipid-modifying proteins. J. Biol. Chem. *274*, 20505–20512.
38. Nakajima, K., Sonoda, H., Mizoguchi, T., Aoki, J., Arai, H., Nagahama, M., Tagaya, M., and Tani, K. (2002). A novel phospholipase A1 with sequence homology to a mammalian Sec23p-interacting protein, p125. J. Biol. Chem. *277*, 11329–11335.
39. Gebremedhin, D., Lange, A.R., Narayanan, J., Aebly, M.R., Jacobs, E.R., and Harder, D.R. (1998). Cat cerebral arterial smooth muscle cells express cytochrome P450 4A2 enzyme and produce the vasoconstrictor 20-HETE which enhances L-type Ca2+ current. J. Physiol. *507*, 771–781.
40. Carroll, M.A., and McGiff, J.C. (2000). A new class of lipid mediators: Cytochrome P450 arachidonate metabolites. Thorax *55* (*Suppl 2*), S13–S16.
41. Imig, J.D., Pham, B.T., LeBlanc, E.A., Reddy, K.M., Falck, J.R., and Inscho, E.W. (2000). Cytochrome P450 and cyclooxygenase metabolites contribute to the endothelin-1 afferent arteriolar vasoconstrictor and calcium responses. Hypertension *35*, 307–312.
42. Chang, P.-A., and Wu, Y.-J. (2010). Neuropathy target esterase: An essential enzyme for neural development and axonal maintenance. Int. J. Biochem. Cell Biol. *42*, 573–575.
43. Aldahmesh, M.A., Mohamed, J.Y., Alkuraya, H.S., Verma, I.C., Puri, R.D., Alaiya, A.A., Rizzo, W.B., and Alkuraya, F.S. (2011). Recessive mutations in ELOVL4 cause ichthyosis, intellectual disability, and spastic quadriplegia. Am. J. Hum. Genet. *89*, 745–750.
44. Gregory, A., and Hayflick, S.J. (2011). Genetics of neurodegeneration with brain iron accumulation. Curr. Neurol. Neurosci. Rep. *11*, 254–261.
45. Schaloske, R.H., and Dennis, E.A. (2006). The phospholipase A2 superfamily and its group numbering system. Biochim. Biophys. Acta *1761*, 1246–1259.
46. Kienesberger, P.C., Oberer, M., Lass, A., and Zechner, R. (2009). Mammalian patatin domain containing proteins: A family with diverse lipolytic activities involved in multiple biological functions. J. Lipid Res. Suppl. *50*, S63–S68.
47. Oka, S., Nakajima, K., Yamashita, A., Kishimoto, S., and Sugiura, T. (2007). Identification of GPR55 as a lysophosphatidylinositol receptor. Biochem. Biophys. Res. Commun. *362*, 928–934.
48. Oka, S., Toshida, T., Maruyama, K., Nakajima, K., Yamashita, A., and Sugiura, T. (2009). 2-Arachidonoyl-sn-glycero-3-phosphoinositol: A possible natural ligand for GPR55. J. Biochem. *145*, 13–20.
49. Oka, S., Ota, R., Shima, M., Yamashita, A., and Sugiura, T. (2010). GPR35 is a novel lysophosphatidic acid receptor. Biochem. Biophys. Res. Commun. *395*, 232–237.
50. Anavi-Goffer, S., Baillie, G., Irving, A.J., Gertsch, J., Greig, I.R., Pertwee, R.G., and Ross, R.A. (2012). Modulation of L-α-lysophosphatidylinositol/GPR55 mitogen-activated protein kinase (MAPK) signaling by cannabinoids. J. Biol. Chem. *287*, 91–104.

51. Rimmerman, N., Bradshaw, H.B., Basnet, A., Tan, B., Widlanski, T.S., and Walker, J.M. (2009). Microsomal omega-hydroxylated metabolites of N-arachidonoyl dopamine are active at recombinant human TRPV1 receptors. Prostaglandins Other Lipid Mediat. *88*, 10–17.
52. Wen, H., Östman, J., Bubb, K.J., Panayiotou, C., Priestley, J.V., Baker, M.D., and Ahluwalia, A. (2012). 20-Hydroxyeicosatetraenoic acid (20-HETE) is a novel activator of transient receptor potential vanilloid 1 (TRPV1) channel. J. Biol. Chem. *287*, 13868–13876.
53. Bénard, G., Massa, F., Puente, N., Lourenço, J., Bellocchio, L., Soria-Gómez, E., Matias, I., Delamarre, A., Metna-Laurent, M., Cannich, A., et al. (2012). Mitochondrial CB_1 receptors regulate neuronal energy metabolism. Nat. Neurosci. *15*, 558–564.
54. Steenbergen, R., Nanowski, T.S., Beigneux, A., Kulinski, A., Young, S.G., and Vance, J.E. (2005). Disruption of the phosphatidylserine decarboxylase gene in mice causes embryonic lethality and mitochondrial defects. J. Biol. Chem. *280*, 40032–40040.
55. Brandner, K., Mick, D.U., Frazier, A.E., Taylor, R.D., Meisinger, C., and Rehling, P. (2005). Taz1, an outer mitochondrial membrane protein, affects stability and assembly of inner membrane protein complexes: implications for Barth Syndrome. Mol. Biol. Cell *16*, 5202–5214.
56. Choi, S.-Y., Huang, P., Jenkins, G.M., Chan, D.C., Schiller, J., and Frohman, M.A. (2006). A common lipid links Mfn-mediated mitochondrial fusion and SNARE-regulated exocytosis. Nat. Cell Biol. *8*, 1255–1262.
57. Benard, G., and Karbowski, M. (2009). Mitochondrial fusion and division: Regulation and role in cell viability. Semin. Cell Dev. Biol. *20*, 365–374.
58. Niemann, A., Wagner, K.M., Ruegg, M., and Suter, U. (2009). GDAP1 mutations differ in their effects on mitochondrial dynamics and apoptosis depending on the mode of inheritance. Neurobiol. Dis. *36*, 509–520.
59. Chang, C.-R., Manlandro, C.M., Arnoult, D., Stadler, J., Posey, A.E., Hill, R.B., and Blackstone, C. (2010). A lethal de novo mutation in the middle domain of the dynamin-related GTPase Drp1 impairs higher order assembly and mitochondrial division. J. Biol. Chem. *285*, 32494–32503.
60. Goizet, C., Depienne, C., Benard, G., Boukhris, A., Mundwiller, E., Solé, G., Coupry, I., Pilliod, J., Martin-Négrier, M.-L., Fedirko, E., et al. (2011). REEP1 mutations in SPG31: frequency, mutational spectrum, and potential association with mitochondrial morpho-functional dysfunction. Hum. Mutat. *32*, 1118–1127.
61. Chevrollier, A., Cassereau, J., Ferré, M., Alban, J., Desquiret-Dumas, V., Gueguen, N., Amati-Bonneau, P., Procaccio, V., Bonneau, D., and Reynier, P. (2012). Standardized mitochondrial analysis gives new insights into mitochondrial dynamics and OPA1 function. Int. J. Biochem. Cell Biol. *44*, 980–988.
62. Girard, M., Larivière, R., Parfitt, D.A., Deane, E.C., Gaudet, R., Nossova, N., Blondeau, F., Prenosil, G., Vermeulen, E.G.M., Duchen, M.R., et al. (2012). Mitochondrial dysfunction and Purkinje cell loss in autosomal recessive spastic ataxia of Charlevoix-Saguenay (ARSACS). Proc. Natl. Acad. Sci. USA *109*, 1661–1666.
63. Misko, A.L., Sasaki, Y., Tuck, E., Milbrandt, J., and Baloh, R.H. (2012). Mitofusin2 mutations disrupt axonal mitochondrial positioning and promote axon degeneration. J. Neurosci. *32*, 4145–4155.
64. Gücüyener, K., Pinarli, F.G., Erbaş, D., Hasanoğlu, A., Serdaroğlu, A., and Topaloğlu, H. (2010). Is oxidative damage in operation in patients with hereditary spastic paraparesis? Brain Dev. *32*, 130–136.
65. Schüle, R., Siddique, T., Deng, H.-X., Yang, Y., Donkervoort, S., Hansson, M., Madrid, R.E., Siddique, N., Schöls, L., and Björkhem, I. (2010). Marked accumulation of 27-hydroxycholesterol in SPG5 patients with hereditary spastic paresis. J. Lipid Res. *51*, 819–823.

Loss of Function of Glucocerebrosidase GBA2 Is Responsible for Motor Neuron Defects in Hereditary Spastic Paraplegia

Elodie Martin,[1,2,3,4,19] Rebecca Schüle,[5,19] Katrien Smets,[6,7,8,19] Agnès Rastetter,[1,2,3,4] Amir Boukhris,[9,10] José L. Loureiro,[11,12] Michael A. Gonzalez,[13] Emeline Mundwiller,[1,2,3,14] Tine Deconinck,[6,8] Marc Wessner,[15] Ludmila Jornea,[1,2,3] Andrés Caballero Oteyza,[5] Alexandra Durr,[1,2,3,16] Jean-Jacques Martin,[8] Ludger Schöls,[5,17] Chokri Mhiri,[9] Foudil Lamari,[18] Stephan Züchner,[13] Peter De Jonghe,[6,7,8] Edor Kabashi,[1,2,3] Alexis Brice,[1,2,3,14,16,*] and Giovanni Stevanin[1,2,3,4,14,16,*]

Spastic paraplegia 46 refers to a locus mapped to chromosome 9 that accounts for a complicated autosomal-recessive form of hereditary spastic paraplegia (HSP). With next-generation sequencing in three independent families, we identified four different mutations in *GBA2* (three truncating variants and one missense variant), which were found to cosegregate with the disease and were absent in controls. *GBA2* encodes a microsomal nonlysosomal glucosylceramidase that catalyzes the conversion of glucosylceramide to free glucose and ceramide and the hydrolysis of bile acid 3-O-glucosides. The missense variant was also found at the homozygous state in a simplex subject in whom no residual glucocerebrosidase activity of GBA2 could be evidenced in blood cells, opening the way to a possible measurement of this enzyme activity in clinical practice. The overall phenotype was a complex HSP with mental impairment, cataract, and hypogonadism in males associated with various degrees of corpus callosum and cerebellar atrophy on brain imaging. Antisense morpholino oligonucleotides targeting the zebrafish *GBA2* orthologous gene led to abnormal motor behavior and axonal shortening/branching of motoneurons that were rescued by the human wild-type mRNA but not by applying the same mRNA containing the missense mutation. This study highlights the role of ceramide metabolism in HSP pathology.

Hereditary spastic paraplegias (HSPs) are heterogeneous inherited neurodegenerative disorders. Affected individuals suffer from pyramidal motor neuron dysfunction such as spasticity, brisk reflexes, and pyramidal weakness of the lower limbs primarily caused by dysfunction or degeneration of upper motor neurons.[1,2] These clinical symptoms are sometimes associated with additional neurological or extraneurological signs and structural abnormalities of the central nervous system (CNS) observed on brain magnetic resonance imaging (MRI), such as thin corpus callosum (TCC), cortical atrophy, and cerebellar atrophy. This clinical heterogeneity partially reflects the large genetic heterogeneity of this group of disorders with ~50 loci mapped to date and accounting for all modes of inheritance.[3]

We mapped *SPG46* to chromosome 9 (MIM 614409) in a consanguineous Tunisian family (TUN35) (Figure 1A) with autosomal-recessive (AR) HSP, mental impairment, cataract, and TCC.[4] We excluded the involvement of large genomic rearrangements in affected individual V.33 by comparative genomic hybridization (NimbleGen chromosome 9-specific 385K array, data not shown). We then sequenced all coding exons of the *SPG46* candidate interval (n = 1,727 exons and their flanking splice sites in 183 genes, including 1 kb of their UTRs) by targeted next-generation sequencing (custom NimbleGen capture and sequencing in a Roche 454-FLX) in affected subjects V.32 and V.33 (Table S1 available online). After exclusion of variants reported as validated polymorphisms in public (1000 Genomes, dbSNP) and local databases, a total of 52 homozygous variants remained common to both individuals, including 48 synonymous or intronic changes or variants in pseudogenes. In the absence of nonsense or intronic/exonic splice-site mutations, we focused our analysis on the four missense variants. Three of them cosegregated with the disease, were predicted to be damaging by various online software packages (PolyPhen-2, Mutation Tasting), and affected conserved amino acids. Two

[1]Unité Mixte de Recherche S975, Centre de Recherche de l'Institut du Cerveau et de la Moelle Epinière, Pitie-Salpêtrière Hospital, Université Pierre et Marie Curie (Paris 6), 75013 Paris, France; [2]Unité 975, Institut National de la Santé et de la Recherche Médicale, 75013 Paris, France; [3]Unité Mixte de Recherche 7225, Centre National de la Recherche Scientifique, 75013 Paris, France; [4]Laboratoire de Neurogénétique, Ecole Pratique des Hautes Etudes, Pitié-Salpêtrière Hospital, ICM building, 75013 Paris, France; [5]Department of Neurodegenerative Disease, Hertie-Institute for Clinical Brain Research and Center for Neurology, 72076 Tübingen, Germany; [6]Neurogenetics Group, Department of Molecular Genetics, VIB, University of Antwerp, 2610 Antwerp, Belgium; [7]Department of Neurology, Antwerp University Hospital, 2610 Antwerp, Belgium; [8]Neurogenetics Laboratory, Institute Born-Bunge, University of Antwerp, 2610 Antwerp, Belgium; [9]Service de Neurologie, Hôpital Universitaire Habib Bourguiba, 3029 Sfax, Tunisia; [10]Faculté de Médecine, Université de Sfax, 3029 Sfax, Tunisia; [11]UnIGENe and Centro de Genética Preditiva e Preventiva, Institute for Molecular and Cellular Biology, 4050 Porto, Portugal; [12]Serviço de Neurologia, Centro Hospitalar entre Douro e Vouga, 4520-211 Santa Maria da Feira, Portugal; [13]Department of Human Genetics and Hussman Institute for Human Genomics, Miller School of Medicine, University of Miami, Miami, FL 33136, USA; [14]Institut du Cerveau et de la Moelle épinière, Pitié-Salpêtrière Hospital, 75013 Paris, France; [15]Genoscope, 91057 Evry, France; [16]Fédération de Génétique, Pitié-Salpêtrière Hospital, Assistance Publique-Hôpitaux de Paris, 75013 Paris, France; [17]German Center of Neurodegenerative Diseases (DZNE), 72076 Tübingen, Germany; [18]Service de Biochimie, Pitié-Salpêtrière Hospital, Assistance Publique-Hôpitaux de Paris, 75013 Paris, France
[19]These authors contributed equally to this work
*Correspondence: alexis.brice@upmc.fr (A.B.), giovanni.stevanin@upmc.fr (G.S.)
http://dx.doi.org/10.1016/j.ajhg.2012.11.021.

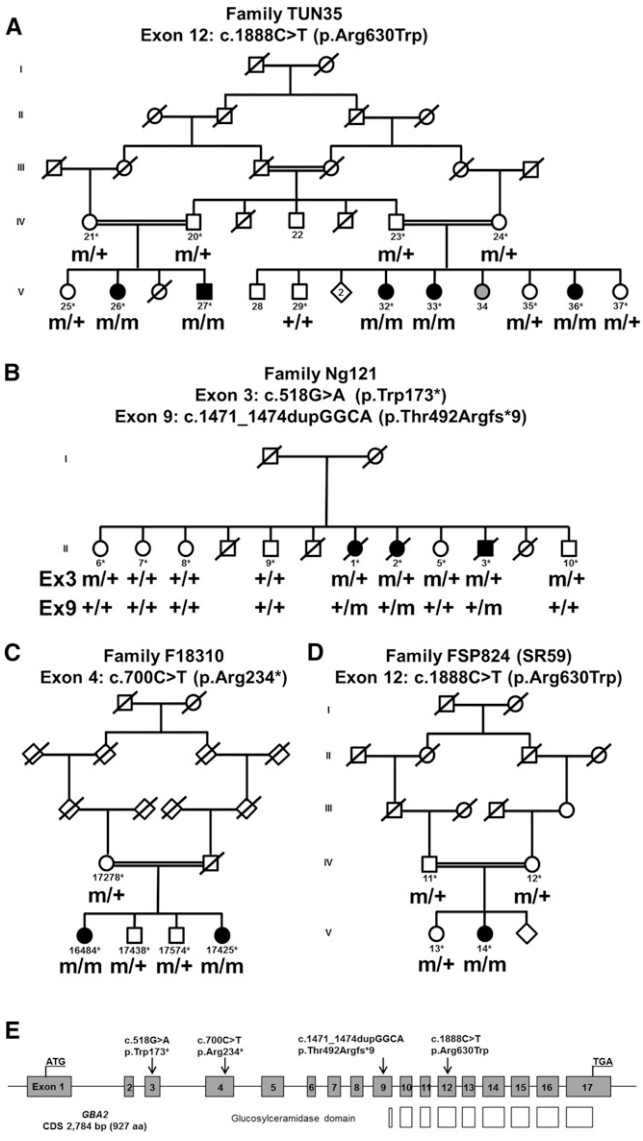

Figure 1. Mutations in *GBA2*

(A–D) Family trees and segregation analysis of the mutations identified in individuals of families TUN35 (A), Ng121 (B), F18310 (C), and FSP824 (D). The following symbols are used: squares for males, circles for females; filled symbols for affected individuals; gray symbols for subjects not clinically assessed; double line for consanguinity; m, mutation; +, wild-type; *, sampled individuals. Sequencing chromatograms of mutations c.518G>A (p.Trp173*), c.700C>T (p.Arg234*), c.1888C>T (p.Arg630Trp), and c.1471_1474dupGGCA (p.Thr492Argfs*9) are in Figure S1.

(E) Graphic representation of the exon organization of *GBA2* on chromosome 9 (gray boxes) and the location of the mutations (black arrows). The *GBA2* transcript is 3,611 bp long (CDS 2,784 bp) and is composed of 17 exons that encode a 927 amino acid protein. White boxes show the exons encoding the glucosylceramidase domain.

were excluded as the cause of the disease either because of the frequency in controls (c.88C>T [p.Arg30Trp], rs75679360, in *FAM166B* [RefSeq accession number NM_001164310.1], found in 8/182 chromosomes of North African controls, including at the homozygous state in one subject) or because the corresponding gene had previously been involved, when mutated, in another autosomal-recessive disease not overlapping with HSP (c.2909T>C [p.Val970Ala] in *NPR2* [MIM 108961, RefSeq NM_003995.3]). Indeed, we did not detect segregating variants in *NPR2* in 68 AR-HSP index subjects and 44 simplex individuals subjected to exome sequencing. The remaining variant, c.1888C>T (p.Arg630Trp), found in exon 12 of *GBA2* (MIM 609471, RefSeq NM_020944.2), segregated with the disease in the family (Figures 1A and S1) and was detected neither in 1,038 control chromosomes of 519 French, West Indian, Brazilian, and North African healthy subjects nor among 6,500 exomes on the Exome Variant Server. The variant affected an amino acid conserved from *Caenorhabditis elegans* and located in the six-hairpin-glucosidase-like domain of the enzyme (Figure 1E).

In parallel, exome capture via the SureSelect Human All Exon 50Mb kit (Agilent) followed by sequencing on a Hiseq 2000 sequencer (Illumina) was performed on the genomic DNA of two index HSP individuals of Belgian and Turkish ancestry, Ng121-II.2 and F18310-V.16484, respectively (Figures 1B and 1C). The Burrows-Wheeler algorithm[5] was used to align 100 bp length paired-end reads to the hg19 version of the human genome (Ensembl); variants were called with the Genome Analysis Toolkit (GATK) software package.[6,7] Data were then imported into the Genomes Management Application (GEM-app) database and its associated toolset for further analysis. On average, 110.4 million reads were produced per sample, 95% of which could be aligned to the targeted sequence. Mean coverage of the targeted sequence was 97-fold. On average, 87,591 single-nucleotide variations (SNV) and 8,876 indels were called per sample. Variants were filtered for occurrence in the normal population (minor allele frequency < 1% in dbSNP135 and at the Exome Variant Server), conservation (Genomic Evolutionary Rate Profiling [GERP] score > 3.5 or PhastCons score > 0.7), and quality (GATK QUAL score > 100, GATK GQ score > 75). Variants occurring and segregating in more than two unrelated families in GEM-app were removed. Compound heterozygous variants in eight genes, in the absence of homozygous variants, were identified in the index subject of family Ng121. In family F18310, 23 homozygous changes and compound heterozygous variants in three genes were identified in the sequenced subject. Among all variants detected in both families, three were truncating mutations and cosegregated with the disease (Figures 1B, 1C, and S1), all located in *GBA2*: c.700C>T (p.Arg234*) at the homozygous state in exon 4 of individual F18310-V.16484, and the heterozygous variants c.518G>A (p.Trp173*) and c.1471_1474dupGGCA (p.Thr492Argfs*9) in exons 3 and 9 of subject Ng121-II.2.

Direct Sanger sequencing (Table S2) of the 17 coding exons of *GBA2* in 95 index HSP subjects with an AR compatible inheritance (study approved by the Paris-Necker ethics committee; approval No. 03-12-07 granted to A.B. and A.D.), identified one simplex subject of Portuguese

ancestry (FSP824-V.14) harboring the same missense mutation (c.1888C>T [p.Arg630Trp]) as in family TUN35, although with a different associated haplotype (Figures 1D and S1). The mutation, which was homozygous, was detected at the heterozygous state in her parents.

The GBA2 protein encoded by *GBA2* is an enzyme of sphingolipid metabolism that is the source of a variety of mediators of cell signaling responses and of structural components of the plasma membrane involved in its dynamics.[8] GBA2 was initially identified as a microsomal bile acid β-glucosidase or β-glucosidase 2,[9,10] but it is also a nonlysosomal glucosylceramidase, a ubiquitous enzyme that catalyzes the conversion of glucosylceramide to free glucose and ceramide as well as the reverse reaction consisting in the transfer of glucose to different lipid substrates.[11,12] The primary catabolic pathway for glucosylceramide involves the lysosomal enzyme glucocerebrosidase GBA1 (MIM 606463), which is defective in persons with Gaucher disease, the most common inherited lysosomal storage disorder.[13] GBA1 is located in the lysosomal compartment and ceramides generated by this enzyme are degraded into sphingosine and fatty acids.[11,14] In contrast, GBA2 has been localized in the endoplasmic reticulum (ER)[12] and at the cell surface,[11] and ceramides formed by this enzyme are rapidly converted into sphingomyelin.[11,12,15] With a published protocol,[16,17] we assessed the GBA2 glucosylceramidase enzymatic activity in lymphoblasts and leukocytes of affected persons harboring the missense c.1888C>T (p.Arg630Trp) mutation in presence of specific inhibitors of the GBA1 enzyme, which is responsible for the vast majority of the glucosylceramidase activity.[18] No detectable GBA2 activity could be observed in the cells of subject FSP824-V.14 compared to healthy controls ($p = 0.001$, Figure S2), indicating a complete loss of function by the mutation. Complete loss of function was also evidenced in nontransformed leukocytes of individuals TUN35-V.27 and V.33 (data not shown).

The neurological phenotype of the 11 affected individuals was similar (Table S3). Onset occurred in infancy or childhood (range 1–16 years) with disturbances that progressed slowly to the need for a cane at 22–32 years and the need for a wheelchair at the age of 54–60. During the course of the disease, cerebellar ataxia and cataract were observed in all individuals. All affected subjects also had mild to moderate mental impairment; two explored during their 50s showed an IQ level equivalent to that of 6-year-old. In the oldest affected subjects, disease course was complicated by a memory deficit in their 60s and they died in a demented state aged 61, 63, and 72 years. The initial phenotypic description[4] was enriched by other frequently observed signs, such as hearing loss ($n = 3$) and axonal neuropathy evidenced at electroneuromyography (ENMG, $n = 5$) and sural nerve biopsy ($n = 3$). Brain MRI showed cerebral, cerebellar, and corpus callosum atrophy in all seven subjects tested, which seemed to worsen with disease duration (Figure 2). Interestingly, the two affected men presented a bilateral testicular hypotrophy in the absence of hormonal dysfunctions. Semen analysis of subject TUN35-V.27 revealed extremely severe spermatozoid head abnormalities with necrospermia and severe reduction in velocity (Table S4). Hormonal and genital exploration of affected woman FSP824-V.14 did not reveal abnormalities but woman Ng121-II.2 was reported to have few pubic hairs. The infertility highlighted in SPG46 males is reminiscent of the consequences of the pharmacological inhibition of glucosylceramidases in mice[19,20] or observed in the *Gba2* knockout (KO) mice in which an abnormal glucosylceramide accumulation in Sertoli cells is observed.[12] This infertility together with the neurological symptoms in our SPG46 subjects points to the critical role of this enzyme in multiple tissues, including testis and brain. Indeed, even if no overt neurological signs, liver dysfunction, or reduced viability were observed in the *Gba2* KO mice at 4 months of age, an

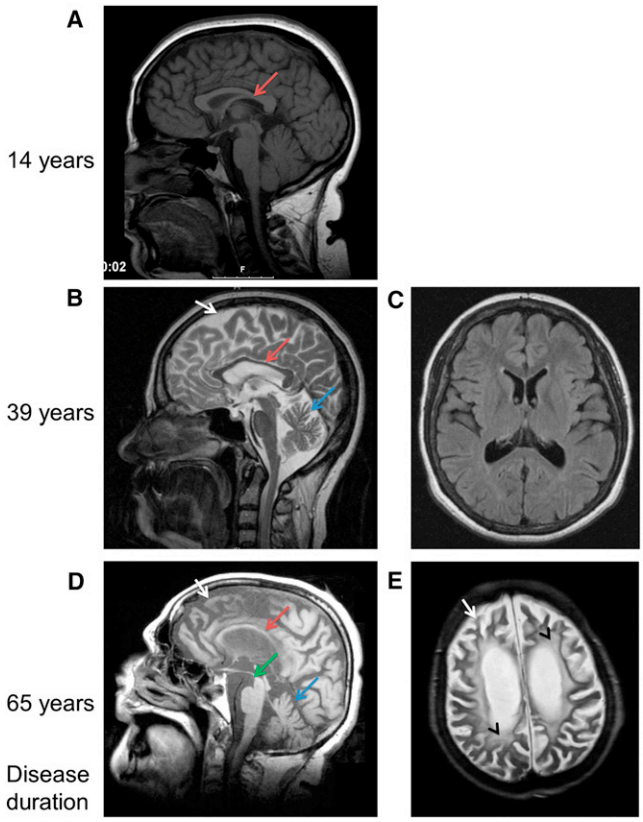

Figure 2. Brain Imaging in SPG46-Affected Individuals
(A) Sagittal brain magnetic resonance imaging (MRI) in subject FSP824-V.14 after 14 years of disease duration, showing a very slight thinning of the corpus callosum (red arrow).
(B and C) Sagittal and transversal flair MRI of individual F18310-V.16484 after 39 years of disease duration. The atrophy of the corpus callosum (B, red arrow) and of the cerebellar (B, blue arrow) and cerebral (B, white arrow) cortex are evident in the absence of relevant white matter disease (C).
(D and E) Sagittal T1- and transversal axial T2-weighted MRI images of subject Ng121-II.2 after 65 years of disease duration, showing severe atrophy of her cerebellum (D, blue arrow) and cerebrum (white arrows) with mesencephalon atrophy (D, hummingbird/colibri sign, green arrow) and pronounced white matter lesions (E, black arrowhead).

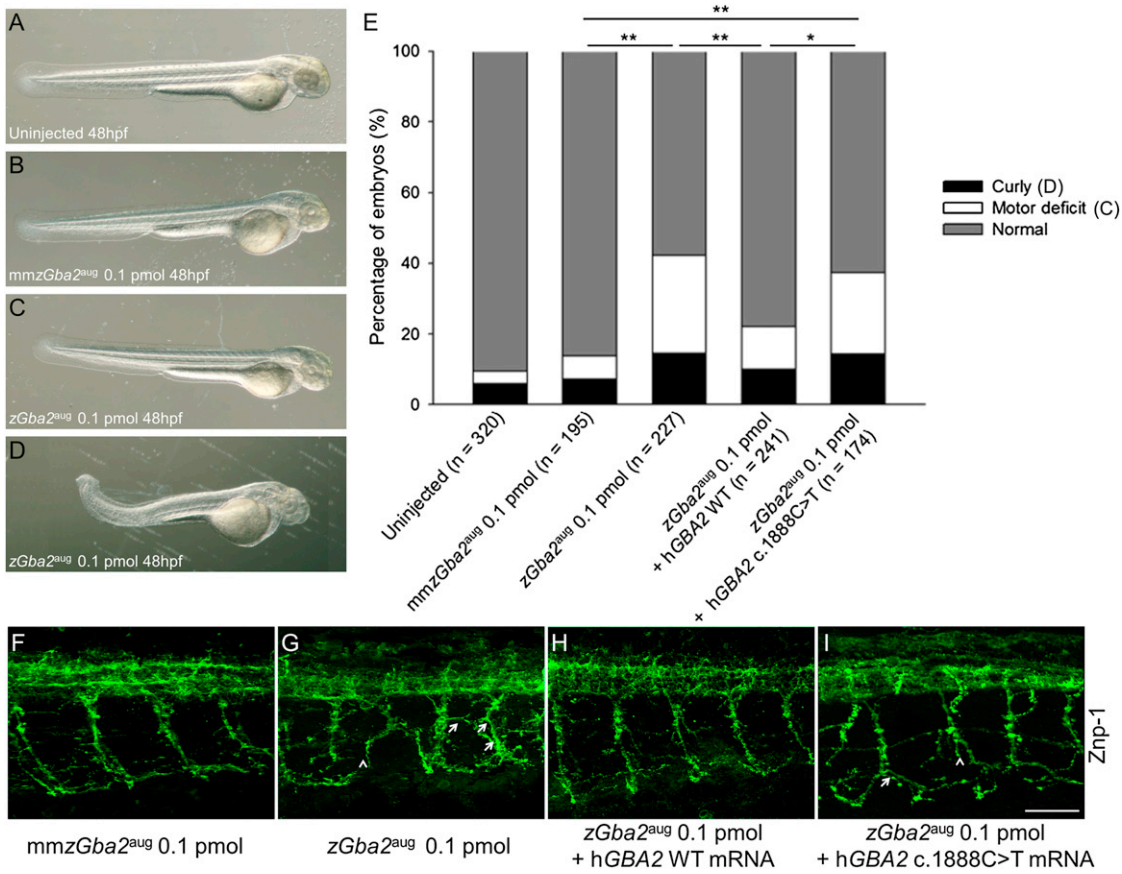

Figure 3. *zGba2* Inactivation Induces Morphological Phenotypes and Abnormal Motoneuronal Outgrowth in Zebrafish Larvae
(A–D) Whereas 48 hpf embryos injected with 0.1 pmol of the control AMO mm*zGba2*^{aug} (B) were phenotypically indistinguishable from noninjected controls (A), injection of 0.1 pmol *zGba2*^{aug} (D) impaired embryonic development of the caudal region, with some morphants showing shortened and/or twisted tails. Most of the injected morphants were normal looking even when they showed abnormal locomotion (C). Magnification ×44.
(E) Classification of morphant phenotypes observed after injection of AMOs with or without mRNA. The numbers of noninjected controls and different *zGba2* morphants are indicated in parentheses. *$p < 0.002$, **$p < 0.001$.
(F–I) Noninjected and *zGba2* morphants were analyzed for Znp-1 staining in spinal neurons. In contrast to noninjected larvae and to morphants injected with mm*zGba2* (F) or *zGba2*^{aug} + *hGBA2* WT mRNA (H), morphants injected with the *zGba2*^{aug} AMO in presence (I) or absence (G) of the mutated c.1888C>T RNA showed dramatically impaired axonal outgrowth leading to truncated axons (arrowheads). Axon trajectories are disturbed; ectopic and aberrant motor axon branches can be seen (arrows). Scale bar represents 50 μm.

accumulation of glycolipid species in the brain, liver, and testis was observed by mass spectrometry.[12] Longer times may be required in mouse as shown in other HSP mouse models in which signs are very subtle during the first months of life.[21,22] The neurological phenotype may also be obscured by the different structure of corticospinal tracts in mice or by compensation by other GBA enzymes early during development. Such compensation in *GBA1* mutated individuals by GBA2 activity has been shown and may explain the absence of notable glucosylceramide accumulation in some Gaucher disease subjects.[17] The reverse situation was not true because, in our study, no difference in GBA1 activity could be observed between lymphoblasts of the Portuguese subject and five controls (data not shown). This compensation may, however, differ between tissues and between different species.[20]

To validate the functional phenotype of the *GBA2* mutations in vivo, and in particular in the CNS, we used the zebrafish model and antisense morpholino oligonucleotide (AMO) technology to knock down the unique *GBA2* ortholog (*zGba2;* RefSeq NM_ENSDARG00000061472) by using classical methodologies.[23] To inactivate *zGba2*, we used an AMO targeting the initiation codon of the mRNA (*zGba2*^{aug}). As a control for our results, we designed a mismatch *zGba2*^{aug} AMO, mm*zGba2*^{aug}, comprising five mismatched bases, whose injection did not significantly lead to the appearance of phenotypes in injected embryos compared to uninjected ones ($p > 0.05$). We determined that microinjection of 0.1 pmol of *zGba2*^{aug} did not cause significant lethality of injected embryos compared to uninjected ($p > 0.05$) or mm*zGba2*^{aug}-injected ($p > 0.05$) embryos. This AMO dose induced a curly tail phenotype in 12.5% of morphants (Figures 3D and 3E) although 73.8% had no visible phenotype (Figure 3C). To further characterize the phenotype of normal-looking embryos (Figure 3C), we assessed their motor behavior by

performing a touch-response test on 2 day postfertilization morphants (Figure S3). We clearly observed that a substantial proportion of the normal-looking *zGba2*^{aug}-injected morphants showed significant motility defects (24%), characterized by slower movements and shorter touch-induced escape distances, when compared to control embryos injected with mm*zGba2*^{aug} (5.6%, $p < 0.001$) (Figure 3E). We next investigated the conservation of the GBA2 protein functions between human and zebrafish by coinjecting *zGba2*^{aug} with the wild-type (WT) human *GBA2* mRNA. When double injected, the number of normal-looking morphants with no locomotor impairment increased significantly (68.4% versus 49.8%) compared to *zGba2*^{aug}-injected larvae (Figure 3E, $p < 0.001$), suggesting that, in zebrafish, human *GBA2* mRNA can compensate, at least partially, for the loss of endogenous zebrafish mRNA. Indeed, the orthologous genes have a 65.8% identity and an 86.5% similarity. In contrast, no significant difference ($p > 0.05$) was observed after the coinjection of the *zGba2*^{aug} AMO with the human *GBA2* mRNA containing the c.1888C>T missense mutation (Figures 3E and 3S), meaning that the mutated mRNA failed to compensate the zebrafish mRNA decrease. Injection of WT or mutant mRNA alone, without morpholinos, did not lead to a curly-tail or a locomotor phenotype and did not influence lethality in embryos compared to mm*zGba2*^{aug}-injected control embryos ($p > 0.05$). Histochemical analyses were then performed on *zGba2*^{aug}-injected morphant embryos showing a motor phenotype without visible anomalies. The Znp-1 antibody, which labels the synaptic protein synaptotagmin 2 in motor neuron axons,[24] showed abnormal development of the spinal motoneurons, observed at mid-distance between head and tail (Figure 3G). We observed and evaluated the morphology of motor neuron axons in embryos injected with *zGba2*^{aug}, which appeared to be shorter and presented with more terminal branches in contrast to the proper axonal outgrowth observed in embryos injected with the mm*zGba2*^{aug} control (Table S5, $p < 0.00001$). This abnormal outgrowth was totally rescued when *zGba2*^{aug} was coinjected with the WT human mRNA (Figure 3H and Table S5, $p = 0.87$), supporting the specificity of our model. In contrast, we did not observe any rescue when the coinjection was performed with the mutated human c.1888C>T mRNA (Figure 3I and Table S5, $p < 0.00001$). These observations suggest that, in SPG46, as in other HSPs,[23,25–29] the neuronal tract formation is defective and they confirm the role of *GBA2* in the CNS development.

Could treatments in use for Gaucher disease, due to *GBA1* mutations, be useful in *GBA2* mutated individuals? Enzyme replacement with imiglucerase (Cerezyme, Genzyme; Velaglucerase alpha, Shire; etc.) will not be effective because it does not cross the blood-brain barrier and has been optimized to target lysosomes, which is not the localization of GBA2. Another therapy, called substrate reduction therapy, uses the iminosugar-based inhibitor N-butyldeoxynojirimycin (miglustat or Zarvesta, Actelion) or a structural analog (Gen 529448, Genzyme) that decrease glucosylceramide biosynthesis in vitro and have been reported to increase survival and motor functions of mice models of Niemann Pick type C1 (MIM 257220) and Sandhoff (MIM 268800) diseases.[20,30–32] However, these inhibitors also acted on GBA2 enzymatic activity,[32] making them unsuitable for SPG46 subjects. Moreover, a pharmacological chaperone strategy, such as isofagomine used in Gaucher disease, may be an interesting therapeutic option in SPG46 subjects due to missense mutations, if adapted to the GBA2 protein, because it was shown to increase GBA1 activity in *GBA1* mutant fibroblasts, reduce glucosylceramide and glucosylsphingosine accumulations in mouse models, and improve neurological symptoms in subjects with type III Gaucher disease (MIM 231000).[33,34]

In conclusion, we have identified mutations in *GBA2* leading to a specific phenotype that connects glucosylceramide metabolism and HSP. Lipid metabolism defects have already been implicated in other forms of HSP,[35] including SPG35 (MIM 612319), SPG28 (MIM 609340), or SPG49 caused by mutations in *FA2H* (MIM 611026), *DDHD1* (MIM 614603), and *CYP2U1* (MIM 610670), respectively.[36,37] Interestingly, measurement of specific activities of enzymes involved in HSP could be useful to facilitate diagnosis in clinical practice and to monitor drug response in future therapeutic trials, even when done in the peripheral blood cells as in SPG5A (MIM 270800)[38] or in SPG46 subjects in our study. Measurement of GBA1 activity is already in use in Gaucher disease assessment.

Supplemental Data

Supplemental Data include three figure and five tables and can be found with this article online at http://www.cell.com/AJHG/.

Acknowledgments

We are grateful to the family members for their participation. We would like to thank S. Ciura, M. Nawara, J. Gomez, P. Coutinho, I. Alonso, N. Jezequel, P. Touraine, G. Gyapay, V. Meyer, S. Rivaud-Péchoux, S. Forlani, and the DNA and Cell Bank of the Centre de Recherche de l'Institut du Cerveau et de la Moelle épinière for their contribution to this study. We also thank F. Mochel, F. Darios, K.H. El-Hachimi, and R. Schiffmann for their advice and the clinicians and collaborators of the Spastic paraplegia and ataxia (SPATAX) network who referred to us some of the affected subjects. This work was supported by the Association Strumpell-Lorrain (to SPATAX), the Agence Nationale de la Recherche (ANR) ("SPAX" to A.D. and "LIGENAX" and "SPG11" to G.S.), the Association Française contre les Myopathies ("LIGENAX" to G.S.), the European Union and ANR through the Eranet E-Rare program ("EUROSPA" to A.B. and L.S.), the Deutsches Zentrum für Neurodegenerative Erkrankungen (to L.S.), the Interdisziplinären Zentrums für Klinische Forschung University of Tübingen (grant 1970-0-0 to R.S.), and the Verum foundation (to A.B.). This study also benefited from funding from the program "Investissements d'avenir" ANR-10-IAIHU-06 (to the Brain and Spine Institute, Paris).

Received: October 3, 2012
Revised: November 15, 2012
Accepted: November 30, 2012
Published: January 17, 2013

Web Resources

The URLs for data presented herein are as follows:

1000 Genomes, http://browser.1000genomes.org/index.html
dbSNP, http://www.ncbi.nlm.nih.gov/projects/SNP/
Ensembl Genome Browser, http://www.ensembl.org/index.html
Genomes Management Application (GEM.app) database, https://genomics.med.miami.edu/gem-app/
Mutalyzer, https://mutalyzer.nl/index
Mutation Taster, http://www.mutationtaster.org/
NHLBI Exome Variant Server Exome Sequencing Project (ESP), http://evs.gs.washington.edu/EVS/
Online Mendelian Inheritance in Man (OMIM), http://www.omim.org/
PolyPhen, http://genetics.bwh.harvard.edu/pph/index.html
RefSeq, http://www.ncbi.nlm.nih.gov/RefSeq

References

1. Harding, A.E. (1983). Classification of the hereditary ataxias and paraplegias. Lancet *1*, 1151–1155.
2. Schüle, R., and Schöls, L. (2011). Genetics of hereditary spastic paraplegias. Semin. Neurol. *31*, 484–493.
3. Finsterer, J., Löscher, W., Quasthoff, S., Wanschitz, J., Auer-Grumbach, M., and Stevanin, G. (2012). Hereditary spastic paraplegias with autosomal dominant, recessive, X-linked, or maternal trait of inheritance. J. Neurol. Sci. *318*, 1–18.
4. Boukhris, A., Feki, I., Elleuch, N., Miladi, M.I., Boland-Augé, A., Truchetto, J., Mundwiller, E., Jezequel, N., Zelenika, D., Mhiri, C., et al. (2010). A new locus (SPG46) maps to 9p21.2-q21.12 in a Tunisian family with a complicated autosomal recessive hereditary spastic paraplegia with mental impairment and thin corpus callosum. Neurogenetics *11*, 441–448.
5. Li, H., and Durbin, R. (2009). Fast and accurate short read alignment with Burrows-Wheeler transform. Bioinformatics *25*, 1754–1760.
6. DePristo, M.A., Banks, E., Poplin, R., Garimella, K.V., Maguire, J.R., Hartl, C., Philippakis, A.A., del Angel, G., Rivas, M.A., Hanna, M., et al. (2011). A framework for variation discovery and genotyping using next-generation DNA sequencing data. Nat. Genet. *43*, 491–498.
7. McKenna, A., Hanna, M., Banks, E., Sivachenko, A., Cibulskis, K., Kernytsky, A., Garimella, K., Altshuler, D., Gabriel, S., Daly, M., and DePristo, M.A. (2010). The Genome Analysis Toolkit: a MapReduce framework for analyzing next-generation DNA sequencing data. Genome Res. *20*, 1297–1303.
8. Mencarelli, C., and Martinez-Martinez, P. (2012). Ceramide function in the brain: when a slight tilt is enough. Cell. Mol. Life Sci.
9. Matern, H., Gartzen, R., and Matern, S. (1992). Beta-glucosidase activity towards a bile acid glucoside in human liver. FEBS Lett. *314*, 183–186.
10. Matern, H., Heinemann, H., Legler, G., and Matern, S. (1997). Purification and characterization of a microsomal bile acid beta-glucosidase from human liver. J. Biol. Chem. *272*, 11261–11267.
11. Boot, R.G., Verhoek, M., Donker-Koopman, W., Strijland, A., van Marle, J., Overkleeft, H.S., Wennekes, T., and Aerts, J.M.F.G. (2007). Identification of the non-lysosomal glucosylceramidase as beta-glucosidase 2. J. Biol. Chem. *282*, 1305–1312.
12. Yildiz, Y., Matern, H., Thompson, B., Allegood, J.C., Warren, R.L., Ramirez, D.M.O., Hammer, R.E., Hamra, F.K., Matern, S., and Russell, D.W. (2006). Mutation of beta-glucosidase 2 causes glycolipid storage disease and impaired male fertility. J. Clin. Invest. *116*, 2985–2994.
13. Tsuji, S., Choudary, P.V., Martin, B.M., Stubblefield, B.K., Mayor, J.A., Barranger, J.A., and Ginns, E.I. (1987). A mutation in the human glucocerebrosidase gene in neuronopathic Gaucher's disease. N. Engl. J. Med. *316*, 570–575.
14. Kolter, T., Winau, F., Schaible, U.E., Leippe, M., and Sandhoff, K. (2005). Lipid-binding proteins in membrane digestion, antigen presentation, and antimicrobial defense. J. Biol. Chem. *280*, 41125–41128.
15. van Weely, S., Brandsma, M., Strijland, A., Tager, J.M., and Aerts, J.M. (1993). Demonstration of the existence of a second, non-lysosomal glucocerebrosidase that is not deficient in Gaucher disease. Biochim. Biophys. Acta *1181*, 55–62.
16. Walden, C.M., Sandhoff, R., Chuang, C.-C., Yildiz, Y., Butters, T.D., Dwek, R.A., Platt, F.M., and van der Spoel, A.C. (2007). Accumulation of glucosylceramide in murine testis, caused by inhibition of beta-glucosidase 2: implications for spermatogenesis. J. Biol. Chem. *282*, 32655–32664.
17. Aureli, M., Bassi, R., Loberto, N., Regis, S., Prinetti, A., Chigorno, V., Aerts, J.M., Boot, R.G., Filocamo, M., and Sonnino, S. (2012). Cell surface associated glycohydrolases in normal and Gaucher disease fibroblasts. J. Inherit. Metab. Dis. *35*, 1081–1091.
18. Dekker, N., Voorn-Brouwer, T., Verhoek, M., Wennekes, T., Narayan, R.S., Speijer, D., Hollak, C.E.M., Overkleeft, H.S., Boot, R.G., and Aerts, J.M.F.G. (2011). The cytosolic β-glucosidase GBA3 does not influence type 1 Gaucher disease manifestation. Blood Cells Mol. Dis. *46*, 19–26.
19. van der Spoel, A.C., Jeyakumar, M., Butters, T.D., Charlton, H.M., Moore, H.D., Dwek, R.A., and Platt, F.M. (2002). Reversible infertility in male mice after oral administration of alkylated imino sugars: a nonhormonal approach to male contraception. Proc. Natl. Acad. Sci. USA *99*, 17173–17178.
20. Bone, W., Walden, C.M., Fritsch, M., Voigtmann, U., Leifke, E., Gottwald, U., Boomkamp, S., Platt, F.M., and van der Spoel, A.C. (2007). The sensitivity of murine spermiogenesis to miglustat is a quantitative trait: a pharmacogenetic study. Reprod. Biol. Endocrinol. *5*, 1.
21. Ferreirinha, F., Quattrini, A., Pirozzi, M., Valsecchi, V., Dina, G., Broccoli, V., Auricchio, A., Piemonte, F., Tozzi, G., Gaeta, L., et al. (2004). Axonal degeneration in paraplegin-deficient mice is associated with abnormal mitochondria and impairment of axonal transport. J. Clin. Invest. *113*, 231–242.
22. Soderblom, C., Stadler, J., Jupille, H., Blackstone, C., Shupliakov, O., and Hanna, M.C. (2010). Targeted disruption of the Mast syndrome gene SPG21 in mice impairs hind limb function and alters axon branching in cultured cortical neurons. Neurogenetics *11*, 369–378.
23. Martin, E., Yanicostas, C., Rastetter, A., Naini, S.M.A., Maouedj, A., Kabashi, E., Rivaud-Péchoux, S., Brice, A.,

Stevanin, G., and Soussi-Yanicostas, N. (2012). Spatacsin and spastizin act in the same pathway required for proper spinal motor neuron axon outgrowth in zebrafish. Neurobiol. Dis. *48*, 299–308.

24. Fox, M.A., and Sanes, J.R. (2007). Synaptotagmin I and II are present in distinct subsets of central synapses. J. Comp. Neurol. *503*, 280–296.
25. Wood, J.D., Landers, J.A., Bingley, M., McDermott, C.J., Thomas-McArthur, V., Gleadall, L.J., Shaw, P.J., and Cunliffe, V.T. (2006). The microtubule-severing protein Spastin is essential for axon outgrowth in the zebrafish embryo. Hum. Mol. Genet. *15*, 2763–2771.
26. Lin, P., Li, J., Liu, Q., Mao, F., Li, J., Qiu, R., Hu, H., Song, Y., Yang, Y., Gao, G., et al. (2008). A missense mutation in SLC33A1, which encodes the acetyl-CoA transporter, causes autosomal-dominant spastic paraplegia (SPG42). Am. J. Hum. Genet. *83*, 752–759.
27. Fassier, C., Hutt, J.A., Scholpp, S., Lumsden, A., Giros, B., Nothias, F., Schneider-Maunoury, S., Houart, C., and Hazan, J. (2010). Zebrafish atlastin controls motility and spinal motor axon architecture via inhibition of the BMP pathway. Nat. Neurosci. *13*, 1380–1387.
28. Southgate, L., Dafou, D., Hoyle, J., Li, N., Kinning, E., Critchley, P., Németh, A.H., Talbot, K., Bindu, P.S., Sinha, S., et al. (2010). Novel SPG11 mutations in Asian kindreds and disruption of spatacsin function in the zebrafish. Neurogenetics *11*, 379–389.
29. Song, Y., Wang, M., Mao, F., Shao, M., Zhao, B., Song, Z., Shao, C., and Gong, Y. (2012). Knockdown of pnpla6 protein results in motor neuron defects in zebrafish. Dis. Model Mech. Published online November 16, 2012. http://dx.doi.org/10.1242/dmm.009688.
30. Overkleeft, H.S., Renkema, G.H., Neele, J., Vianello, P., Hung, I.O., Strijland, A., van der Burg, A.M., Koomen, G.J., Pandit, U.K., and Aerts, J.M. (1998). Generation of specific deoxynojirimycin-type inhibitors of the non-lysosomal glucosylceramidase. J. Biol. Chem. *273*, 26522–26527.
31. Cox, T.M. (2001). Gaucher disease: understanding the molecular pathogenesis of sphingolipidoses. J. Inherit. Metab. Dis. *24*(*Suppl 2*), 106–121, discussion 87–88.
32. Nietupski, J.B., Pacheco, J.J., Chuang, W.-L., Maratea, K., Li, L., Foley, J., Ashe, K.M., Cooper, C.G.F., Aerts, J.M.F.G., Copeland, D.P., et al. (2012). Iminosugar-based inhibitors of glucosylceramide synthase prolong survival but paradoxically increase brain glucosylceramide levels in Niemann-Pick C mice. Mol. Genet. Metab. *105*, 621–628.
33. Sun, Y., Ran, H., Liou, B., Quinn, B., Zamzow, M., Zhang, W., Bielawski, J., Kitatani, K., Setchell, K.D.R., Hannun, Y.A., and Grabowski, G.A. (2011). Isofagomine in vivo effects in a neuronopathic Gaucher disease mouse. PLoS ONE *6*, e19037.
34. Sun, Y., Liou, B., Xu, Y.-H., Quinn, B., Zhang, W., Hamler, R., Setchell, K.D.R., and Grabowski, G.A. (2012). Ex vivo and in vivo effects of isofagomine on acid β-glucosidase variants and substrate levels in Gaucher disease. J. Biol. Chem. *287*, 4275–4287.
35. Stevanin, G., Ruberg, M., and Brice, A. (2008). Recent advances in the genetics of spastic paraplegias. Curr. Neurol. Neurosci. Rep. *8*, 198–210.
36. Edvardson, S., Hama, H., Shaag, A., Gomori, J.M., Berger, I., Soffer, D., Korman, S.H., Taustein, I., Saada, A., and Elpeleg, O. (2008). Mutations in the fatty acid 2-hydroxylase gene are associated with leukodystrophy with spastic paraparesis and dystonia. Am. J. Hum. Genet. *83*, 643–648.
37. Tesson, C., Nawara, M., Salih, M.A., Rossignol, R., Zaki, M.S., Al Balwi, M., Schüle, R., Mignot, C., Obre, E., Bouhouche, A., et al. (2012). Alteration of fatty-acid-metabolizing enzymes affects mitochondrial form and function in hereditary spastic paraplegia. Am. J. Hum. Genet. *91*, 1051–1064.
38. Schüle, R., Siddique, T., Deng, H.-X., Yang, Y., Donkervoort, S., Hansson, M., Madrid, R.E., Siddique, N., Schöls, L., and Björkhem, I. (2010). Marked accumulation of 27-hydroxycholesterol in SPG5 patients with hereditary spastic paresis. J. Lipid Res. *51*, 819–823.

Alteration of Ganglioside Biosynthesis Responsible for Complex Hereditary Spastic Paraplegia

Amir Boukhris,[1,2,3] Rebecca Schule,[4] José L. Loureiro,[5] Charles Marques Lourenço,[6] Emeline Mundwiller,[3,7] Michael A. Gonzalez,[8] Perrine Charles,[9] Julie Gauthier,[10] Imen Rekik,[1,3] Rafael F. Acosta Lebrigio,[8] Marion Gaussen,[3,11,12,13] Fiorella Speziani,[8] Andreas Ferbert,[14] Imed Feki,[1,2] Andrés Caballero-Oteyza,[4] Alexandre Dionne-Laporte,[10] Mohamed Amri,[1,2] Anne Noreau,[10] Sylvie Forlani,[3,11,12] Vitor T. Cruz,[5] Fanny Mochel,[3,9,11,12] Paula Coutinho,[5] Patrick Dion,[10,15] Chokri Mhiri,[1,2] Ludger Schols,[4,16] Jean Pouget,[17] Frédéric Darios,[3,11,12] Guy A. Rouleau,[10] Wilson Marques, Jr.,[6] Alexis Brice,[3,7,9,11,12,*] Alexandra Durr,[3,9,11,12] Stephan Zuchner,[8,18] and Giovanni Stevanin[3,7,9,11,12,13,18,*]

Hereditary spastic paraplegias (HSPs) form a heterogeneous group of neurological disorders. A whole-genome linkage mapping effort was made with three HSP-affected families from Spain, Portugal, and Tunisia and it allowed us to reduce the *SPG26* locus interval from 34 to 9 Mb. Subsequently, a targeted capture was made to sequence the entire exome of affected individuals from these three families, as well as from two additional autosomal-recessive HSP-affected families of German and Brazilian origins. Five homozygous truncating (n = 3) and missense (n = 2) mutations were identified in *B4GALNT1*. After this finding, we analyzed the entire coding region of this gene in 65 additional cases, and three mutations were identified in two subjects. All mutated cases presented an early-onset spastic paraplegia, with frequent intellectual disability, cerebellar ataxia, and peripheral neuropathy as well as cortical atrophy and white matter hyperintensities on brain imaging. *B4GALNT1* encodes β-1,4-N-acetyl-galactosaminyl transferase 1 (B4GALNT1), involved in ganglioside biosynthesis. These findings confirm the increasing interest of lipid metabolism in HSPs. Interestingly, although the catabolism of gangliosides is implicated in a variety of neurological diseases, SPG26 is only the second human disease involving defects of their biosynthesis.

Hereditary spastic paraplegias (HSPs) constitute a clinically and genetically heterogeneous group of neurodegenerative conditions. They are characterized by a slowly progressive spasticity of the lower extremities resulting from the axonal degeneration and/or dysfunction observed in long axons of the corticospinal tracts.[1,2] HSPs are classified according to the following criteria: (1) absence (uncomplicated or pure HSP) or presence (complicated or complex HSP) of additional neurological signs and symptoms, including intellectual disability, cerebellar ataxia, peripheral neuropathy, retinopathy, cataract, epilepsy, and ichthyosis; and (2) mode of inheritance in the case of familial forms, which can be autosomal-dominant, autosomal-recessive (AR), mitochondrial, or X-linked.[3] To date, more than 55 HSP loci (denoted *SPG*) have been mapped. Among them, mutations have been found in ~33 genes; the proteins encoded by these genes are often involved in intracellular trafficking, lipid metabolism, or mitochondrial functions.[2,4–8]

In 2005, Wilkinson et al. mapped the *SPG26* locus (MIM 609195) to a 22.8 cM region flanked by markers D12S59 and D12S1676 (34.2 Mb) on chromosome 12p11.1–12q14 in a Kuwaiti family with AR complicated HSP.[9] In the present study, we linked additional HSP families to the *SPG26* locus, refined the locus region, identified the segregating mutations in seven of these families, and described the associated phenotype.

We selected three families in which diagnosis of AR HSP was established according to Harding's criteria and careful exclusion of alternative disorders.[10] Blood samples and clinical assessments were performed after informed consent and after local ethics approvals. The disease was not caused by mutations in any of the frequently involved genes previously linked to HSPs. All available affected

[1]Service de Neurologie, Hôpital Universitaire Habib Bourguiba, 3029 Sfax, Tunisia; [2]Faculté de Médecine, Université de Sfax, 3029 Sfax, Tunisia; [3]Unité 975, Institut National de la Santé et de la Recherche Médicale, 75013 Paris, France; [4]Department of Neurodegenerative Diseases and Hertie-Institute for Clinical Brain Research, University of Tübingen, 72076 Tübingen, Germany; [5]UnIGENe and Centro de Genética Preditiva e Preventiva, Institute for Molecular and Cellular Biology, 4050 Porto, Portugal; [6]Departamento de Neurologia, Faculdade de Medicina de Ribeirão Preto, Universidade de São Paulo, SP 14049-900 Ribeirão Preto, Brazil; [7]Institut du Cerveau et de la Moelle épinière, Pitié-Salpêtrière Hospital, 75013 Paris, France; [8]Department of Human Genetics and Hussman Institute for Human Genomics, Miller School of Medicine, University of Miami, Miami, FL 33136, USA; [9]APHP, Fédération de Génétique, Pitié-Salpêtrière Hospital, 75013 Paris, France; [10]Montreal Neurological Institute and Hospital, Department of Neurology and Neurosurgery, McGill University, Montreal, QC H3A 2B4, Canada; [11]Unité Mixte de Recherche S975, Centre de Recherche de l'Institut du Cerveau et de la Moelle épinière, Pitié-Salpêtrière Hospital, Université Pierre et Marie Curie (Paris 6), 75013 Paris, France; [12]Unité Mixte de Recherche 7225, Centre National de la Recherche Scientifique, 75013 Paris, France; [13]Neurogenetics team, Ecole Pratique des Hautes Etudes, Institut du Cerveau et de la Moelle épinière, Pitié-Salpêtrière Hospital, 75013 Paris, France; [14]Department of Neurology, Klinikum Kassel, 34125 Kassel, Germany; [15]Département de pathologie et biologie cellulaire, Faculté de médecine, Université de Montréal, Montréal, QC H2L 2W5, Canada; [16]German Center of Neurodegenerative Diseases (DZNE), 72076 Tübingen, Germany; [17]Centre de référence des maladies neuromusculaires et de la SLA, CHU La Timone, 13005 Marseille, France
[18]These authors contributed equally to this work
*Correspondence: alexis.brice@upmc.fr (A.B.), giovanni.stevanin@upmc.fr (G.S.)
http://dx.doi.org/10.1016/j.ajhg.2013.05.006.

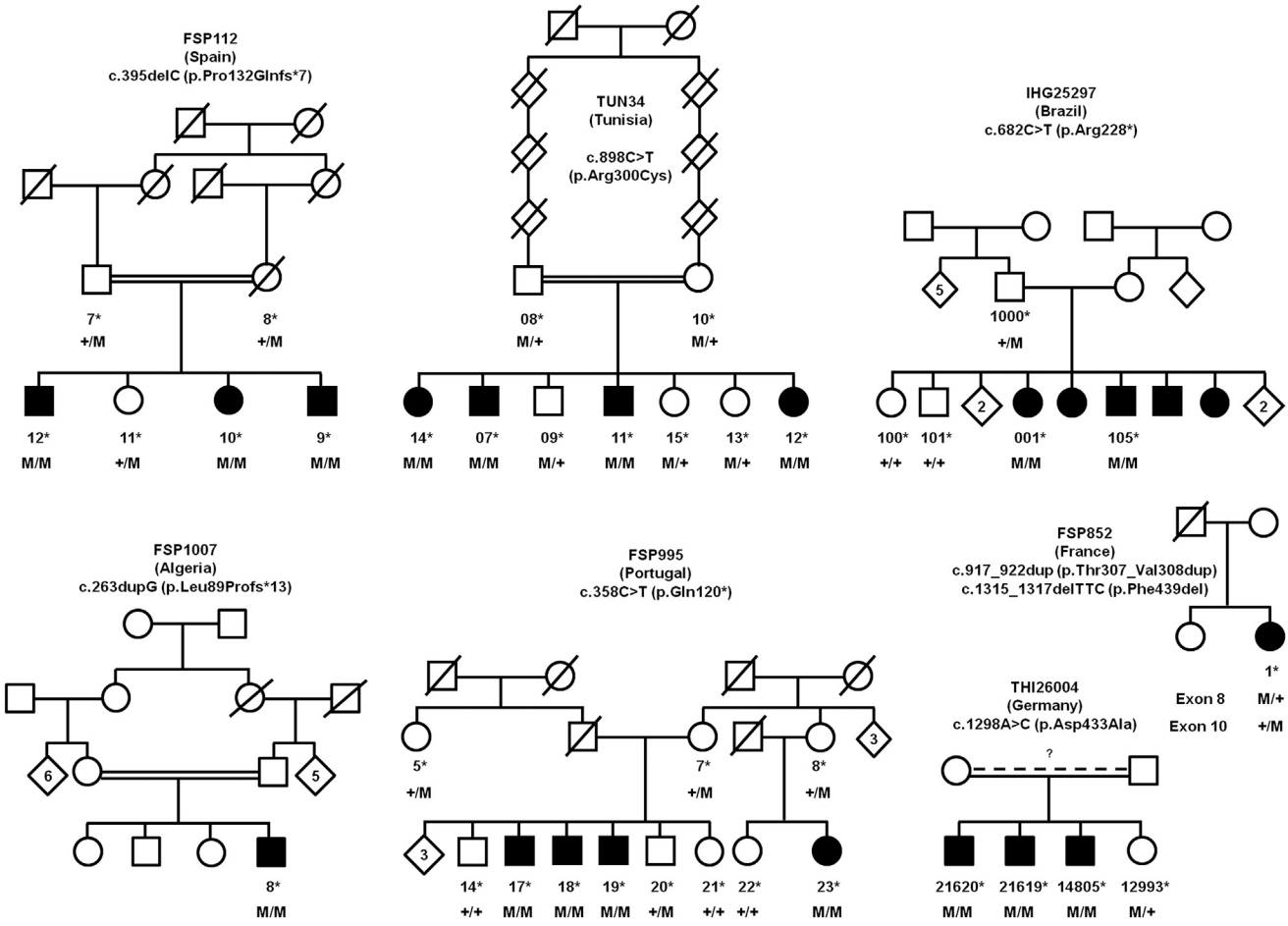

Figure 1. SPG26 Pedigrees and Segregation of the Mutations Detected in *B4GALNT1*
Square symbols indicate males and circles indicate females. Filled symbols indicate affected individuals. The numbers are an internal reference for each sampled individual. Stars indicate sampled subjects. Abbreviations are as follows: M, mutation; +, wild-type.

(n = 4) and unaffected (n = 5) members of a Tunisian family (TUN34) were subjected to a genome-wide linkage mapping that used 6,090 SNP markers (LINKAGE_24 Illumina) and an additional 30 microsatellite markers, as previously described.[11] All four affected individuals shared a single region of homozygosity of 22.5 cM (24 Mb) on chromosome 12 flanked by markers D12S1632 (56,415,415 bp) and D12S2074 (80,431,457 bp) (Figure S1 available online). Pairwise LOD scores reached the significance value of +3 at 19 consecutive markers with a multipoint LOD score of +4.45 (data not shown). In three affected and three unaffected subjects of a Spanish family (FSP112), the genome-wide scan was performed with 428 microsatellite markers, including the ABI Mapping set (Applied Biosystems), as described.[12] In a single homozygous region of 33 cM (41 Mb), a maximal multipoint LOD score of +2.53 reached the maximal expected value in this pedigree, flanked by markers D12S1617 and D12S1686 (Figure S1). Both homozygous regions in families TUN34 and FSP112 overlapped with the *SPG26* candidate interval and allowed its reduction from 34.2 Mb (27 cM) to 9.3 Mb (6.9 cM) between D12S1632 and D12S1686 (Figure S1). In a third family, of Portuguese origin without known consanguinity (FSP995), the same strategy was employed using the Illumina SNP panel and identified 10 regions with positive LOD score values ranging from +0.2 to +2.25, including a large portion of chromosome 12 containing *SPG26*.

Exome sequencing was performed on affected subjects of families FSP112, FSP995, and TUN34 as well as in two additional families, IHG25297 from Brazil and THI26004 from Germany (Figure 1). Coding exons and flanking intronic sequences were enriched with the SureSelect Human All Exon 50 Mb kit (Agilent) according to the manufacturer's standard protocol. Enriched samples were prepared for the Hiseq2000 instrument (Illumina) and paired-end reads of 100 bp length were produced. The Burrows-Wheeler algorithm was applied to align sequence reads to the UCSC Genome Browser hg19 version of the human genome and variants were called via the GATK software package.[13] Data were then imported into dedicated analysis toolsets, including the online GEnomes Management application (GEM.app)[14] and Eris (Integragen), for further analysis. In families TUN34, FSP995, and FSP112, the variants were filtered according to their quality, functional class (nonsynonymous and/or affecting splicing), presence in chromosomal regions with putative or

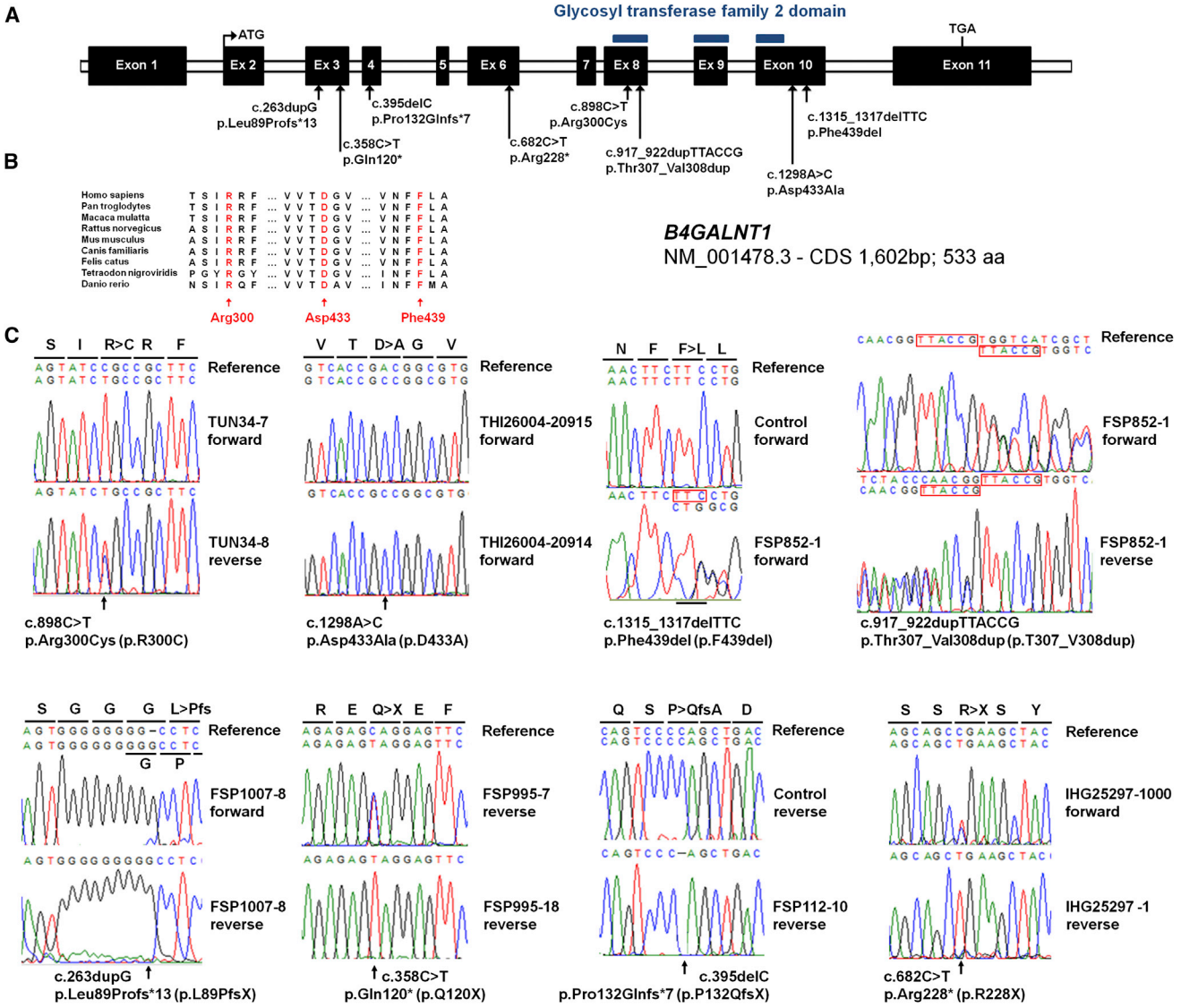

Figure 2. Schematic Representation of *B4GALNT1*/*SPG26* and Location of the Mutations
(A) Exon-intron structure of *B4GALNT1*, with positions of mutations identified in seven SPG26-affected families. Exons are indicated as black boxes. The region encoding a functional domain is indicated by blue bars.
(B) Phylogenetic conservation of three amino acids mutated in SPG26-affected individuals.
(C) Electropherograms of the mutations identified. Mutation nomenclature is in agreement with ALAMUT 2.2 and Mutalyzer software with transcript NM_001478.3.

nonexcluded linkage, and frequency ≤1% in publically available genomic databases. Together, these criteria helped to reduce the list of variants to two to five variants per family (Table S1). Based on conservation and variant class, we restricted this list to single mutations for each family that were all in the same gene, *B4GALNT1* (MIM 601873; RefSeq accession number NM_001478.3): c.898C>T (p.Arg300Cys), c.358C>T (p.Gln120*), and c.395delC (p.Pro132Glnfs*7), respectively. In family IHG25397, filtering of exome variants under a recessive model identified three candidate variants, one being a homozygous stop mutation in *B4GALNT1* (c.682C>T [p.Arg228*]). Similarly, a single homozygous variant in *B4GALNT1* remained under the same filters in family THI26004 (c.1298A>C [p.Asp433Ala]) (Table S1).

We then screened a series of 65 index cases of HSP families compatible with an AR mode of inheritance and found three other mutations in two simplex cases. One homozygous truncating mutation was identified in a consanguineous Algerian subject (FSP1007-8: c.263dupG [p.Leu89Profs*13]). A French HSP case harbored compound heterozygote changes: one codon deletion affecting a conserved amino acid and one in-frame duplication of two codons (FSP852-1: c.1315_1317delTTC [p.Phe439del] and c.917_922dup [p.Thr307_Val308dup]). For the latter case, it was not possible to verify whether they segregated in *cis* or in *trans* (Figures 1 and 2).

These mutations all segregated with the disease in their respective pedigree, when it could be tested (Figure 1), and they were also absent from the Exome Variant Server

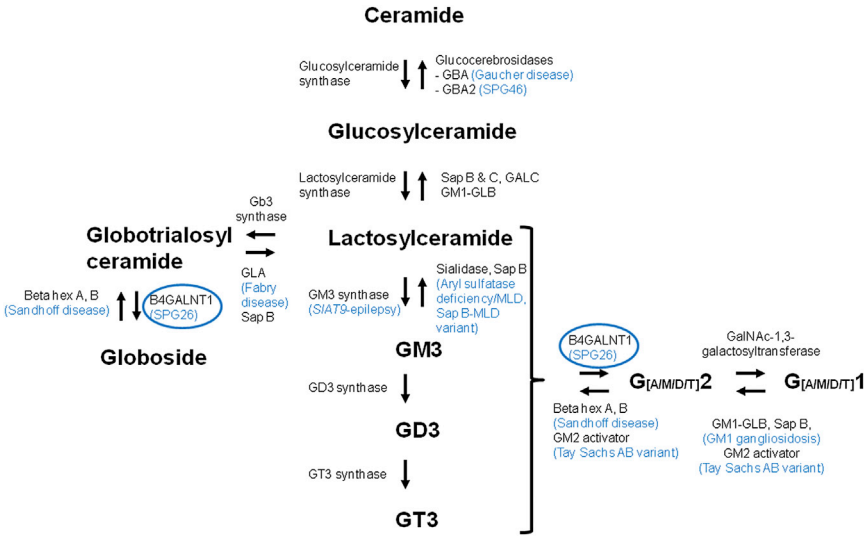

Figure 3. Simplified Representation of Ganglioside Metabolism and Their Related Disorders

Arrows indicate the orientation of the enzymatic reactions and the corresponding enzymes are indicated in black. Metabolic diseases are indicated in blue at the corresponding altered reaction. Ganglioside formation is performed in the endoplasmic reticulum and Golgi by successive glycosylations. Their degradation takes place in lysosomes. Abbreviations are as follows: hex, hexosaminidase; Gb3, globotrioaosylceramide; GBA, glucocerebrosidase; GD, disialic ganglioside; GALC, galactosylceramide-beta-galactosidase; GLA, alpha galactosidase; GLB, beta galactosidase; GM, monosialic ganglioside; GT, trisialic ganglioside; GT3 synthase, alpha-N-acetyl-neuraminide alpha-2,8-sialyltransferase; MLD, metachromatic leukodystrophy; Sap, saposin.

(EVS; 13,006 chromosomes) and our local databases (>3,340 chromosomes). The two missense variants and the codon deletion affected strongly conserved amino acids (Figure 2) in *B4GALNT1* and they were all predicted to be pathogenic when examined with algorithms designed to assess the impact of genetic variations (Polyphen, MutationTaster, Sift).

B4GALNT1 encodes β-1,4-N-acetyl-galactosaminyl transferase 1 (GM2/GD2 synthase; EC 2.4.1.92), an enzyme involved in the biosynthesis of complex gangliosides (G), which are mono- (M), di- (D), and tri- (T) sialic acid-containing glycosphingolipids generated by sequential glycosylations (Figure 3).[15] Gangliosides are part of the larger family of glycosphingolipids and are components of the synaptic plasma membrane involved in synaptic plasticity, signal transduction, and endocytosis and then are critical for CNS development. B4GALNT1 catalyzes the transfer of N-acetyl-galactosamine into GM3, GD3, and globotriaosylceramide by a β-1,4 linkage (Figure 3). The reverse reaction is performed by β-hexosaminidase and its cofactor (GM2 activator). Molecular defects in the degradation of glycosphingolipids led to well-known lysosomal storage diseases, including Gaucher disease caused by *GBA* (MIM 606463) mutations,[16,17] Fabry disease (MIM 301500), metachromatic leukodystrophy (MIM 250100 and 249900), Tay-Sachs AB variant/GM2 gangliosidosis (MIM 272750), Sandhoff disease (MIM 268800), and GM1 gangliosidosis (MIM 230500) (Figure 3). Conversely, to our knowledge, a single proven case of a human disorder resulting from disruption of ganglioside biosynthesis has been described.[18] Mutations in *ST3GAL5* (also known as *SIAT9* [MIM 604402]) coding for GM3 synthase, also called lactosylceramide α-2,3 sialyltransferase, resulted in infantile epileptic encephalopathy (MIM 609056) with severe developmental delay and blindness. *ST3GAL5*-mutated individuals displayed a complete lack of plasma GM3 and its downstream biosynthetic derivatives but had increased levels of plasma lactosylceramide and increased flux through the globoside and paragloboside pathways.[18] Therefore, SPG26 resulting from *B4GALNT1* mutations is the second ganglioside biosynthesis defect and is expected to lead to the accumulation of globotriaosylceramide and gangliosides G[M/D/T]3. Of note, another complex AR HSP, SPG46 (MIM 614409), is caused by loss-of-function mutations in *GBA2* (MIM 609471), coding for an enzyme acting on glucosylceramides, substrates of lactosylceramides (Figure 3).[8]

The clinical features of 18 affected individuals from the 7 SPG26 families identified in this study are summarized in Table S2. Gait difficulties occurred early, from 2 to 19 years of age. All subjects had predominant spasticity of the lower limbs (with variable spastic involvement of the upper limbs in 33%), increased reflexes, and bilateral Babinski sign. Pseudobulbar dysarthria was present in 47% (7/15). After a mean disease duration of 32.2 ± 19.5 years (range 1–60), four subjects were confined to a wheelchair or bedridden. Severity was variable: one was bedridden after 13 years (TUN34-11) whereas another was confined to a wheelchair after 47 years of disease evolution (FSP995-17). Lower motor neuron involvement was variably present, indicated by lower limb muscle wasting (11/18, 61%) at later disease stages, decrease or absence of lower limb tendon reflexes (11/18, 61%) during the course of the disease (as in family THI26004), and peripheral neuropathy predominantly of the axonal type in four families (7/11, 64%). Mild to moderate cognitive impairment and developmental delay was noted in all individuals, often preceding motor deficits. Cognitive dysfunction was noted to worsen with time in some subjects. Cerebellar signs (10/18, 55%) and extrapyramidal signs (8/18, 44%), such as facial dyskinesia and dystonia, were also noted. Further commonly observed signs and symptoms included bladder disturbances (6/18, 33%), peripherally decreased vibration sense (9/15, 60%), scoliosis (10/15, 67%), pes cavus (9/16, 56%), and strabismus (4/18, 22%). Four subjects had psychiatric features (the three German cases and one Brazilian individual). In

addition, several signs were confined to one family: mild dysmorphic features in the Brazilian subjects and congenital posterior capsular cataract in the three Spanish individuals. Brain magnetic resonance imaging (MRI) was either normal or, after long disease durations, showed cortical atrophy (n = 5/10), subcortical atrophy (n = 1/10), and/or white matter hyperintensities (WMHs) on FLAIR sequence (n = 4/10) (Figure S2). In subject FSP995-19, WMHs worsen with time, as observed in two brain MRIs performed 12 years apart. We noted a slightly enlarged corpus callosum in 4/10 subjects; some of them with otherwise unremarkable MRIs. Finally, serum testosterone was reduced or at the lower limit in four of the six young men tested (67%), and one of them (IHG25297-105) had hypogonadism and delayed puberty.

Interestingly, the *B4galnt1*$^{-/-}$ mouse[19] shows progressive gait disorder reminiscent of clinical features of SPG26. This phenotype could result from decreased central myelination in dorsal spinal cord and increased numbers of unmyelinated fibers,[20,21] increased astrocyte/microglia proliferation, or alteration of lipid content in glycolipid-enriched membrane (raft) domains.[22,23] Cerebellar granule cells of *B4galnt1*$^{-/-}$ mice are also more prone to degeneration in depolarizing conditions, very probably due to an alteration of calcium homeostasis.[24] In addition, knockout males have progressive testicular atrophy with the presence of diffuse vacuoles in Sertoli cells and, despite almost normal testosterone levels per mg of testis, a severe reduction of serum testosterone.[25] All these phenotypes could be due to the accumulation of globotriaosylceramide and simple gangliosides and/or the lack of complex gangliosides.[19,24] Interestingly, GM3 accumulation has been reported in a simplex case with liver and brain disease.[26,27] Whether the disease in this subject is the result of a mutation in *B4GALNT1* remains unknown.

In conclusion, we used a combined mapping and exome sequencing approach to identify *B4GALNT1* variants as the cause of an AR complicated form of HSP. This was achieved with 18 SPG26-affected individuals that belonged to 7 unrelated families from Europe, South America, and North Africa (indicating the world-wide distribution of this particular form of HSP). In accordance with previous reports,[9] the phenotype of SPG26 consisted in early-onset and slowly progressive spastic paraparesis and cognitive impairment, complicated by cerebellar ataxia. We extended this clinical spectrum to include extrapyramidal involvement and peripheral neuropathy as well as cortical atrophy with white matter hyperintensities at brain MRI and low levels of testosterone in males. Disease progression seemed slow: most affected subjects were still able to walk after long disease durations but heterogeneity in disease progression was frequent among families. Altogether, SPG26 is the second human disorder of ganglioside biosynthesis. Abnormal glycosphingolipid profile may be detectable in peripheral samples from SPG26 subjects: this would hasten clinical diagnosis and facilitate monitoring in therapeutic trials as for other HSPs, such as SPG5A (MIM 270800) associated with 25- and 27-hydroxycholesterol accumulation[28] and X-linked adrenoleukodystrophy (MIM 300100).

Supplemental Data

Supplemental Data include two figures and two tables and can be found with this article online at http://www.cell.com/AJHG/.

Acknowledgments

The authors are grateful to the family members who participated in this study, to M.A.M. Salih and M. Koenig for family referral, and to S. Trefouret and P. Ribai as well as the DNA and cell Bank of CRICM and the Centre National de Genotypage (Evry, France) for their help. This work was financially supported by the French-Tunisian Cooperation Project (to A. Brice and C.M.) led by INSERM (France) and DGRSRT (Tunisia), the VERUM Foundation (to A. Brice), the French Agency for Research (ANR) (to G.S. and A.D.), the Association Française contre les Myopathies ("LIGENAX" to G.S.), the Strumpell-Lorrain association (to the SPATAX network), the Deutsches Zentrum für Neurodegenerative Erkrankungen (to L.S.), the Interdisziplinären Zentrums für Klinische Forschung University of Tübingen (grant 1970-0-0 to R.S.), and the European Community with the ANR ("Eurospa" project to A. Brice and L.S.; 7th Framework Programme Neuromics to A. Brice). This study also benefited from funding from the program "Investissements d'avenir" ANR-10-IAIHU-06 (to the Brain and Spine Institute, Paris), a Canadian Institutes of Health Research grant (#119191) entitled "Emerging Team to identify and characterize novel and existing Hereditary Spastic Paraplegia (HSP) disease genes," and a National Institutes of Health grant (R01NS072248 to S.Z.).

Received: April 7, 2013
Revised: May 6, 2013
Accepted: May 8, 2013
Published: June 6, 2013

Web Resources

The URLs for data presented herein are as follows:

1000 Genomes, http://browser.1000genomes.org
Alamut, http://www.interactive-biosoftware.com/
dbSNP, http://www.ncbi.nlm.nih.gov/projects/SNP/
Ensembl Genome Browser, http://www.ensembl.org/index.html
ERIS, http://eris.integragen.com/
GEM.app, https://genomics.med.miami.edu
Mutalyzer, https://mutalyzer.nl/index
MutationTaster, http://www.mutationtaster.org/
NHLBI Exome Sequencing Project (ESP) Exome Variant Server, http://evs.gs.washington.edu/EVS/
Online Mendelian Inheritance in Man (OMIM), http://www.omim.org/
PolyPhen-2, http://www.genetics.bwh.harvard.edu/pph2/
RefSeq, http://www.ncbi.nlm.nih.gov/RefSeq
SIFT, http://sift.bii.a-star.edu.sg/
UCSC Genome Browser, http://genome.ucsc.edu

References

1. Behan, W.M., and Maia, M. (1974). Strümpell's familial spastic paraplegia: genetics and neuropathology. J. Neurol. Neurosurg. Psychiatry *37*, 8–20.

2. Stevanin, G., Ruberg, M., and Brice, A. (2008). Recent advances in the genetics of spastic paraplegias. Curr. Neurol. Neurosci. Rep. *8*, 198–210.
3. Fink, J.K. (2006). Hereditary spastic paraplegia. Curr. Neurol. Neurosci. Rep. *6*, 65–76.
4. Schüle, R., and Schöls, L. (2011). Genetics of hereditary spastic paraplegias. Semin. Neurol. *31*, 484–493.
5. Finsterer, J., Löscher, W., Quasthoff, S., Wanschitz, J., Auer-Grumbach, M., and Stevanin, G. (2012). Hereditary spastic paraplegias with autosomal dominant, recessive, X-linked, or maternal trait of inheritance. J. Neurol. Sci. *318*, 1–18.
6. Tesson, C., Nawara, M., Salih, M.A.M., Rossignol, R., Zaki, M.S., Al Balwi, M., Schule, R., Mignot, C., Obre, E., Bouhouche, A., et al. (2012). Alteration of fatty-acid-metabolizing enzymes affects mitochondrial form and function in hereditary spastic paraplegia. Am. J. Hum. Genet. *91*, 1051–1064.
7. Schuurs-Hoeijmakers, J.H.M., Geraghty, M.T., Kamsteeg, E.-J., Ben-Salem, S., de Bot, S.T., Nijhof, B., van de Vondervoort, I.I.G.M., van der Graaf, M., Nobau, A.C., Otte-Höller, I., et al.; FORGE Canada Consortium. (2012). Mutations in DDHD2, encoding an intracellular phospholipase A(1), cause a recessive form of complex hereditary spastic paraplegia. Am. J. Hum. Genet. *91*, 1073–1081.
8. Martin, E., Schüle, R., Smets, K., Rastetter, A., Boukhris, A., Loureiro, J.L., Gonzalez, M.A., Mundwiller, E., Deconinck, T., Wessner, M., et al. (2013). Loss of function of glucocerebrosidase GBA2 is responsible for motor neuron defects in hereditary spastic paraplegia. Am. J. Hum. Genet. *92*, 238–244.
9. Wilkinson, P.A., Simpson, M.A., Bastaki, L., Patel, H., Reed, J.A., Kalidas, K., Samilchuk, E., Khan, R., Warner, T.T., and Crosby, A.H. (2005). A new locus for autosomal recessive complicated hereditary spastic paraplegia (SPG26) maps to chromosome 12p11.1-12q14. J. Med. Genet. *42*, 80–82.
10. Harding, A.E. (1983). Classification of the hereditary ataxias and paraplegias. Lancet *1*, 1151–1155.
11. Boukhris, A., Feki, I., Elleuch, N., Miladi, M.I., Boland-Augé, A., Truchetto, J., Mundwiller, E., Jezequel, N., Zelenika, D., Mhiri, C., et al. (2010). A new locus (SPG46) maps to 9p21.2-q21.12 in a Tunisian family with a complicated autosomal recessive hereditary spastic paraplegia with mental impairment and thin corpus callosum. Neurogenetics *11*, 441–448.
12. Stevanin, G., Bouslam, N., Thobois, S., Azzedine, H., Ravaux, L., Boland, A., Schalling, M., Broussolle, E., Dürr, A., and Brice, A. (2004). Spinocerebellar ataxia with sensory neuropathy (SCA25) maps to chromosome 2p. Ann. Neurol. *55*, 97–104.
13. McKenna, A., Hanna, M., Banks, E., Sivachenko, A., Cibulskis, K., Kernytsky, A., Garimella, K., Altshuler, D., Gabriel, S., Daly, M., and DePristo, M.A. (2010). The Genome Analysis Toolkit: a MapReduce framework for analyzing next-generation DNA sequencing data. Genome Res. *20*, 1297–1303.
14. Gonzalez, M.A., Lebrigio, R.F., Van Booven, D., Ulloa, R.H., Powell, E., Speziani, F., Tekin, M., Schule, R., and Zuchner, S. (2013). GEnomes Management Application (GEM.app): A New Software Tool for Large-Scale Collaborative Genome Analysis. Hum. Mutat. *34*, 860–863.
15. Xu, Y.-H., Barnes, S., Sun, Y., and Grabowski, G.A. (2010). Multi-system disorders of glycosphingolipid and ganglioside metabolism. J. Lipid Res. *51*, 1643–1675.
16. Tsuji, S., Choudary, P.V., Martin, B.M., Stubblefield, B.K., Mayor, J.A., Barranger, J.A., and Ginns, E.I. (1987). A mutation in the human glucocerebrosidase gene in neuronopathic Gaucher's disease. N. Engl. J. Med. *316*, 570–575.
17. Cox, T.M. (2001). Gaucher disease: understanding the molecular pathogenesis of sphingolipidoses. J. Inherit. Metab. Dis. *24*(*Suppl 2*), 106–121, discussion 87–88.
18. Simpson, M.A., Cross, H., Proukakis, C., Priestman, D.A., Neville, D.C.A., Reinkensmeier, G., Wang, H., Wiznitzer, M., Gurtz, K., Verganelaki, A., et al. (2004). Infantile-onset symptomatic epilepsy syndrome caused by a homozygous loss-of-function mutation of GM3 synthase. Nat. Genet. *36*, 1225–1229.
19. Takamiya, K., Yamamoto, A., Furukawa, K., Yamashiro, S., Shin, M., Okada, M., Fukumoto, S., Haraguchi, M., Takeda, N., Fujimura, K., et al. (1996). Mice with disrupted GM2/GD2 synthase gene lack complex gangliosides but exhibit only subtle defects in their nervous system. Proc. Natl. Acad. Sci. USA *93*, 10662–10667.
20. Sheikh, K.A., Sun, J., Liu, Y., Kawai, H., Crawford, T.O., Proia, R.L., Griffin, J.W., and Schnaar, R.L. (1999). Mice lacking complex gangliosides develop Wallerian degeneration and myelination defects. Proc. Natl. Acad. Sci. USA *96*, 7532–7537.
21. Ma, Q., Kobayashi, M., Sugiura, M., Ozaki, N., Nishio, K., Shiraishi, Y., Furukawa, K., Furukawa, K., and Sugiura, Y. (2003). Morphological study of disordered myelination and the degeneration of nerve fibers in the spinal cord of mice lacking complex gangliosides. Arch. Histol. Cytol. *66*, 37–44.
22. Ohmi, Y., Tajima, O., Ohkawa, Y., Yamauchi, Y., Sugiura, Y., Furukawa, K., and Furukawa, K. (2011). Gangliosides are essential in the protection of inflammation and neurodegeneration via maintenance of lipid rafts: elucidation by a series of ganglioside-deficient mutant mice. J. Neurochem. *116*, 926–935.
23. Ohmi, Y., Ohkawa, Y., Yamauchi, Y., Tajima, O., Furukawa, K., and Furukawa, K. (2012). Essential roles of gangliosides in the formation and maintenance of membrane microdomains in brain tissues. Neurochem. Res. *37*, 1185–1191.
24. Wu, G., Xie, X., Lu, Z.H., and Ledeen, R.W. (2001). Cerebellar neurons lacking complex gangliosides degenerate in the presence of depolarizing levels of potassium. Proc. Natl. Acad. Sci. USA *98*, 307–312.
25. Takamiya, K., Yamamoto, A., Furukawa, K., Zhao, J., Fukumoto, S., Yamashiro, S., Okada, M., Haraguchi, M., Shin, M., Kishikawa, M., et al. (1998). Complex gangliosides are essential in spermatogenesis of mice: possible roles in the transport of testosterone. Proc. Natl. Acad. Sci. USA *95*, 12147–12152.
26. Max, S.R., Maclaren, N.K., Brady, R.O., Bradley, R.M., Rennels, M.B., Tanaka, J., Garcia, J.H., and Cornblath, M. (1974). GM3 (hematoside) sphingolipodystrophy. N. Engl. J. Med. *291*, 929–931.
27. Fishman, P.H., Max, S.R., Tallman, J.F., Brady, R.O., Maclaren, N.K., and Cornblath, M. (1975). Deficient Ganglioside Biosynthesis: a novel human sphingolipidosis. Science *187*, 68–70.
28. Schüle, R., Siddique, T., Deng, H.-X., Yang, Y., Donkervoort, S., Hansson, M., Madrid, R.E., Siddique, N., Schöls, L., and Björkhem, I. (2010). Marked accumulation of 27-hydroxycholesterol in SPG5 patients with hereditary spastic paresis. J. Lipid Res. *51*, 819–823.

European Journal of Human Genetics (2013) 21, 1214–1218

www.nature.com/ejhg

ARTICLE

Mutations in phospholipase DDHD2 cause autosomal recessive hereditary spastic paraplegia (SPG54)

Michael Gonzalez[1], Sheela Nampoothiri[2], Cornelia Kornblum[3], Andrés Caballero Oteyza[4], Jochen Walter[3], Ioanna Konidari[1], William Hulme[1], Fiorella Speziani[1], Ludger Schöls[4,5], Stephan Züchner[1] and Rebecca Schüle*[,4]

Hereditary spastic paraplegias (HSP) are a genetically heterogeneous group of disorders characterized by a distal axonopathy of the corticospinal tract motor neurons leading to progressive lower limb spasticity and weakness. Intracellular membrane trafficking, mitochondrial dysfunction and myelin formation are key functions involved in HSP pathogenesis. Only recently defects in metabolism of complex lipids have been implicated in a number of HSP subtypes. Mutations in the 23 known autosomal recessive HSP genes explain less than half of autosomal recessive HSP cases. To identify novel autosomal recessive HSP disease genes, exome sequencing was performed in 79 index cases with autosomal recessive forms of HSP. Resulting variants were filtered and intersected between families to allow identification of new disease genes. We identified two deleterious mutations in the phospholipase *DDHD2* gene in two families with complicated HSP. The phenotype is characterized by early onset of spastic paraplegia, mental retardation, short stature and dysgenesis of the corpus callosum. Phospholipase DDHD2 is involved in intracellular membrane trafficking at the golgi/ endoplasmic reticulum interface and has been shown to possess phospholipase A1 activity *in vitro*. Discovery of *DDHD2* mutations in HSP might therefore provide a link between two key pathogenic themes in HSP: membrane trafficking and lipid metabolism.
European Journal of Human Genetics (2013) **21,** 1214–1218; doi:10.1038/ejhg.2013.29; published online 13 March 2013

Keywords: Hereditary spastic paraplegia; exome sequencing; neurodegenerative disease

INTRODUCTION

The genetically diverse group of hereditary spastic paraplegias (HSP) is clinically defined by a progressive spasticity and weakness of the lower limbs, caused by distal axonopathy of the long motor axons of the corticospinal tract. Identification of more than 39 HSP[1] genes highlights intracellular membrane trafficking, mitochondrial metabolism and myelin formation as key functions involved in HSP pathogenesis.[2] Only recently lipid metabolism has emerged as another main theme in HSP pathophysiology, backed by the discovery of mutations in a number of genes involved in lipid metabolism and signaling including *CYP2U1*,[3] *CYP7B1*,[4] *DDHD1*,[3] *FA2H*,[5] *GBA2*[6] and *PNPLA6*.[7]

In this study, we have identified deleterious mutations in phospholipase *DDHD2*, the sister enzyme of PA-PLA1/*DDHD1* in two families with complicated HSP.

MATERIALS AND METHODS

Exome sequencing was performed in 79 index patients with familial forms of autosomal recessive HSP. The SureSelect Human All Exon 50 Mb kit (Agilent, Santa Clara, CA, USA) was used for in-solution enrichment; exome sequencing was performed using the Hiseq2000 instrument (Illumina, San Diego, CA, USA). Paired-end reads of 100 bp length were produced. BWA and GATK software packages[8,9] were used to align sequence reads to the reference and call variant positions. The data were then imported into Gem.app, a web-based database and analysis tool for next generation sequencing data developed by the group of S Züchner (https://secureforms.med.miami.edu/hihg/gem-app/)[10] for further analysis. An average of 82 613 347 sequence reads was produced per sample, 98.7% of which could be aligned to the targeted sequence. Mean coverage was 75.9-fold; 85.5% of the targeted sequence was covered by at least 10 reads. Variants were filtered for impact on the coding sequence, presence of either one homozygous or two heterozygous variants in one gene, frequency in public databases (minor allele frequency in dbSNP135 and NHLBI ESP6500 $<0.5\%$), conservation (GERP score >2 or PhastCons score >0.6) and genotyping quality (GATK quality index >30 and genotype quality GQ >30). Additionally, variants segregating in more than two families in Gem.app were removed. In addition to 79 families with complex HSP, Gem.app contained $\sim$130 families with pure HSP and $\sim$450 families with non-HSP phenotypes at the time of analysis.

Informed consent was obtained from all individuals and the Institutional Review Boards at the participating medical centers approved the study.

RESULTS

Gene identification

In family THI26003, seven homozygous SNVs and one homozygous Indel were present; two of the SNVs as well as the Indel didn't segregate with the disease. Segregating homozygous missense variants were found in *C14orf166* (NM_016039.2: c.311C>T, p.Pro104Leu; rs149288575), *FUT10* (NM_032664.3: c.473T>C, p.Leu158Pro), *IMPA1* (NM_001144879.1: c.542C>T, p.Thr181Ile) and *OTOGL*

[1]Hussman Institute for Human Genomics, University of Miami Miller School of Medicine, Miami, FL, USA; [2]Department of Pediatric Genetics, Amrita Institute of Medical Sciences and Research Center, Kerala, India; [3]Department of Neurology, University of Bonn, Bonn, Germany; [4]Department of Neurodegenerative Disease, Hertie Institute for Clinical Brain Research and Center for Neurology, Tübingen, Germany; [5]German Center of Neurodegenerative Diseases (DZNE), Tübingen, Germany
*Correspondence: Dr R Schüle, Department of Neurodegenerative Disease, Hertie Institute for Clinical Brain Research and Center for Neurology, Otfried-Müller-Str. 27, Tübingen 72076, Germany. Tel: +49 7071 29 82057; Fax: +49 7071 294254; E-mail: Rebecca.schuele-freyer@uni-tuebingen.de
Received 6 December 2012; revised 18 January 2013; accepted 22 January 2013; published online 13 March 2013

(NM_173591.3: c.3461A>G, p.Asp1154Gly); a homozygous nonsense variant in *DDHD2* (NM_001164234: c.859C>T, p.Arg287*) was the only truncating change present. Details on all the five segregating variants in family THI26003 are given in Supplementary Table 1. As it was not possible to further narrow down the list of candidate genes in family THI26003 alone based on the available in silico parameters, the resulting list of five candidate genes was used as a seed and intersected with the resulting candidate gene lists obtained by exome sequencing in the remaining 78 autosomal recessive HSP families. Another deleterious *DDHD2* variant was identified in family IHG25194 (NM_001164232.1: c.1982_1983delAT, p.Tyr661Cysfs*8) that segregates with the disease (Figure 1). Parents of the two affected siblings of this family were not available for genetic analysis, therefore a genomic deletion of one DDHD2 allele cannot be ruled out with certainty. Independent analysis of the exome data of family IHG25194 did not yield any nonsense or truncating variants other than the above described DDHD2 mutation.

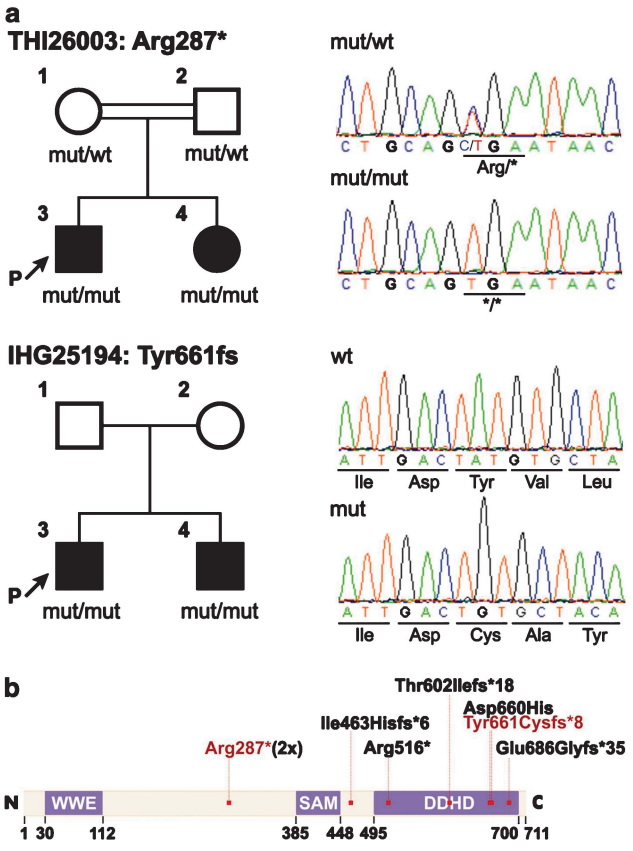

Figure 1 Pedigrees and mutations. (**a**) Pedigrees and sequence traces of the DDHD2 families. The c.859C>T mutation segregates in family THI26003 and leads to the formation of a preterminal stop signal at codon 287. The c.1982_1983delAT mutation segregates in family IHG25194; it results in a frameshift at amino acid position 661. (**b**) Schematic of the DDHD2 gene. The DDHD2 gene contains three known protein domains. The WWE domain is predicted to mediate protein interactions in ubiquitin and ADP ribose conjugation systems. The tandem SAM (sterile alpha motif domain) – DDHD domain is required for phosphoinositide binding.[14] Integrity of the family-defining DDHD domain, present in DDHD2 as well as its homolog DDHD1, is necessary for the PLA1 catalytic activity and homo-oligomerization of DDHD2. Catalytic function as well as a positively charged cluster in the SAM domain (Arg434-Lys435-Lys436) also required for phosphoinositide binding are necessary to promote membrane localization.[11,14] Mutations previously described[28] are indicated in black, novel mutations in red.

In none of the other four candidate genes additional variants were found in the remaining autosomal recessive HSP families.

Both *DDHD2* mutations will destroy the integrity of the DDHD domain and thereby affect catalytic function, membrane localization, phosphoinositide binding and homo-oligomerization (Figure 1). Both mutations therefore likely lead to a complete loss of phospholipase DDHD2 function.

Clinical description

The two siblings of family THI26003 originating from Azerbaijan (Iran) from a consanguineous family background (first degree cousins) developed a progressive spastic gait disorder since early childhood. At the time of examination (disease duration 22–13 years) they were still able to walk unsupported. Due to mental retardation both had attended a special school for mentally disabled children and were working in a sheltered workshop. Spastic paraplegia was further complicated by short stature, high arched palate and dysgenesis of the corpus callosum especially in the dorsal parts (Figures 2a and b).

The two brothers of family IHG25194 were of Indian origin and had spastic paraplegia from early childhood. No consanguinity was reported, but both parents originated from the same village and were part of the Muslim community, explaining a possible founder effect. Additional clinical signs and symptoms in both the siblings included mental retardation, mild facial dysmorphism, short stature and dysgenesis of the corpus callosum (Figures 2c and d).

Considering the usually high phenotypic variability in HSP, the phenotype between the two unrelated *DDHD2* families is astonishingly similar. Key features of *DDHD2*-related HSP appear to be spastic paraplegia, mental retardation, short stature and dysgenesis of the corpus callosum (Table 1).

DISCUSSION

Phospholipids are a key component of biological membranes. They are metabolized by the large family of phospholipases that can be classified according to their site of cleavage. The phospholipase A_1 family, consisting of extracellular and intracellular enzymes, hydrolyzes the ester bond at the sn-1 position of phospholipids, producing 2-acyl-lysophospholipids and fatty acids. In contrast to most eukaryotic organisms, mammals have three different intracellular phospholipase A_1s: phosphatidic acid preferring phospholipase A_1 (PA-PLA1/iPLA1α; *DDHD1*), the SEC23-interacting protein p125 (iPLA1β; *SEC23IP*) and phospholipase DDHD2 (iPLA1ψ; *DDHD2*).

The biological function of phospholipase DDHD2 is not fully understood. DDHD2 is ubiquitously expressed; a cytosolic and a membrane-associated pool, localizing to the cis-Golgi and the ER-Golgi intermediate compartment (ERGIC) are in a dynamic equilibrium.[11–13] Overexpression of DDHD2 leads to dispersion of the Golgi and enlargement of the perinuclear ERGIC.[12,14] Conflicting data exists about the effect of DDHD2 depletion. Morikawa *et al*[13] report a specific defect of retrograde transport from the Golgi to the ER; this defect is not confirmed by Sato *et al*[11] who instead postulate a anterograde transport defect from the Golgi to the plasma membrane. The authors contribute these differences to their use of different oligonucleotides for the knockdown of *DDHD2* in HeLa cells and possible off-target effects. In spite of these contradictions, the role of *DDHD2* in intracellular membrane trafficking is further supported by its homology to another member of the PLA1 family – p125 – that has been shown to be involved in vesicular transport from the ER to the Golgi by interacting with Sec23p, a component of the COP II complex.[15]

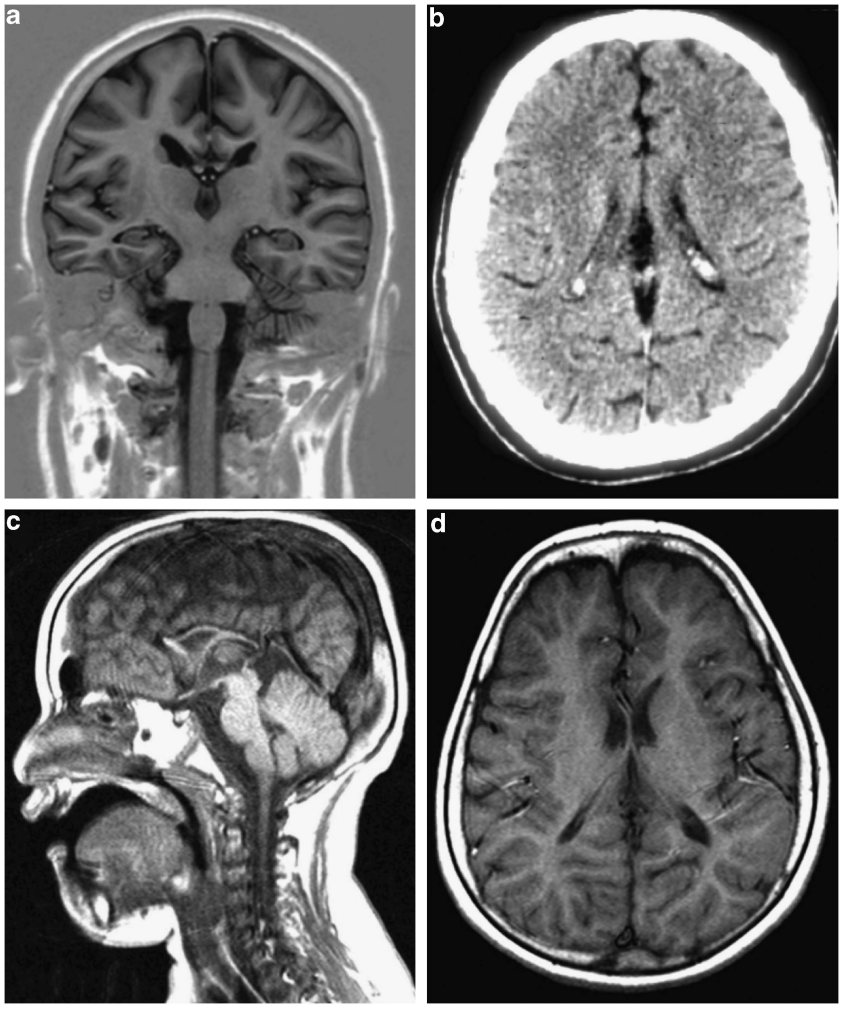

Figure 2 Cranial MRI/CT scans of DDHD2 patients. MRI/CT scans of DDHD2 patients show dysgenesis of the corpus callosum as well as some paucity of the periventricular white matter (**d**). (**a**): coronal MRI (T1 inversion recovery) of THI26003-4. (**b**): axial CT-scan of THI26003-3. (**c**): sagittal MRI (T1) of IHG25194-3. (**d**): axial MRI (T1) of IHG25194-3.

Changes in morphology and dynamics of Golgi and ER functionally connect several subtypes of HSP: Atlastin-1 (*SPG3*), the CNS expressed member of the atlastin family of GTPases, localizes predominantly to the tubular ER and to a lesser extent to the ERGIC and the cis-Golgi. It is required for the formation of three-way junctions of the ER.[16] Receptor expression-enhancing proteins (REEPs) and reticulons form large oligomeric complexes in the ER membrane that are involved in curving the ER membrane, thereby forming the characteristic tubular structure of the smooth ER. Mutations in *REEP1* (SPG31) as well as reticulon 2 (*RTN2*, SPG12) genes cause autosomal dominant forms of HSP.[17] Point mutations in *BSCL2*, causing SPG17, lead to upregulation of ER stress markers.[18] The long isoform of spastin mutated in the most common autosomal dominant subtype of HSP (*SPAST*, SPG4) forms a protein complex with atlastin-1 and REEP1 in the tubular ER network and is thought to coordinate microtubule regulation and membrane modeling.[2,17] The identification of mutations in the gene encoding DDHD2, another protein acting at the ER-to-Golgi interface therefore comes as no surprise.

In addition to its involvement in membrane trafficking, DDHD2 has been shown to possess phospholipase A1 catalytic activity towards phosphatidic acid and other phospholipids,[12,19] a function shared also by DDHD1. Phosphatidic acid has diverse biological functions. It is a precursor for the biosynthesis of triacylglycerols and phosphoglycerols. In addition to its structural functions in biological membranes,[20] it is also involved in lipid signaling.[21] This phospholipase A1 catalytic activity puts DDHD2 into context with a number of recently discovered HSP genes involved in lipid metabolism. Both seipin (*SPG17*)[22] and spartin (*SPG20*)[23] are involved in formation and regulation of lipid droplets. These dynamic organelles consist of a core of neutral lipids that are covered by a monolayer of amphiphatic lipids containing cholesterol and phospholipids. Phosphatidic acid, preferred substrate for DDHD1 and DDHD2, is essential for lipid droplet assembly.[24] The acetyl-CoA transporter *SLC33A1* located in the ER membrane and required for the formation of O-acetylated gangliosides is mutated in SPG42. Defects in the metabolism of complex lipids cause at least four more HSP subtypes: in SPG39 the deacetylation of phosphatidylcholine, the major membrane phospholipid, is defective due to mutations in phospholipase B/neuropathy target esterase (*PNPLA6*),[7] mutations in fatty acid-2 hydroxylase (*FA2H*) affect synthesis of 2-hydroxysphingolipids in

Table 1 Clinical features of genetically confirmed DDHD2 patients

Identifier	*Gender*	*Age at onset*	*Age at examination*	*Spasticity, UL/LL*	*Brisk tendon reflexes, UL/LL*	*Extensor plantar response*	*Bladder disturbance*	*Sensory deficits*	*Other signs/ symptoms*	*Imaging*	*Neurophysiology*
THI26003-3	M	~3	25	−/+	+/+	+	−	None	Mental retardation short stature high arched palate hypertelorism	TCC	NCV normal; SEP/MEP: prolonged latencies to the LL
THI26003-4	F	6	19	−/+	+/+	+	−	Vibration sense	Mental retardation saccadic eye pursuit short stature high arched palate IgA deficiency	TCC	NCV normal; SEP/MEP normal
IHG25194-3	M	0	2	−/+	+/+	+	Unknown	Unknown	Mental retardation short stature antemongoloid slant, telecanthus	TCC	Not done
IHG25194-4	M	0	9	−/+	+/+	+	Unknown	Unknown	Mental retardation short stature	TCC	NCV normal; SEP/MEP normal

Abbreviations: F, female; LL, lower limbs; M, male; MEP, motor evoked potentials; NCV, nerve conduction velocity; SEP, sensory evoked potentials; TCC, thin corpus callosum; UL, upper limbs; WMC, white matter changes.

SPG35[25] and *CYP2U1* mutations in SPG49 lead to disturbed ω- and w-1 fatty acid hydroxylation.[3] In *GBA2*, mutated in autosomal recessive HSP SPG46, the conversion of glucosylceramide to free glucose and ceramide by the non-lysosomal glucosylceramidase is deficient.[6] In SPG5 mutations in the 7α-hydroxylase gene *CYP7B1* not only lead to accumulation of oxysterols in SPG5 patients[26] but may also influence neurosteroid metabolism.[27]

During preparation of this manuscript Schuurs-Hoeijmakers *et al*[28] reported mutations in *DDHD2* in four families with autosomal recessive HSP. The phenotype in these families is strikingly similar to the clinical features reported in families THI26003 and IHG25194 with early onset spasticity, mental retardation and TCC being the overlap between all affected family members. The seven DDHD2 mutations described in Schuurs-Hoeijmakers *et al*[28] and our study comprise four frameshift, two nonsense and only one missense mutation so far (Figure 1). Of note, most mutations cluster in the DDHD domain, located in the C-terminal half of the protein. Further studies will have to clarify whether a toxic gain of function of potentially expressed truncated or mutant DDHD2 protein contributes to the phenotype. The nonsense mutation Arg287* that we identified in the Iranian family THI26003 has been described by Schuurs-Hoeijmakers *et al*[28] in another Iranian family; a founder effect is therefore possible.

The identification of mutations in *DDHD2*, which is involved in Golgi-/ER membrane trafficking and lipid metabolism further demonstrates the critical roles of these essential cellular processes in motor neuron function and helps to understand the molecular mechanisms underlying the pathogenesis of HSPs.

CONFLICT OF INTEREST

The authors declare no conflict of interest.

ACKNOWLEDGEMENTS

This study was supported by the National Institute of Health (NIH) (grants 5R01NS072248, 1R01NS075764, 5R01NS054132 to SZ), the Interdisciplinary Center for Clincial Research IZKF Tübingen (grant 1970-0-0 to RS) and the German HSP-Selbsthilfegruppe eV (grant to RS and LS). We thank Dr Tobias Lindig for his critical comments on the neuroradiological findings.

1 Schule R, Schols L: Genetics of hereditary spastic paraplegias. *Semin Neurol* 2011; **31**: 484–493.
2 Blackstone C: Cellular pathways of hereditary spastic paraplegia. *Annu Rev Neurosci* 2012; **35**: 25–47.
3 Tesson C, Nawara M, Salih MA *et al*: Alteration of Fatty-Acid-metabolizing enzymes affects mitochondrial form and function in hereditary spastic paraplegia. *Am J Hum Genet* 2012; **91**: 1051–1064.
4 Tsaousidou MK, Ouahchi K, Warner TT *et al*: Sequence alterations within CYP7B1 implicate defective cholesterol homeostasis in motor-neuron degeneration. *Am J Hum Genet* 2008; **82**: 510–515.
5 Dick KJ, Eckhardt M, Paisan-Ruiz C *et al*: Mutation of FA2H underlies a complicated form of hereditary spastic paraplegia (SPG35). *Hum Mutat* 2010; **31**: E1251–E1260.
6 Martin E, Schule R, Smets K *et al*: Loss of function of glucocerebrosidase GBA2 is responsible for motor neuron defects in hereditary spastic paraplegia. *Am J Hum Genet* 2013; **92**: 238–244.
7 Rainier S, Bui M, Mark E *et al*: Neuropathy target esterase gene mutations cause motor neuron disease. *Am J Hum Genet* 2008; **82**: 780–785.
8 Li H, Durbin R: Fast and accurate long-read alignment with Burrows-Wheeler transform. *Bioinformatics* 2010; **26**: 589–595.
9 McKenna A, Hanna M, Banks E *et al*: The Genome Analysis Toolkit: a MapReduce framework for analyzing next-generation DNA sequencing data. *Genome Res* 2010; **20**: 1297–1303.
10 Gonzalez M, Acosta Lebrigio R, van Booven DJ *et al*: GEnomes Management Application (GEM.app): A new web tool for large-scale collaborative genome analysis. *Hum Mutat* 2013 (in press).
11 Sato S, Inoue H, Kogure T, Tagaya M, Tani K: Golgi-localized KIAA0725p regulates membrane trafficking from the Golgi apparatus to the plasma membrane in mammalian cells. *FEBS Lett* 2010; **584**: 4389–4395.
12 Nakajima K, Sonoda H, Mizoguchi T *et al*: A novel phospholipase A1 with sequence homology to a mammalian Sec23p-interacting protein, p125. *J Biol Chem* 2002; **277**: 11329–11335.
13 Morikawa RK, Aoki J, Kano F *et al*: Intracellular phospholipase A1gamma (iPLA1-gamma) is a novel factor involved in coat protein complex I- and Rab6-independent retrograde transport between the endoplasmic reticulum and the golgi complex. *J Biol Chem* 2009; **284**: 26620–26630.
14 Inoue H, Baba T, Sato S *et al*: Roles of SAM and DDHD domains in mammalian intracellular phospholipase A(1) KIAA0725p. *Biochim Biophys Acta* 2012; **1823**: 930–939.
15 Shimoi W, Ezawa I, Nakamoto K *et al*: p125 is localized in endoplasmic reticulum exit sites and involved in their organization. *J Biol Chem* 2005; **280**: 10141–10148.
16 Rismanchi N, Soderblom C, Stadler J, Zhu PP, Blackstone C: Atlastin GTPases are required for Golgi apparatus and ER morphogenesis. *Hum Mol Genet* 2008; **17**: 1591–1604.
17 Park SH, Zhu PP, Parker RL, Blackstone C: Hereditary spastic paraplegia proteins REEP1, spastin, and atlastin-1 coordinate microtubule interactions with the tubular ER network. *J Clin Invest* 2010; **120**: 1097–1110.
18 Yagi T, Ito D, Nihei Y, Ishihara T, Suzuki N: N88S seipin mutant transgenic mice develop features of seipinopathy/BSCL2-related motor neuron disease via endoplasmic reticulum stress. *Hum Mol Genet* 2011; **20**: 3831–3840.
19 Tani K, Mizoguchi T, Iwamatsu A, Hatsuzawa K, Tagaya M: p125 is a novel mammalian Sec23p-interacting protein with structural similarity to phospholipid-modifying proteins. *J Biol Chem* 1999; **274**: 20505–20512.

20 Kooijman EE, Chupin V, de Kruijff B, Burger KN: Modulation of membrane curvature by phosphatidic acid and lysophosphatidic acid. *Traffic* 2003; **4**: 162–174.
21 Wang X, Devaiah SP, Zhang W, Welti R: Signaling functions of phosphatidic acid. *Prog Lipid Res* 2006; **45**: 250–278.
22 Boutet E, El Mourabit H, Prot M *et al*: Seipin deficiency alters fatty acid Delta9 desaturation and lipid droplet formation in Berardinelli-Seip congenital lipodystrophy. *Biochimie* 2009; **91**: 796–803.
23 Eastman SW, Yassaee M, Bieniasz PD: A role for ubiquitin ligases and Spartin/SPG20 in lipid droplet turnover. *J Cell Biol* 2009; **184**: 881–894.
24 Fei W, Shui G, Zhang Y *et al*: A role for phosphatidic acid in the formation of "supersized" lipid droplets. *PLoS Genet* 2011; **7**: e1002201.
25 Hama H: Fatty acid 2-Hydroxylation in mammalian sphingolipid biology. *Biochim Biophys Acta* 2010; **1801**: 405–414.
26 Schule R, Siddique T, Deng HX *et al*: Marked accumulation of 27-hydroxycholesterol in SPG5 patients with hereditary spastic paresis. *J Lipid Res* 2010; **51**: 819–823.
27 Fex Svenningsen A, Wicher G, Lundqvist J, Pettersson H, Corell M, Norlin M: Effects on DHEA levels by estrogen in rat astrocytes and CNS co-cultures via the regulation of CYP7B1-mediated metabolism. *Neurochem Int* 2011; **58**: 620–624.
28 Schuurs-Hoeijmakers JH, Geraghty MT, Kamsteeg EJ *et al*: Mutations in DDHD2, Encoding an Intracellular Phospholipase A(1), Cause a Recessive Form of Complex Hereditary Spastic Paraplegia. *Am J Hum Genet* 2012; **91**: 1073–1081.

Supplementary Information accompanies this paper on European Journal of Human Genetics website (http://www.nature.com/ejhg)

Motor protein mutations cause a new form of hereditary spastic paraplegia

Andrés Caballero Oteyza, MSc
Esra Battaloğlu, PhD
Levent Ocek, MD
Tobias Lindig, MD
Jennifer Reichbauer, BSc
Adriana P. Rebelo, PhD
Michael A. Gonzalez, MSc
Yasar Zorlu, MD
Burcak Ozes, MSc
Dagmar Timmann, MD
Benjamin Bender, MD
Günther Woehlke, PhD
Stephan Züchner, MD, PhD
Ludger Schöls, MD
Rebecca Schüle, MD

Correspondence to Dr. Schüle: r.schule@med.miami.edu

ABSTRACT

Objective: To identify a novel disease gene in 2 families with autosomal recessive hereditary spastic paraplegia (HSP).

Methods: We used whole-exome sequencing to identify the underlying genetic disease cause in 2 families with apparently autosomal recessive spastic paraplegia. Endogenous expression as well as subcellular localization of wild-type and mutant protein were studied to support the pathogenicity of the identified mutations.

Results: In 2 families, we identified compound heterozygous or homozygous mutations in the kinesin gene *KIF1C* to cause hereditary spastic paraplegia type 58 (SPG58). SPG58 can be complicated by cervical dystonia and cerebellar ataxia. The same mutations in a heterozygous state result in a mild or subclinical phenotype. *KIF1C* mutations in SPG58 affect the domains involved in adenosine triphosphate hydrolysis and microtubule binding, key functions for this microtubule-based motor protein.

Conclusions: *KIF1C* is the third kinesin gene involved in the pathogenesis of HSPs and is characterized by a mild dominant and a more severe recessive disease phenotype. The identification of *KIF1C* as an HSP disease gene further supports the key role of intracellular trafficking processes in the pathogenesis of hereditary axonopathies. ***Neurology*® 2014;82:2007–2016**

GLOSSARY

ATP = adenosine triphosphate; **BICDR-1** = bicaudal-D-related protein 1; **DMEM** = Dulbecco's modified Eagle medium; **FCS** = fetal calf serum; **HSP** = hereditary spastic paraplegia; ***HSP60*** = heat shock 60kDa protein 1; ***KIF1C*** = kinesin family member 1C; **p-loop** = phosphate-binding loop; **SPG58** = hereditary spastic paraplegia type 58; **WB** = Western blot; **WES** = whole-exome sequencing.

Hereditary spastic paraplegias (HSPs) are among the most heterogeneous mendelian diseases.[1] The pathologic hallmark of HSPs is a length-dependent distal axonopathy of the upper motor neurons. To maintain their high degree of polarization, corticospinal tract motor neurons critically depend on efficient mechanisms to selectively distribute proteins and membrane components throughout the cell. It is therefore not surprising that a large number of HSP proteins interfere with membrane trafficking pathways in various ways: by affecting membrane curvature and/or the morphology of the endoplasmic reticulum (Reep1, RTN2, spastin, atlastin-1), by modifying vesicle sorting and trafficking along the secretory or endosomal pathway (adapter protein complexes, strumpellin, vcp, vps37a), or by disturbing axonal transport (KIF5A, spastin) (reviewed in reference 2).

In this study, we used whole-exome sequencing (WES) to identify the genetic cause of a novel form of complicated HSP, termed hereditary spastic paraplegia type 58 (SPG58).

METHODS

Exome sequencing. WES was performed on the index patients of families THI26001 (P3) and IHG25215 (P5) (figure 1A). After exome capture via the SureSelect Human All Exon 50 Mb kit (Agilent, Santa Clara, CA), samples were sequenced on HiSeq2000 instruments (Illumina, San Diego, CA). An average of 70,811,663 sequence reads of 100–base pair length were produced per sample, 98.8% of

Supplemental data at Neurology.org

From the Hertie-Institute for Clinical Brain Research (A.C.O., J.R., L.S., R.S.), Department of Neurodegenerative Diseases, University of Tübingen, Germany; Bogazici University (E.B., B.O.), Department of Molecular Biology and Genetics, Istanbul; Tepecik Research and Training Hospital (L.O., Y.Z.), Clinics of Neurology, Izmir, Turkey; Diagnostic and Interventional Neuroradiology (T.L., B.B.), Department of Radiology, University Hospital Tübingen; German Research Center for Neurodegenerative Diseases (DZNE) (J.R., R.S., L.S.), Tübingen, Germany; Dr. John T. Macdonald Foundation Department of Human Genetics and John P. Hussman Institute for Human Genomics (A.P.R., M.A.G., S.Z., R.S.), University of Miami Miller School of Medicine, FL; Department of Neurology (D.T.), University of Duisburg-Essen; and Department of Physics E22 (Biophysics) (G.W.), Technical University Munich, Garching, Germany.

Go to Neurology.org for full disclosures. Funding information and disclosures deemed relevant by the authors, if any, are provided at the end of the article.

Figure 1 Pedigrees and mutations in the *KIF1C* gene

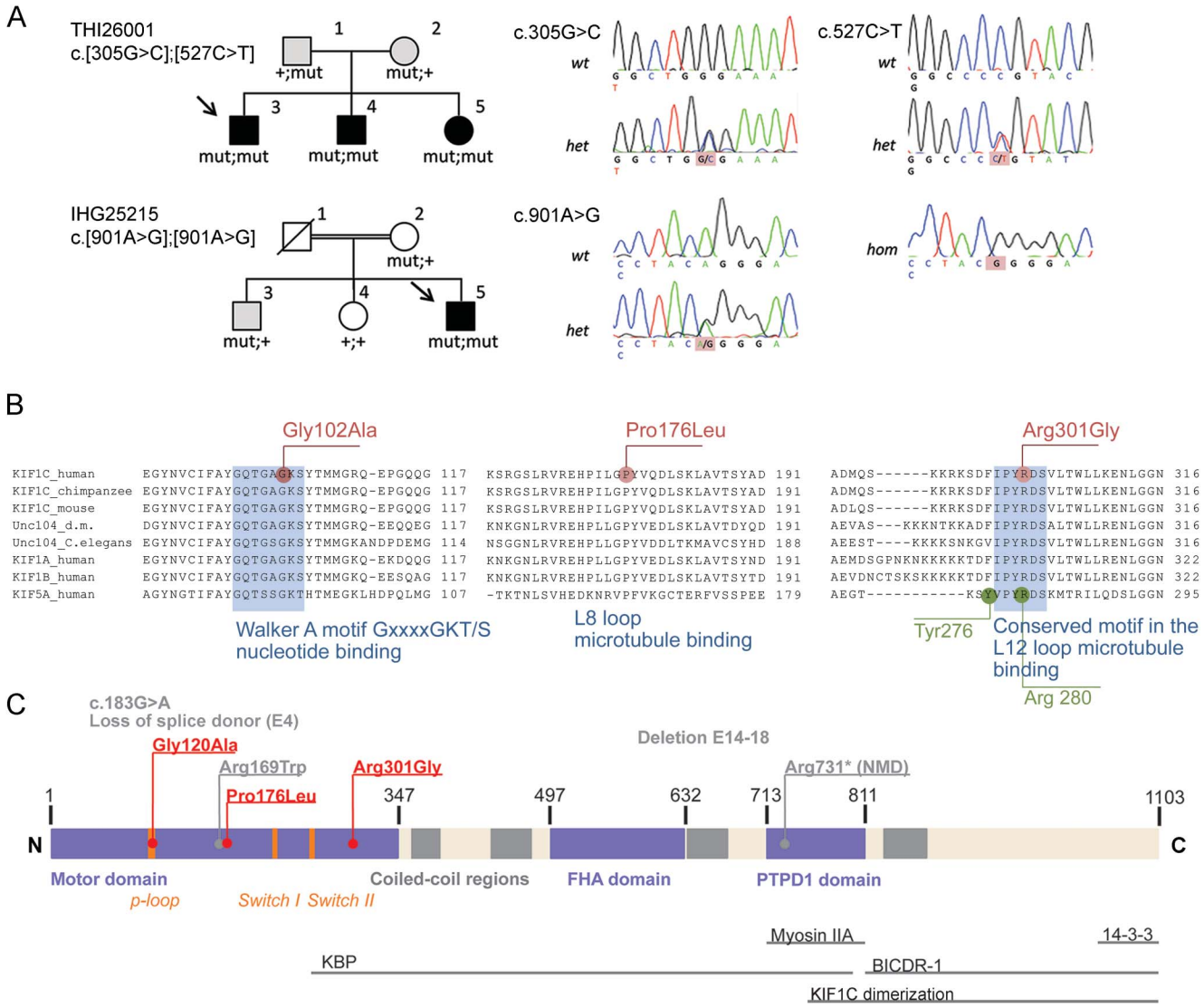

(A) The *KIF1C* variants c.[305G>C];[527C>T], p.[Gly102Ala];[Pro176Leu], and c.[901A>G];[901A>G], p.[Arg301Gly];[Arg301Gly] segregate in families THI26001 and IHG25215, respectively. Severely affected family members are depicted by black boxes and are homozygous or compound heterozygous for the respective mutations. Mildly or subclinically affected family members are depicted by gray boxes and are carriers of one mutant allele each. Electropherograms are shown on the right. (B) All 3 *KIF1C* mutations (red) affect amino acids that are highly conserved across species as well as among kinesin-3 and -1 families. Gly102Ala is located within the Walker A motif (GxxxxGKT/S) of the so called p-loop, essential for nucleotide binding, and therefore likely renders KIF1C catalytically inactive. Both Pro176Leu (loop 8) and Arg301Gly (loop 12) affect the microtubule binding interface of KIF1C. *KIF5A* mutations causing autosomal dominant SPG10 are shown in green. The uniprot alignment tool was used to generate alignments with the following protein identifiers: KIF1C_human: O43896; KIF1C_chimpanzee: K7BP32; KIF1C_mouse: O35071; unc104_d.m.: A1ZAJ2; unc104_*C elegans*: P23678; KIF1A_human: Q12756; KIF1B_human: O60333; and KIF5A_human: Q12840. (C) Domain structure of the *KIF1C* gene. Known interaction partners and putative binding regions of *KIF1C* are depicted by horizontal lines. Mutations detected in this study are indicated in red, mutations published by Dor et al.[26] in gray.

which could be aligned to the target sequence. Mean coverage was 57-fold. Data were analyzed using the browser interface of the Genomes Management Application GEM.app.[3] Candidate variants were confirmed with conventional Sanger sequencing.

Cell culture. Fibroblast lines were established from skin biopsies using standard procedures. Cells were grown in Dulbecco's modified Eagle medium (DMEM) plus 10% fetal calf serum (FCS) and maintained at 37°C and 5% CO_2. Lymphocytes were isolated from blood samples and immortalized by exposure to Epstein-Barr virus. Cells were cultivated in Roswell Park Memorial Institute medium plus 20% FCS and maintained at 37°C and 5% CO_2. The motor neuron–like hybrid cell line NSC-34 and the fibroblast-like cell line COS-7 were cultured in DMEM plus 10% FCS at 37°C, 5% CO_2.

Quantitative PCR. RNA was extracted and transcribed using standard protocols. Control fibroblasts and lymphoblasts were matched to patient cells for age (±5 years), sex, and cell passage (±2 passages). Quantitative PCR was run on a LightCycler 480 device (Roche Applied Science, Penzberg, Germany).

Western blot. Protein was isolated from primary fibroblast and lymphoblast cell lines using standard protocols. After sodium dodecyl sulfate–polyacrylamide gel electrophoresis, samples were

transferred onto a polyvinylidene difluoride membrane, washed 3 times with 1x Tris-buffered saline/Tween 20, and blocked with 1x Tris-buffered saline/Tween 20 + 5% skimmed milk. The membrane was incubated with the primary antibody overnight in blocking buffer and with the secondary antibody for 1 hour at room temperature. Detection was performed using ECL reagent (Thermo Fisher Scientific, Waltham, MA).

Cloning. The *KIF1C* ORF was amplified from a complementary DNA clone[4] and transferred into a pcDNA3.1/CT-GFP-TOPO expression vector (Invitrogen, Carlsbad, CA). Site-directed mutagenesis was performed on the resulting pTOPO-GFP-KIF1C$_{wt}$, using QuikChange II XL (Agilent), introducing the human mutations c.305G>C (pTOPO-GFP-KIF1C$_{Gly102Ala}$), c.527C>T (pTOPO-GFP-KIF1C$_{Pro176Leu}$), and c.901A>G (pTOPO-GFP-KIF1C$_{Arg301Gly}$). Identity with the reference sequence (NM_006612.5) and introduction of the desired mutations was confirmed by conventional sequencing. Restriction enzyme digest was used to transfer the inserts to pmCherry-N1 (Clontech Laboratories, Mountain View, CA).

Immunofluorescence. Cells were fixed in 4% paraformaldehyde and stained with specific primary antibodies and Alexa-conjugated secondary antibodies. Cells were mounted on coverslips with Prolong Gold Antifading Reagent with DAPI (4',6-diamidino-2-phenylindole) (Invitrogen). Pictures were taken with a Zeiss LSM 710 inverted confocal microscope using the ZEN2010 software (Carl Zeiss Corporation, Oberkochen, Germany). Finally, images were processed with the ImageJ software (http://rsbweb.nih.gov).

Antibodies. The following antibodies were used: rabbit polyclonal anti-KIF1C (AKIN11; Cytoskeleton Inc., Denver, CO), dilution 1:250 (immunofluorescence) and 1:500 (Western blot [WB]); mouse monoclonal anti-α-tubulin (A-11126; Invitrogen), dilution 1:200 (immunofluorescence); mouse monoclonal anti-α-tubulin (T6074; Sigma-Aldrich, St. Louis, MO), dilution 1:5,000 (WB); and mouse anti-GAPDH (glyceraldehyde 3-phosphate dehydrogenase) (clone 6C5; Millipore Corporation, Billerica, MA), dilution 1:5,000 (WB).

Statistics. Statistical analyses were performed using SPSS software version 20 for Mac (IBM Corporation, Armonk, NY). Two-sided *t* tests were used to compare KIF1C levels between groups.

Standard protocol approvals, registrations, and patient consents. Informed consent was obtained from all individuals involved in the study, and the institutional review boards of the participating medical centers approved the study.

RESULTS

Exome sequencing and identification of the *KIF1C* gene (SPG58). We performed WES in the index patient of a German family with apparently autosomal recessive HSP (THI26001, figure 1A) and filtered the resulting variants for allele frequency (EVS6500 <0.5%), genotype frequency in the GEM.app database (number of families with segregating variant ≤10), conservation across species (GERP score >1 or PhastCons score >0.4), effect on protein function (Polyphen-2 score >0.3), and quality (GATK QUAL score >50, genotype quality GQ >50). None of the known HSP genes contained any variants matching the filter criteria. Only 5 potentially novel candidate genes remained on the hit list, containing either 2 heterozygous (n = 4) or 1 homozygous (n = 1) variant: *KIF1C*, *LYST*, *TENM1*, *SAMD11*, and *OVOS*. To narrow down this candidate gene list, we analyzed all variants for cosegregation with the disease. Only the 2 variants in the *KIF1C* gene (NM_006612.5) cosegregated completely: c.[305G>C];[527C>T], p.[Gly102Ala];[Pro176Leu] (figure 1A, table e-1 on the *Neurology*® Web site at Neurology.org).

To further support the role of *KIF1C* as a disease gene, we revisited the exomes of 186 index patients with genetically unresolved HSP (n = 126), ataxia (n = 30), or spastic ataxia (n = 30) compatible with autosomal recessive modes of inheritance. One additional family (IHG25215) carried a highly conserved unknown homozygous *KIF1C* variant: c.[901A>G];[901A>G], p.[Arg301Gly];[Arg301Gly]. This variant cosegregated with disease (figure 1A).

Clinical description of SPG58 families. *THI26001.* All 3 affected siblings presented with adult-onset (18–30 years) spastic ataxia with predominant lower limb spasticity and weakness. Cerebellar ataxia was present in all 3 with cerebellar oculomotor disturbance (2/3) and upper > lower limb ataxia (3/3). Dorsal column sensory deficits (3/3) were rather pronounced compared with most other HSP subtypes. Although not formally tested, none of the family members showed an indication of cognitive involvement. Details on the phenotype are given in table 1.

Neurophysiologic studies indicated a widespread demyelinating process with central and peripheral involvement. Motor evoked potentials showed increased central motor conduction times at early disease stages and were later absent when recorded from the upper and the lower limbs. The long sensory tracts were similarly involved with prolonged or absent cortical potentials. Increased latencies were also observed for visual (2/3) and auditory (1/3) evoked potentials. One sibling showed peripheral involvement with a demyelinating sensory-motor peripheral neuropathy.

MRIs revealed signs of widespread T2 hyperintensities primarily affecting the pre- and postcentral white matter, pyramidal tracts, superior cerebellar peduncles, and the occipital white matter with relative sparing of the optic radiations (figure 2).

Both parents are carriers of one of the *KIF1C* mutations. The father had consulted a neurologist a few weeks prior because of a subjective limping and some sensory deficits in his legs. The mother reported no gait problems. Closer clinical examination revealed a carrier phenotype in both of them, consisting of lower limb weakness with central distribution (proximal > distal, hip abductors > hip adductors) and demyelinating sensory-motor neuropathy in the father (Gly102Ala) and mild signs of pyramidal involvement (brisk reflexes, extensor plantar response) in the mother (Pro176Leu). The MRIs of both parents also showed T2

Table 1 Phenotypes and characteristics of the families

	THI26001-3	THI26001-4	THI26001-5	THI26001-1	THI26001-2	IHG25125-5	IHG25125-3
Origin	Germany	Germany	Germany	Germany	Germany	Turkey	Turkey
Sex	Male	Male	Female	Male	Female	Male	Male
Genotype	Gly102Ala/Pro176Leu	Gly102Ala/ Pro176Leu	Gly102Ala/Pro176Leu	Gly102Ala/wt	Wt/Pro176leu	Arg301Gly/ Arg301Gly	Arg301Gly/wt
Age at onset, y	18	30	18	69	NA	10	16
Age at last examination, y	48	45	42	69	67	48	46
Severity SPRS	30	26	27	7	3	ND	ND
UL							
Spasticity	–	–	+	–	–	–	–
Reflexes	Normal	Normal	Increased	Decreased	Increased	Normal	
Weakness	–	–	–	–	–	–	–
Amyotrophy	–	–	–	–	–	–	–
LL							
Spasticity	+++	++	+++	-	-	+++	++
Reflexes	Increased	Increased	Increased	Normal	Increased	Increased	Increased
Weakness	+ (distal predominant)	+	++ (distal predominant)	+ (proximal predominant)	–	++ (distal predominant)	+ (distal predominant)
Amyotrophy	–	–	–	–	–	–	–
Extensor plantar sign	+	+	+	–	+	+	+
Cognition	Normal	Normal	Normal	Normal	Normal	Normal	Normal
Oculomotor disturbance	Upward vertical gaze palsy	Cerebellar (saccadic pursuit, gaze-evoked nystagmus)	Cerebellar (saccadic pursuit, gaze-evoked nystagmus, dysmetric saccades)	–	–	–	–
Cerebellar ataxia	UL > LL limb ataxia, UL intention tremor	UL > LL limb ataxia, UL intention tremor	UL > LL limb ataxia, UL intention tremor	–	–	–	–
Dysarthria	Mild	Mild	Moderate			Mild	–
Dystonia	–	–	Mild cervical dystonia	–	–	–	–
Vibration sense	LL distal absent	LL distal reduced	LL distal reduced	LL distal reduced	LL distal absent	LL distal absent	LL distal absent
Urinary symptoms	–	–	–	–	–	–	–
Other symptoms	Irregular head tremor	–	–	–	–	–	–
Nerve conduction studies	Normal	Demyelinating sensory-motor neuropathy	Normal	Demyelinating sensory-motor neuropathy	ND	ND	Sensory-motor neuropathy
Evoked potentials	VEP: increased latency; AEP: normal; MEP: not possible because of head tremor; Tib-SEP: no cortical potential	VEP: increased latency; AEP: increased latency over brainstem; MEP: UL/LL no potential; Tib-SEP: no cortical potential	VEP: normal; AEP: normal; MEP: UL/LL no potential (at age 34 prolonged CMCT); Tib-SEP: increased latency cortical potential	ND	ND	ND	VEP: normal; AEP: normal; MEP: ND; Tib-SEP: no cortical potential
Imaging	MRI: T2 hyperintensities (pre-/postcentral/occipital white matter, pyramidal tract, superior cerebellar peduncles), mild global cerebral atrophy, pronounced tegmental and vermian cerebellar atrophy	ND	MRI: T2 hyperintensities (pre-/postcentral/ occipital white matter, pyramidal tract, superior cerebellar peduncles), mild vermian cerebellar and spinal atrophy	MRI: mild T2 hyperintensities (pyramidal tract, optic radiation), mild cerebellar atrophy	MRI: mild T2 hyperintensities (pyramidal tract, superior cerebellar peduncles)	ND	MRI: mild T2 hyperintensities (pyramidal tract)

Abbreviations: AEP = auditory evoked potentials; CMCT = central motor conduction time; LL = lower limbs; MEP = motor evoked potentials; ND = not done; Tib-SEP = tibial sensory evoked potentials; SPRS = Spastic Paraplegia Rating Scale; UL = upper limbs; VEP = visual evoked potentials; wt = wild-type.

Figure 2 Brain MRI of family THI26001

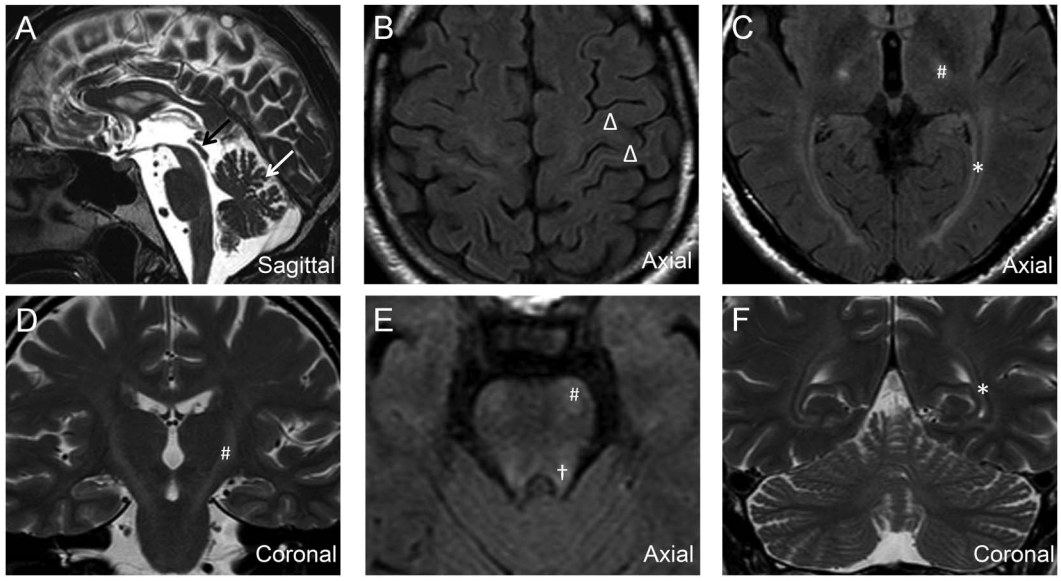

Brain T2-weighted imaging (B, C, E, fluid-attenuated inversion recovery) of THI26001-3 (age 48 years) reveals symmetrical T2-hyperintense cerebral and mild cerebellar demyelination affecting the pre- and postcentral white matter (Δ in B), the pyramidal tracts (# in C–E), the occipital white matter with relative sparing of the optic radiations (* in C and F), and the superior cerebellar peduncles († in E). The midsagittal view (A) shows mild tegmental (black arrow) and vermian cerebellar (white arrow) atrophy.

hyperintensities with a similar pattern, albeit less intense than in the affected offspring (figure e-1).

IHG25215. The 2 affected siblings of consanguineous descent (parents first-degree cousins) of family IHG25215 both reported an unsteady gait since their adolescence, but with different disease course. While the disease progressed insidiously in the younger brother (IHG25215-5), leading to loss of the ability to walk and caregiver dependency in his early 40s, the disease was apparently stable in the older brother (IHG25215-3) who is working full-time and displays only mildly spastic gait not interfering with his daily activities at age 46.

On examination, both brothers exhibited a lower limb spastic paraparesis, mild in IHG25215-3 and severe in IHG25215-5. In the latter, additionally mild cervical dystonia and loss of vibration sense in the lower extremities were noted. The mother of the 2 siblings (IHG25215-2) reported no gait problems at the age of 67 and her neurologic examination was normal. Cognition appeared normal in all family members.

IHG25215-2 and -3 received a neurophysiologic examination. While normal in the mother, the mildly affected sibling showed absence of somatosensory evoked cortical potentials and sensory-motor neuropathy.

Localization of mutations. KIF1C is a kinesin-type microtubule-dependent motor protein that belongs to the kinesin-3 subfamily. It contains an N-terminal conserved kinesin motor domain with several characteristic features: the phosphate-binding loop (p-loop) responsible for adenosine triphosphate (ATP) hydrolysis and propagation of nucleotide-dependent conformational changes from the ATP binding pocket to the microtubule binding region. The latter is often called switch-2 cluster and is formed by helix α4, loop L12, helix α5, and supporting structures[5] (figure 1C). In addition, members of the kinesin-3 subfamily contain a stretch of positively charged lysine residues thought to enhance microtubule binding[6] (k-loop). The SPG58 mutations are found in the p-loop and the switch-2 cluster.

Gly102 is located within the highly conserved Walker A motif of the nucleotide binding p-loop. Mutation of this glycine residue to alanine presumably renders KIF1C catalytically inactive, as noted for the neighboring Lys103Ala mutation.[7] The mutant may no longer be capable of binding nucleotide, and is possibly less stable (see below).

Pro176 is part of loop 8 of the kinesin's motor domain and thus close to the microtubule interaction domain. Functional studies are lacking. Arg301 lies at the core of a highly conserved motif in the L12 loop, involved in microtubule interaction. The homologous amino acid in KIF5A (Arg280) is a mutational hotspot in the autosomal dominant HSP subtype SPG10.[8,9] The Arg280Ala mutant has been shown to reduce microtubule affinity in vitro, suggesting impaired transport rates.[10]

Impact of identified mutations on KIF1C expression. To check whether the mutations affect expression levels of

KIF1C, we compared messenger RNA and protein levels between lymphoblasts and fibroblasts of family THI26001 with age- and sex-matched controls. KIF1C messenger RNA levels among those affected, heterozygous carriers, and controls (figure e-2A) were not significantly different applying quantitative real-time PCR to lymphoblasts. In contrast, protein levels of KIF1C in lymphoblasts of affected persons were reduced to 45% in WBs. These results were confirmed in patient-derived fibroblasts, in which KIF1C protein was reduced to a level of 58% (figure e-2, B and C). The polyclonal antibody used is directed against the KIF1C neck domain and does not specifically recognize wild-type or mutant KIF1C. Of note, the heterozygous carrier of the Gly102Ala mutation (father, P1) showed KIF1C protein levels comparable to his affected offspring (P3-5), whereas KIF1C protein levels in the carrier of the Pro176Leu mutation (mother, P2) were comparable to the control probands' levels. This pattern indicates that the Gly102Ala mutation renders the KIF1C protein less stable, leading to significantly reduced protein levels.

Subcellular localization of endogenous KIF1C protein. We have studied the localization of KIF1C in several cell lines, including human primary fibroblasts (data not shown), a fibroblast-like cell line (COS-7), a human

Figure 3 Subcellular localization of endogenous and overexpressed KIF1C

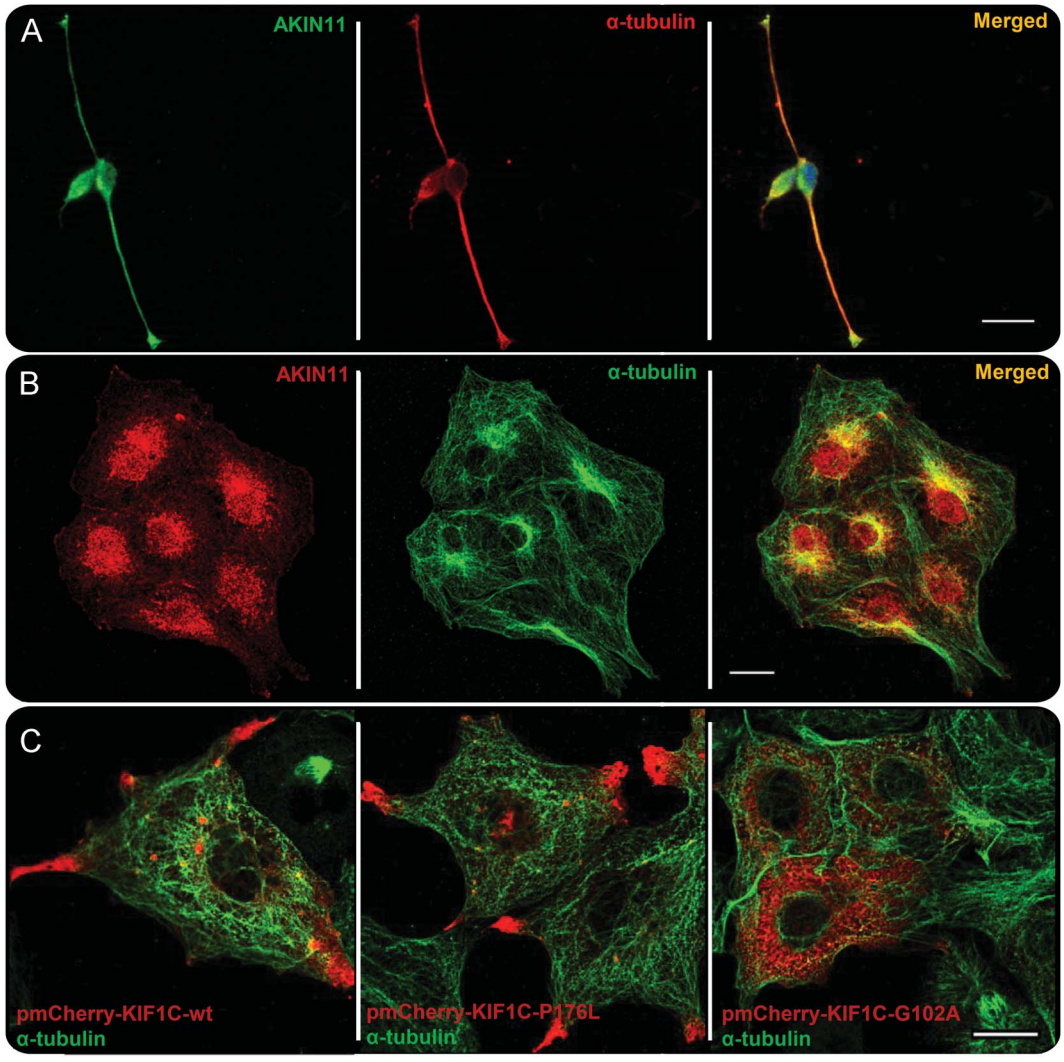

(A, B) Endogenous KIF1C. In the mouse motor neuron–like spinal cord cell line NSC-34, endogenous KIF1C is found throughout the cell body with an accumulation in the pericentrosome and along the neurites, and strong accumulation at the neurite tips (A). In fibroblast-like COS-7 cells, endogenous KIF1C is sparsely distributed throughout the cell and accumulates perinuclear in a reticular pattern (B). In COS-7 cells displaying cellular processes, accumulation at the tips of these processes can be seen (not shown). (C) Overexpressed, mCherry-tagged KIF1C accumulates at the tips of cellular processes in the COS-7 monkey fibroblast cell line (left). The same localization pattern can be observed for mCherry-tagged KIF1C-$_{Pro176Leu}$ (middle). In contrast, mCherry-tagged KIF1C$_{Gly102Ala}$ (right) fails to reach cellular processes and instead is observed in a reticular pattern around the nucleus. 200-μm scale bar.

neuroblastoma cell line (SH-SY5Y, data not shown), and a mouse spinal cord motor neuron cell line (NSC-34). As described in the literature,[7,11,12] KIF1C was located mainly in the perinuclear area with an accumulation in the pericentrosomal region. In cells forming cellular processes, i.e., NSC-34 cells or a subset of COS-7 cells, KIF1C was additionally localized along cellular processes and enriched at their tips (figure 3, A and B).

Subcellular localization of overexpressed wild-type and mutant KIF1C protein. Similarly, we found overexpressed wild-type KIF1C (pmCherry-KIF1C$_{wt}$) in the perinuclear region and strongly accumulating in the cellular processes of COS-7 cells (figure 3C). Overexpressed KIF1C$_{Pro176Leu}$ (pmCherry-KIF1C$_{Pro176Leu}$) showed a localization pattern indistinguishable from wild-type. Overexpressed KIF1C$_{Gly102Ala}$ (pmCherry-KIF1C$_{Gly102Ala}$) as well as KIF1C$_{Arg301Gly}$, however, failed to reach the tips of cellular processes and instead accumulated in a reticular pattern in a wide area around the nucleus of COS-7 cells (figure 3C, data for KIF1C$_{Arg301Gly}$ not shown).

In family THI26001, severely affected subjects carry a mixture of 2 mutant alleles, whereas the very mildly affected heterozygous mutation carriers possess only one of the mutant copies in a wild-type background. Two kinesin-3 motors closely related to KIF1C have been studied in vitro, mouse KIF1A and *Caenorhabditis elegans* Unc104.[13–15] Both appear to be active in vivo as dimers. To mimic the human situation more closely, we simultaneously overexpressed each of the mutants together with wild-type and a combination of both mutants together. As expected from the mono-overexpression experiments, simultaneous overexpression of KIF1C$_{Pro176Leu}$ and KIF1C$_{wt}$ led to colocalization of both alleles in a distribution indistinguishable from wild-type (figure 4B). Of note, upon co-overexpression of KIF1C$_{Gly102Ala}$ and KIF1C$_{wt}$, the normal distribution pattern could partially be restored and both KIF1C$_{Gly102Ala}$ and KIF1C$_{wt}$ colocalized at the tips of cellular processes (figure 4C). Overexpression of KIF1C$_{Pro176Leu}$ together with KIF1C$_{Gly102Ala}$, however, failed to restore the localization at the tips of cellular processes. Moreover, KIF1C$_{Pro176Leu}$, which shows a normal localization pattern when overexpressed alone or together with KIF1C$_{wt}$, also became trapped in the reticular perinuclear localization pattern typical for the KIF1C$_{Gly102Ala}$ mutant (figure 4D).

DISCUSSION HSPs are genetically highly heterogeneous. However, despite at least 38 known HSP genes, approximately one-third of dominant and at least half of recessive cases still cannot be explained by mutations in known genes. In this study, we uncovered the genetic basis for a new subtype of HSP with autosomal dominant and recessive inheritance—termed SPG58.

Our approach exemplifies the power of exome sequencing to identify novel disease genes even in small families, especially when combined with classic segregation analysis and access to a "validation cohort" of cases with similar phenotypes. Considering the long lists of candidate genes typically generated by exome sequencing of single families, the latter is absolutely essential to gain additional evidence for the pathogenic relevance of a novel disease gene. Collection of these "exome repositories," however, can be challenging, especially for rare diseases, and requires large collaborative efforts.[3]

KIF1C belongs to the large family of kinesin motor proteins and represents the third kinesin gene involved in the pathogenesis of HSP: mutations in the kinesin heavy chain gene *KIF5A*, encoding the main neuronal motor for long-range axonal transport, cause autosomal dominant SPG10,[16,17] and mutations in *KIF1A* cause autosomal recessive SPG30.[18,19] Kinesins are a large family of microtubule-dependent motor proteins that are involved in intracellular transport and organization of the mitotic spindle. KIF1C was first identified as a binding partner of tyrosine phosphatase PTPD1 and recognized, together with KIF1A, as a member of the so-called kinesin-3/KIF1 family based on sequence homology and the presence of a forkhead-associated domain.[7] Endogenous KIF1C is localized at the pericentrosome, in the region of the Golgi apparatus,[7] and in the cell periphery with accumulation at the tips of cellular processes, colocalizing with microtubule plus-ends.[12,20] Although the precise function of KIF1C still is not clear, it has been implicated in retrograde vesicular transport between Golgi and endoplasmic reticulum,[7] maintenance and reformation of podosomes in macrophages,[20] and stabilization of trailing adhesions in migrating cells.[12] Knockdown of KIF1C in hippocampal neurons leads to defective neurite outgrowth.[11] Most known protein interactions of KIF1C require the C-terminus (figure 1C); known interaction partners comprise 14-3-3 family proteins,[21] the nonmuscle myosin II A,[20] bicaudal-D-related protein 1 (BICDR-1),[11] and kinesin binding protein KBP.[22] Notably, some of these interaction partners are themselves associated with hereditary disorders: mutations in the myosin II A *MYH9* cause sensorineural deafness, mutations in the bicaudal D homolog 2 (*BICD2*) gene, a close homolog of BICDR-1, have recently been shown to cause a spectrum of motor neuron disorders including HSP,[23] and KBP mutations are responsible for autosomal recessive Shprintzen-Goldberg syndrome.

The 3 mutations we describe in this study are all located within the highly conserved KIF1C motor domain. The p-loop mutation Gly102Ala affects the ATP binding site of the motor. Mutations of this amino acid in KIF1A and other kinesins have been shown to impair ATP hydrolysis, lead to "rigor" binding of the immobilized motor on microtubules,[24,25] and

Figure 4 Double overexpression of mCherry- and GFP-tagged mutant and wild-type *KIF1C* alleles

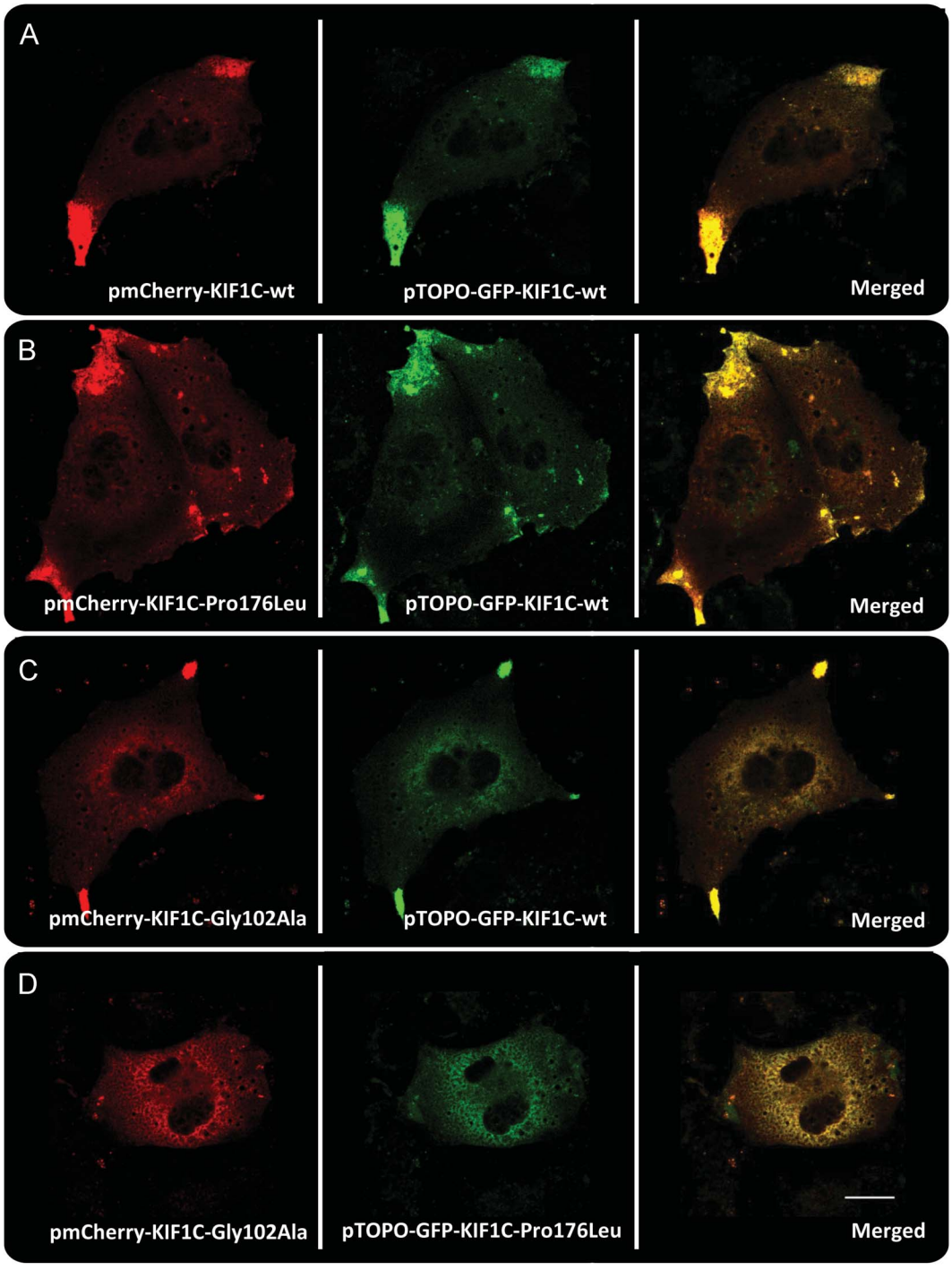

In double transfections of COS-7 cells with 2 wild-type alleles (A) or one Pro176Leu and one wild-type allele (B), the normal localization pattern consisting of a slight cytoplasmic staining combined with accumulation in cellular processes can be seen. The localization defect observed in $KIF1C_{Gly102Ala}$ mono-overexpression experiments can be partially rescued by simultaneous overexpression of $KIF1C_{wt}$ (C), but not by simultaneous overexpression of $KIF1C_{Pro176Leu}$ (D). 200-μm scale bar.

have a dominant negative effect when expressed in wild-type background.[25] Similar to the Arg301Gly mutation for which we have demonstrated reduced microtubule binding affinity and consequently reduced transport rates in the corresponding amino acid in KIF5A (Arg278),[10] the position of the Pro176Leu mutation suggests a microtubule binding defect.

While overexpression of wild-type KIF1C can rescue the perinuclear mislocalization of KIF1CGly102Ala, the KIF1CPro176Leu protein does not rescue this defect, supporting the pathogenicity of both variants.

The phenotype of SPG58 is—as is typical for HSP—variable, ranging from seemingly pure HSP to a spastic ataxia phenotype with signs of widespread

demyelination in neurophysiologic examinations and T2 hyperintensities compatible with demyelination on MRI. While this report was under review, another report of *KIF1C* mutations in 2 consanguineous families of Palestinian/Moroccan origin was published.[26] The phenotype was very similar to that of our families, with an early-onset spastic ataxia, normal cognitive function, and a similar pattern of T2 hyperintensities on MRI. Cervical dystonia, neuropathy, and reduced visual acuity were variably present.

Notably, 3 of 4 heterozygous mutation carriers that were available for examination in our study expressed a mild clinical disease phenotype as well as mild MRI changes. This dual mode of inheritance with a mild dominant disease phenotype and a more severe recessive disease expression has been previously described for at least 2 HSP subtypes. In autosomal recessive SPG7, a mild carrier phenotype mimicking autosomal dominant inheritance has been described in some families.[27] While heterozygous mutations in the heat shock protein 60 gene, *HSP60*, cause autosomal dominant pure HSP,[28] homozygous *HSP60* mutations cause an early-onset fatal hypomyelinating leukodystrophy.[29] In many ways, SPG58 exemplifies the diagnostic and counseling challenge rare hereditary diseases pose: phenotypic variability that impedes pattern recognition strategies for diagnosis, a phenotype overlapping with other disorders (hereditary ataxias and spastic paraplegias), and a mode of inheritance that blurs the lines between traditional mendelian inheritance patterns.

AUTHOR CONTRIBUTIONS

Andrés Caballero Oteyza was involved in the conceptualization of the study, acquired and analyzed most of the functional data on *KIF1C* mutations, and critically revised the article. Esra Battaloğlu was involved in design and conceptualization of the study, analyzed the genetic data on family IHG25215, and critically revised the article. Levent Ocek recruited and examined family IHG25215 and participated in drafting of the article. Tobias Lindig acquired and interpreted the MRI of family THI26001and participated in drafting of the article. Jennifer Reichbauer performed sequencing and segregation analysis of variants in family THI26001 and critically revised the manuscript. Adriana Rebelo was involved in design and conceptualization of the study and advised on the interpretation of functional data on *KIF1C* mutations; she critically revised the article. Michael Gonzalez performed exome sequencing in both families and critically revised the manuscript. Yasar Zorlu recruited and examined family IHG25215 and critically revised the article. Burcak Ozes performed sequencing and segregation analysis of variants in family IHG25215 and critically revised the manuscript. Dagmar Timmann recruited and examined family THI26001 and critically revised the article. Benjamin Bender acquired and analyzed the MRIs of family THI26001 and critically revised the article. Günther Woehlke analyzed the position of the *KIF1C* mutations and participated in drafting of the article. Stephan Züchner was involved in design of the study and critically revised the article. Ludger Schöls was involved in design of the study and critically revised the article. Rebecca Schüle was responsible for conception and design of the study, analyzed and interpreted the exome sequencing data, supervised and coordinated the study, and drafted the article. All authors approved the final version of the manuscript to be submitted.

ACKNOWLEDGMENT

The authors thank Prof. Rainer Lammers, University of Tübingen, for kindly providing the *KIF1C* cDNA.

STUDY FUNDING

Supported by the Interdisciplinary Center for Clinical Research IZKF Tübingen (grant 1970-0-0 to R.S.), the European Union (PIOF-GA-2012-326681 HSP/CMT genetics to R.S. and FP7 grant NeurOmics [2012-305121] to L.S.), the NIH (grants 5R01NS072248, 1R01NS075764, and 5R01NS054132 to S.Z.), and the German HSP-Selbsthilfegruppe e.V. (grant to R.S. and L.S.).

DISCLOSURE

A. Caballero Oteyza, E. Battaloğlu, L. Ocek, T. Lindig, J. Reichbauer, A. Rebelo, M. Gonzalez, Y. Zorlu, B. Ozes, and D. Timmann report no disclosures relevant to the manuscript. B. Bender has received travel support from Bayer Vital GmbH. G. Woehlke reports no disclosures relevant to the manuscript. S. Züchner has received license fee payments from Athena Diagnostics and is funded by NIH grants 5R01NS072248, 1R01NS075764, and 5R01NS054132. L. Schöls is funded by the EU FP7 grant 2012-305121 NeurOmics and the German HSP-Selbsthilfegruppe. R. Schüle is funded by the Interdisciplinary Center for Clinical Research IZKF Tübingen (grant 1970-0-0), the EU grant PIOF-GA-2012-326681 HSP/CMT genetics, and the German HSP-Selbsthilfegruppe e.V. Go to Neurology.org for full disclosures.

Received November 25, 2013. Accepted in final form March 3, 2014.

REFERENCES

1. Schule R, Schols L. Genetics of hereditary spastic paraplegias. Semin Neurol 2011;31:484–493.
2. Blackstone C. Cellular pathways of hereditary spastic paraplegia. Annu Rev Neurosci 2012;35:25–47.
3. Gonzalez MA, Acosta Lebrigio RF, Van Booven D, et al. GEnomes Management Application (GEM.app): a new software tool for large-scale collaborative genome analysis. Hum Mutat 2013;34:842–846.
4. Lammers R, Bossenmaier B, Cool DE, et al. Differential activities of protein tyrosine phosphatases in intact cells. J Biol Chem 1993;268:22456–22462.
5. Marx A, Hoenger A, Mandelkow E. Structures of kinesin motor proteins. Cell Motil Cytoskeleton 2009;66:958–966.
6. Okada Y, Hirokawa N. Mechanism of the single-headed processivity: diffusional anchoring between the K-loop of kinesin and the C terminus of tubulin. Proc Natl Acad Sci USA 2000;97:640–645.
7. Dorner C, Ciossek T, Muller S, Moller PH, Ullrich A, Lammers R. Characterization of KIF1C, a new kinesin-like protein involved in vesicle transport from the Golgi apparatus to the endoplasmic reticulum. J Biol Chem 1998;273:20267–20275.
8. Fichera M, Lo Giudice M, Falco M, et al. Evidence of kinesin heavy chain (KIF5A) involvement in pure hereditary spastic paraplegia. Neurology 2004;63:1108–1110.
9. Goizet C, Boukhris A, Mundwiller E, et al. Complicated forms of autosomal dominant hereditary spastic paraplegia are frequent in SPG10. Hum Mutat 2009;30:E376–E385.
10. Ebbing B, Mann K, Starosta A, et al. Effect of spastic paraplegia mutations in KIF5A kinesin on transport activity. Hum Mol Genet 2008;17:1245–1252.
11. Schlager MA, Kapitein LC, Grigoriev I, et al. Pericentrosomal targeting of Rab6 secretory vesicles by bicaudal-D-related protein 1 (BICDR-1) regulates neuritogenesis. EMBO J 2010;29:1637–1651.
12. Theisen U, Straube E, Straube A. Directional persistence of migrating cells requires Kif1C-mediated stabilization of trailing adhesions. Dev Cell 2012;23:1153–1166.
13. Hirokawa N, Nitta R, Okada Y. The mechanisms of kinesin motor motility: lessons from the monomeric motor KIF1A. Nat Rev Mol Cell Biol 2009;10:877–884.

14. Klopfenstein DR, Tomishige M, Stuurman N, Vale RD. Role of phosphatidylinositol(4,5)bisphosphate organization in membrane transport by the Unc104 kinesin motor. Cell 2002;109:347–358.
15. Yue Y, Sheng Y, Zhang HN, et al. The CC1-FHA dimer is essential for KIF1A-mediated axonal transport of synaptic vesicles in C. elegans. Biochem Biophys Res Commun 2013; 435:441–446.
16. Reid E, Kloos M, Ashley-Koch A, et al. A kinesin heavy chain (KIF5A) mutation in hereditary spastic paraplegia (SPG10). Am J Hum Genet 2002;71:1189–1194.
17. Schule R, Kremer BP, Kassubek J, et al. SPG10 is a rare cause of spastic paraplegia in European families. J Neurol Neurosurg Psychiatry 2008;79:584–587.
18. Erlich Y, Edvardson S, Hodges E, et al. Exome sequencing and disease-network analysis of a single family implicate a mutation in KIF1A in hereditary spastic paraparesis. Genome Res 2011;21:658–664.
19. Klebe S, Lossos A, Azzedine H, et al. KIF1A missense mutations in SPG30, an autosomal recessive spastic paraplegia: distinct phenotypes according to the nature of the mutations. Eur J Hum Genet 2012;20:645–649.
20. Kopp P, Lammers R, Aepfelbacher M, et al. The kinesin KIF1C and microtubule plus ends regulate podosome dynamics in macrophages. Mol Biol Cell 2006;17:2811–2823.
21. Dorner C, Ullrich A, Haring HU, Lammers R. The kinesin-like motor protein KIF1C occurs in intact cells as a dimer and associates with proteins of the 14-3-3 family. J Biol Chem 1999;274:33654–33660.
22. Wozniak MJ, Melzer M, Dorner C, Haring HU, Lammers R. The novel protein KBP regulates mitochondria localization by interaction with a kinesin-like protein. BMC Cell Biol 2005;6:35.
23. Oates EC, Rossor AM, Hafezparast M, et al. Mutations in BICD2 cause dominant congenital spinal muscular atrophy and hereditary spastic paraplegia. Am J Hum Genet 2013;92:965–973.
24. Meluh PB, Rose MD. KAR3, a kinesin-related gene required for yeast nuclear fusion. Cell 1990;60:1029–1041.
25. Wedlich-Soldner R, Straube A, Friedrich MW, Steinberg G. A balance of KIF1A-like kinesin and dynein organizes early endosomes in the fungus Ustilago maydis. EMBO J 2002;21: 2946–2957.
26. Dor T, Cinnamon Y, Raymond L, et al. KIF1C mutations in two families with hereditary spastic paraparesis and cerebellar dysfunction. J Med Genet 2013;51:137–142.
27. Klebe S, Depienne C, Gerber S, et al. Spastic paraplegia gene 7 in patients with spasticity and/or optic neuropathy. Brain 2012;135:2980–2993.
28. Hansen JJ, Durr A, Cournu-Rebeix I, et al. Hereditary spastic paraplegia SPG13 is associated with a mutation in the gene encoding the mitochondrial chaperonin Hsp60. Am J Hum Genet 2002;70:1328–1332.
29. Magen D, Georgopoulos C, Bross P, et al. Mitochondrial hsp60 chaperonopathy causes an autosomal-recessive neurodegenerative disorder linked to brain hypomyelination and leukodystrophy. Am J Hum Genet 2008;83:30–42.

RNA metabolism meets axonopathy: the HSP protein KIF1C binds RNA and ribosomal components

Authors and affiliations

Andrés Caballero-Oteyza[1,#], Stefan Kotschote[2], Beibei Chen[3], Jennifer Reichbauer[1,4], Angelos Skodras[5], Adriana P Rebelo[6], Alleene Strickland[6], Günther Woehlke[7], Stephan Züchner[6], Michael Bonin[2], Ludger Schöls[1,4], Rebecca Schüle[1,4#].

1. Center for Neurology and Hertie Institute for Clinical Brain Research, Eberhard-Karls-University, 72076 Tübingen, Germany

2. IMGM Laboratories GmbH, Martinsried 82152, Germany;

3. QBRC Centre, Dallas (TX) 75390, U.S.A;

4. German Center of Neurodegenerative Diseases (DZNE), Tübingen, Germany

5. Hertie-Institute for brain clinical research, Cell biology and neurological diseases department, Tübingen 72076, Germany;

6. Hussman Institute for Human Genomics, Miami (FL) 33136, U.S.A;

7. Technical University Munich, Molecular and cellular biophysics, Garching 85748, Germany.

 # Corresponding authors:

Rebecca Schüle, telephone: +49 7071 2982057; e-mail: rebecca.schuele-freyer@uni-tuebingen.de

Andrés Caballero-Oteyza, telephone: +49 761 270-77769; e-mail: andres.caballero.garcia.oteyza@uniklinik-freiburg.de

Conflict of interest: The authors have declared that no conflict of interest exists.

Abstract

Hereditary spastic paraplegias (HSPs) are highly heterogeneous neurodegenerative disorders characterized by lower limb spasticity and weakness. All HSPs share a common trait – a progressive length-dependent degeneration of the motor axons that compose the corticospinal tract. However, many underlying mechanisms of the pathology still remain unknown. In the present study we aim to elucidate the pathological mechanism of spastic paraplegia type 58 (SPG58), an autosomal recessive subtype of HSP complicated by ataxia, which is caused by mutations in the Kinesin-like protein 1C (*KIF1C)* gene. Here we demonstrate that KIF1C functions as an RNA-binding protein (RBP), that it interacts with other RBPs such as the polyadenylate binding protein cytoplasmic I (PABP), the heat-shock 70KDa protein 8 isoform 1 (HSPA8) and the insulin-like growth factor II mRNA binding protein I (IMP-1); and that the KIF1C-PABP mutual interaction is RNA-mediated. We report that KIF1C-bound transcripts are involved in pathways such as gene expression, cell cycle, RNA processing and RNA splicing, and that ribosomal RNAs are strongly enriched among these transcripts. Finally, we show that immobilizing mutations in KIF1C lead to a dramatic re-distribution of ribosomes. These findings suggest KIF1C as an axonal transporter for ribosomes.

Introduction

Hereditary spastic paraplegias (HSPs) are a group of inherited neurodegenerative disorders characterized by a progressive spasticity and weakness of the lower limbs. With a prevalence of 1,3 to 9,6 in 100.000 individuals (1, 2). HSPs are rare, yet they rank among the clinically and genetically most heterogeneous Mendelian diseases. HSPs can be inherited in autosomal dominant, autosomal recessive and X-linked manner. To date, at least 76 different loci and 59 corresponding spastic paraplegia genes (SPG) have been identified (3, 4). Despite this diversity all forms of HSP share a common pathology, a length-dependent distal axonopathy of the upper motor neurons, which compose the corticospinal tract.

Corticospinal tract motor neurons critically depend on efficient transport mechanisms throughout the axons to deliver vesicles and other organelles such as mitochondria, RNA-granules and polyribosomes to their respective target sites (5, 6). Polyribosomes - complexes of ribosomes linked to messenger RNA (mRNA) molecules - are transported as stably paused complexes from the nucleus to the synapse to allow rapid on-site translation (6). Local protein translation is essential for synaptic plasticity (6), dysregulation of which can cause common neurological disorders such as Alzheimer's disease (AD) (7), Parkinson's disease (PD) (8), and Huntington's disease (HD) (9). RNA-binding proteins (RBPs) play a critical role in translational control of mRNA and dysfunction of RBPs such as TDP-43, FMRP or SMN can lead to Amyotrophic lateral sclerosis (ALS) and Frontotemporal dementia (FTLD) (10), Fragile X syndrome (FXS) (11), or Spinal muscular atrophy (SMA) (12) respectively.

Corticospinal tract axons are among the longest in the central nervous system (CNS) and therefore are arguably most vulnerable to disturbances of axonal transport (13). Thus it is not surprising that several HSP-associated proteins are directly involved in axonal transport, including kinesin heavy chain 5A (*KIF5A*), kinesin-like protein 1A (*KIF1A*) and spastin (*SPAST*) (14–16). We have recently discovered that loss-of-function mutations in *KIF1C*, encoding the kinesin-like protein 1C (KIF1C), cause autosomal recessive HSP type 58 (SPG58) (17). The biological function of KIF1C as well as the molecular mechanism of SPG58 pathogenesis, however, are still incompletely understood. Endogenous KIF1C is expressed ubiquitously and can be spotted around the centrosome and Golgi

apparatus (18, 19). It also accumulates in the cell periphery and verges of cellular extensions (20, 21). Functionally, KIF1C has been shown to be involved in retrograde vesicular transport between Golgi and endoplasmic reticulum (ER) (19), in Golgi membrane organization (22), formation and maintenance of podosomes in macrophages (21, 23) and stabilization of trailing focal adhesions in migrating cells (20).

In the present study, we set out to elucidate the molecular function of KIF1C. We demonstrate that KIF1C directly binds RNA and RNA-binding proteins. Ribosomal components are strongly enriched among KIF1C-bound transcripts. We speculate that KIF1C might be an axonal transporter for ribosomes and show that immobilizing mutations in KIF1C lead to a dramatic re-distribution of ribosomal components.

Results

Identification of KIF1C interacting partners

Specific cargoes as well as cargo adapters and regulators of KIF1C are still unknown. To identify interaction partners we immunoprecipitated protein complexes bound to wildtype KIF1C ($KIF1C_{WT}$) or pathogenic KIF1C ($KIF1C_{G102A}$ and $KIF1C_{P176L}$) isoforms overexpressed (17) in the monkey fibroblast-like COS-7 cell line as well as in the human kidney HEK293T line. Silver staining of SDS-PAGE gels (Figure S1) loaded with the respective precipitates, demonstrated the enrichment of a specific protein band of approximately 70 KDa in both wildtype and mutant KIF1C samples in comparison to controls (proteins pulled down with an IgG antibody). Mass spectrometry indicated the presence of several proteins (Table S1) including the polyadenylate binding protein cytoplasmic I (PABP), the heat-shock 70KDa protein 8 isoform 1 (HSPA8), the insulin-like growth factor II mRNA binding protein I (IMP-1), and the insulin-like growth factor II mRNA binding protein III (IMP-3).

Validation of KIF1C interactions

We then performed co-immunoprecipitation (Co-IP) assays and co-localization analysis by immunofluorescence (IF) to validate the potential new KIF1C interaction partners PABP, IMP-1 and HSPA8.

a) Protein interaction was confirmed by Co-IP by overexpression of the HA-tagged fusion proteins $KIF1C_{WT}$, $KIF1C_{G102A}$, $KIF1C_{P176L}$ or $KIF1C_{R301G}$ in HEK293T cells. All three candidate interactors - PABP, IMP-1 and HSPA8 - could be detected by western blot after being pulled down with an anti-HA antibody (Figure 1A). Quantification of the relative ratio of the respective candidate interactor over KIF1C in three independent experimental repetitions revealed that mutant KIF1C isoforms bind to interactors with the same affinity as wildtype KIF1C (Figure 1B). The same results were observed with a reverse Co-IP, when an anti-PABP antibody was used to pull down the protein complex, instead of an anti-HA antibody (Figure 1C), thus confirming the specificity of the interaction. As expected none of the candidate interactors could be immunoprecipitated with an IgG control antibody (Figure 1A,C).

The dynein motor adaptor Bicaudal D Homolog 2 (BICD2), which has been implicated in the pathogenesis of spinal muscular atrophy and HSP (24), has been previously reported to interact with KIF1C (25). However, we were not able to confirm a KIF1C-BICD2 interaction through immunoprecipitation (Figure 1A).

b) Co-localization by confocal microscopy of endogenous KIF1C with its respective candidate interaction partners: PABP, IMP-1 and HSPA8 were observed in the human neuronal SH-SY5Y cell line (Figure 2). KIF1C is sparsely distributed throughout the cell with a propensity to accumulate at the centrosome and at the tips of cellular processes where it co-localizes with PABP. KIF1C also co-localizes with HSPA8 at the edge of cellular protrusions, and with IMP-1 at the periphery of cellular extensions and partially around the nucleus. Similar results were obtained in the monkey fibroblast-like COS-7 cell line (Figure S2), although both the staining pattern of endogenous KIF1C as well as the co-localization pattern between KIF1C and its interaction patterns are less distinct than in the neuronal SH-SY5Y cell line.

In line with our results obtained with immunoprecipitation, we observed no co-localization between BICD2 and KIF1C, when overexpressing $KIF1C_{WT}$ or $KIF1C_{G102A}$ (Figure S3, Figure S4).

Impact of pathogenic p.G102A mutation on KIF1C interactions

To test whether immobilizing mutations in the motor domain of KIF1C affect the co-localization pattern with the candidate interaction partners, we proceeded to overexpress $KIF1C_{WT}$ and mutant $KIF1C_{G102A}$ in COS-7 cells. As previously described in (17), overexpressed $KIF1C_{WT}$ accumulates at the cell periphery or tips of cellular protrusions. We observed almost complete co-localization of endogenous PABP with overexpressed $KIF1C_{WT}$; both proteins accumulate at the tips of cellular processes (Figure 3). The extent of $KIF1C_{WT}$:PABP co-localization is near complete and comparable to co-localization of GFP- and mCherry-tagged $KIF1C_{WT}$ fusion proteins (control). HSPA8 co-localizes with $KIF1C_{WT}$ at sites of $KIF1C_{WT}$ accumulation while maintaining a strong cytoplasmic staining pattern seemingly independent of $KIF1C_{WT}$. IMP-1 shows a predominantly cytoplasmic

staining pattern in COS-7 cells and co-localizes with $KIF1C_{WT}$ in a few small spots in the cell periphery.

We have previously shown that the p.G102A mutation in the motor domain of KIF1C completely abolishes the peripheral staining pattern observed for overexpressed $KIF1C_{WT}$ (17). Interestingly, $KIF1C_{G102A}$ also recruits PABP to the cytoplasm, preventing its localization at the verge of cellular processes (Figure 4). Similarly, IMP-1 and HSPA8 lose their predilection for peripheral accumulation and display a more homogeneous cytoplasmic distribution while retaining a limited co-localization with $KIF1C_{G102A}$.

Further analysis looking at Pearson's co-localization coefficient of $KIF1C_{WT}$ or $KIF1C_{G102A}$ with each of the respective interactors showed no relevant differences in the ratio interactor/KIF1C between wildtype and mutant KIF1C isoforms (Data not shown). This observation supports our hypothesis that pathogenic p.G102A mutation alters the distribution of KIF1C complexes without affecting its binding affinity to interactors.

Study of KIF1C distribution

For a better understanding of KIF1C localization and function we also studied its distribution in relation to different subcellular compartments such as the Golgi apparatus, the endoplasmic reticulum (ER) and the mitochondrial network. Previous publications have associated KIF1C with Golgi-ER transport or Golgi compartment organization (19, 22). Also the kinesin-like protein 1B (KIF1B), a strong homolog of KIF1C, is known to be involved in mitochondrial transport (26). However, in COS-7 cells KIF1C did not co-localize with any of the tested markers for the ER (pmKate2-ER), Golgi (GM130), or the mitochondrial network (TRAK2). These results were consistent for endogenous KIF1C (Figure S5), overexpressed $KIF1C_{WT}$ (Figure S3) as well as $KIF1C_{G102A}$ (Figure S4).

In a previous study about the role of KIF1C in podosome dynamics in macrophages, the motor protein had been reported to interact indirectly with the actin cytoskeleton (21). Thus we decided to employ immunofluorescent imaging to evaluate the effects of $KIF1C_{G102A}$ overexpression on actin cytoskeleton architecture. However, the actin cytoskeleton looked unaltered compared to cells

overexpressing $KIF1C_{WT}$ (Figure S6). Additionally, we also observed that pathogenic p.G102A mutation caused no apparent disturbance on the microtubule architecture when compared to cells overexpressing the wildtype form or cells with endogenous protein levels (Figure S7).

KIF1C-PABP interaction is RNA-mediated

PABP, IMP-1 and HSPA8 are known RNA-binding proteins that are involved in RNA metabolism in various functions (27–29). This suggested that KIF1C might also be involved in RNA metabolism through regulation and/or transport. To test whether KIF1C binds to its interactors directly or indirectly by mutual interaction with RNA, we performed an "RNAse-COIP" experiment. We focused on KIF1C-PABP interaction because it had proven to be the strongest (Figure 1). We added increasing concentrations of RNAse I to the lysis buffer before pulling down protein complexes with an anti-HA antibody in HEK293T cells transiently overexpressing *KIF1C-HA*. The interaction between KIF1C and PABP was markedly reduced by addition of RNAse I in a dose-dependent manner (Figure 5A,B). This could also be confirmed when pulling down protein complexes using an anti-PABP antibody (Figure 5A,B). To control for the relative excess of KIF1C due to transient overexpression, we repeated the experimental setup overexpressing both KIF1C (HA-tagged) and PABP (GFP-tagged). Again, a reduced interaction between KIF1C and PABP after addition of RNAse I was confirmed using either an anti-HA or anti-GFP antibody for the precipitation of complexes (Figure 5C,D). Lastly, the dependence of the KIF1C-PABP interaction on the presence of RNA was confirmed under endogenous conditions (Figure 5E,F). The latter experiment was carried out in HeLa cells as they express rather strong endogenous levels of both KIF1C and PABP compared to other cell types (Figure S8A).

The results of these three similar approaches suggest that KIF1C and PABP interact indirectly and that the interaction is mediated through mutual binding of RNA.

Identification of transcripts bound to KIF1C

Given that the interaction between KIF1C and PABP is RNA-mediated we hypothesized that KIF1C might be an RBP itself. To test this hypothesis and identify KIF1C-bound transcripts, we performed

individual-nucleotide resolution UV crosslinking immunoprecipitation (iCLIP) in HEK293T cells transiently overexpressing either KIF1C-mCherry or mCherry encoded by the empty pmCherry-N1 plasmid. We applied the protocol detailed in (30) with slight modifications (see material and methods). In short, RNA-protein binding sites were crosslinked (CL) by irradiation with UV light (254nm), allowing for subsequent rigorous purification of RNA-protein complexes. Lysates were immunoprecipitated with anti-mCherry, separated using SDS-PAGE, transferred to a nitrocellulose membrane and visualized with Ponceau staining. Complexes ranging between 150-250 kDa in size were retrieved from the membrane (blue box in Figure S9A) and proteins were removed by proteinase K treatment. Then the remaining RNA (tagged with small peptides at CL sites) was reverse transcribed with a specific "Rclip" primer. Resulting cDNA was loaded on a TBE-Urea gel (not shown), where we artificially defined three different cutting fractions of 120-200 nt (high), 85-120 nt (medium) and 70-85 nt (low). cDNA fragments of all fractions were purified from the gel and circularized, linearized again and amplified with specific primers. Finally, a quality control of amplified cDNA fragments (Figure S9B) revealed that only lanes 7 and 8, which represent the high and medium size fraction of the KIF1C-mCherry crosslinked sample, contained significant amounts of amplified DNA. Consequently, a cDNA library was generated from the mix of lanes 7 and 8 together. Four different concentrations of this library were prepared in duplicates to obtain eight separate replicates which were subjected to next generation sequencing. In the two negative controls, i) overexpression of empty mCherry plasmid and ii) overexpression of KIF1C-mCherry without cross-linking, no DNA could be amplified in any of the size fractions.

Analysis of next generation sequencing data

An average of about 157 million read-pairs of ~100bp in length were produced per sample (8 replicates). About 48 million read-pairs could be mapped to the hg19 reference genome (Figure 6A). Consecutively, mapped reads were processed with the PIPE-CLIP analysis tool (31). Filtering for minimum read length and maximum base mismatch retrieved a mean of about 500 thousand reads per sample. Aggregation of adjacent reads overlapping by at least one nucleotide identified a mean of 1.065 ± 141 enriched clusters per sample. Clustering of all cDNA truncations (indicating RNA-protein

crosslinking sites) found at a given genomic location identified a mean of 3.017 ± 167 reliable truncation sites (Figure 6A). Finally, the mapping of the truncation sites to the enriched clusters allowed us to identify a mean of 1.858 ± 116 crosslinking mutations clustered in 602 ± 70 CL sites, which matched to 427 ± 52 genes per sample (Table S2). These values were within the expected range for PIPE-CLIP analysis as shown in the summary table for the Nova iCLIP data (31).

The crosslinking sites across all 8 replicates mapped to a total of 515 unique genes (Table S3). The candidate gene lists resulting from the 8 replicates were highly correlated (correlation coefficients > 0.997); 86% of genes were represented in at least four samples and 57% of genes were present in all 8 replicates (Table S3). The genes present in three or less samples without exception had low peak scores (number of reads per cluster), 40fold lower than average peak scores in genes present in ≥4 lanes. We therefore decided to pool all replicates for further analysis and include only genes detected in at least four samples (n=441) in the joint analysis. 99.1% of genes had peak scores below 5.000 with a median of 133. Among the four genes represented by transcripts with the highest peak scores were two ribosomal DNA genes: *RNA45S5* from which the ribosomal 28S, 5.8S, and 18S subunits are transcribed, and *RNA5-8S5* that encodes the ribosomal 5S subunit (Figure S9C). Very high peak scores were further observed for KIF1C and HYDIN (hydrocephalus inducing protein homologue) (Figure S9C).

Confirmation of RNA transcripts

To validate the iCLIP results, we performed an RNA-immunoprecipitation (RIP) assay in HEK293T cells, either untransfected or transiently overexpressing KIF1C-HA. In short, after immunoprecipitation of the RNA-protein complex, recovered RNA was retro-transcribed and amplified with specific primers to verify presence and relative abundance of a specific transcript in the immunoprecipitated sample. Preliminary RNA quality control addressed by a Bioanalyzer showed rRNA and mRNA present in the sample immunoprecipitated with an anti-HA but absent in the IgG control (Figure S10). We selected five genes - *KIF1C, HYDIN, HFM1, PDE3 & RAPGEF* – all of which were among the 10 highest scoring genes in the iCLIP analysis (Table S3). As expected all these transcripts were not only present in the IP sample (under endogenous or overexpressing

conditions) but also overrepresented in comparison to the RNA from the input sample (Figure 6B). GAPDH ranked the 330th position in the list and therefore was used to show a case of low representation, whereas amplification of RPLP0 (absent in the list, Table S3) served as a negative control.

Pathway enrichment analysis

To determine cellular pathways and components that the transcripts bound to KIF1C play a role in, we used the DAVID Bioinformatics Database (32) to functionally annotate the genes (n=441) whose RNA we found to interact with KIF1C. 420/441 could be mapped by DAVID; the 21 genes that could not be mapped by DAVID included 16 RNA genes (ncRNA, miRNA, lncRNA, mt-rRNA) (Figure 6c), 4 pseudogenes and 1 fusion protein gene. We performed functional annotation using several pathway tools (BBID, BIOCARTA, KEGG pathway, Panther pathway, REACTOME, GO terms) and then created a pathway enrichment map using the Cytoscape pathway enrichment plugin. Significant enrichment was demonstrated for genes involved in RNA/DNA metabolism, gene expression, cell cycle, RNA processing and RNA splicing pathways (Figure 6C). This analysis suggests that KIF1C has a clear prevalence for transcripts involved in a certain aspect of RNA metabolism. This hypothesis is further supported by the presence of two ribosomal genes: *RNA45S5* and *RNA5-8S5*, which are among the transcripts with highest peak scores in (Table S3).

KIF1C interacts with Ribosomes

The strong over-representation of RNA-related functional pathways among the interactions of KIF1C suggested that KIF1C might cooperate with ribosomes. We therefore studied the interaction between the ribosomal protein RPS6 and the KIF1C motor through IF and IP. Immunofluorescent imaging of COS-7 cells overproducing $KIF1C_{WT}$ demonstrates strong co-localization between RPS6 and $KIF1C_{WT}$ in the cell periphery accumulating at the tip of cellular processes (Figure 7A). Overexpression of the immobile motor $KIF1C_{G102A}$ on the other hand leads to cytoplasmic redistribution of kinesin and recruitment of RPS6 from the cell periphery to the cytoplasm. Under endogenous conditions the KIF1C-RPS6 co-localization is not complete but is clearly detected at the

cell edges in COS-7 cells (Figure 7A) and it is even more clearly perceptible in SH-SY5Y cells (Figure 7B).

The interaction between KIF1C and the ribosomal protein RPS6 could also be confirmed in HEK293T cells transiently overexpressing KIF1C$_{WT}$-HA and immunoprecipitated with an anti-HA or anti-RPS6 antibody (Figure 7C); in both cases the two proteins, as well as PABP, were co-immunoprecipitated, thus proving to be part of the same complex.

Discussion

Previous studies have implicated KIF1C in anterograde transport of α5β1-integrins, retrograde Golgi to ER transport (19, 20) or Golgi membrane shaping (22). However, it is currently unclear, how these different functions may be related and which properties of KIF1C may be critical for its role in HSP disease pathology. Therefore we hypothesized that identification of KIF1C interaction partners might reveal previously unrecognized functional connections. Peptide identification (Table S1) in KIF1C complexes indeed revealed novel interactions with the proteins PABP, IMP-1 and HSPA8, all of which were successfully confirmed by co-immunoprecipitation and co-localization studies. Interestingly, PABP is a protein that binds to the 3' poly(A) tail of messenger RNAs to regulate mRNA stability, splicing, translation and nonsense-mediated decay (NMD) (33, 34). Moreover, when PABP binds to the adenine-rich auto-regulatory sequence (ARS) in the 5'UTR of its own mRNA to repress translation, it is assisted by IMP-1 forming an auto-regulatory complex (ARC) *in vitro* (35). In addition, IMP-1 binds to the 3'UTR of β-actin (ACTB) mRNA forming and mRNP complex that is responsible to deliver ACTB mRNA to leading edges of cells as seen for chicken fibroblasts and neurons and for growth cones of Xenopus laevis. This localization is essential for growth cone motility and guidance (36–38). Lastly, HSPA8 is a component of the PRP19-CDC5L complex in the spliceosome, which is required to activate mRNA splicing (39). The fact that all three novel interactors are known RNA-binding proteins (27–29), strongly suggested a role of KIF1C in RNA metabolism and/or transport. And indeed, RNA-immunoprecipitation in HEK293T cells transiently overexpressing KIF1C-HA confirmed presence of messenger and ribosomal RNA in KIF1C complexes (Figure S10).

However, neither the protein- nor the RNA-immunoprecipitation experiments we had initially performed were suitable to discriminate between direct and indirect interactions. We first speculated that the RBPs might mediate interaction between KIF1C and RNA. We were however surprised to find that instead, the interaction between KIF1C and the other RBPs is seemingly mediated by their mutual capacity to bind RNA, as shown exemplarily for PABP (Figure 5). This hypothesis is supported by two independent studies in which high-throughput screenings had previously identified

KIF1C as a candidate RBP as one of 860 and 800 identified candidate proteins respectively (40, 41). To validate these findings we used iCLIP, a state-of-the-art technique that allows identification of RNA transcripts covalently bound to a specific protein (30). Compared to normal RNA-immunoprecipitation, crosslinking-immunoprecipitation (CLIP) allows for more stringent purification, thus reducing unspecific interactions (42). In none of the negative controls (overexpression of an 'empty' pmCherry vector; overexpression of KIF1C-mCherry without crosslinking) RNA transcripts were present (Figure S9B). Analysis of the 441 transcripts consistently present in our dataset consolidated the role of KIF1C in RNA metabolism and/or transport. For one, pathway analysis - using the DAVID bioinformatics tool - revealed a strong enrichment of genes related to RNA/DNA metabolism, gene expression, cell cycle, RNA processing and RNA splicing pathways (Figure 6C). Secondly, 46% of all reads represented the ribosomal genes *RNA45S5* and *RNA5-8S5* (Table S3). As no ribosomal contamination was present in the negative controls we consider these reads to be specific to our dataset. The abundance of ribosomal RNA, overrepresentation of transcripts related to RNA metabolism in the broader sense, and presence of known RNA-binding proteins in the KIF1C complex suggested an interaction of KIF1C with ribosomes. This hypothesis was tested by studying KIF1C interaction with a representative ribosomal protein such us RPS6 by IF and IP assays (Figure 7). Ribosomal protein S6 has been used as a marker to measure dendritic mRNA transport as RNA granules in hippocampal neurons (43). Judging by RPS6-KIF1C co-localization, overexpression of $KIF1C_{WT}$ induces a ribosomal recruitment to the cell periphery and accumulation at the tips of cellular processes. However, this localization pattern is lost after overexpression of $KIF1C_{G102A}$; the cytoplasmic phenotype reflects how pathogenic p.G102A mutation in KIF1C alters ribosome distribution. Immunofluorescence results are supported by the reciprocal co-immunoprecipitation of KIF1C and RPS6. Taken together, these observations strongly suggest that KIF1C interacts with ribosomes and that it is likely involved in active ribosomal transport.

Surprisingly little is known about such a basic mechanism as ribosomal transport. We know that in neurons, ribosomal subunits are found in RNA granules - large macromolecular structures containing RNAs and proteins - (44) however, it is not known how those RNA granules are carried. A few studies have described the implication of certain kinesins in the transport of ribosomes. It is known that a

member of the human kinesin-5 family: KIF11 is required to link ribosomes to microtubules, and that its inhibition causes slowed ribosome transit and affects translation, which is physiologically dependent on KIF11's ATPase activity. Although it is unknown whether KIF11 binds directly or indirectly to the ribosome, it has been proposed as a motile microtubule-ribosome linker that enhances translation efficiency and that could also play a role in translation elongation and termination (45). KIF1C, KIF1B and kinesin-like protein 1A (KIF1A) belong to the kinesin-3 family. A kinesin-3 homolog in the fungus Ustilago maydis: Kin3, is responsible for the endosome-mediated anterograde shuttling of mRNPs that contain the RBP: Rrm4, in the elongated hyphal cell (46). Furthermore, the mouse homolog of the Kinesin-4 family in humans: KIF4 interacts with the ribosomal protein P0 (component of the 60s subunit) in dorsal root ganglia (DGR) neurons; as KIF1C does with RPS6 in our cellular models. In addition, as it happens with the p.G102A mutation in KIF1C, mutations in KIF4 alter the intracellular distribution of ribosomes, represented by P0 localization. Finally, RNAi suppression reveals that KIF4 is essential for the anterograde translocation of ribosomal constituents to developing axons (47).

Implication of these kinesins in ribosomal transport further strengthens our hypothesis that KIF1C might be an axonal transporter for ribosomes involved in maintenance and regulation of synaptic translation in neurons. However, a more comprehensive live imaging testing will be needed to prove the hypothesis. As a next step we will study in vivo ribosomal transport of KIF1C in a more suitable neuronal model such as iPS-derived neurons.

Our study for the first time implicates RNA transport and/or metabolism in the pathogenesis of HSP and thus moves HSPs closer to the growing number of related neurodegenerative diseases like ALS and FTD (10) in which mutations in RNA-binding proteins are recognized to be intricately involved in disease pathology.

Methods

Cloning. KIF1C cDNA was amplified from pRK5-KIF1C kindly provided by Dr. Reiner Lammers and cloned into a pENTR/D-TOPO vector (#K2400-20, Invitrogen) accordingly to manufacturer's instructions. Subsequently we introduced the changes c.305G>C (p.G102A); c.527C>T (p.176P>L) and c.901A>G (p.301R>G) respectively into pENTR-KIF1C$_{WT}$, using the Q5 site-directed mutagenesis kit (#E0554S, NEB). KIF1C coding sequence was amplified from all resulting constructs: pENTR-KIF1C$_{WT}$, pENTR-KIF1C$_{G102A}$, pENTR-KIF1C$_{P176L}$, pENTR-KIF1C$_{R301G}$, with specific primers (Reverse primer containing sequence coding for an HA-tag) to introduce them into a pCS2+ vector (kindly donated by Dr. Alexander Abrams), thus obtaining: pCS2+KIF1C$_{WT}$-HA, pCS2+KIF1C$_{G102A}$-HA, pCS2+KIF1C$_{P176L}$-HA, pCS2+KIF1C$_{R301G}$-HA. All plasmids were sequenced to confirm changes - primers available in (TableS4) - and no other mutations were found. Additional plasmids used such us pTOPO-GFP-KIF1C$_{WT}$, pTOPO-GFP-KIF1C$_{G102A}$, pmCherryN1-KIF1C$_{WT}$ and pmCherryN1-KIF1C$_{G102A}$ were previously cloned as described in (17).

Other plasmids. pmCherryN1 (#632523, Clontech Laboratories), pmKate2-ER (#FP324, Evrogen), pEGFP-N3-ITGA5 (#15238, Addgene), p.α5-integrin-GFP and pKIF1C-mCherry were provided by Dr. Anne Straube, pTOPO-TRAK2-GFP was provided by Dr. Adriana Rebelo and pPABP-eGFP was kindly donated by Dr. Matthias Hentze.

Cell culture. Human Embryonic Kidney (HEK) 293T, HeLa, human glioblastoma U-87 MG, human neuroblastoma SH-SY5Y, mouse motoneuron-like NSC-34 and the monkey fibroblast-like kidney COS-7 cell lines were all cultured in Dubelco's modified eagle medium (DMEM) (Biochrom) supplemented with 10% Fetal calf serum (FCS) (#10270106, Thermofisher) and maintained at 37°C and 5% CO_2.

Transfection. Mammalian cell transfection of COS-7 or HEK293T with any of the above mentioned plasmids was done using Turbofect reagent (#R0531, ThermoScientific) dissolved in Opti-MEM (#31985047, Thermofisher) following the manufacturer's instructions. 24 hours after transfection cells

were harvested and stored as frozen cell pellets or used directly for WB or IP, or either fixed in-situ for immunofluorescent microscopy purposes.

Cell pellet stocks. All different cell types used: COS-7, HEK293T, HeLa, SH-SY5Y and U-87 MG -transfected or untransfected- were grown in normal DMEM + 10% FCS medium, harvested when the plate was full and re-suspended in PBS (#8537, Sigma Aldrich), aliquoted (2-3 aliquots per 100mm culture dish, depending on cell type) and centrifuged at 500g for 10 min at 4°C. After aspiring supernatant, resulting cell pellets were snap-frozen on dry-ice and kept at -80°C until further use.

KIF1C pull-down. Performed in parallel in COS-7 and HEK293T cells, both lines were transfected with three different constructs: pCS2+KIF1C$_{WT}$-HA, pCS2+KIF1C$_{G102A}$-HA and pCS2+KIF1C$_{P176L}$-HA. Cells were harvested and re-suspended in 1 ml of Lysis buffer (#87788, ThermoScientific) and centrifuged at maximum speed for 30 min. Following the Crosslink Magnetic IP and Co-IP Kit (#88805, ThermoScientific) collected supernatants were incubated with protein A/G magnetic beads previously coupled to the respective antibody (HA or IgG) and then protein complexes were eluted from beads. Eluted samples were loaded into an SDS-PAGE gel which was later fixed and silver stained to detect protein bands. The desired band was cut off the gel and sent to the TSRI Center for Mass Spectometry in Miami (FL, USA) for further analysis.

(CO-) Immunoprecipitation (CO-IP). Was performed following the Classic Magnetic IP and Co-IP Kit (#88804, ThermoScientific). Cell pellets were thawed and re-suspended in 0.5 ml of Lysis buffer supplemented with Proteinase inhibitor (Sigma) and incubated at 4ºC for 30 min with rotation. Cell lysates were then centrifuged at 14.000 r.p.m. for 15 min. 50 µl of supernatant was saved as "input" sample and the rest (0.5-1mg protein) was incubated with 2-10 µg of the respective antibody (HA, KIF1C, PABP, RPS6 or IgG) overnight at 4°C rotating and then linked to 0.25 mg protein A/G Magnetic beads for 1 hour at room temperature (RT). After washings, immunoprecipitated protein complexes were finally eluted from the beads in 100µl of loading buffer (10µl 10x DTT, 20µl 5x loading dye, 70µl H2O) for 10 min at RT.

Western Blot. Either 1/2 or 1/3 of eluted IP samples and 30-50µg of input samples were loaded into 8% BIS-TRIS gels and run at a constant 20mA per gel for 2 hours in 1x MOPS buffer. Proteins were then transferred onto a PVDF membrane (Milipore), or to Nitrocellulose for iCLIP, at 4°C overnight and 25V. Blocking was done in TBST + 5% milk and antibodies were incubated at 4°C overnight (Primary) and at RT for 1 hour (Secondary) in TBST + 1% milk. ECL detection was done with 10 ml of ECL-solution (10% Tris[1M] pH 8,5 + 0,5% Luminol[4,4%] + 0,22% PCA[1,5%] in water) plus 10µl 30% H_2O_2. Blots were imaged using the ChemiDoc System (Bio-Rad) and images were processed and analyzed with Image Lab 5.1 software (Bio-Rad).

Immunofluorescent microscopy. Untransfected or transfected COS-7 or SH-SY5Y cells were fixed in 4% Paraformaldehyde (PFA) in PBS for 20 minutes, washed once with PBS + 0.1% Triton X-100 (TPBS) and blocked for 1 hour at RT with TPBS + 5% FCS. Primary and secondary antibodies were incubated in TPBS + 1% Bovine serum albumin (BSA) inside a moist chamber at 4°C overnight and for 1 hour at RT respectively. Coverslips were mounted into the slides with Dako fluorescent mounting media (Dako, Agilent). Cells were imaged using a LSM 510 Confocal Axiovert 200M inverted microscope (Zeiss), the resulting images were processed and analyzed with Fiji software and employing the "Coloc2" plugin to quantify co-localization through the Pearson's-R correlation coefficient measured above threshold.

RNAse-COIP. Followed the same procedure as for a CO-IP but adding either RNAse I (RNAse If, NEB) or RNAse inhibitor (RNAseOUT, Invitrogen) to the Lysis buffer.

Individual-nucleotide resolution UV crosslinking immunoprecipitation. Following the method described by Huppertz I. and colleagues (30) we used HEK293T cells transfected either with pmCherryN1-KIF1C$_{WT}$ or pmCherryN1 empty vector (as a control). Transfected cells were irradiated with a pulse of 150 mJ/cm^2 at 254 nm in a Stratalinker 2400 (Stratagene) and harvested in PBS (a non-crosslinked control was included). Cells were lysed in lysis buffer containing a low RNAse dilution (1:500) and incubated with magnetic beads for overnight immunoprecipitation. IP was followed by high-salt buffer washes; dephosphorylation of RNA 3'-ends with polynucleotide kinase (PNK) (NEB); ligation to RNA 3'-ends of linker L3 (5'P-AAGATCGGAAGAGCGGTTCAG-3ddC); and a final

RNA 5’-end ATP labelling with PNK. Then samples were loaded on a SDS-PAGE and transferred to Nitrocellulose membrane which was stained with Ponceau solution to visualize protein bands. Desired region was cut off and treated with proteinase K (ThermoScientific) to degrade proteins, leaving just small peptides bound to RNA molecules at CL sites. This was followed by phenol/chloroform RNA isolation and overnight ethanol (ETOH) precipitation. Recovered RNA was mixed with Rclip13 primer (5'P-NNTCCGNNNAGATCGGAAGAGCGTCGTGGATCCTGAACCGC) and reverse transcribed using Superscript III kit (Invitrogen). Resulting cDNA was precipitated overnight in ETOH and then loaded into a 6% TBE-urea gel (Invitrogen) to purify and separate by size. Three fractions at 120-200 nt (high), 85-120 nt (medium) and 70-85 nt (low) were cut off from each sample, which were later purified and precipitated overnight in ETOH. On the next day a cut_oligo (GTTCAGGATCCACGACGCTCTTCaaaa) was annealed to 5’-ends of cDNA fragments and molecules were circularized using CircLigase II (Epicentre) to be later again linearized with BamHI (Fermentas). After cDNA purification and precipitation, samples were PCR amplified with P5/P3 solexa primers (AATGATACGGCGACCACCGAGATCTACACTCTTTCCCTACACGACGCTCTTCCGATCT / CAAGCAGAAGACGGCATACGAGATCGGTCTCGGCATTCCTGCTGAACCGCTCTTCCGATCT) using Accuprime Supermix enzyme (Invitrogen). Finally, aliquots of the samples were used for quality control on the Agilent bioanalyzer (High sensitivity DNA chip) to visualize cDNA bands.

Library preparation & next generation sequencing. Positive samples on the TBE gel were retrieved, purified and prepared for sequencing. A cDNA library was generated pooling lanes 7 and 8 together (Figure S9B), and then four different concentrations (6, 8, 10 and 12 pM) of this library were prepared in duplicates, thus obtaining eight separate replicates**.** High-throughput sequencing of the replicates was carried out by IMGM Laboratories GmbH (Germany) with an Illumina HiSeq 2500 system. Sequencing was set as a non-stranded paired-end run (2x50bp). Sequencing data containing the reads was retrieved and stored as fastq files.

Analysis of sequencing data. Fastq files were processed with Galaxy (https://usegalaxy.org) (48) as follows: all files from each sample (8 repetitions) were uploaded and treated independently and

concatenated into 2 files containing either all R1 reads (50bp) or all R2 reads (50bp). Concatenated read files were formatted with the FastqGrommer tool, QC read quality was checked and reads were finally aligned to the hg19 human genome using the Bowtie2 tool with default settings: Pair-end library (fastq file for R1 concatenate and fastq file for R2 concatenate); Minimum fragment length for valid pair-end alignment: 0; Maximum fragment length for valid pair-end alignment: 450; upstream/downstream mate orientations for a valid paired-end alignment against the forward reference strand: --fr; no-mixed behavior: No; no-discordant behavior: No; Allow mate dovetailing: No; Allow one mate alignment to contain another: No; Allow mate alignments to overlap: No. Resulting .BAM files were analyzed using the PIPE-CLIP pipeline developed by Dr. Beibei Chen (31) from QBRC (TX, USA). Since PIPE-CLIP deals with pair-end as two single fragments, in order to reduce noise introduced by the second fragment of each sequenced pair, only the first fragment (R1 reads) containing the CLIP site were kept for further analysis. Mapped reads were filtered to exclude reads shorter than 20bp and with a maximum mismatch of 2bp. Crosslinking sites were predicted and annotated without removing the PCR duplicates and FDR for both enriched clusters and reliable mutations were set to 0.05 (-r 0 –M 0.05 –C 0.05). An individual output file was retrieved for each sample (8 replicates) containing a list of identified crosslinking sites and their matching transcripts. These were later mapped to the respective genes and sorted by descending peak score (number of reads). Then all genes identified across the 8 replicates were pooled together, with their respective peak score values, into a final list containing unique genes (Table S3). To normalize for peak score, genes in the list were given 8 values depending on how they ranked in the respective origin lists and then these values were summed up to allow gene sorting by ascending ranking value. Finally the total number of genes per replicate was estimated by giving 1-values if a gene was present or 0-values if absent and summing numbers up.

RNA-Immunoprecipitation. We used cell pellets of untransfected HEK293T and HEK293T cells transfected with pCS2+KIF1C-HA for the endogenous and overexpressed RIP respectively; and followed the above mentioned IP protocol although prior to protein elution we proceeded to the purification of RNA: Samples were washed repeatedly and digested with proteinase K solution, RNA was then extracted using the Phenol-Chloroform method and isolated through ethanol precipitation

following the Magna RIP protocol (#17-700, Milipore). After RNA recovery, equal amounts of input and immunoprecipitated sample were retro-transcribed to cDNA using the High fidelity cDNA synthesis kit (#05081955001, Roche), and then used the cDNA as PCR template using different primers (Table S4) specifically designed for quantitative PCR amplification and a GoTaq2 polymerase (M7801, Promega). PCR products were loaded into a 2% agarose gel and ran at 120V for 30min, images were captured with the Bio-Capt software on a UV-light Vilber Lourmat device.

Functional Annotation. Only genes (Table S3) detected in at least four of the eight replicates (n=441) were included in the joint analysis with DAVID Bioinformatics Resources 6.7, NIAID/NIH (david.ncifcrf.gov) (32). Since DAVID does not recognize all HGNC symbols, some were sequentially converted to different ID symbols and mapped to other gene lists: 396 IDs were mapped using Ensembl's IDs (GRCH38.p3), 21 IDs mapped with HGNC symbols, 2 IDs mapped to Unigene accession symbols, 1 mapped to Ensembl Transcript IDs (GRCH38.p3) and 21 genes couldn't be mapped to DAVID, including 16 RNA genes (ncRNA, miRNA, lncRNA, mt-rRNA), 4 pseudogenes, and 1 fusion protein gene. All gene IDs were then combined and submitted to DAVID. Fort the creation of the functional annotation chart EASE parameter was set to 0.05 and the rest were set as default; and for the Enrichment map we used the Cytoscape 3.2 plugin with the following parameters (p-value: 0.0001, FDR Q-value: 0.05, similarity overlap: 0.4). Finally, enrichment map was edited in Adobe Illustrator, changing node colors to represent data source: GO-terms: red, Reactome: orange, Panther biological process: purple, Panther molecular function: yellow, RNA genes were added manually in green.

Antibodies. Mouse monoclonal PABP(10E10) (NB120-6125, Novus Biologicals), rabbit polyclonal PABP (ab21060, Abcam), goat polyclonal IMP-1(E-20) (sc-21026, Santa Cruz Biotechnology), mouse monoclonal HSC70(13D3) (MA3-014, ThermoScientific), rabbit monoclonal HSPA8(D12F2) (8444, Cell Signaling), mouse monoclonal anti-HA (26183, ThermoScientific), rabbit monoclonal HA-Tag(C29F4) (3724, Cell Signaling), mouse monoclonal ß-Tubulin (32-2600, Invitrogen), mouse monoclonal ß-Actin (A5441, Sigma), rabbit polyclonal anti-BICD2 (HPA023013, Sigma Life Science), rabbit polyclonal anti-KIF1C (AKIN11, Cytoskeleton), rabbit polyclonal anti-KIF1C

(ab72238, abcam), mouse monoclonal anti-GM130 (610823, BD Biosciences), mouse monoclonal GAPDH (H86504M, Meridian Life Science), rabbit polyclonal mCherry (PA5-34974, ThermoScientific), mouse GFP-tag (GF28R, ThermoScientific), mouse S6 Ribosomal protein (2317, Cell Signaling), rabbit S6 Ribosomal protein (710405, Novex), normal mouse IgG (sc-2025, Santa Cruz Biotechnology), normal rabbit IgG (sc-2027, Santa Cruz Biotechnology), Anti-rabbit/mouse IgG HRP-linked (7074 & 7076, Cell Signaling), donkey anti-goat IgG-HRP (sc-2020, Santa Cruz Biotechnology), goat anti-mouse alexa-488, goat anti-rabbit alexa-488, goat anti-mouse alexa-568, goat anti-rabbit alexa-568 (A-11001, A-11008, A-11004, A-11011, Invitrogen).

Primers. All primers used for the study can be found within Table S4 in the supplement.

Statistics and Graphics. GraphPad Prism 5 (GraphPad Software Inc., CA, USA) was the software of choice for the statistical analysis using 1 way ANOVA with Dunnett's Multiple Comparison Test when comparing two or more groups against a control group; or performing an unpaired t-test when comparing only two groups against each other. Graphs were also created using GraphPad Prism 5 software, bars drawn in the graphs represent the mean + SEM.

Author contributions

Andrés Caballero-Oteyza contributed with conceptualization and design; acquisition, analysis and interpretation of data; generation of figures for publication, drafting and revising the manuscript.

Stefan Kotschote contributed with acquisition, analysis and interpretation of data; and critical review of the manuscript.

Beibei Chen contributed with analysis and interpretation of data; and critical review of the manuscript.

Jennifer Reichbauer contributed with acquisition of data and critical review of the manuscript.

Angelos Skodras contributed with analysis and interpretation of data; and critical review of the manuscript.

Alleene Strickland contributed with analysis and interpretation of data; and critical review of the manuscript.

Adriana Rebelo contributed with acquisition, analysis and interpretation of data; and critical review of the manuscript.

Günther Woehlke contributed critically reviewing the manuscript.

Ludger Schöls contributed with supervision and critical review of the manuscript.

Stephan Züchner contributed critically reviewing the manuscript.

Michael Bonin contributed with supervision and critical review of the manuscript.

Rebecca Schüle contributed with conceptualization and design; supervision; analysis and interpretation of data; drafting and critically revising the manuscript.

Acknowledgements

This study was supported by the European Union within the 7th European Community Framework Programme through funding for the NEUROMICS network (F5-2012-305121 to L.S.), the E-Rare Network NEUROLIPID (01GM1408B to RS) and a Marie Curie International Outgoing Fellowship (grant PIOF-GA-2012-326681 to R.S. and L.S.), and the Center for Clinical Research (IZKF) Tübingen (grant 1970-0-0 to R.S.).

We would like to acknowledge Caro Schönfeld for her technical assistance and we would like to thank Dr. Anne Straube and Dr. Matthias Hentze for the materials provided.

References

1. Sedel F, Fontaine B, Saudubray JM, Lyon-Caen O. Hereditary spastic paraparesis in adults associated with inborn errors of metabolism: a diagnostic approach.. *J. Inherit. Metab. Dis.* 2007;30(6):855–864.

2. McMonagle P, Webb S, Hutchinson M. The prevalence of "pure" autosomal dominant hereditary spastic paraparesis in the island of Ireland.. *J. Neurol. Neurosurg. Psychiatry* 2002;72(1):43–46.

3. Klebe S, Stevanin G, Depienne C. Clinical and genetic heterogeneity in hereditary spastic paraplegias: From SPG1 to SPG72 and still counting. *Rev. Neurol. (Paris).* 2015;171(6-7):505–530.

4. Schule R, Schols L. Genetics of hereditary spastic paraplegias.. *Semin. Neurol.* 2011;31(5):484–493.

5. Lin MY, Sheng ZH. Regulation of mitochondrial transport in neurons. *Exp. Cell Res.* 2015;334(1):35–44.

6. Graber TE et al. Reactivation of stalled polyribosomes in synaptic plasticity. TL - 110 [Internet]. *Proc. Natl. Acad. Sci. U. S. A.* 2013;110 VN - (40):16205–16210.

7. Frandemiche ML et al. Activity-dependent tau protein translocation to excitatory synapse is disrupted by exposure to amyloid-beta oligomers.. *J. Neurosci.* 2014;34(17):6084–6097.

8. Ferrer I. Neurons and their dendrites in frontotemporal dementia.. *Dement. Geriatr. Cogn. Disord.* 1999;10 Suppl 1:55–60.

9. Raymond LA et al. Pathophysiology of Huntington's disease: time-dependent alterations in synaptic and receptor function.. *Neuroscience* 2011;198:252–273.

10. Lagier-Tourenne C, Polymenidou M, Cleveland DW. TDP-43 and FUS/TLS: emerging roles in RNA processing and neurodegeneration.. *Hum. Mol. Genet.* 2010;19(R1):R46–64.

11. Darnell JC et al. FMRP stalls ribosomal translocation on mRNAs linked to synaptic function and autism.. *Cell* 2011;146(2):247–261.

12. Piazzon N et al. In vitro and in cellulo evidences for association of the survival of motor neuron complex with the fragile X mental retardation protein.. *J. Biol. Chem.* 2008;283(9):5598–5610.

13. Beirowski B. Concepts for regulation of axon integrity by enwrapping glia.. *Front. Cell. Neurosci.*

2013;7:256.

14. F??ger P et al. Spastic Paraplegia Mutation N256S in the Neuronal Microtubule Motor KIF5A Disrupts Axonal Transport in a Drosophila HSP Model. *PLoS Genet.* 2012;8(11). doi:10.1371/journal.pgen.1003066

15. Kasher PR et al. Direct evidence for axonal transport defects in a novel mouse model of mutant spastin-induced hereditary spastic paraplegia (HSP) and human HSP patients. *J. Neurochem.* 2009;110(1):34–44.

16. Lo KY, Kuzmin A, Unger SM, Petersen JD, Silverman MA. KIF1A is the primary anterograde motor protein required for the axonal transport of dense-core vesicles in cultured hippocampal neurons. *Neurosci. Lett.* 2011;491(3):168–173.

17. Caballero Oteyza A et al. Motor protein mutations cause a new form of hereditary spastic paraplegia. [Internet]. *Neurology* [published online ahead of print: 2014]; doi:10.1212/WNL.0000000000000479

18. Schlager MA et al. Bicaudal D Family Adaptor Proteins Control the Velocity of Dynein-Based Movements. *Cell Rep.* 2014;8(5):1248–1256.

19. Dorner C et al. Characterization of KIF1C, a new kinesin-like protein involved in vesicle transport from the Golgi apparatus to the endoplasmic reticulum.. *J. Biol. Chem.* 1998;273(32):20267–20275.

20. Theisen U, Straube E, Straube A. Directional Persistence of Migrating Cells Requires Kif1C-Mediated Stabilization of Trailing Adhesions. *Dev. Cell* 2012;23(6):1153–1166.

21. Kopp P et al. The kinesin KIF1C and microtubule plus ends regulate podosome dynamics in macrophages.. *Mol. Biol. Cell* 2006;17(6):2811–2823.

22. Lee PL, Ohlson MB, Pfeffer SR. Rab6 regulation of the kinesin family KIF1C motor domain contributes to Golgi tethering. [Internet]. *Elife* 2015;4. doi:10.7554/eLife.06029

23. Efimova N et al. Podosome-regulating kinesin KIF1C translocates to the cell periphery in a CLASP-dependent manner. [Internet]. *J. Cell Sci.* 2014;127(24):5179–88.

24. Oates EC et al. Mutations in BICD2 cause dominant congenital spinal muscular atrophy and hereditary spastic paraplegia.. *Am. J. Hum. Genet.* 2013;92(6):965–973.

25. Novarino G et al. Exome sequencing links corticospinal motor neuron disease to common

neurodegenerative disorders. [Internet]. *Science* 2014;343(6170):506–11.

26. Wozniak MJ, Melzer M, Dorner C, Haring H-U, Lammers R. The novel protein KBP regulates mitochondria localization by interaction with a kinesin-like protein. [Internet]. *BMC Cell Biol.* 2005;6(1):35.

27. Zhang H et al. PABPC1 interacts with AGO2 and is responsible for the microRNA mediated gene silencing in high grade hepatocellular carcinoma.. *Cancer Lett.* 2015;367(1):49–57.

28. Bley N et al. Stress granules are dispensable for mRNA stabilization during cellular stress.. *Nucleic Acids Res.* 2015;43(4):e26.

29. Kakumani PK et al. Dengue NS3, an RNAi suppressor, modulates the human miRNA pathways through its interacting partner.. *Biochem. J.* 2015;471(1):89–99.

30. Huppertz I et al. iCLIP: Protein-RNA interactions at nucleotide resolution. *Methods* 2014;65(3):274–287.

31. Chen B, Yun J, Kim MS, Mendell JT, Xie Y. PIPE-CLIP: a comprehensive online tool for CLIP-seq data analysis. [Internet]. *Genome Biol.* 2014;15(1):R18.

32. Huang DW, Sherman BT, Lempicki RA. Systematic and integrative analysis of large gene lists using DAVID bioinformatics resources.. *Nat. Protoc.* 2009;4(1):44–57.

33. Kini HK, Silverman IM, Ji X, Gregory BD, Liebhaber SA. Cytoplasmic poly(A) binding protein-1 binds to genomically encoded sequences within mammalian mRNAs [Internet]. *RNA (New York, NY)* 2015;61–74.

34. Singh G, Rebbapragada I, Lykke-Andersen J. A competition between stimulators and antagonists of Upf complex recruitment governs human nonsense-mediated mRNA decay. *PLoS Biol.* 2008;6(4):860–871.

35. Patel GP, Ma S, Bag J. The autoregulatory translational control element of poly(A)-binding protein mRNA forms a heteromeric ribonucleoprotein complex.. *Nucleic Acids Res.* 2005;33(22):7074–7089.

36. Ross AF, Oleynikov Y, Kislauskis EH, Taneja KL, Singer RH. Characterization of a beta-actin mRNA zipcode-binding protein.. *Mol. Cell. Biol.* 1997;17(4):2158–2165.

37. Yao J, Sasaki Y, Wen Z, Bassell GJ, Zheng JQ. An essential role for beta-actin mRNA localization and translation in Ca2+-dependent growth cone guidance.. *Nat. Neurosci.* 2006;9(10):1265–1273.

38. Zhang HL et al. Neurotrophin-induced transport of a beta-actin mRNP complex increases beta-actin levels and stimulates growth cone motility.. *Neuron* 2001;31(2):261–275.

39. Vickers TA, Crooke ST. Antisense oligonucleotides capable of promoting specific target mRNA reduction via competing RNase H1-dependent and independent mechanisms.. *PLoS One* 2014;9(10):e108625.

40. Castello A et al. Insights into RNA Biology from an Atlas of Mammalian mRNA-Binding Proteins. *Cell* 2012;149(6):1393–1406.

41. Baltz AG et al. The mRNA-Bound Proteome and Its Global Occupancy Profile on Protein-Coding Transcripts. *Mol. Cell* 2012;46(5):674–690.

42. König J, Zarnack K, Luscombe NM, Ule J. Protein–RNA interactions: new genomic technologies and perspectives [Internet]. *Nat Rev Genet* 2012;13(2):77–83.

43. Kim HK, Kim Y-B, Kim E-G, Schuman E. Measurement of dendritic mRNA transport using ribosomal markers.. *Biochem. Biophys. Res. Commun.* 2005;328(4):895–900.

44. Krichevsky AM, Kosik KS. Neuronal RNA granules: a link between RNA localization and stimulation-dependent translation.. *Neuron* 2001;32(4):683–696.

45. Bartoli KM, Jakovljevic J, Woolford JLJ, Saunders WS. Kinesin molecular motor Eg5 functions during polypeptide synthesis.. *Mol. Biol. Cell* 2011;22(18):3420–3430.

46. Baumann S, Pohlmann T, Jungbluth M, Brachmann A, Feldbrugge M. Kinesin-3 and dynein mediate microtubule-dependent co-transport of mRNPs and endosomes.. *J. Cell Sci.* 2012;125(Pt 11):2740–2752.

47. Bisbal M et al. KIF4 mediates anterograde translocation and positioning of ribosomal constituents to axons.. *J. Biol. Chem.* 2009;284(14):9489–9497.

48. Goecks J, Nekrutenko A, Taylor J. Galaxy: a comprehensive approach for supporting accessible, reproducible, and transparent computational research in the life sciences [Internet]. *Genome Biol.* 2010;11(8):1–13.

Figures and Figure legends

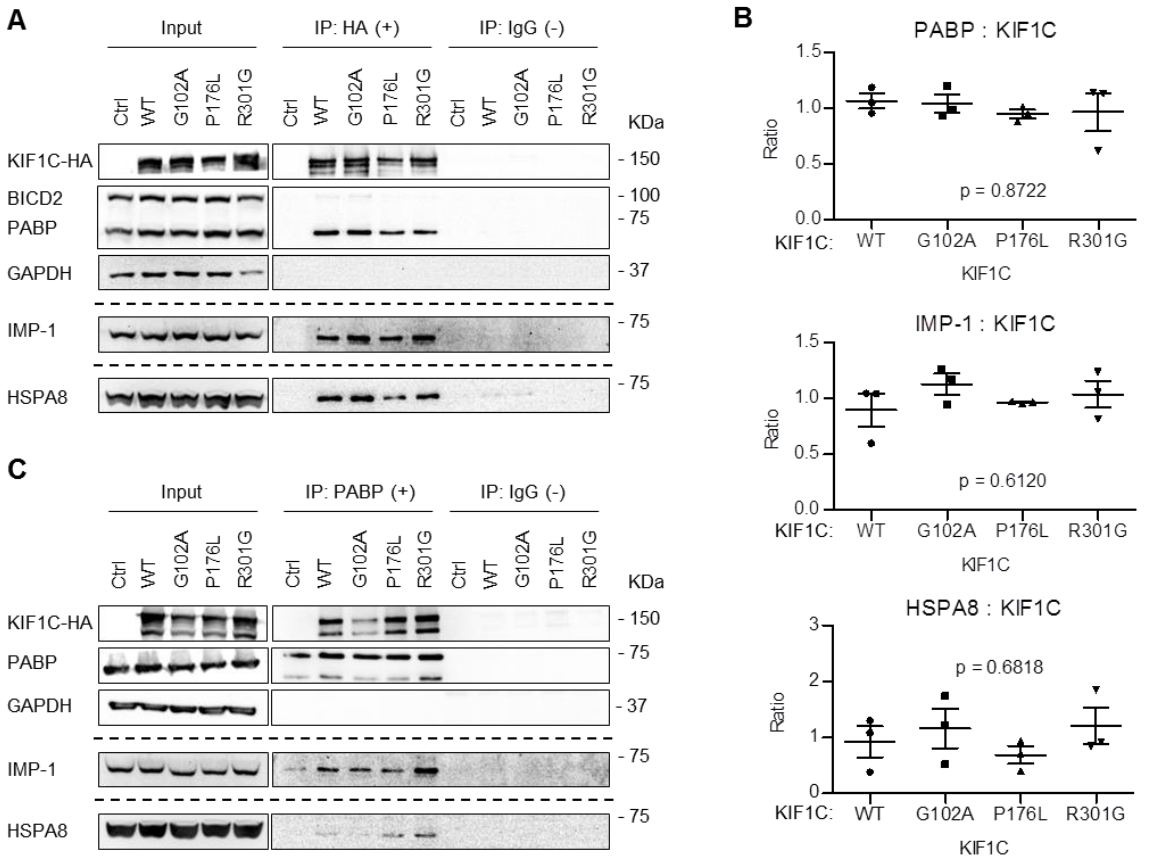

Figure 1. Immunoprecipitation of KIF1C protein complexes from lysates of HEK293T cells untransfected (Ctrl) or transfected with plasmids encoding $KIF1C_{WT}$-HA, $KIF1C_{G102A}$-HA, $KIF1C_{P176L}$-HA or $KIF1C_{R301G}$-HA respectively and co-immunoprecipitated with an anti-HA antibody **(A)** or an anti-PABP antibody **(C).** Proteins $KIF1C_{WT}$-HA, PABP, IMP-1 and HSPA8 co-immunoprecipitate and are positively detected by western blot on both IP and input (50µg) lanes, whereas proteins BICD2 and GAPDH are absent on the IP lanes. Dotted lines delimit different blots. **(B)** Quantification of the relative amount of PABP, IMP-1 or HSPA8 bound to KIF1C between $KIF1C_{WT}$ and the different mutant isoforms, for the Co-IP seen in **(A)**, using data from 3 independent IP experiments. Statistics: 1way ANOVA with Dunnett's Multiple Comparison Test, bars represent mean+SEM, p-values given for each comparison.

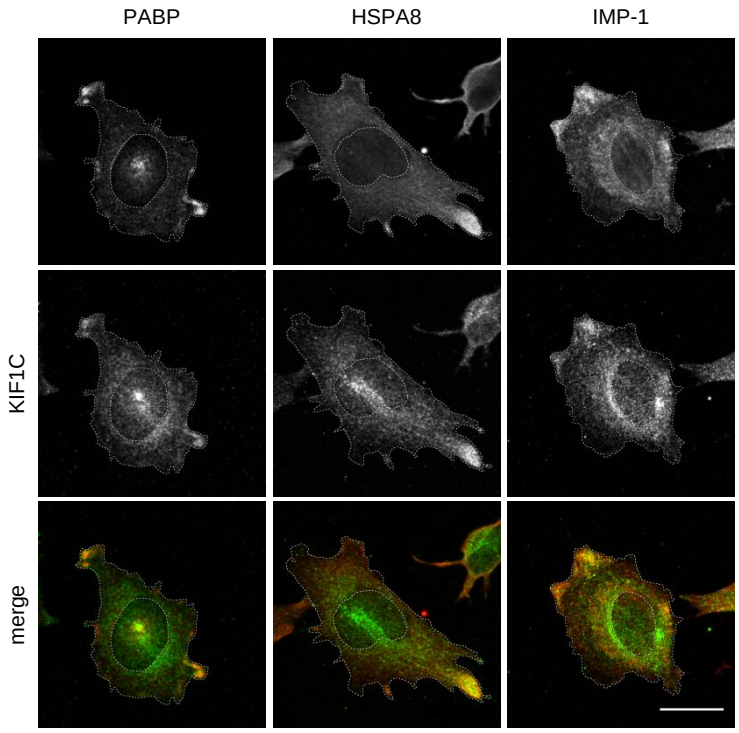

Figure 2. Co-localization of endogenous KIF1C Images show fluorescent immunostainings of SH-SY5Y cells where endogenous KIF1C co-localizes with PABP mainly around the centrosome and at the tips of cellular extensions. KIF1C-HSPA8 co-localization is mainly found at the tip of cellular processes. KIF1C-IMP-1 co-localization also happens at the edges of cellular protrusions and partially around the nucleus. Fine dotted lines delimit nucleus and cell contours, scale bar: 20µm.

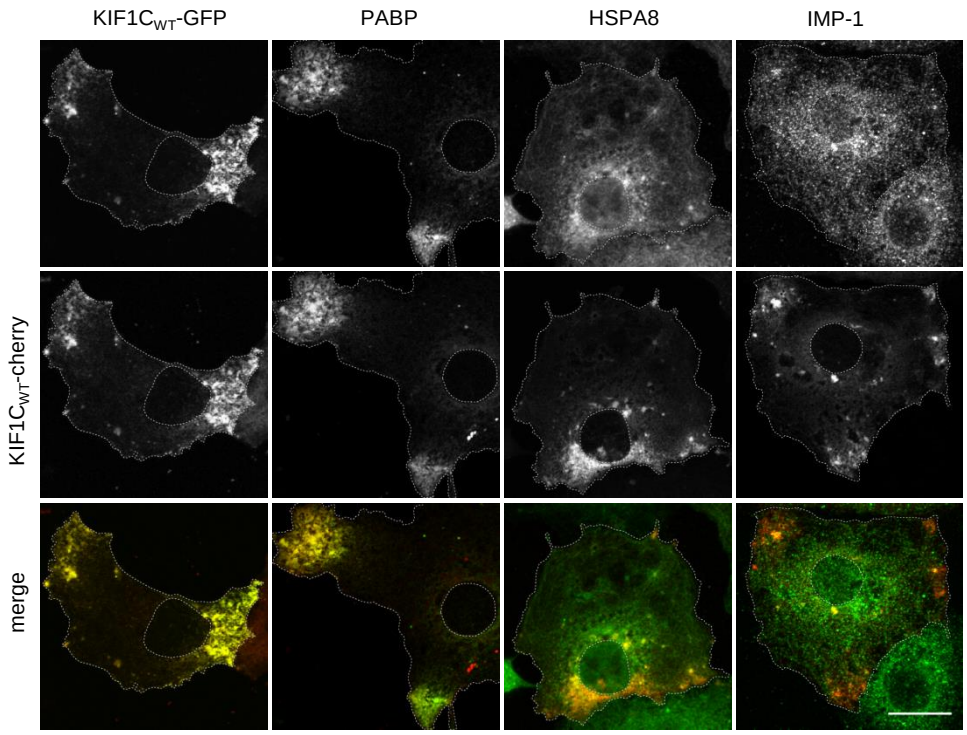

Figure 3. Co-localization of overexpressed KIF1C$_{WT}$ Images show distribution of overexpressed KIF1C$_{WT}$-cherry in COS-7 cells immunolabelled with endogenous PABP, HSPA8 or IMP-1 or co-transfected with KIF1C$_{WT}$-GFP (control for co-localization). Co-localization between KIF1C$_{WT}$ and PABP is almost complete. KIF1C-HSPA8 co-localization is restricted to sites of KIF1C accumulation, and KIF1C-IMP1 co-localization is limited to a few specific spots. Fine dotted lines delimit nucleus and cell contours, scale bar: 20µm.

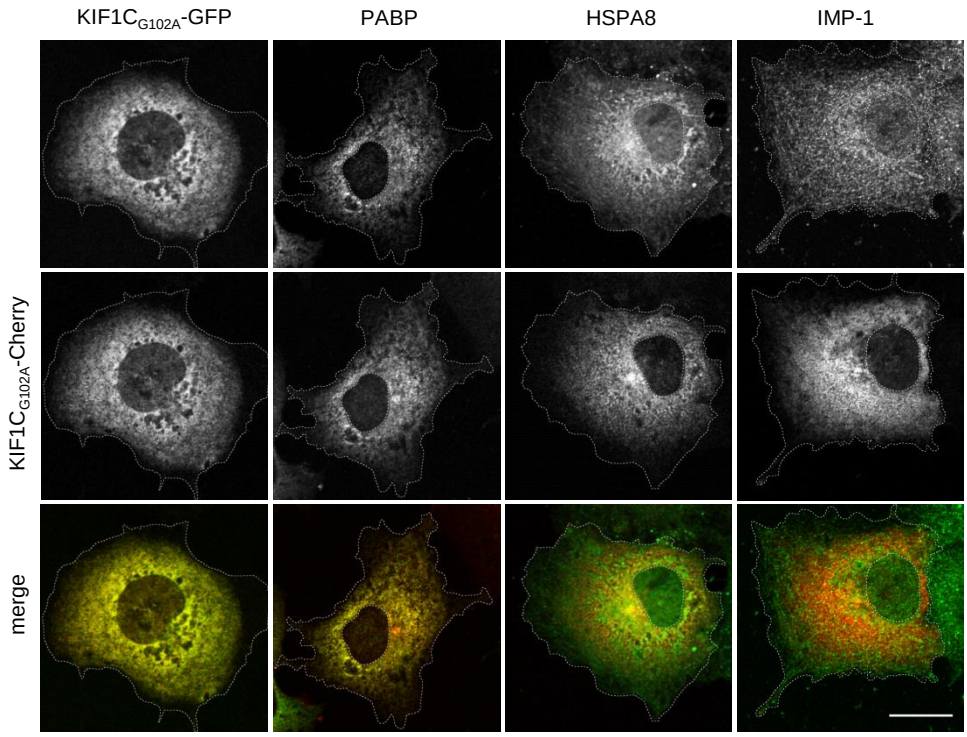

Figure 4. Co-localization of overexpressed KIF1C$_{G102A}$ Images show distribution of overexpressed KIF1C$_{G102A}$-cherry in COS-7 cells immunolabelled with endogenous PABP, HSPA8 or IMP-1, or co-transfected with KIF1C$_{G102A}$-GFP (control for co-localization). Mutant KIF1C$_{G102A}$ loses its predilection for the cell periphery leading to redistribution of PABP, the co-localization between the two proteins is almost complete. HSPA8 is drawn to sites of KIF1C$_{G102A}$ accumulation, while IMP-1 and KIF1C$_{G102A}$ co-localize in few specific spots. In summary, the distribution of the KIF1C$_{G102A}$ complex is altered compared to KIF1C$_{WT}$, however the extent of interaction with PABP, HSPA8 and IMP-1 seems unperturbed. Fine dotted lines delimit nucleus and cell contours, scale bar: 20µm.

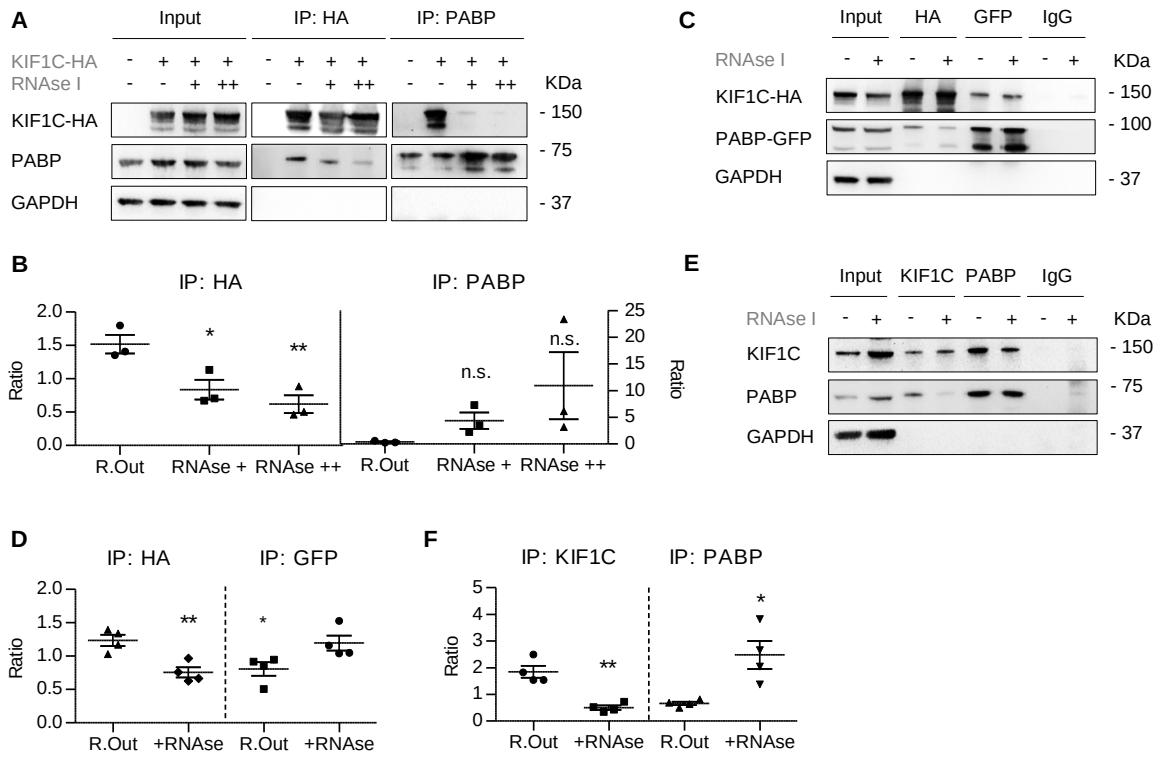

Figure 5. RNAse-COIP experiment on HEK293T cells untransfected or overexpressing KIF1C$_{WT}$-HA. **(A)** KIF1C$_{WT}$-HA and PABP co-immunoprecipitate either with anti-PABP or anti-HA antibodies**.** As expected no KIF1C$_{WT}$-HA was pulled-down in the untransfected sample. Addition of RNAse I to the lysis buffer reproducibly led to a reduction in the affinity between KIF1C and PABP; quantification of this phenomenom is represented in **(B)** (n=3). **(C)** RNAse-COIP of HEK293T co-expressing KIF1C$_{WT}$-HA and PABP-GFP fusion proteins; both proteins co-immunoprecipitate with anti-GFP and anti-HA antibodies. As expected nothing was pulled-down with an IgG control antibody. Addition of RNAse I to the lysis buffer reproducibly led to a reduction in the affinity between KIF1C$_{WT}$-HA and PABP-GFP; quantification of this phenomenom is represented in **(D)** (n=4). **(E)** Same experiment in HeLa cells using antibodies against endogenous KIF1C and PABP for co-immunoprecipitation; quantification of this effect is represented in **(F)** (n=4). Bars in Graphs represent mean+SEM. Statistics: 1 way ANOVA with Dunnets test for **(B)** and unpaired t-tests for **(D)** and **(F)**.

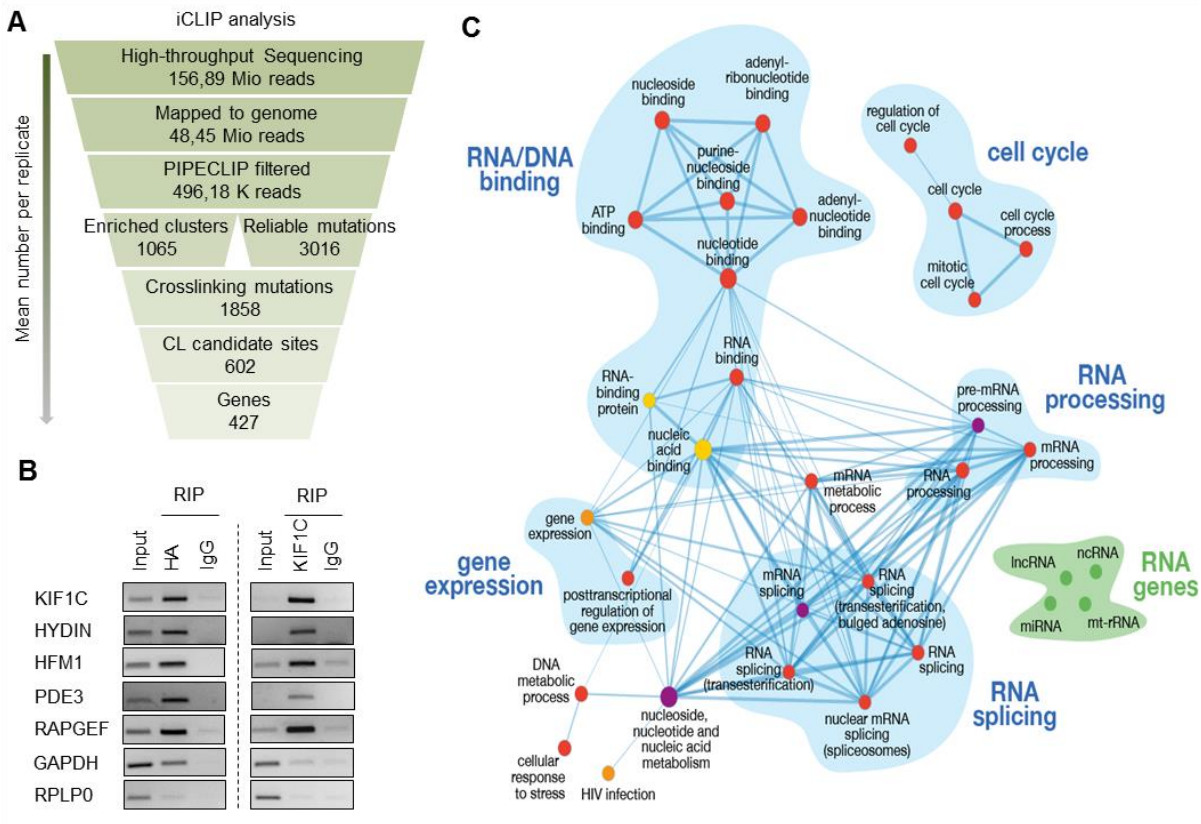

Figure 6. Identification and characterization of transcripts bound to KIF1C (**A**) Funnel shows the filtering of iCLIP sequencing data with PIPE-CLIP tool. (**B**) Confirmation of RNA transcripts bound to KIF1C was done through RIP and later RT-PCR of the recovered RNA. Agarose gels show the presence and over-representation on the IP-positive sample of 5 transcripts which were among the first 10 genes with the highest peak score in the list (Table S3). GAPDH is representative of genes with low peak score and RPLP0 is a negative control. Left-side gels show cDNA from immunoprecipitated RNA of HEK293T overexpressing KIF1C$_{WT}$-HA pulled-down with anti-HA or -IgG antibody; right-side gels show cDNA from immunoprecipitated RNA of untransfected HEK293T. **(C)** Enrichment map of functional pathways in which the transcripts bound to KIF1C are involved. The network contains all genes present in at least 4 of the 8 replicates of the iCLIP experiment and annotated with DAVID bioinformatic functional tool. Node colors represent data source: GO-terms: red, Reactome: orange, Panther biological process: purple, Panther molecular function: yellow, RNA genes were added manually in green.

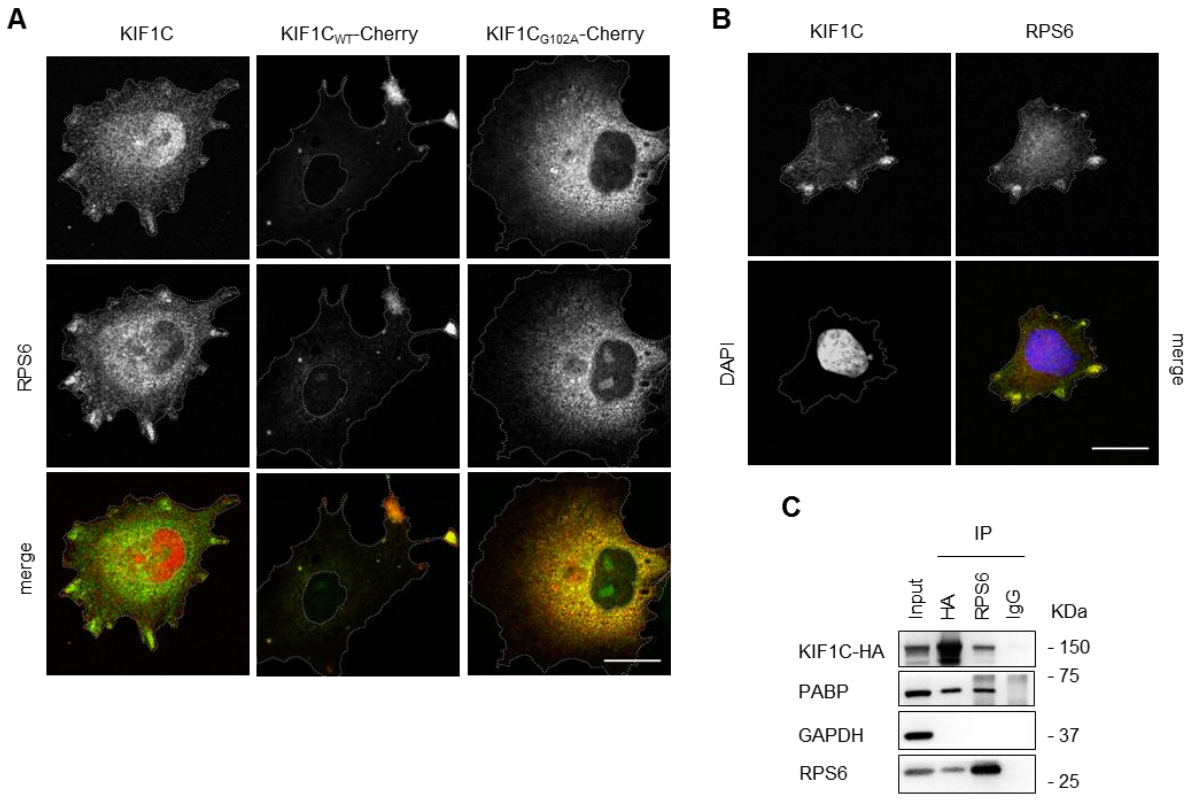

Figure 7. KIF1C interacts with Ribosomes (A) Images show fluorescent immunostainings of either endogenous KIF1C, overexpressed KIF1C$_{WT}$-Cherry or KIF1C$_{G102A}$-Cherry with the ribosomal protein S6 (RPS6) in COS-7 cells. In endogenous conditions KIF1C co-localizes with RPS6 at the tips of cellular protrusions, however after KIF1C overexpression almost all RPS6 is sequestered resulting in a stronger co-localization pattern. Fine dotted lines delimit nucleus and cell contours, scale bar: 20µm. **(B)** Co-staining of endogenous KIF1C and PABP in SH-SY5Y cells also shows co-localization at the cell verges. **(C)** Membrane shows how KIF1C$_{WT}$-HA co-immunoprecipitates with RPS6 in HEK293T cells transfected with KIF1C$_{WT}$-HA and pulled down with an anti-HA or anti-RPS6 antibody. As previously shown PABP protein also co-immunoprecipitates with KIF1C$_{WT}$-HA and RPS6; as expected nothing was pulled down with the IgG control antibody (30µg of input sample was loaded as control).

Supplemental data

Evaluation of other previously reported KIF1C interaction.

KIF1C has been also implicated in the vesicular transport of α5-integrins (1). Indeed, overexpressed α5-integrin (ITGA5) and endogenous KIF1C seem to co-localize in the perinuclear region to some extent (Figure S5), however, this could not be confirmed when overexpressing $KIF1C_{WT}$ or $KIF1C_{G102A}$ (Figure S3, Figure S4). Moreover, we were not able to reproduce the perinuclear vesicular staining pattern for α5-integrin and KIF1C described by Theisen et al. in human retinal pigment epithelial cells (1). To exclude that we were missing the vesicular pattern due to artifacts of paraformaldehyde cell fixation we repeated the experiment under live cell conditions in COS-7 cells co-transfected with plasmids respectively encoding for ITGA5 and $KIF1C_{WT}$, which were kindly provided by Theisen et al., nevertheless we could not reproduce the co-localization pattern described by them (1) (data not shown).

References

1. Theisen U, Straube E, Straube A. Directional Persistence of Migrating Cells Requires Kif1C-Mediated Stabilization of Trailing Adhesions. *Dev. Cell* 2012;23(6):1153–1166.

Supplemental figures

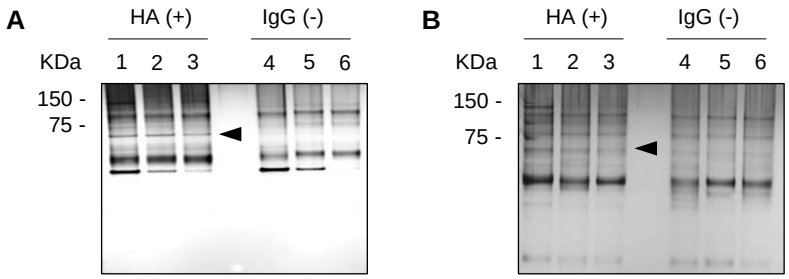

Figure S1. KIF1C pull-down Images represent two different silver stained SDS-PAGE gels to detect all loaded proteins with high sensitivity. Samples correspond to **COS-7 (A)** cells overexpressing $KIF1C_{WT}$ (Lanes 1,4), $KIF1C_{G102A}$ (2,5) or $KIF1C_{P176L}$ (3,6) lysates of which were co-immunprecipitated with an anti-HA or an IgG control antibody. **(B)** Same experiment as in (A) but done in **HEK293T** cells. Arrowheads pinpoint protein bands that were overrepresented in lanes 1-3 compared to lanes 4-6. These bands were cut and analyzed by Mass Spectometry.

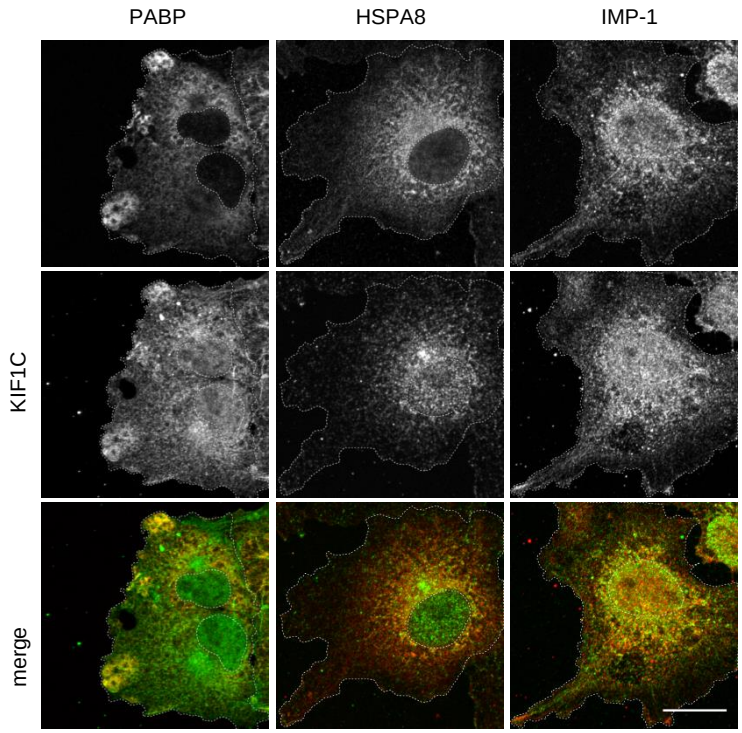

Figure S2. Co-localization of endogenous KIF1C Images show fluorescent immunostainings in COS-7 cells of endogenous KIF1C co-localizing with PABP at specific peripheral regions and partially around the nucleus. KIF1C co-localizes with HSPA8 mostly in a perinuclear manner, and with IMP-1 also around the nucleus. Fine dotted lines delimit nucleus and cell contour, scale bar 20µm.

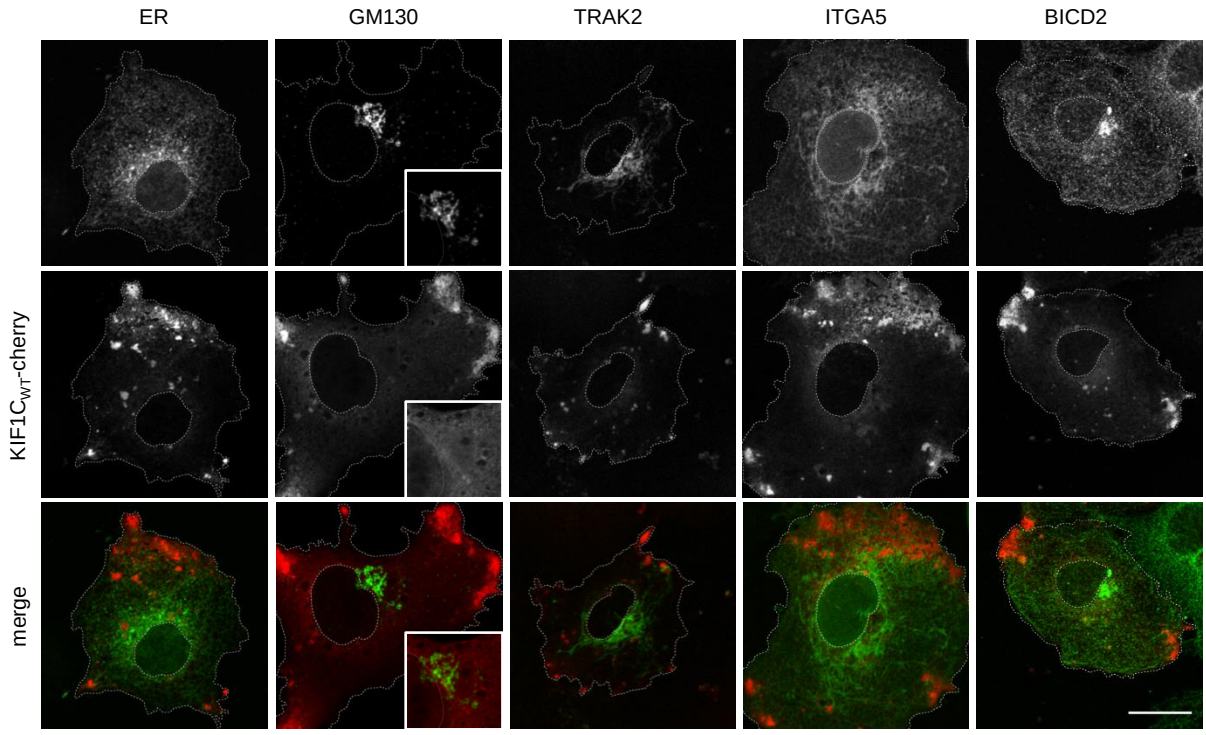

Figure S3. Study of overexpressed KIF1C$_{WT}$ co-localization Images show distribution of overexpressed KIF1C$_{WT}$-cherry in COS-7 cells immunolabelled with markers for endoplasmic reticulum (pmKate2-ER), Golgi (GM130), mitochondrial network (TRAK2), α5-integrin (pEGFPN3-ITGA5) and BICD2 protein. KIF1C does not seem to co-localize with any of the markers displayed here. Fine dotted lines delimit nucleus and cell contour, scale bar 20µm.

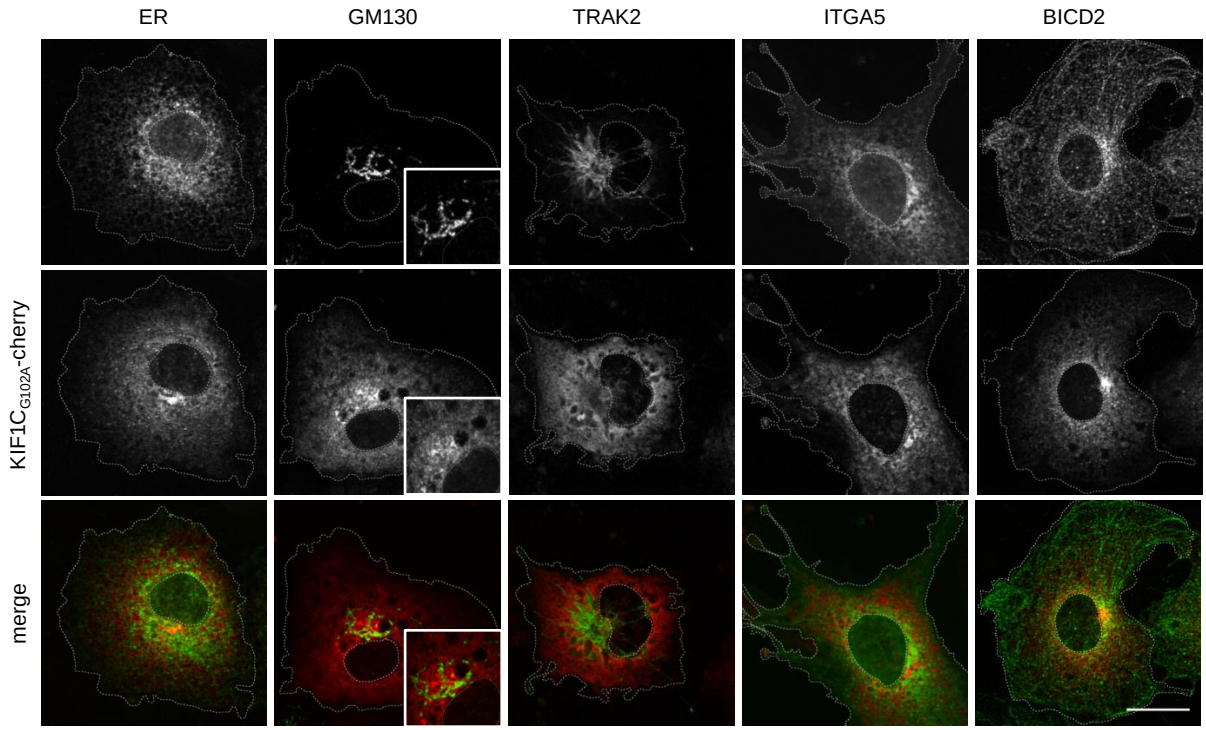

Figure S4. Study of overexpressed KIF1C$_{G102A}$ co-localization Images show distribution of overexpressed KIF1C$_{G102A}$-cherry in COS-7 cells immunolabelled with markers for endoplasmic reticulum (pmKate2-ER), Golgi (GM130), mitochondrial network (TRAK2), α5-integrin (pEGFPN3-ITGA5) and BICD2 protein. KIF1C does not seem to co-localize with any of the markers displayed here. Fine dotted lines delimit nucleus and cell contour, scale bar 20µm.

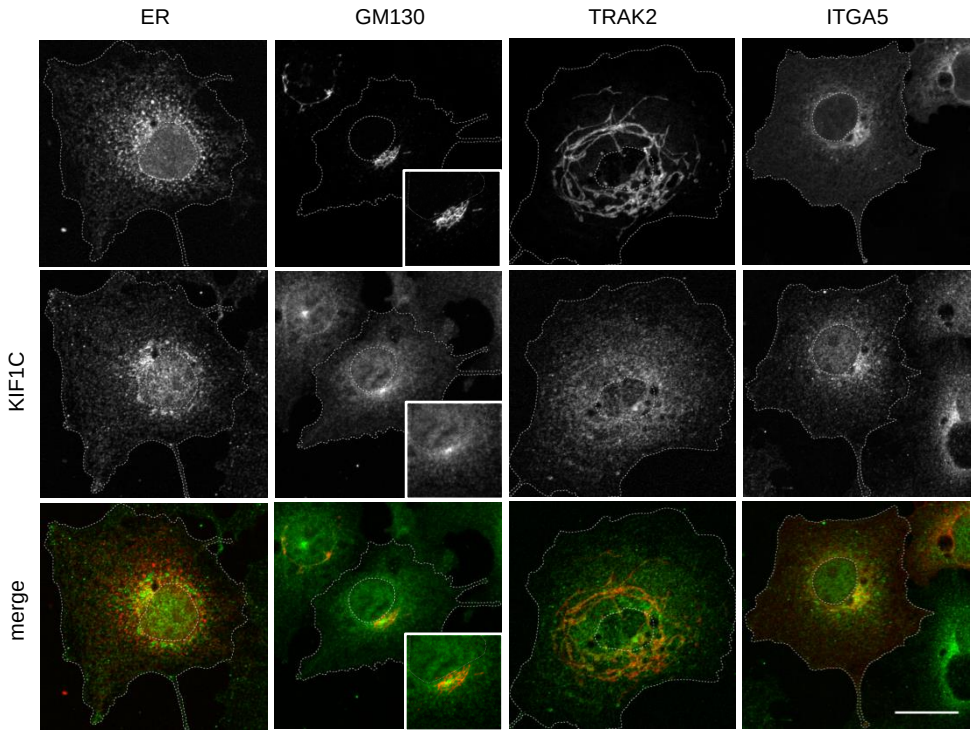

Figure S5. Study of endogenous KIF1C co-localization Images show immunofluorescent co-stainings of endogenous KIF1C with markers for endoplasmic reticulum (pmKate2-ER), Golgi (GM130), mitochondrial network (TRAK2) and α5-integrin (pEGFPN3-ITGA5) in COS-7 cells. KIF1C does not appear to co-localize with any of the markers for ER, Golgi or mitochondria, although it might co-localize in few restricted points with ITGA5 around the nucleus. Fine dotted lines delimit nucleus and cell contour, scale bar 20µm.

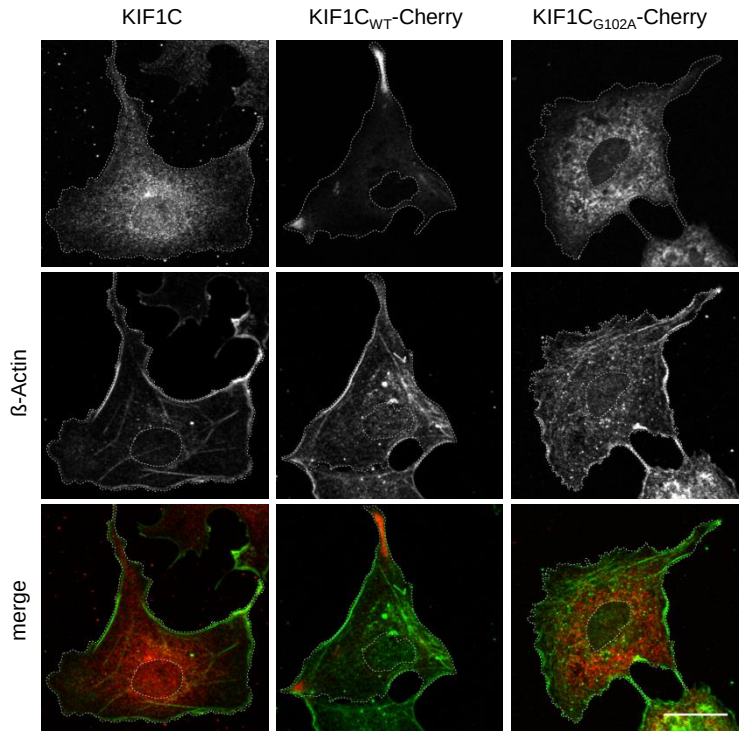

Figure S6. Overexpression of KIF1C$_{G102A}$ does not affect the actin cytoskeleton. Images show COS-7 cells either untransfected or transfected with KIF1C$_{WT}$-cherry or KIF1C$_{G102A}$-cherry respectively and immunolabelled with ß-actin to visualize the actin cytoskeleton. Fine dotted lines delimit nucleus and cell contour, scale bar 20µm.

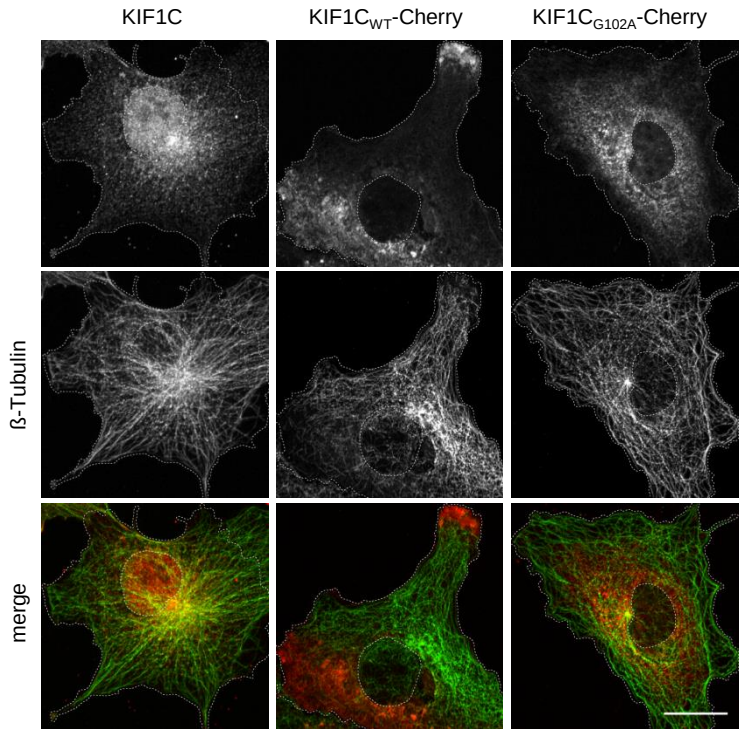

Figure S7. Overexpression of KIF1C$_{G102A}$ does not affect the microtubular architecture. Images show COS-7 cells either untransfected or transfected with KIF1C$_{WT}$-cherry or KIF1C$_{G102A}$-cherry respectively and immunolabelled with ß-tubulin to visualize microtubular network. Fine dotted lines delimit nucleus and cell contour, scale bar 20µm.

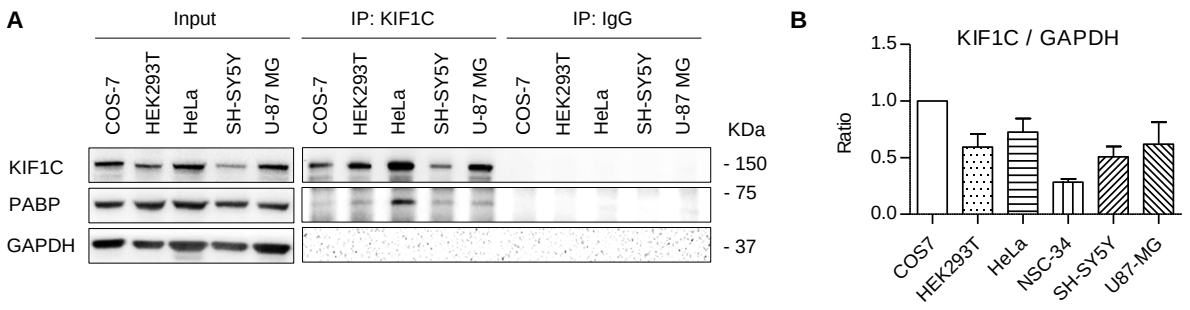

Figure S8. **KIF1C expression and PABP co-immunoprecipitation depending on the cell type**. **(A)** Western blot membrane shows co-immunoprecipitation of endogenous KIF1C with PABP performed on different cell lines, using an antibody against KIF1C or a control IgG antibody. HeLa cells seem to work best for this experiment. **(B)** Graph shows the relative amount of KIF1C per GAPDH as a way to address relative protein expression depending on the cell type (normalized to COS-7 cells), bars represent mean + SEM (n = 2-5).

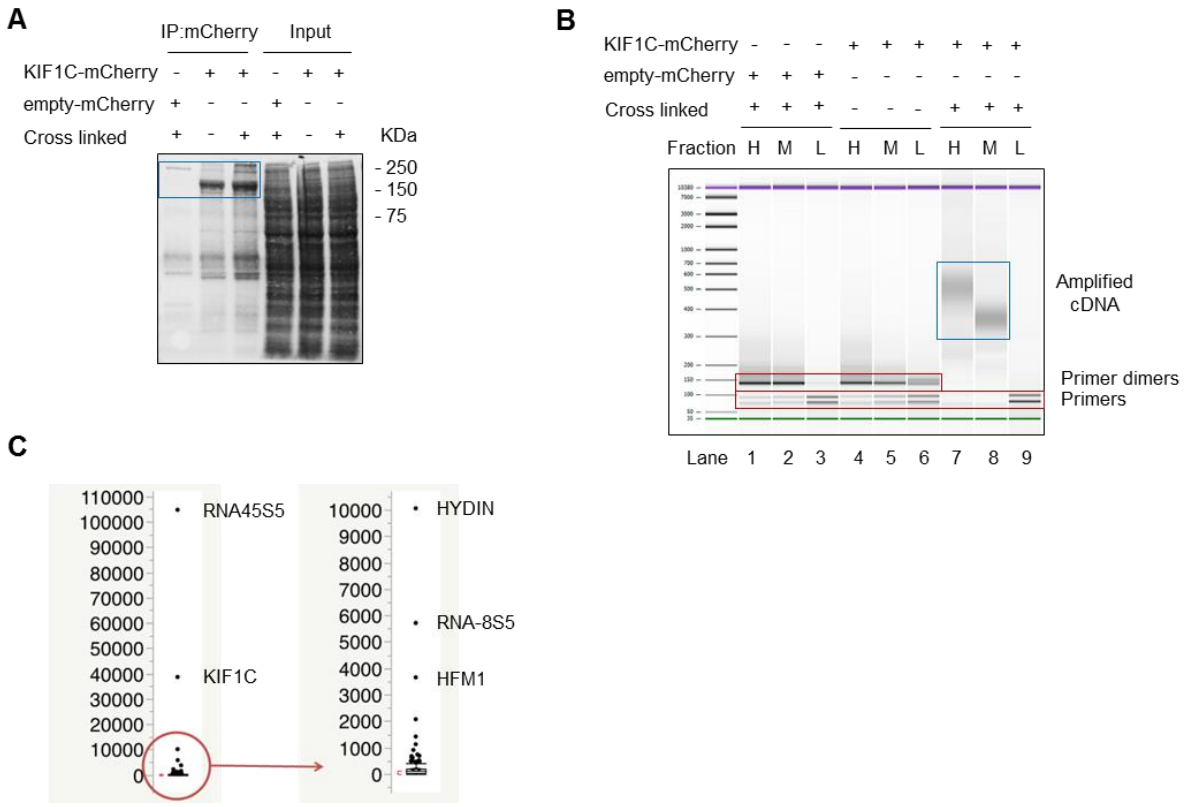

Figure S9. iCLIP experiment and analysis (A) Ponceau staining of nitrocellulose membrane reveals all loaded proteins. Blue region delimits where KIF1C-RNA complex is located, which was cut out to isolate RNA. **(B)** The high sensitivity Agilent DNA chip shows amplification of high and medium size fragments of cDNA for KIF1C-mCherry_crosslinked (CL) sample. As expected nothing is amplified on any of the fractions of the negative controls "empty-mCherry_CL" (lanes 1-3) and "KIF1C-mCherry_non-crosslinked" (lanes 4-6), thus proving the efficiency of the method. **(C)** Represents the peak score distribution of KIF1C-bound gene transcripts extracted from Table S3.

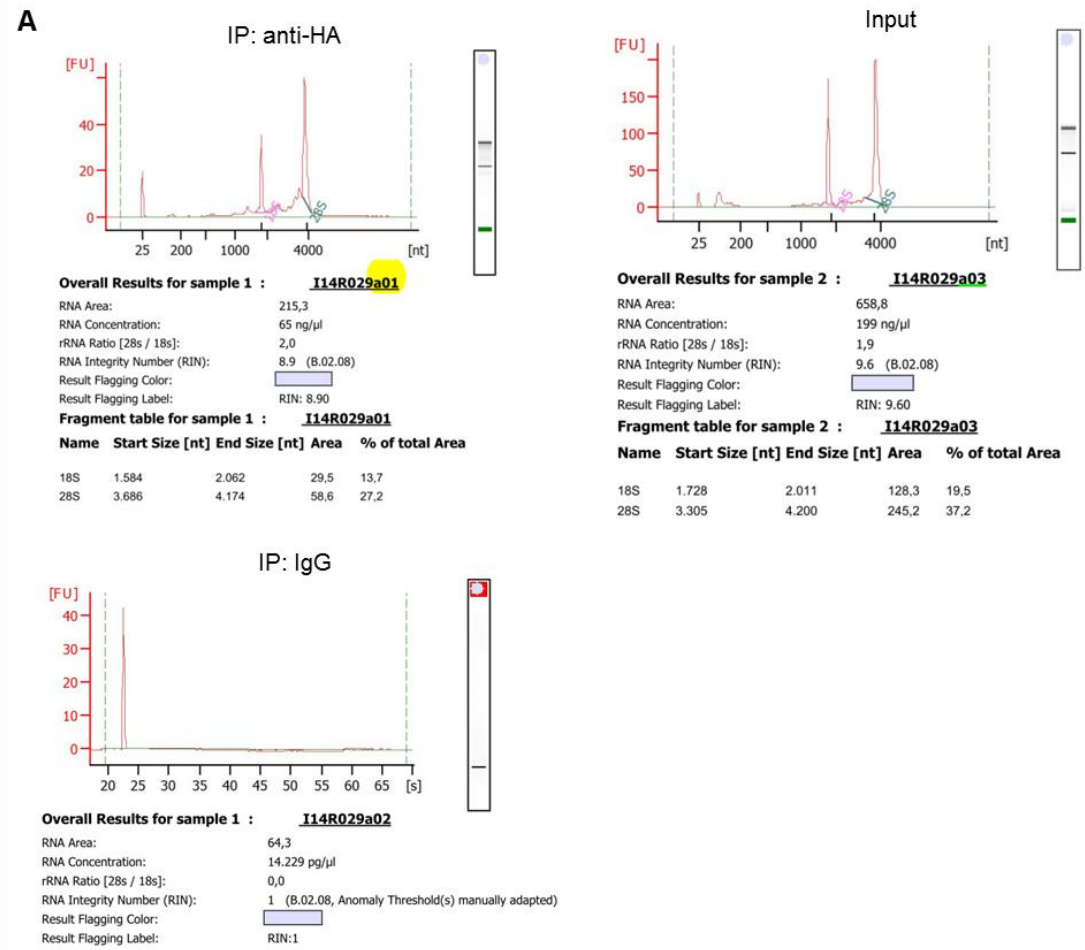

Figure S10. Quality control for RNA-immunoprecipitation Bioanalyzer analysis shows presence and quality of RNA for the different samples.

Tables

Protein hits	Name	Mass	Score	Matches	Peptides	emPAI
gi|11935049	Keratin I	66198	963	39(37)	15(15)	1.27
gi|547754	Keratin, type II	66110	876	31(29)	14(13)	1.15
gi|40254834	**Kinesin family member 1C**	123725	791	25(21)	14(12)	0.51
gi|28317	Unnamed protein product	59720	796	30(29)	12(12)	1.07
gi|693937	**Polyadenylate binding protein II**	58709	511	17(17)	9(9)	0.74
gi|55956899	Keratin 9	62255	464	12(12)	7(7)	0.59
gi|5729877	**Heat schock 70KDa protein 8 isoform 1**	71082	360	15(15)	5(5)	0.43
gi|56237027	**Insulin-like growth factor 2 mRNA binding protein 1**	63783	328	8(8)	6(6)	0.4
gi|386785	Heat shock protein	70110	310	11(11)	5(5)	0.29
gi|119581150	Keratin 14	44865	237	10(9)	4(4)	0.38
gi|386850	Keratin 5	54649	185	5(5)	3(3)	0.22
gi|30795212	**Insulin-like growth factor 2 mRNA binding protein 3**	64008	113	3(2)	2(1)	0.12
gi|37460	Unnamed protein product	27329	72	1(1)	1(1)	0.14
gi|292059	MTHSP75	74019	64	4(4)	1(1)	0.05
gi|16751921	Dermicidin preprotein	11391	57	2(1)	1(1)	0.35
gi|51476370	Hypothetical protein	199652	48	2(2)	1(1)	0.02
gi|114682771	Predicted: similar to ribosomal protein L36 (P.troglodytes)	5528	45	1(1)	1(1)	0.78
gi|20149993	Chain A, structure of Human Trysin IV	24832	43	1(1)	1(1)	0.15

Table S1. Protein hits found by Mass spectrometry

Proteins followed up functionally are marked in bold font. The remaining peptides mapped mostly to keratins, probably due to contamination during handling, and to KIF1C which presence is likely attributable to its abundance after *KIF1C* overexpression.

Rep.	sequencing paired-reads	mapped pair-end (Bowtie2)	# reads after filtering	reliable mutations	clusters	enriched clusters	CL mutations	CL candidate sites	# genes
1	118680109	38978481	394871	2926	3654	1010	1792	567	405
2	151318478	48552947	495051	3065	3904	1105	1895	623	439
3	171310069	55163189	564032	3070	3937	1122	1891	633	450
4	194101960	62960780	650985	3190	4074	1203	1977	668	472
5	117122886	21077481	212942	2651	3128	743	1602	444	307
6	145283635	46230734	469958	3018	3768	1075	1878	609	434
7	173089145	55665454	570315	3091	3895	1127	1898	630	449
8	184224256	58944226	611268	3124	3896	1138	1934	645	456
mean	156891317	48446661	496178	3017	3782	1065	1858	602	426
stdev	28808260	13425569	140654	167	291	141	116	70	52
min	117122886	21077481	212942	2651	3128	743	1602	444	307
max	194101960	62960780	650985	3190	4074	1203	1977	668	472

Rep.: replicate, #: number of, CL: crosslinking

Table S2. PIPE-CLIP analysis of iCLIP sequencing data

	Sum Peak Score in sample								Ranking in sample									
Gene	**1**	**2**	**3**	**4**	**5**	**6**	**7**	**8**	**1**	**2**	**3**	**4**	**5**	**6**	**7**	**8**	**Present in**	**Mean Peak Score**
RNA45S5	82841	104145	120074	135786	44940	99078	119569	127662	1	1	1	1	1	1	1	1	8	104736
KIF1C	30802	38287	43893	50048	16850	36436	43773	46624	2	2	2	2	2	2	2	2	8	38594
HYDIN	7678	9899	10513	14022	4035	9431	11825	13525	3	3	3	3	3	3	3	3	8	10051
RNA5-8S5	4605	5648	6566	7474	2391	5314	6527	7098	4	5	5	4	4	4	4	4	8	5714,6
HFM1	1554	2066	2391	2710	900	1968	2391	2553	6	6	6	5	6	6	6	5	8	2073,1
SLC26A3	1193	1360	1461	2005	565	1321	1643	1820	7	7	7	6	7	7	7	6	8	1416,8
PDE3A	917	1156	1207	1498	472	1067	1280	1363	8	8	8	7	8	8	8	7	8	1124,5
RAPGEF6	662	882	983	1314	338	809	1088	1343	9	9	9	8	9	9	9	8	8	910,15
LINC01019	552	758	784	991	283	715	845	1017	10	10	11	9	11	10	10	9	8	736,54
RPS29	542	704	783	781	283	642	771	865	12	11	12	14	12	11	12	10	8	675,26
MFSD11	552	677	819	903	299	637	786	826	11	12	10	10	10	12	11	11	8	690,82
SLCO5A1	502	593	695	785	268	597	685	805	13	14	15	13	14	14	14	12	8	619,87
MAZ	471	634	727	827	281	603	762	798	14	13	13	12	13	13	13	13	8	639,92
EFTUD1P1		575	657	835		559	660	762		15	16	11		15	15	14	6	445,08
MALAT1	382	460	559	656	176	510	511	657	17	18	20	17	21	16	21	15	8	483,9
GARS	373	534	703	673	208	461	606	613	18	16	14	16	18	17	16	16	8	518,2
FN1	412	443	628	682	223	437	575	608	16	21	18	15	17	20	17	17	8	503,15
HSPA1B	318	428	636	631	105	406	546	594	22	22	17	19	83	21	19	18	8	437,99
CCDC107	415	457	561	642	226	445	553	578	15	19	19	18	15	19	18	19	8	490,82
DCTN1	352	461	540	544	224	451	531	565	19	17	21	24	16	18	20	20	8	466,23
RPL23	284	451	467	561	152	355	466	560	31	20	25	22	25	29	23	21	8	405,71
BRD4	312	390	488	559	182	381	483	541	24	26	24	23	19	24	22	22	8	417,1
MKNK1	226	342	359	563	106	295	414	536	57	37	47	21	79	50	35	23	8	341,28
CDH11	347	400	530	588	174	393	443	508	20	24	22	20	22	23	25	24	8	422,76
PPP1R7	285	370	410	532	182	367	448	507	29	27	31	26	20	27	24	25	8	390,13

BYSL	298	396	419	505	149	369	416	476	26	25	27	28	26	25	33	26	8	377,57
SLC30A10	286	318	349	463	145	312	421	469	28	46	53	34	30	44	32	27	8	345,35
ZFP64	258	367	417	536	136	347	424	467	40	28	29	25	39	31	31	28	8	363,4
HIST2H2AA3	315	405	498	514	119	394	440	464	23	23	23	27	54	22	27	29	8	386,53
IMP4	284	366	426	480	147	345	410	460	30	29	26	31	28	32	36	30	8	363,95
WDFY3	259	362	400	497	140	340	442	453	39	31	34	29	36	33	26	31	8	358,22
PIM3	329	356	419	493	157	368	424	438	21	32	28	30	23	26	30	32	8	375,69
PCNX	269	346	413	411	141	351	416	435	36	34	30	50	35	30	34	33	8	348,23
PCGF3	276	314	371	449	142	314	372	434	33	49	43	38	33	42	46	34	8	334,86
TMC7	271	324	383	438	144	315	399	424	35	44	39	43	31	41	38	35	8	338,25
TACC3	221	261	333	473	132	259	371	419	61	73	57	33	42	67	48	36	8	305,66
NCBP2	232	319	367	458	111	316	366	418	56	45	46	35	68	40	51	37	8	317,51
C18orf54	247	308	370	420	113	316	375	415	45	50	44	47	63	39	44	38	8	316,54
MDK	301	336	386	477	132	358	428	414	25	38	37	32	41	28	28	39	8	352,74
KNTC1	222	316	373	436	134	300	350	413	60	48	42	44	40	48	57	40	8	316,73
AKAP13	242	282	388	412	149	316	389	411	48	60	36	49	27	37	41	41	8	325,72
NUP107	250	336	407	447	132	307	391	404	44	39	33	41	44	45	40	42	8	332,32
EIF4H	233	304	347	380	70	281	362	389	53	52	54	60	166	54	52	43	8	285,84
LAMC1	237	331	389	389	140	283	408	388	50	42	35	56	37	52	37	44	8	321,66
CHAF1A	279	332	410	452	154	317	394	383	32	40	32	37	24	35	39	45	8	343,43
OAZ1	243	328	333	448	132	301	359	383	47	43	55	40	43	47	53	46	8	315,81
DENR	253	354	378	448	146	330	374	382	43	33	41	39	29	34	45	47	8	335,19
HIST2H2BC	257	346	385	445	124	313	385	377	41	35	38	42	48	43	43	48	8	327,09
GTF2H1	223	332	355	373	138	241	371	375	59	41	50	61	38	76	49	49	8	302,84
COL1A1	220	304	370	430	110	282	351	371	62	53	45	45	70	53	55	50	8	300,25

Table S3. Gene list resulting from iCLIP data filtering with PIPE-CLIP; only first 50 genes (Total: 515) are represented.

Primer name	Sequence	Application
kif1c_topo_for	atggctggtgcctcgg	Cloning
kif1c_topo_nonstop_rev	tcacagctgccccact	Cloning
kif1c_g305c_for	gcagaccggggctgcgaaatcctataccat	Mutagenesis
kif1c_g305c_rev	atggtataggatttcgcagccccggtctgc	Mutagenesis
kif1c_c527t_for	cccatcctgggcctgtacgtgcaggac	Mutagenesis
kif1c_c527t_rev	gtcctgcacgtacaggcccaggatggg	Mutagenesis
kif1c_a901g_for	ggattttatcccctacggggactctgtgctcac	Mutagenesis
kif1c_a901g_rev	gtgagcacagagtccccgtaggggataaaatcc	Mutagenesis
BamHI-kif1c_for	taggatccatggctggtgcctcggtg	Cloning
kif1c-ha-XhoI_rev	atctcgagtcaagcgtaatctggaacatcgtatgggtacacagctgccccactctcc	Cloning
kif1c_seq_1_for	gtgaaagtggcagtgagggt	Sequencing
kif1c_seq_2_rev	cctccgtcgaagtgtgtgac	Sequencing
kif1c_seq_2_for	ctcttgaaccccaagagtcg	Sequencing
kif1c_seq_3_for	gctgctcaaggaaaatttgg	Sequencing
kif1c_seq_4_for	agaggctgcaggagacagag	Sequencing
kif1c_seq_5_for	agaaccacgttttccgcttc	Sequencing
kif1c_seq_6_for	tcgcagggtttatcagatcc	Sequencing
kif1c_seq_7_for	gatcagaggcagcagaggag	Sequencing
kif1c_seq_8_for	gcaggaactccctggatg	Sequencing
kif1c_for_ex16-17	ctccaaagaagactccccacc	qPCR
kif1c_rev_ex19	ctccgtcacaagcttcccat	qPCR
rna28s5_for	acctctcacgtctcttcacc	qPCR
rna28s5_rev	aggcgcatgaatggatgaac	qPCR
gapdh_qpcr_for	cctgttcgacagtcagccgcat	qPCR
gapdh_qpcr_rev	caggcgcccaatacgaccaa	qPCR
actb_qpcr_for	cgcgagaagatgacccagat	qPCR
actb_qpcr_rev	tcaccggagtccatcacgat	qPCR
hydin_qpcr2_for	gcggggaatggaggtagaat	qPCR
hydin_qpcr2_rev	tctgagggtgtaagcattcgg	qPCR
hfm1_qpcr_for	tgtccgcagggagatttatgac	qPCR
hfm1_qpcr_rev	agcaggagggagaaaccaatc	qPCR
pde3a_qpcr_for	tcccggtgtttaagaggagg	qPCR
pde3a_qpcr_rev	ggttcctgaagactgtgatcct	qPCR
rapgef6_qpcr_for	cttgcctccttgcagttttgg	qPCR
rapgef6_qpcr_rev	aatggtttggcgctctcctt	qPCR
rplp0_qpcr_f	acgggtacaaacgagtcctg	qPCR
rplp0_qpcr_r	cgactcttccttggcttcaa	qPCR

Table S4. Primers used in the study